AN ABSTRACT OF THE DISSERTATION OF

Kellie T. Wall for the degree of Doctor of Philosophy in Geology presented on March 8, 2022.

Title: The 3.1 Ma to 100 ka Goat Rocks volcanic complex: Persistence and evolution of magmatism at a long-lived major andesite locus on the Cascade Arc

Abstract approved:

Anita L. Grunder

The imposing andesite stratovolcano is the characteristic expression of subduction zone magmatism, posing hazards to coastal populations and bearing insight into deep Earth processes. On a map of a typical volcanic arc, one can easily distinguish the approximately linear alignment and regular spacing of these major edifices that stand out from a diffuse distribution of mafic volcanoes (e.g. the Quaternary Cascades; Hildreth, 2007). The andesitic composite volcanoes have a reputation for being complex, open systems: crystal zoning "stratigraphies," diverse crystal cargoes including antecrysts or xenocrysts, quenched magmatic inclusions, and variations in isotopic signatures are among the many lines of evidence that these systems involve a variety of igneous processes and melt sources. To investigate the development and evolution of such transcrustal magma factories, I have conducted a detailed temporal, spatial, and geochemical characterization of a long-lived arc volcanic center in the southern Washington Cascades, the Goat Rocks volcanic complex.

Results from $^{40}Ar/^{39}Ar$ and U/Pb geochronology constrain the lifespan of the Goat Rocks volcanic complex from ~3.1 Ma to ~100 ka. During this time, four major composite volcanoes were built (as well as several smaller volcanoes). From oldest to youngest, these are Tieton Peak, Bear Creek Mountain, Lake Creek volcano, and Old Snowy Mountain. Four volcanic stages are defined based on the lifespans of these centers and distinct compositional changes that occur from one to the next: Tieton Peak stage (3.1-2.6 Ma), Bear Creek Mountain stage (1.6-1.1 Ma), Lake Creek stage (1.1 Ma to 456 ka), and Old Snowy Mountain stage (440 ka to 115 ka). Two lava flow remnants also have ages in the interim between Tieton Peak stage and Bear Creek Mountain stage (2.3 Ma and 2.1 Ma), and their sources are not yet identified. The ages of the Bear Creek Mountain and Lake Creek stages in fact overlap, and the gap between Lake Creek stage and Old Snowy Mountain stage is only on the

order of 10^4 years. Based on supporting compositional evidence, the Bear Creek Mountain, Lake Creek, and Old Snowy Mountain stage volcanoes are considered to be the migrating surface expressions of a continuous magmatic system that was active over at least ~1.5 million years. It remains uncertain whether the gaps between the Tieton Peak stage, scattered early Pleistocene andesites, and Bear Creek Mountain stage are due to incomplete exposure/sampling or real quiescent periods earlier in the development of the Goat Rocks volcanic complex.

Throughout the construction of the andesitic complex, mafic volcanoes were active on its periphery. These include the Miriam Creek volcano (~3.6-3.1 Ma), Devils Washbasin volcano (3.0-2.7 Ma), Hogback Mountain (1.1 Ma – 891 ka), Lakeview Mountain (194 ka), and Walupt Lake volcano (65 ka). Two basalt and basaltic andesite units (Qob_1 and Qob_2, 1.4 and 1.3 Ma; Hammond, 2017) also erupted from the Goat Rocks area, likely an older incarnation of Hogback Mountain. The suite of mafic magmas erupted in this region are all calcalkaline basalt (or basaltic andesite; CAB), but two compositional groups emerge from the trace element and isotopic data. Group 1 is LILE and LREE-enriched, with higher $^{87}Sr/^{86}Sr$ isotopes, and includes compositions from Devils Washbasin, Lower Hogback Mountain, and Lakeview Mountain. Group 2 is less enriched in LILE and LREE and lower in $^{87}Sr/^{86}Sr$, and includes the compositions of Miriam Creek, Qob_1, Upper Hogback Mountain, Walupt Lake, and Coleman Weedpatch. The two groups are recurrent through time and with no geographic distinction; in fact, both types were tapped by the Hogback Mountain volcano. Together both of these groups, alongside CABs from Mount Adams and various basalts from Mount St. Helens, form a compositional array between the basalts of the High Cascades and the intraplate-type basalts (IPB) of Mount Adams and Simcoe volcanic field. These results lead to three conclusions. 1) Variably subduction-modified mantle is distributed across the region, perhaps either as stratified layers or a web-like network of fluid pathways amongst less metasomatized mantle. 2) Transitional compositions between the IPBs and typical "High Cascades" CAB/HAOT signature suggest a broader influence of the mantle domain that feeds IPBs—if asthenospheric mantle through a slab window, as suggested by Mullen et al. (2017), then perhaps it bleeds in smaller quantities over a broader area. This compositional trend solidifies the interpretation of the southern Washington Cascades as a unique and coherent "segment" of the arc (the Washington segment of Pitcher and Kent, 2019). 3) The recurrence of variable mafic magma types through time, and with no geographic boundaries, indicates that the compositional evolution of the Goat Rocks volcanic complex was not likely driven by a change in mafic input.

Indeed, the Sr, Nd, Hf, and Pb isotope ratios of the intermediate to felsic suite are closely aligned with the local basalts and suggest a limited role of crustal assimilation. Importantly, several mineral thermometers (zircon, ilmenite-magnetite pairs, and amphibole) align in recording higher crystallization temperatures in Bear Creek Mountain to early Lake Creek time, a cooling trend through the Lake Creek stage, and a more diverse range of temperatures in the transition to Old Snowy Mountain stage. Thus, it is suggested that the compositional evolution at Goat Rocks represents a thermal cycle of waxing and waning magmatic flux: where the period of Bear Creek Mountain to early Lake Creek volcanism was the climactic phase of a vertically extensive magma homogenization factory, then the system waned and cooled, ultimately losing its ability to filter, homogenize, and enrich magmas.

©Copyright by Kellie T. Wall
March 8, 2022
(All Rights Reserved or Creative Commons License)

The 3.1 Ma to 100 ka Goat Rocks volcanic complex: Persistence and evolution of magmatism at a long-lived major andesite locus on the Cascade Arc

by
Kellie T. Wall

A DISSERTATION

submitted to

Oregon State University

in partial fulfillment of
the requirements for the
degree of

Doctor of Philosophy

Presented March 8, 2022
Commencement June 2022

Doctor of Philosophy dissertation of Kellie T. Wall presented on March 8, 2022.

APPROVED:

____

Anita L. Grunder, representing Geology

____

(Head, Chair, Director, Dean) of the (Department, School, College) of Geology and Geophysics

____

Dean of the Graduate School

I understand that my dissertation will become part of the permanent collection of Oregon State University libraries. My signature below authorizes release of my thesis to any reader upon request.

____

Kellie T. Wall, Author

In loving memory of my mom,

whose eyes sparkled when I told her about my lava rocks.

ACKNOWLEDGEMENTS

It took a village to craft this dissertation—there are so many who have helped me on my graduate research adventure in ways both big and small. I thank each of you who have contributed to this work by supporting me financially, intellectually, and/or emotionally. From years-long mentorship and collaboration to the briefest conversations, all have enriched my experience and shaped this research.

Numerous funding sources made this work possible. The National Science Foundation (NSF) Graduate Research Fellowship Program funded my stipend for three years and a summer internship at the USGS Cascades Volcano Observatory. NSF also supported this work via a research grant to my advisor Anita Grunder and co-PI Anthony Koppers. In addition, I received a grant from the NSF Earthscope Awards for Geochronology Student Research (AGeS) program. I also benefitted from the generous support of the Geological Society of America (GSA), the Jack Kleinman Memorial Fund for Volcano Research, the American Association of Petroleum Geologists (AAPG) Grants-in-Aid program, and the National Center for Airborne Laser Mapping (NCALM) seed proposal program. Last but not least, the College of Earth, Ocean, and Atmospheric Sciences provided many terms of teaching assistantship opportunities, a Jean Bowman Clark Education Award, and created a scholarship from the Geology program's Foundation to support me in my final term. I am immensely grateful to all of the donors, organizers, and volunteers whose generosity made this education and research possible. In particular I thank those who dedicated their precious time to read my proposals and who believed in me and my work.

I am lucky to have had Anita Grunder as my advisor and mentor through this experience. Anita, thank you for seeing potential in me and accepting me as your student. I am grateful for our stimulating science chats, your understanding in difficult times, and your balanced criticism and encouragement.

I thank my committee members Adam Kent, Anthony Koppers, Andrew Meigs, and Kevin Gable for challenging and supporting me. Thanks to my professors and the VIPERs for a broad education from the theoretical to the practical, and for interesting discussions both inside and outside the classroom.

Thank you, Don Swanson, for so generously sharing your field notes, maps, and analyses from your many years of work on the Goat Rocks area. I appreciate the time you have spent organizing those documents, answering my long-winded emails, and meeting with me at conferences. Your perspective has been critical to this project and I have thoroughly enjoyed our discussions.

Thanks to the numerous other experts on Cascade Arc geology and geochemistry who have made time to share their perspectives with me, including Dominique Weis, Judy Fierstein, Wes Hildreth, Mike Clynne, and many folks at the USGS Cascades Volcano Observatory.

Thanks to the many individuals who have trained me in proper laboratory techniques, including Dan Miggins, Daniel Heaton, and the rest of the Argon Lab crew; Frank Tepley and Marie Takach of the microprobe lab; Matt Coble at the USGS-Stanford SHRIMP-RG lab; Ashley Steiner and company at the WSU GeoAnalytical Lab; sample processing extraordinaires Nikki Moore, Nansen Olson, Brad Pitcher, Jordan Lubbers, and certainly many others whom I am forgetting.

My field work would have been impossible without the help of these assistants, colleagues, and mentors: Tommy Moore, Daryl Gusey, John Lasher, William Otto, Nathan Van Cleave, Peter Davidson, Marina Marcelli, Zoe Dilles, Nansen Olson, Tim Facemire, Will Gapasín, Leo Dilles, Henry Westly, Joe Biasi, Marcel Griffioen, Sage Reuter, Sydney Acito, and of course Anita Grunder. I am grateful for their good company, hard work, and many lessons on science, safety, and fun in the backcountry.

To my partner of six years and counting, Tommy Moore, thank you for guiding my first ever backpacking trip(!) and joining me on several other excursions to provide physical and moral support. From the Lost Lake trail to our home office, thank you for the countless occasions you have offered your hankie to dry my tears. Your love, humor, groundedness, resilience, and example of work-life balance have inspired and helped me immensely. Thanks for being a constant support through calm and chaos.

I thank my family and friends near and far for your encouragement and love. Thank you, Dad, Jennie, Tara, the Moore and Childress clan, Aunt Barb, and Granny. Thank you, OSU/Corvallis friends for many years of fun and camaraderie. Thank you to all who showed me kindness, understanding, and support during the difficult period when the pandemic took my mom from me.

Mom, thanks for cheering me on and listening so attentively to my chatter about volcanic rocks and the many ways I dissect and transform them in the lab. I cherish the night when we visited the Argon Lab to look at my samples under a microscope and you were thrilled by the gleaming crystals of plagioclase and sugary flakes of groundmass. Your eager questions encouraged me that this work is meaningful.

CONTRIBUTION OF AUTHORS

Chapter 1 was written by Kellie Wall and Anita Grunder with assistance of Dan Miggins and Matt Coble.

Chapter 2 was written by Kellie Wall with assistance from Anita Grunder and the paleomagnetic expertise of Joe Biasi.

Chapters 3 and 4 were written by Kellie Wall with guidance from Anita Grunder and Dominique Weis.

TABLE OF CONTENTS

LIST OF FIGURES

Page

LIST OF TABLES

Page

LIST OF APPENDICES

Optional. If list of appendices is short, it may be attached to the table of contents. For more than 5 appendices, or if different heading levels are listed in the appendices, a separate List of Appendices is required. If two or more figures appear in the appendices, a List of Appendix Figures and/or a List of Appendix Tables are required.

LIST OF APPENDIX FIGURES

LIST OF APPENDIX TABLES

MULTISTAGE GROWTH AND COMPOSITIONAL CHANGE AT THE GOAT ROCKS VOLCANIC COMPLEX, A MAJOR PLIOCENE-PLEISTOCENE ANDESITE CENTER IN THE SOUTHERN WASHINGTON CASCADES

Kellie T. Wall[1], Anita L. Grunder[1], Daniel P. Miggins[1], Matthew A. Coble[2]

[1]*College of Earth, Ocean, and Atmospheric Sciences, Oregon State University, 104 CEOAS Administration Bldg, Corvallis, OR 97331*

[2]*Department of Geological Sciences, Stanford University, 367 Panama Street Room 89, Stanford, CA 94305*

The Geological Society of America

P.O. Box 9140, Boulder, CO 80301-9140

Special Paper 538

Citation:

Wall, K.T., Grunder, A.L., Miggins, D.P., and Coble, M.A., 2018, Multistage growth and compositional change at the Goat Rocks volcanic complex, a major Pliocene–Pleistocene andesite center in the southern Washington Cascades, *in* Poland, M.P., Garcia, M.O., Camp, V.E., and Grunder, A., eds., Field Volcanology: A Tribute to the Distinguished Career of Don Swanson: Geological Society of America Special Paper 538, p. 63–91, https://doi.org/10.1130/2018.2538(04).

CHAPTER 1 - MULTISTAGE GROWTH AND COMPOSITIONAL CHANGE AT THE GOAT ROCKS VOLCANIC COMPLEX, A MAJOR PLIOCENE-PLEISTOCENE ANDESITE CENTER IN THE SOUTHERN WASHINGTON CASCADES

ABSTRACT

The deeply eroded Goat Rocks volcanic complex was a major locus of andesitic volcanism in the Cascade arc in southwest Washington during the late Pliocene to Pleistocene. This volcanic complex includes the remnants of multiple andesitic edifices over an area of ~200 km^2, centered ~35 km north of Mount Adams on the arc axis. New $^{40}Ar/^{39}Ar$ ages for seven samples and U/Pb zircon ages for nine samples indicate a 2.5 to 2.9 Myr eruptive history at Goat Rocks. Four eruptive stages are delineated: Tieton Peak (potentially 3.0 to 2.6 Ma), Bear Creek Mountain (>1.6 to 1.3 Ma), Lake Creek (1.1-0.6 Ma), and Old Snowy Mountain (0.4 to 0.1 Ma), each named for the major vent that was active during that time. Lake Creek volcano was the most voluminous of these edifices and probably rose at least 3400 m above sea level with a volume of ~60 km^3, comparable to nearby active composite volcanoes. Thirty new bulk composition XRF and ICP-MS analyses from the volcanic complex are presented, in addition to 54 previously unpublished XRF analyses for samples collected by Don Swanson. The compositional variability is greatest in the early and late stages, ranging from basaltic andesite to rhyolite, whereas the more voluminous middle stages are dominated by andesite to dacite. The middle eruptive stages are interpreted to have been a time of peak thermal energy with a mature subvolcanic plexus. In addition, compositions shift from high-K to medium-K with time, which mimics variation across the arc; early eruptive products are similar in composition to those of Mount Adams, and Old Snowy Mountain stage compositions are more similar to Mount St. Helens. The life cycle of Goat Rocks volcanic complex provides new perspective on the longevity and evolution of major arc volcanoes, and on the complex distribution of magma in the Cascade arc at the latitudes of southern Washington and adjacent Oregon.

INTRODUCTION

A distinctive feature of convergent margins is the magnificent active volcanoes of “orogenic andesite” (Gill, 1981), which inspire art and legends, provide recreation and resources, and threaten life and property. Arc andesite centers, in the form of individual volcanoes or volcanic clusters, are spaced several tens to a few hundred kilometers along subduction zones. This along-arc spacing has been modeled to result from distributed buoyant rise from the deep mantle wedge (e.g. de Bremond d'Ars, 1995; Tamura et al., 2001), a response to lithospheric thickness (e.g. ten Brink, 1991), and/or crustal influences (Savant and de Silva, 2005). The productivity, timing and composition of arc volcanoes inform the balance of geochemical cycling in subduction zones. Arc volcanoes have typical lifespans of a few tens of thousands of years to a few hundred thousand years, whereas clusters of volcanoes have lifespans ranging from about 1 million to more than 10 million years (Jicha and Singer, 2005; Grunder et al., 2006). Many basic facts remain to be assembled about the distribution, longevity, and geochemical evolution of arc volcanoes before arc-scale models of subduction zone magmatism can be tested.

The focus in this paper is on the Cascade arc, which despite its modest length of 1250 km, features great variety in setting and composition amongst its 22 broadly andesitic Quaternary arc volcanoes (see compilation by Hildreth, 2007). In the central segment of the arc (southern Washington to northern Oregon), the arc front is not linear, as it is to the north and south. Instead, the volcanoes Mount St. Helens and Mount Rainier lie trenchward of the arc axis defined by Mount Hood and Mount Adams; farther east lies the alkalic Simcoe volcanic field (Figure 1). Compositions are generally more alkalic with distance from the trench (Leeman et al., 1990, 2005). In addition, the volcanoes in this arc segment exhibit variable eruptive histories and behavior. Mount Hood, for example, has a history dating back to about 3.1 Ma, and has infrequently erupted silicic andesite to mafic dacite (i.e. quite monotonous) lavas over the last several thousand years (Wise, 1969; Sherrod and Scott, 1995; Scott and Gardner, 2017). In contrast, Mount St. Helens is a relative newcomer to the arc, having initiated about 300,000 years ago, and has had frequent explosive eruptions ranging in composition from basalt to dacite (Mullineaux and Crandell, 1981; Clynne et al., 2008). To give perspective to the distribution, longevity, and relative timing of volcanoes in this segment of the arc, as well as spatial and temporal variation in their compositions, we turn our attention to the age and compositional record of the Goat Rocks volcanic complex ('Goat Rocks,' for short), a young but extinct cluster of andesitic volcanoes located approximately within the Goat Rocks Wilderness of Washington State (Figure 1).

New age determinations for thirty-nine samples from Goat Rocks, including $^{40}Ar/^{39}Ar$ ages for seven samples and U/Pb ages for nine samples, provide a geochronological framework to augment mapping and age relations established by other authors (Swanson and Clayton, 1983; Clayton, 1983; Swanson, 1996a,b, and unpublished; Hammond, 2017; Gusey et al., this volume). Goat Rocks was active as recently as ~100,000 years ago and was a major andesitic locus over a period of approximately three million years. Goat Rocks reached its maximum volcanic output in its third of four eruptive stages, overlapping in time with the construction of ancestral Mount Rainier and Mount Hood. Activity at Goat Rocks waned as Mount Adams and Mount St. Helens emerged.

Changes through time in compositions erupted at Goat Rocks are illustrated by 30 new and 54 previously unpublished bulk rock compositional analyses presented in this paper. Early volcanism was compositionally similar to the medium- to high-K suite of Mount Adams, while late-stage eruptions were least potassic and most adakite-like, similar to compositions of Mount St. Helens. The compositional variation at Goat Rocks through time thus mimics the compositional variation observed across the arc in this segment of the Cascades.

GEOLOGIC SETTING

The Goat Rocks volcanic complex is part of the Cascade volcanic arc, which extends 1250 km from British Columbia to California and includes >2300 Quaternary volcanoes related to subduction of the Explorer, Juan de Fuca and Gorda plates beneath the North American plate (Figure 1; Hildreth, 2007). Goat Rocks is the northernmost major volcanic center on the main arc axis that extends from Crater Lake in southern Oregon, through the Oregon Cascades and Mount Adams in southern Washington, and passes through Goat Rocks toward Bumping Lake (Figure 1). Neighboring major arc volcanoes Mount Rainier and Mount St. Helens are offset to the west, and the Simcoe mafic volcanic field lies to the east (Figure 1).

The Rainier-to-Hood segment of the Cascade arc is geomorphologically distinct; abundant mafic volcanic vents and major andesitic centers span ~160 km across the arc (Figure 1; Guffanti and Weaver, 1988; Hildreth, 2007). The region lies at a major structural transition between extension to the south and compression to the north. To the south, clockwise rotation of the Oregon coast range (Wells et al., 1998; Wells and McCaffrey, 2013) yields eastward migration of the Oregon arc through time, and east-west extension affects the present arc (Hughes and Taylor, 1986; Conrey et al., 2002, 2004). To the north, northeasterly compression prevails, and the position of the arc axis has been relatively fixed with minor westward migration (see vent loci in Hildreth, 2007).

The crust beneath the southern Washington Cascades is 40-45 km thick (Shen et al., 2013). Underlying the Cascade arc volcanic products is a patchwork of Paleozoic to Eocene accreted terranes including Paleozoic to Mesozoic mélange belts (Miller, 1989) and the Early Paleogene Siletz Terrane, a fossil oceanic plateau that crops out in the Washington and

Oregon forearc and may underlie the arc (Trehu et al., 1994; Wells et al., 2014). In addition, the locations of Goat Rocks and neighboring Mount Rainier, Mount Adams, and Mount St. Helens coincide with the Southern Washington Cascades Conductor, a complex conductive feature (Stanley, 1990; Hill et al., 2009). Recent high-resolution magnetotelluric studies (e.g. Bowles-Martinez et al., 2016) reveal a complex network of mid-crustal conductive regions near and between the major volcanic centers. These conductive areas have been interpreted as regions of melting and (or) fluid or sulfide-rich metasedimentary layers (Stanley, 1990; Hill et al., 2009; Bowles-Martinez et al., 2016).

Like elsewhere in the Cascade arc, multiple primitive magma types have erupted throughout the Rainier-to-Hood section, including calk-alkaline basalt and low-K tholeiite (Bacon et al., 1997, Conrey et al., 1997) as well as intraplate basalt (Leeman et al., 2005). The latter are a distinctive component of this segment of the arc (Schmidt et al., 2008). Mullen et al. (2017) use Pb, Hf, Nd, and Sr isotope characteristics to define the High Cascades (Mount Rainier to Lassen Peak) as a single arc segment, albeit with a distinct array for Mount Adams and the Simcoe volcanic field. The major volcanic centers from Mount Rainier to Mount Hood have distinct geochemical compositions, with K2O and other incompatible element concentrations being generally lower at a given SiO2 in the forearc (Mount St. Helens), higher on-arc (Mount Adams), and highest in the back-arc (Simcoe volcanic field; Leeman et al., 1990).

PREVIOUS WORK

Our present understanding of the Goat Rocks volcanic complex is the culmination of more than a century of geologic research. In 1893, during reconnaissance fieldwork, USGS geologist Israel C. Russell discovered a thick outcrop of columnar andesite on the bank of the Naches River that he inferred to be a lava flow from “somewhere in the elevated region drained by Tiaton[sic] creek.” Smith (1903) named the great lava flow the Tieton (pronounced tī-eton) andesite. Later, Ellingson (1968) proposed that its source was a volcanic plug at the peak called Black Thumb, west of Gilbert Peak. Noting the similarity of the Tieton andesite to other pyroxene andesite lava flows exposed in the Goat Rocks area, Ellingson (1968) envisioned that Black Thumb had been the center of a major composite volcano, the Goat Rocks volcano, that stood >12,000 feet tall prior to its destruction by glacial erosion.

Clayton (1980, 1983) conducted extensive and detailed fieldwork across the White Pass and Goat Rocks area. He described the Devils Horns rhyolite, a thick sequence of (probably caldera-filling) rhyolite tuff, lava flows, and breccias that crops out on the eastern side of Goat Rocks. Two samples from this rhyolite sequence yielded zircon fission-track ages of 3.20 ± 0.14 Ma and 3.17 ± 0.16 Ma (Clayton, 1983). The overlying Devils Washbasin basalt yielded a stratigraphically inconsistent K/Ar age of 3.80 ± 0.31 Ma (Clayton, 1983). Clayton (1983) described the Devils Washbasin basalt as intercalated with the andesites of nearby Tieton Peak: his sample GRTP-8, from a lava flow cropping out on the lower northeast side of the Tieton Peak stratigraphy, is a basaltic andesite with nearly identical composition to my sample GR20-20 from the upper part of the Devils Washbasin pile. The normal magnetic polarity of the Devils Washbasin basalts and Tieton Peak andesites suggested to Clayton (1983) that these eruptions took place during the Gauss Chron, between 3.2 Ma (post-Devils Horns rhyolite) and ~2.6 Ma (2.581 Ma is the revised age given by Cande and Kent, 1995, for the Gauss-Matuyama reversal). Clayton (1983) concluded that a large composite volcano, with a total eruptive volume of at least 60 km^3 (comparable to present-day Mt. Hood), was active between ~3.2 and 1.0 Ma (based on an unpublished K/Ar age of 1.0 ± 0.1 Ma for Tieton andesite reported by Swanson, 1978).

U.S. Geological Survey geologist Don Swanson began working with Clayton in 1981 as part of a multi-decadal mapping campaign to contextualize the stratigraphy of the Southern Washington Cascades with that of the Mount Rainier-White Pass area (Fiske et al., 1963) and to investigate the influence of the Southern Washington Cascades Conductor (Stanley et al., 1987, 1992) on the regional geology. Products of this work include a preliminary geologic map and open-file report of the Goat Rocks Wilderness (Swanson and Clayton, 1983), several 7.5-minute quadrangle maps and open-file reports (Hamilton Buttes, Packwood Lake, and Packwood quadrangles include volcanic products of the Goat Rocks volcanic complex; Swanson, 1996a, 1996b, 1997), a nearly complete Old Snowy Mountain quadrangle map, and additional notes and mapping from adjacent quadrangles Ohanapecosh Hot Springs, White Pass, Pinegrass Ridge, Jennies Butte, and Walupt Lake.

In their 1983 report, Swanson and Clayton described numerous dikes crosscutting lava flows near Johnson Peak and Goat Lake, and postulated that they are the remnants of a radial dike swarm at the center of a major composite volcano, now deeply eviscerated to form the valley occupied by Upper Lake Creek. Additional geologic mapping by Swanson (1996a, 1996b, and unpublished) details a magnetostratigraphic sequence of normal-reversed-normal in the pyroxene andesites near and west of Johnson Peak, indicating that this vent was active through multiple magnetic reversals, and possibly recording the Brunhes-Matuyama transition. In addition, Swanson (1996a, 1996b, unpublished) reported andesite (± dacite >

rhyolite) lava flows that postdate this activity and occupy deep glacial valleys like those of Upper Lake Creek, Johnson Creek, Jordan Creek, and Goat Creek. These include the lava flows of Old Snowy Mountain, Jordan Creek, Goat Ridge, and Clear Fork Cowlitz River. Swanson (1996a, 1996b) proposed that these valleys were deepened by the glaciers that in nearby regions deposited the Hayden Creek Drift, for which the age has been variably estimated to be between 300 ka and 60 ka (Colman and Pierce, 1981; Crandell, 1987; Dethier, 1988; Evarts et al., 2003), and so the volcanic units occupying them are likely younger.

Gusey et al. (2018) concluded that the Tieton andesite includes two channelized lava flows of enormous length; one ~74 km long and dated at 1.64 ± 0.07 Ma, the other ~52 km long with an age of 1.39 ± 0.10 Ma ($^{40}Ar/^{39}Ar$ ages reported by Hammond, 2017). Based on field relations and compositional similarity, the source of the Tieton andesite is Bear Creek Mountain (Gusey et al., 2018), rather than Black Thumb as proposed by Ellingson (1968).

Extent of the Goat Rocks Volcanic Complex

The broadly andesitic vents of the Goat Rocks volcanic complex lie within a ~200 km^2 ellipsoidal area. We include in the Goat Rocks volcanic complex: a) an inferred vent at Tieton Peak (Clayton, 1983; Swanson, unpublished); b) Bear Creek Mountain, source of the Tieton andesites (Gusey et al., 2018); c) the region of dikes that define the center of Lake Creek Volcano (so named for the dikes' convergence upon the valley of Upper Lake Creek; Swanson and Clayton, 1983; Swanson, 1996b); d) the Old Snowy Mountain-Ives Peak area, where there are dikes and shallow intrusions (Swanson and Clayton, 1983; Swanson, unpublished); e) late-stage andesitic to rhyolitic vents at Goat Ridge and Coyote Lake (Swanson, 1996a,b); f) Hogback Mountain, a dominantly mafic shield volcano, but also a source of andesites (Clayton, 1983); and g) Black Thumb, a source of dacite near Gilbert Peak (Figure 2; Ellingson, 1968; Clayton, 1983).

The locations of peripheral mafic volcanoes are used to constrain the extent of the Goat Rocks volcanic complex. The Devils Washbasin basaltic volcano marks the eastern boundary at the time of the earliest activity at Goat Rocks, though andesitic volcanism later expanded eastward to Bear Creek Mountain. The dominantly basaltic Hogback Mountain volcano defines a northeastern boundary. The Walupt Lake basaltic tuya (subglacial volcano; Swanson, 1996a), nearby mafic vents of Coleman Weedpatch, and the Lakeview Mountain basaltic andesite volcano mark the southern limit to Goat Rocks during its last stage of activity. Andesitic to dacitic vents to the north and northeast of Hogback Mountain (e.g.

Spiral Butte, Round Mountain) are not considered a part of the Goat Rocks volcanic complex, as they lie beyond the "shadow zone" (Walker, 2000) defined by these mafic volcanoes.

Four Volcanic Stages

The Goat Rocks volcanic complex was constructed in four major eruptive stages. From oldest to youngest, these are: Tieton Peak stage, Bear Creek Mountain stage, Lake Creek stage, and Old Snowy Mountain stage. The stages are defined based on the chronologic sequence of migrating vents inferred from mapping, paleomagnetic measurements, and geochronology by previous authors (Clayton, 1980, 1983; Swanson and Clayton, 1983; Swanson, 1996a, 1996b, unpublished; Gusey et al., 2018).

The first eruptive stage, Tieton Peak stage, marks the onset of andesitic volcanism at Goat Rocks, which was centered near Tieton Peak at the western margin of the inferred Devils Horns caldera (Clayton, 1983; Swanson, unpublished). Present-day Tieton Peak is built of a sequence of lava flows (and possibly shallow intrusions in the lower stratigraphy; Judy Fierstein, personal communication) ranging from basaltic andesite to rhyolite. Note that Tieton Peak is not the Miocene feature that Swanson (1966) describes as Tieton Volcano, nor the source of the Tieton andesite flows (Gusey et al., 2018).

Andesitic lava flows from Tieton Peak are reportedly intercalated with mafic lava flows erupted from the nearby Devils Washbasin volcano (this intercalation of units was not observed directly by this author, but mapped and sampled by Clayton, 1983). The remains of Devils Washbasin volcano consist of basaltic dikes crosscutting basaltic lava flows and scoriaceous pyroclastic deposits (Clayton, 1983). Radiometric ages determined during this study (discussed in Chapter 2) confirm the coeval activity of the Devils Washbasin and Tieton Peak volcanoes.

Lava flows or shallow intrusive rocks to the south of Tieton Peak and northeast of Gilbert Peak are heavily altered, commonly bleached or greenish in color, and mineralized with pyrite, suggesting near-vent hydrothermal alteration (Swanson, unpublished). A lava flow that is low in this stratigraphic section, directly overlying Devils Horns rhyolite on the divide between Conrad Creek and South Fork Tieton River, was determined to be ~3 Ma, erupted shortly after emplacement of the rhyolite (see Chapter 2). However, the source of these units (whether also proximal to Tieton Peak, or a different location) and the details of the stratigraphy comprising the Gilbert Peak massif (the summit of which appears from satellite imagery to be part of a plug or coulee erupted near Black Thumb, ~800 ka; Chapter 2) remain poorly defined. Based on the limited fieldwork completed by this author, the bulk of these units are interpreted to be associated with the Tieton Peak eruptive stage, and later capped by an eruption at Black Thumb during the Lake Creek stage; but more work is required in that area.

The Bear Creek Mountain eruptive stage includes the andesitic volcanic products comprising Bear Creek Mountain and extending from there northeastward along the Tieton River valley (the two Tieton Andesite lava flows; Gusey et al., 2018). Bear Creek Mountain is built of two-pyroxene (sometimes olivine-bearing) andesite lava flows and breccias that are crosscut by dikes and plugs (Gusey et al., 2018). The Bear Creek Mountain lava flows are reversely magnetized, and recent age determinations of the Tieton Andesite lava flows confirm emplacement during the Matuyama chron (Hammond, 2017). During this time, basalt and basaltic andesite units were also erupted nearby, from uncertain source(s) but possibly Hogback Mountain (Units Qob_1 and Qob_2 of Hammond, 2017; Gusey et al., 2018; this study).

Following the eruptions of Bear Creek Mountain, the primary locus of Goat Rocks volcanism moved about 12 km west to the Lake Creek Volcano. The location of this volcano can be inferred from the ridge-forming sections of andesitic to dacitic lava flows that dip radially away from the basin of Upper Lake Creek and are cut by a radial array of andesitic to dacitic dikes (map units Qgr_1, Qgr_2, and Qgr_3 of Swanson, 1996b). Paleovalley-filling sections of lava flows can be thicker than 500 m and extend as far as 12 km to the northwest and northeast (Swanson, 1996b, and unpublished). At Hogback Mountain, andesite and dacite lavas of Lake Creek Volcano are intercalated with and capped by basaltic lava flows younger than ~1 Ma (Swanson, unpublished, and this study). The volcanic products of the Lake Creek stage are deeply incised and glacially sculpted at high elevation. Geochronology (discussed in Chapter 2) indicates that the dacite plug or coulée of Black Thumb was also erupted during this stage.

After the Lake Creek stage had waned and a period of deep glacial erosion occurred, volcanism of Old Snowy Mountain stage commenced. The most voluminous eruptions occurred from vents near Old Snowy Mountain and Ives Peak (Swanson and Clayton, 1983; Swanson, unpublished). Other andesitic eruptions occurred at the southern end of Goat Ridge, and from a vent at Coyote Lake that fed the voluminous Clear Fork andesite (Swanson, 1996b; Gapasin et al., 2019). Young andesitic lava flows from minor vents or of uncertain source (e.g. the andesite of Chimney Creek and hornblende andesite described in Old Snowy Mountain quadrangle by Swanson, unpublished) are also tentatively assigned to this youngest eruptive stage, although samples were not dated. Lava flows from Old Snowy Mountain are present low in the valley of Upper Lake Creek, attesting to the deep erosion between the Lake Creek and Old Snowy Mountain stages. Old Snowy Mountain stage lavas are mainly andesite, lesser dacite, and rarely rhyolite. Amphibole is a common component of the typical two-pyroxene mafic assemblage, and in some cases is the dominant mafic mineral.

METHODS

Mapping and Sample Collection

Petrographic descriptions and chemical analyses for 54 Pliocene to Pleistocene volcanic samples were provided by Don Swanson. Swanson collected these and other samples between 1981 and 1996 in Packwood Lake, Old Snowy Mountain, Pinegrass Ridge, and Walupt Lake quadrangles, and mapped these regions with the aid of a portable fluxgate magnetometer.

We revisited in 2015, 2016, and 2017 the areas mapped by Swanson in the above quadrangles and Hamilton Buttes quadrangle. In 2017, we used a portable fluxgate magnetometer (MEDA µMAG-01) at selected outcrops, taking at least three readings per site to confirm whether the rock was magnetically normal or reversed. If the reading induced by the rock was indistinguishable from small movements of the handheld sensor probe during measurement, we assigned an indeterminate magnetic polarity for the outcrop.

We collected a total of 143 rock samples from the Goat Rocks volcanic complex. Thirteen of these samples have been dated by either the $^{40}Ar/^{39}Ar$ or U/Pb methods, and thirty samples have been geochemically analyzed (locations in Tables 1, A2, Figure 2).

Analytical Methods

$^{40}Ar/^{39}Ar$ Geochronology

Samples for $^{40}Ar/^{39}Ar$ dating were prepared and analyzed at the Oregon State University Argon Geochronology Laboratory. Samples were crushed and sieved to 125-355 microns, washed, then passed through a Frantz magnetic separator to isolate groundmass from phenocrysts. All groundmass, plagioclase, and amphibole separates were cleaned by a rigorous acid leaching procedure involving one hour each of 1N HCl, 6N HCl, 1N HNO_3, 3N HNO_3, and triple distilled H_2O. Plagioclase separates were additionally treated with 5% HF for eight minutes to remove adhering glass and/or volcanic matrix, and cleaned with triple distilled water for an additional 1 hour in an ultrasonic bath. High-purity separates were hand-picked under a binocular microscope, with particular attention to removing plagioclase crystals with visible inclusions. Between 10 and 50 mg of each separate were encapsulated in aluminum foil and loaded with the Fish Canyon Tuff sanidine flux monitor (FCT-NM; age

28.201 ± 0.023 Ma (1σ); Kuiper et al., 2008) and vacuum-sealed in quartz vials. Sample heights were determined using a vernier caliper. The samples and flux monitors were irradiated for six hours in three separate irradiations (15-OSU-06, 17-OSU-01, 17-OSU-06) in the CLICIT-position at the TRIGA nuclear reactor at Oregon State University.

The $^{40}Ar/^{39}Ar$ ages were determined by incremental heating using a CO_2 laser and analyzed using a multi-collector ARGUS-VI mass spectrometer at the Argon Geochronology Laboratory at Oregon State University. Ages were calculated using the decay constant of $5.530 \pm 0.097 \times 10^{-10}$ yr^{-1} (2σ) as reported by Min et al. (2000); for other constants refer to Table 2 in Koppers et al. (2003) or Appendix 1. Plateau and isochron ages were calculated as weighted mean ages with $1/\sigma^2$ as the weighting factor (Taylor, 1997) and as YORK2 least-square fits with correlated errors (York, 1969) using the ArArCALC v2.6.2 software from Koppers (2002). All $^{40}Ar/^{39}Ar$ ages are reported at 2σ uncertainty (Table 1, Figure 3, Appendix 1). When the inverse isochron for a sample suggests an initial $^{40}Ar/^{36}Ar$ ratio that is not within 2σ error of the standard value for air (295.5), we use the data-defined $^{40}Ar/^{36}Ar(i)$ value to recalculate the plateau age (propagating the error on the $^{40}Ar/^{36}Ar(i)$ through the calculation). Ages presented here contain between 52% and 96% of the cumulative ^{39}Ar released for a given sample. In this paper, we define a plateau as 3 or more contiguous heating steps that represent at least 50% of the cumulative ^{39}Ar released. Each of our plateau ages has an MSWD below the 95% confidence limit as defined by Mahon (1996), except for one groundmass sample (GR16-12). All plagioclase separates yield age spectra and inverse isochrons that suggest excess argon, probably from microscopic melt inclusions. Plagioclase separates for two samples yield plateau ages within uncertainty of the groundmass plateau or total fusion ages, but plagioclase for three samples (GR15-04, GR16-07, GR16-25) do not yield plateau ages. Pseudo-plateaus (containing 27% to 33% of the ^{39}Ar released) for those plagioclase separates are significantly older than the groundmass ages for those samples and are not considered reliable eruption ages; however, the analytical data for those plagioclase analyses can be found in Appendix 1.

U/Pb Geochronology

Samples for U/Pb dating were crushed and panned under running water to concentrate high-density minerals. The nonmagnetic fraction was recovered from the high-density material via a Frantz magnetic separator and examined under binocular microscope with the aid of polarizing film. Zircons were hand selected, mounted in epoxy and polished, or pressed into an indium metal mount for analysis of surfaces (rims), then imaged using cathodoluminescence (CL) at either the Oregon State University Electron Microscopy

Facility or Stanford University to identify internal zonation, cracks, or inclusions, and to guide in-situ analyses.

Zircon mounts were analyzed using the sensitive high-resolution ion microprobe with reverse geometry (SHRIMP-RG) at the Stanford-USGS MicroAnalysis Center (SUMAC) to obtain U/Pb ages and trace element compositions. The spot size for individual analyses was approximately 25 microns in diameter and 1-2 microns deep, providing the high spatial resolution needed to avoid identifiable cracks as well as apatite and melt inclusions (Schaltegger et al., 2015). On polished mounts, spots were analyzed on individual zircons of variable appearance (size, morphology, CL brightness, zonation pattern), targeting rims, intermediate zones, and cores in efforts to survey the range of ages and compositions present in each sample. For the four samples mounted in indium, spots were analyzed on surfaces of zircons in order to determine the age of the most recent crystallization (e.g. Vazquez and Lidzbarski, 2012; Matthews et al., 2015; Coble et al., 2017).

Calculated model ages for zircon were standardized relative to Temora-2 (416.8 Ma; Black et al., 2004), which was analyzed repeatedly throughout the duration of the analytical sessions. Early-erupted Bishop Tuff zircon (EBT; Crowley et al., 2007) was analyzed as a secondary standard and yielded a weighted mean age of 786 ± 23 ka (see Table A1 for full dataset). This age is within 2σ error of the ID-TIMS age of 767.1 ± 0.9 ka by Crowley et al. (2007) for Bishop Tuff zircon. Samples were corrected for disequilibrium of the ^{230}Th intermediate daughter product using the method of Schärer (1984) and initial $^{232}Th/^{238}U_{melt}$ values based on new U and Th concentrations measured by ICP-MS (samples GR16-30 and GR16-38) or estimated at 3.0 for all other samples not yet analyzed for bulk composition. $^{238}U/^{206}Pb$ dates were corrected for common Pb using measured $^{207}Pb/^{206}Pb$ (Ireland and Williams, 2003) and assuming a $^{207}Pb/^{206}Pb_{common}$ value from Stacey and Kramers (1975). Zircon trace element concentrations were standardized relative to sample MAD-559 (U = 3435 ppm), a homogeneous in-house zircon standard calibrated relative to MAD-green (Barth and Wooden, 2010). Individual spot ages are reported at 1σ analytical error. The youngest zircon crystallization age for each sample is interpreted as either: 1) weighted mean and 2σ standard error of interiors of compositionally and texturally similar crystals, for samples only in polished mounts, 2) weighted mean and 2σ standard error of crystal surfaces which define a coherent population, or 3) weighted mean and 2σ standard error of both interior ages and surface ages, when these individual ages overlap within 2σ uncertainty.

Bulk XRF and ICP-MS Geochemistry

Samples collected in 2015 (prefix GR15) and 2016 (GR16) were prepared and analyzed via XRF and ICP-MS at the Peter Hooper GeoAnalytical Lab at Washington State University. Samples for XRF analyses were prepared following the procedures of Johnson et al. (1999). The accuracy and precision of the major element XRF analyses are as described in Johnson et al. (1999), with modifications summarized by Kelly (2016). Improved accuracy of Zr and Cr for samples analyzed since 2004 and 2007, respectively, is described by Sawlan et al. (2018).

Uncertainty for each XRF elemental analysis is based on the relative percent absolute difference (RPAD; eq.1) in the measured concentration of an element for two aliquots of the same sample (Kelly, 2016).

$$RPAD = \left|(Aliquot\ 1 - Aliquot\ 2) \div \frac{(Aliquot\ 1 + Aliquot\ 2)}{2}\right| * 100 \qquad (1)$$

The mean RPAD value for each element, used here as a measure of uncertainty (Table 2), combines RPAD values determined from over 250 samples and their repeat analyses (Kelly, 2016). Samples for ICP-MS were prepared and analyzed following procedures noted on the WSU lab website (Peter Hooper GeoAnalytical Lab, "ICP-MS Method," https://environment.wsu.edu/facilities/geoanalytical-lab/technical-notes/icp-ms-method/) and modified by Steenberg et al. (2017). Based on ~100 ICP-MS analyses of several certified reference materials (CRMs), Steenberg et al. (2017) determined average relative percent differences from GeoReM accepted values that range from 6.32% (Ho) to 1.66% (Ba), with an average of 3.37%. Samples collected by Swanson were analyzed at the USGS lab in Lakewood, Colorado or in 1996 at Washington State University.

RESULTS

Geochronology

Eruption and shallow intrusion of andesite and dacite lavas persisted at Goat Rocks for 2.5 to 2.9 million years (from between 3.0-2.6 Ma to 0.1 Ma; Figure 5), based on a combination of new $^{40}Ar/^{39}Ar$ ages and U/Pb ages for thirteen samples and ten previous ages (Table 1), in concert with field relations and magnetic polarity measurements. The new ages constrain the Devils Washbasin basalt, Lost Lake andesite, andesites and dacites from Lake Creek volcano, Black Thumb dacite, Old Snowy Mountain andesites, Goat Ridge rhyolite, and Clear Fork andesite (see Table 1 and Figure 2 for sample locations). Previous ages (K/Ar, zircon fission-track, and $^{40}Ar/^{39}Ar$) are of the Devils Horns rhyolite, Devils Washbasin basalt, a dacite tuff along Miriam Creek, Tieton andesite, Hogback Mountain basalt, and the Cispus Pass pluton (Table 1).

Tieton Peak to Bear Creek Mountain Stage

Two samples have ages that predate the Lake Creek stage. Sample GR16-07, collected from a basaltic lava flow northeast of Bear Creek Mountain, is from the Devils Washbasin volcano (Gusey et al., this volume). Groundmass from this sample yielded a $^{40}Ar/^{39}Ar$ plateau age of 2.68 ± 0.01 Ma (Figure 3a), which we interpret as the eruption age for this lava flow. No absolute ages have been determined for the lava flows (or shallow intrusions) of Tieton Peak, but these rocks are normally-magnetized like the Devils Washbasin basalts (Clayton, 1983; Swanson, unpublished). Based on the magnetization, the possible intercalation of the Tieton Peak and Devils Washbasin lavas (Clayton, 1983), and the basalt groundmass age, we tentatively assign the duration of Tieton Peak stage to within the normal subchron between 3.04 and 2.58 Ma at the end of the Gauss chron (Cande and Kent, 1995; Figure 5).

Sample GR16-12, collected near Lost Lake, is the oldest andesite dated in this study. We take the eruption age to be 2.27 ± 0.01 Ma based on the groundmass plateau age (Figure 3b), which is within error of the groundmass total fusion age (2.25 ± 0.01 Ma, Appendix 1) and the plagioclase plateau age of 2.29 ± 0.01 Ma (Figure 3c). Both the groundmass and plagioclase separates have age spectra that are discordant: the groundmass indicates slight ^{39}Ar recoil, and the plagioclase has a climbing age spectrum indicating slight excess argon. Although the groundmass plateau age has a higher MSWD than the 95% confidence limit for a homogeneous population (Mahon, 1996), we prefer it to the total fusion age which includes anomalously young steps at high temperature (Figure 3b). This lava flow was measured to have reversed magnetic polarity and was originally mapped as unit Qgr_2 from Lake Creek volcano, given its proximity to that eruptive center (Swanson, 1996b), but it is older than Qgr_1 and Qgr_2 lavas that we analyzed. We arbitrarily include the andesite near Lost Lake with the Bear Creek Mountain stage on composition diagrams, but its eruptive stage remains undefined.

Lake Creek Stage

Ages for each of the Lake Creek volcano map units (one sample from Qgr_1, four from Qgr_2, and one from Qgr_3) indicate that Lake Creek volcano was active from at least 1.1 to 0.6 Ma. In addition, the dacite of Black Thumb erupted at about 0.8 Ma, and therefore we include it with the Lake Creek stage. Three of these samples yield ages that appear to record brief magnetic excursions during the late Matuyama and Brunhes chrons. We retain the map units as assigned by Swanson and further supported by our field magnetometer measurements, and rely on the $^{40}Ar/^{39}Ar$ and U/Pb ages for age constraints.

The lowest lava flow in the Lake Creek sequence southeast of Goat Lake (sample GR16-36) marks the base of the normally-magnetized unit Qgr_1 (Figure 2; Swanson, 1996b). We take the eruption age to be 1.11 ± 0.01 Ma based on the groundmass total fusion age (Figure 3d, Figure 5, Table 1). This age corresponds to the Punaruu normal magnetic excursion during late Matuyama chron (1.12 Ma, Channell et al., 2002). Plagioclase from the same sample yielded a plateau age of 1.13 ± 0.01 Ma and contains slight excess argon. Nevertheless, the plagioclase plateau age is within error of the groundmass total fusion age (Figure 3e). Our U/Pb age for this sample is based on 12 spots analyzed on polished interiors of zircons (Figure 4a). The youngest spot analysis was excluded from the weighted mean because it has high common Pb (29%) and does not overlap with others at 1σ error. The youngest population of eight spots overlapping at 1σ error yields a weighted mean age (weighting by 1σ spot error) of 1.11 ± 0.03 Ma, which is within error of the $^{40}Ar/^{39}Ar$ groundmass total fusion age.

Zircon from sample GR16-30, collected from a dacite lava flow near the base of magnetically reversed unit Qgr_2 (Figure 2), yielded a U/Pb age of 987 ± 57 ka from ten spots analyzed on polished interiors (Figure 4b). The oldest spot age overlaps at 1σ error with younger spot ages, but we exclude it from the weighted mean because it is an outlier in composition (Th, U, and Y concentrations are more than double those of the main population; Table A1). The zircon crystallization age of this sample, considered to be a maximum estimate for eruption age, is within the magnetically reversed period from 988 to 925 ka (Horng et al., 2002).

The andesite lava flow capping Hawkeye Point (sample GR16-34) is mid-section in the reversely magnetized unit Qgr_2. Our $^{40}Ar/^{39}Ar$ age determination for a groundmass separate yielded a plateau age of 820 ± 3 ka (Figure 3f), which we consider the eruption age for this lava flow. Spot analyses from polished zircons yield a weighted mean age of 920 ± 33 ka (MSWD=2.5) including all 10 grains analyzed. This MSWD is larger than expected for a homogeneous population (e.g., Mahon, 1996), thus we prefer a weighted mean of the youngest six spots, 874 ± 30 ka (MSWD=1.3) as the zircon crystallization age (Figure 4c). Each of these ages is within the magnetically reversed period from 920 to 781 ka (Horng et al., 2002). We prefer the younger and more precise groundmass plateau age as the best estimate for the eruption age. The difference between the zircon age(s) and groundmass age suggests a protracted period of zircon crystallization prior to eruption, possibly in magma reservoirs that fed previous eruptions from Lake Creek volcano.

The U/Pb age of 817 ± 24 ka for Black Thumb dacite (sample GR16-47A, Figure 4d) indicates that this vent was active at the same time as Lake Creek volcano. This age is a weighted mean of spot analyses on both polished interiors and surfaces of zircons. Polished interiors alone yield an age of 822 ± 27 ka (MSWD=0.60), excluding one resorbed-looking core that is slightly older than the weighted mean age at the 1σ level. Seven spots on surfaces yield an age of 837 ± 40 ka (MSWD=2.2), excluding two outliers that are also interpreted to be inherited crystals (Figure 4d). Since the mean surface age and mean interior age overlap at 2σ error, we calculate a weighted mean of all spots included in those ages, 817 ± 24 ka (MSWD=0.67; Figure 4d). Importantly, this age confirms that Black Thumb was not the source of the >1.3 Ma Tieton andesite flows (Table 1, Figure 5), as Gusey et al. (this volume) determined by comparing their bulk compositions.

An andesite lava flow (sample GR17-72A) within the upper normally magnetized unit Qgr_3 from Lake Creek volcano yielded a U/Pb age of 742 ± 17 ka from polished interiors of zircons. The age is a weighted mean of 11 spot ages overlapping at the 1σ level; three older crystals were excluded (Figure 4e). The age matches the normal magnetic polarity for this eruptive unit as determined by Swanson (1996b; Figure 5).

In accord with Swanson's (1996b) mapping as unit Qgr_2, we measured reversed magnetic polarity for the dacitic dike from which sample GR17-75 was collected (this sample is equivalent to GR15-02, Table 2). Surfaces of 9 (out of 10) zircon crystals analyzed yield a weighted mean age of 600 ± 29 ka, which we take as the best estimate for the emplacement age for this dike (Figure 4f). The one older surface spot age was interpreted as antecrystic and excluded from this mean. The mean surface age is within error of two brief magnetic excursions during the early Brunhes chron: Big Lost (or stage 15a), recorded at 560-580 ka (575 ka), and stage 15b, at 605 ka (Laj and Channell, 2007; Lund et al., 2006). Ten polished crystal interiors yield 9 spot ages overlapping at the 1σ level and one outlier (Figure 4f). The weighted mean of these 9 spot ages is 679 ± 20 ka and is significantly older than the surface age, suggesting residence of crystallizing zircons of several tens of thousands of years. Sample GR15-04 is from a magnetically-reversed dacitic lava flow also from map unit Qgr_2. Groundmass from this sample yielded a plateau age of 593 ± 4 ka (Figure 3g), which we take as the best estimate of the eruption age of this lava flow. This age is between, but close to, the reported ages for the Big Lost and stage 15b excursions (see above). An amphibole separate yields a plateau age of 626 ± 77 ka (Figure 3h), within error of the groundmass age.

Old Snowy Mountain Stage

We determined ages for two samples from Old Snowy Mountain, one sample from Goat Ridge, and one sample of the Clear Fork andesite. Lavas from Old Snowy Mountain erupted from ~440 ka to <217 ka, broadly coeval with those at Goat Ridge, where a rhyolite low in the section yields an age of ~443 ka. Clear Fork andesite, at ~107 ka, is the youngest lava flow yet dated in the Goat Rocks volcanic complex.

Sample GR16-38 of Old Snowy Mountain andesite is low in the Old Snowy Mountain eruptive sequence, overlying Tertiary volcanic rock on the saddle east of Goat Lake (map number 67, Figure 2). The eruption age is based on a groundmass separate that yielded a plateau age of 440 ± 3 ka, based on higher temperature heating steps, despite slight ^{39}Ar recoil (Figure 3i). Polished interiors of 17 zircon crystals yielded a complex range of ages. The weighted mean age of the youngest nine crystals is 453 ± 8 ka (Figure 4g). While the MSWD for this age (7.22) is much higher than expected for a homogeneous population (Mahon, 1996), it is challenging to isolate a smaller coherent population via composition or crystal appearance, given the relatively small number of grains analyzed. We therefore consider the zircon age to represent a complex and extended period(s) of pre-eruptive crystallization, and prefer the groundmass ^{40}Ar/^{39}Ar plateau age as a better estimate for the eruption age.

For a dacitic lava flow higher in the Old Snowy Mountain section (sample GR16-25), the groundmass yielded a ^{40}Ar/^{39}Ar plateau age of 217 ± 5 ka, which we assign as the eruption age for this lava flow (Figure 3j).

Sample GR17-71 is from a rhyolite lava flow exposed in a creek drainage about 2 km west of the southern extent of Goat Ridge (map number 86, Figure 2). This sample yields a U/Pb age of 443 ± 10 ka, which overlaps with early activity at Old Snowy Mountain (Figures 4h, 5). Spot analyses on polished interiors of zircons from this sample define two compositional populations (a low-Y population with [Y] 359-1817 ppm, and a high-Y population with [Y] 2424-5655 ppm; Table A1), plus one older outlier (Figure 4h). The weighted mean age of the younger, low-Y population (n=5) is 446 ± 13 ka (MSWD=0.94). Four crystal surfaces group with the low-Y interior spots. The weighted mean of the surface spot ages is 438 ± 16 ka (MSWD=1.7). Since the low-Y interior mean age and surface mean age overlap at 2σ standard error, we prefer a combined mean age using all of the spots included in those two ages, 443 ± 10 ka.

At 107 ± 5 ka, the Clear Fork andesite (sample GR17-78; unit Qacf, Figure 2) is the youngest at Goat Rocks to be dated thus far, while also bearing the longest record of zircon crystallization. The U/Pb age we determined is a weighted mean of spots from both interiors and surfaces of zircons. The youngest spot ages approach the limit of the resolution of U/Pb geochronology, so more scatter can be expected due to poor counting statistics on ^{206}Pb. Crystal interiors yielded a wide range of ages from 30 ka to 177 Ma, indicating many xenocrystic populations (see Table A1 for full dataset). Five of the seven analyses from zircon interiors have a weighted mean age of 104 ± 6 ka (MSWD=1.8). We exclude the youngest two analyses in the population because they have high common Pb and are likely inaccurate. The youngest four of six surface analyses all contain high common Pb and are overall less precise, but yield a weighted mean age of 118 ± 13 ka (MSWD=2.4) that overlaps with the age from interiors. We therefore prefer a weighted mean age of 107 ± 5 ka including spot analyses from both surfaces and interiors (Figure 4i). This age is younger than MIS stage 6 (Figure 5; Lisiecki and Raymo, 2005), which may correlate with the Hayden Creek glaciation (Evarts, 2005), supporting Swanson's (1996b) interpretation that the Clear Fork andesite erupted after that glacial event.

Rock Compositions

The suite of Pliocene to Pleistocene volcanic rocks at Goat Rocks is dominantly andesites and dacites, with sparse rhyolites only in the early and late stages (Table 2, Figure 6). A paucity of samples between 55 and 58 weight percent SiO_2 separates the intermediate suite from contemporaneous basalts and basaltic andesites. These mafic samples fall within the field of mafic volcanic rocks in the southern Washington Cascades, but do not extend to highly alkaline compositions (Figure 7a). As a whole, the Goat Rocks andesite to rhyolite suite ranges from medium- to high-K character, overlapping and spanning beyond the entire range of composition at neighboring arc volcanoes (Figures 7a, 8). Two temporal patterns emerge. First, there is a general decrease in potassium in time, with highest K_2O in the Tieton Peak and Bear Creek Mountain stages, comparable to the high-K suite of Mount Adams, and lowest K_2O in the Old Snowy Mountain suite, overlapping with the suite of Mount St. Helens (Figures 7a, 8). We note that high-K compositions manifest at greater than ~59 weight percent SiO_2. The temporal potassium pattern at Goat Rocks mimics the spatial, trench-ward decrease in potassium in the arc, along with parallel declining Y, Zr, Rb, and increasing Sr/Y (Figure 9). The second temporal pattern is compositional restriction in the middle two stages compared to early and late stages, mainly owing to the absence of rhyolite. While we believe regional sampling has captured the variability of volcanic rocks, the number sampled is not a reliable proxy for relative volumes of the different stages.

The **Tieton Peak stage** has a wide range in bulk composition, but andesites dominate (Figures 6,8). K_2O, Zr, and Y values reach their highest during this stage in comparison to later stages (Figure 7a, 9c,d) and concentrations of CaO, MgO, and particularly TiO_2 are generally lower at a given weight percent SiO_2.

During the **Bear Creek Mountain stage**, the range in composition is restricted to mainly silicic andesite (Figures 6, 8c). Andesites of Bear Creek Mountain stage have the highest K_2O of the Goat Rocks suite, and for other elements, define an upper or lower limit to the range of andesites (e.g. lowest Al_2O_3, FeO*/MgO; highest TiO_2, MgO, Rb, Zr; Figures 7, 8, 9).

The **Lake Creek stage** is the most voluminous and most compositions are between 60 and 68 weight percent SiO_2, with scarce basaltic andesite (Figures 6, 8). This stage has the greatest range in incompatible elements (e.g., Zr, Rb, U, and Y; Figure 9) among andesites and dacites and makes a compositional bridge between potassic compositions of Bear Creek Mountain andesites and late, low-K compositions of the Old Snowy Mountain stage.

The **Old Snowy Mountain stage** is broad in composition (57 to 75 weight percent SiO_2; Figures 6) and has two compositional modes, one at ~60-61 weight percent SiO_2 and one at ~67 weight percent SiO_2 (Figure 8a). Andesites and dacites of Old Snowy Mountain stage differ from their predecessors not only in lower K_2O, Zr and Y, but also in higher concentrations of Al_2O_3 and Sr, resulting in high Sr/Y, one of the adakitic signatures defined by Defant and Drummond (1993) (Figures 7, 8, 9).

DISCUSSION

The Goat Rocks volcanic complex provides new perspective into the timing of volcanism within the central Cascade arc. Below we discuss how our new $^{40}Ar/^{39}Ar$ and U/Pb ages refine both the eruptive timeline at Goat Rocks as well as the magnetic polarity timescale recorded by its lavas. We then consider the size, longevity, and compositional variation at Goat Rocks and compare these to neighboring Cascade volcanoes.

Integrating Magnetostratigraphy and Geochronology

Prior to this study, the chronology of the Goat Rocks volcanic complex was primarily based on magnetostratigraphy and calibrated with a handful of K-Ar, $^{40}Ar/^{39}Ar$, and zircon fission-track ages. While the overall chronology of eruptive stages has largely held true, our new ages refine these stages and reveal additional complexity in the Lake Creek volcanic sequence.

New ages indicate that the Lake Creek eruptive sequence captures multiple magnetic polarity subchrons and excursions during the late Matuyama to early Brunhes chrons. For example, early Qgr_1 lava sample GR16-36 (normally magnetized) has a groundmass age of 1.11 ± 0.1 Ma, within uncertainty of the Punaruu normal excursion reported by previous authors (1.105 Ma, Singer et al., 1999; 1.115 Ma, Channel et al., 2002; 1.075 ± 0.032 Ma, Ownby et al., 2007; 1.095 ± 0.210, Michalk et al., 2013). The interval of time between this early Qgr_1 lava and early Qgr_2 lava (reversed, e.g. GR16-30, 987 ± 57 ka) also includes the Jaramillo normal subchron (Figure 5). It is possible that all of the normally-magnetized Qgr_1 lava flows were erupted during the brief ~5000 year Punaruu excursion, or that eruptions continued over tens of thousands of years into the Jaramillo subchron; further work is required to constrain the ages of younger Qgr_1 lavas. In addition, lavas from map unit Qgr_2 are from multiple reversed periods, and show that magnetic polarity alone cannot resolve age relationships where exposures are discontinuous or there are cryptic unconformities. Two Qgr_2 samples date to late Matuyama chron (GR16-30 and -34), while two (GR17-75, 600 ± 29 ka, and GR15-04, 593 ± 4 ka) were erupted during a brief excursion in early Brunhes chron (variable ages of potentially multiple excursions reported by Lund et al., 2006; Laj and Channell, 2007; Singer et al., 2008; Michalk et al., 2013), making them younger than a Qgr_3 lava flow that we dated (Table 1, Figure 5). Full reconstruction of the growth of Lake Creek volcano awaits further chronologic calibration of more detailed magnetostratigraphy.

Volcano Size and Volume

Extensive erosion makes it difficult to estimate the dimensions of the Goat Rocks volcanic complex during its construction. Clayton (1983) inferred that >60 km^3 of dominantly pyroxene andesite lava flows were erupted from a central volcanic edifice. Hildreth (2007) estimates 40 km^3 for the eroded remnants of the Goat Rocks. We estimate a total erupted volume between 90-100 km^3 for the entire Goat Rocks volcanic complex, as follows.
The Lake Creek stage was the most voluminous and has a volcanic apron with a radius of at least 12 km from the inferred vent in the present-day valley of Upper Lake Creek. The radii of lava aprons around Mount Hood, Mount Adams, and Mount Rainier are slightly larger at approximately 14, 18, and 14 km, respectively, while the respective relief of their central peaks is 1800, 2300, and 2100 m above basement (Hildreth, 2007; Figure 10). The ratio of relief to radius at these centers ranges from 0.13 to 0.15; applying these ratios to the lava radius at Goat Rocks (12 km) gives a range of 1500 to 1800 m relief. We make a conservative estimate of 1500 m for the full height of the Lake Creek volcano edifice above basement (Figure 10). This relief is in keeping with the average relief of ~1565 m for 10 major Cascade

andesitic volcanoes, excluding dome complexes and deeply glaciated or eroded centers (Table 2 in Hildreth, 2007). Similarly, the average relief of Andean arc volcanoes in the Southern Volcanic Zone is ~1625 m, independent of considerable variation in crustal thickness (Hildreth and Moorbath, 1988).

We estimate the volume of the Lake Creek volcano at ~60 km^3 by adding the volume of a central cone to that of a surrounding hollow disc. The inner 5-km-radius portion of the edifice can be approximated by a cone of height 1500 m and volume 40 km^3 (Figure 10). The remaining volume of the lava apron is difficult to estimate: while preserved exposures of lava flows are as thick as 500 km in paleodrainages (Swanson, 1996b), this thickness is neither radially nor concentrically continuous. Estimating a distributed thickness of 50 m over the remaining hollow disc that extends to the 12 km radius, we calculate an additional ~20 km^3 of lava and other ejecta for a total of ~60 km^3. For comparison, the erupted volume of Mount Hood is estimated at 50 to 100 km^3 (Hildreth, 2007). If the other major andesitic vents (Tieton Peak, Bear Creek Mountain, Old Snowy Mountain) each contributed 10 to 15 km^3 (the Tieton andesite flows from Bear Creek Mountain add to ~9 km^3; Gusey et al., this volume), the Goat Rocks volcanic complex as a whole could exceed 90 km^3 erupted volume.

Persistence of Andesite in the Cascade Arc

The lifespan of andesitic volcanism at Goat Rocks is 2.5 to 2.9 Myr, based on the magnetic correlation and possible intercalation of the oldest Tieton Peak stage andesite lavas with 2.7-Ma Devils Washbasin basalt. Eruptions of the subsequent Bear Creek Mountain stage occurred a few km to the east and lasted at least 300,000 years, from >1.6 to 1.3 Ma. The Lake Creek stage lasted about 500,000 years, from 1.1 Ma to ~600 ka, during which the Lake Creek volcano was constructed from an inferred center near Upper Lake Creek. This stage marks a ~9 km westward shift of the andesite focus. The youngest stage, Old Snowy Mountain stage, lasted approximately 330,000 years from ~440 ka to 107 ka from regionally distributed vents.

Similarly persistent andesitic volcanism as at Goat Rocks occurred in the Mount Hood area. There, andesitic volcanism is as old as 3.1 ± 0.2 Ma at Lookout Mountain, which is ~14 km to the east of Mount Hood (Wise, 1969; Sherrod and Scott, 1995). The Vista Ridge cone and Sandy Glacier volcano were active between 1.5 and 0.8 Ma and lie under and slightly west of Mount Hood, respectively. The modern edifice has been active since ~500 ka (Scott et al., 1997; Scott and Gardner, 2017).

Andesitic volcanism near Mount Rainier has persisted for at least ~1.4 Ma. Possibly juvenile clasts in the Lily Creek formation have been dated at 1.36 ± 0.05 Ma and 1.16 ± 0.05

Ma (2σ uncertainty; plagioclase $^{40}Ar/^{39}Ar$ ages), and exposures at Panhandle Gap and Glacier Basin have been dated at 1.06 ± 0.05 Ma and 1.03 ± 0.00 Ma (groundmass $^{40}Ar/^{39}Ar$ ages), indicating that a previous edifice was active between ~1.4 and 1.0 Ma (Sisson and Calvert, written communication). It is unknown whether activity continued between 1.0 Ma and the growth of the modern Rainier edifice, where activity had commenced by 0.6 Ma, based on two widely separated lavas dated at 601 ± 16 ka and 596 ± 4 ka (groundmass $^{40}Ar/^{39}Ar$ ages; Sisson and Calvert, written communication). Frequent voluminous eruptions, with major pulses from 500 to 420 ka and from 280 to 180 ka, built the present-day edifice (Sisson et al., 2001).

In the vicinity of Mount Adams, basaltic eruptions have occurred in a broad volcanic field since ~940 ka (Hildreth and Lanphere, 1994; Hildreth and Fierstein, 1995, 1997). The andesitic Hellroaring volcano was active from ~520 ka to 450 ka, when the eruptive center shifted ~5 km northwest to the modern Mount Adams vent (ibid.). Like Mount Rainier, the Hellroaring volcano-Mount Adams edifice was built fitfully in major cone-building episodes centered at ~500 ka, ~450 ka, and 30 ka, separated by lesser activity (Hildreth and Lanphere, 1994).

To the southwest of Goat Rocks, Mount St. Helens grew in stages a few tens to 100 kyr long resulting in a total volcanic history of ~300 kyr, but ages of entrained zircons suggest that intermediate magmatism was active for as long as 500-600 kyr (Clynne et al., 2008; Claiborne et al., 2010). The modern stratocone was built only in the last 2.5 kyr (Mullineaux and Crandell, 1981).

The record of andesite activity at Goat Rocks is comparable to Mount Hood and longer than at other neighboring centers (Figure 11). Lake Creek and Old Snowy Mountain stages together represent a nearly continuous period of eruptive activity lasting 1 million years, comparable to the 0.7 Myr period of activity at Vista Ridge and Sandy Glacier volcanoes (Mount Hood predecessors). If the long life span of the Goat Rocks volcanic complex is an analog, then one might expect Mount Hood to be near the end of its life and that the other neighboring centers can expect another 0.5 to 1.5 Myr of activity.

A picture emerges in which at ~2.5 Ma, Tieton Peak and Lookout Mountain (Mount Hood area) dominated the arc at these latitudes. At ~1.5 Ma, proto-Mount Rainier, Bear Creek Mountain, and Vista Ridge and/or Sandy Glacier volcanoes were active. Flare-ups at Mount Rainier and Mount Adams at ~500 ka coincide with the onset of the modern cone at Mount Hood and with the end of the productive Lake Creek volcano. Less voluminous, more distributed activity at Goat Rocks followed Lake Creek volcano during Old Snowy Mountain stage. Mount St. Helens emerged during this final Goat Rocks stage and became increasingly productive as activity at Goat Rocks ended. In summary, the Goat Rocks volcanic complex further illuminates an arc-wide history of waxing and waning of andesitic arc volcanoes, which invites speculation about the distribution of energy delivered from the mantle to the crust at subduction zones.

Geochemical Variations through Time

The Goat Rocks volcanic complex has a wide range of compositions and is an excellent case for grappling with the complex processes that produce andesitic arc volcanoes. Abundant quenched inclusions of variably more mafic magmas, large ranges in composition at similar silica, and diverse populations of zircons attest to a complex magmatic history typical of arc volcanoes. While a comprehensive petrologic treatment awaits fuller characterization of the suite, we point out some major patterns and their implications. We first address variability within the Goat Rocks suite, then consider the temporal pattern of larger compositional variability in early and late stages compared to in the middle two stages. Finally, we compare the temporal pattern toward less potassic, adakite-like compositions to across-arc variations.

Stages of the Goat Rocks Volcanic Complex

The Tieton Peak stage has high-K silicic compositions, moderate-K mafic compositions, and an array of varied-K intermediate compositions (Figures 7,8). Lower Ti in the mafic compositions compared to the rest of the Goat Rocks suite suggests a different mantle contribution for this part of the suite (Figure 9). The high variability of potassium amongst andesites, without a high-K mafic parent, implies that the high-K signature is crustally derived.

The Bear Creek Mountain stage produced tightly clustered andesites that are as potassic as the high-K andesites of Tieton Peak stage, but differ from those in having higher Ti and lower Sr (Figures 7, 8, 9), thus putting them on a different liquid line of descent more akin to highest-K andesites of the Lake Creek stage. Andesites and dacites of the Bear Creek Mountain and Lake Creek stages are tightly clustered along similar major element trends. Declining CaO, Al_2O_3, and Sr, with silica (Figure 7b,e, Figure 9b) signal plagioclase-dominated fractionation. On the other hand, strong scatter with respect to incompatible elements including K and Rb indicates a complex of processes, likely variable proportions of crystal fractionation, magma mixing, and crustal assimilation, to be unraveled in future work. The Lake Creek stage also includes compositions with lower K_2O, transitional to the Old Snowy Mountain stage. No rhyolites were erupted during these middle two stages.

The Old Snowy Mountain stage is distinct from the middle stages in having a wide compositional spread and the most linear distribution of data among the four stages on both major and trace element variation diagrams (Figures 7, 9). The linear trends suggest a dominance of magma mixing between mafic andesite and a rhyolitic composition similar to that of Devils Horns. Higher Al_2O_3 among mafic andesites indicates suppression of plagioclase in their derivation, likely owing to deeper and (or) wetter conditions, consistent with more phenocrystic amphibole in this suite. While most of the data fall along a moderate K-enrichment with silica, overlapping the field of Mount Rainier, a smattering of samples define a separate trend similar to the relatively K-poor andesites and dacites of Mount St. Helens.

Compositional Range in Time

Volcanism at Goat Rocks is strongly dominated by silicic andesite and dacite, especially in the middle eruptive stages, but varies from basaltic andesite to rhyolite in early and late stages (Figure 7). The pattern invites comparison to other long-lived intermediate suites where volcanism exhibits a middle period of restricted composition that also corresponds to the largest erupted volume (e.g. Aucanquilcha Volcanic Cluster and other examples, Grunder et al., 2006; Yanacocha Volcanics, Longo et al., 2010; eastern Great Basin, Gans et al., 1989; Mount Jefferson volcanic field, Conrey et al., 2001, and DiGiulio, 2016). We postulate that the more homogenous phase represents a time when the magmatic underpinnings of the complex were well established and created an extensive mushy zone in the crust where rising more mafic magmas were trapped and hybridized (e.g. Aucanquilcha Volcanic Cluster, Walker et al., 2012) and rhyolitic crustal melts effectively assimilated. Basaltic magmas can ascend and erupt before and after the creation of the mushy crustal magma complex, or they may penetrate along the margins (the shadow zone effect, e.g. Walker, 2000).

Adakitic Signature in Time Versus Space

The Old Snowy Mountain stage has the highest Sr/Y of the Goat Rocks suite, an adakitic indicator defined by Defant and Drummond (1993; Figure 9f). Such an adakitic signature can be acquired by melting of the slab, which is appealing for the young hot slab beneath Cascadia. Although we cannot at this point exclude mantle-hosted influence, the temporal context for the adakitic signature in the last stage of a protracted andesitic history suggests that the adakitic character is derived during crustal residence. Smith and Leeman (1987) argue that the adakitic character of Mount St. Helens dacite reflects deep amphibolite-derived crustal magma sources. Contribution of deep, young mafic sources has been supported by Os isotopic studies of Mount Adams (Jicha et al., 2009). In an analysis of across-arc increases in K_2O in the central Andes, Michelfelder et al. (2013) propose amphibolitic crustal influence for less potassic arc-front volcanoes and the influence of increasingly felsic crust with distance from the arc to produce more potassic suites. In any case, at Goat Rocks, the temporal compositional changes within a relatively confined area mimic the trans-arc variability in southern Washington, and can serve as a test for the significance of these spatial variations.

CONCLUSION

The Goat Rocks volcanic complex is a long-lived Pliocene to Pleistocene andesitic locus in the southern Washington Cascades. Goat Rocks was active over a period of about 2.5 to 2.9 million years, from at least 2.6 Ma (and possibly as long ago as 3.0 Ma), to ~100 ka. Activity at Goat Rocks occurred in four stages from vents within an ellipsoidal area of ~200 km^2, surrounded by contemporaneous mafic vents.

1. Tieton Peak stage (tentatively 3.0 to 2.6 Ma) marks the onset of activity at Goat Rocks. Volcanism was centered at Tieton Peak near the margin of, and over, the 3.2 Ma Devils Horns rhyolite caldera. The compositional range is broad, ranging from basaltic andesite to rhyolite.
2. During Bear Creek Mountain stage (>1.6 to 1.3 Ma), eruptions occurred at Bear Creek Mountain and include the Tieton andesite lavas that flowed as far as 74 km down paleovalleys to the east (Gusey et al., 2018, this volume). In contrast to Tieton Peak stage, compositions are restricted to high-K andesites.
3. During Lake Creek stage (1.1 to 0.6 Ma), a ~3500-m high, ~60 km^3 andesite-dacite composite cone was constructed at what is now the Upper Lake Creek basin. Andesite and dacite lavas extended to a radius of at least 12 km. This was the most voluminous, climactic stage at Goat Rocks, dominated by compositionally variable andesites and dacites.
4. Old Snowy Mountain stage (0.4 to 0.1 Ma) included eruptions at Old Snowy Mountain and from distributed vents across the Goat Rocks area. This suite marks the waning of volcanism at Goat Rocks and includes diverse compositions from basaltic andesite to rhyolite.

Early in the Goat Rocks eruptive history, the main andesitic volcanoes in this region of the Cascade arc were Tieton Peak and proto-Mount Hood. At the time of Bear Creek Mountain to

Lake Creek volcano, Mount Rainier and Mount Adams emerged. With the growth of Mount St. Helens, activity at Goat Rocks waned and ceased.

Volcanic rock compositions of the Goat Rocks suite are less potassic with time: Tieton Peak through Lake Creek stages generally constitute a high-K suite, while vents of Old Snowy Mountain stage erupted medium-K compositions. Magmas of the Old Snowy Mountain stage were more water-rich as indicated by higher Al_2O_3 compositions and a prevalence of amphibole. The compositional changes through time at Goat Rocks mimic compositional diversity across the Cascade arc: earlier magmas are more Mount Adams-like, while some Old Snowy Mountain stage magmas are similar to Mount St. Helens compositions. We attribute the change to a more adakitic character to the influences of more mafic crust and more water in differentiation.

FIGURES

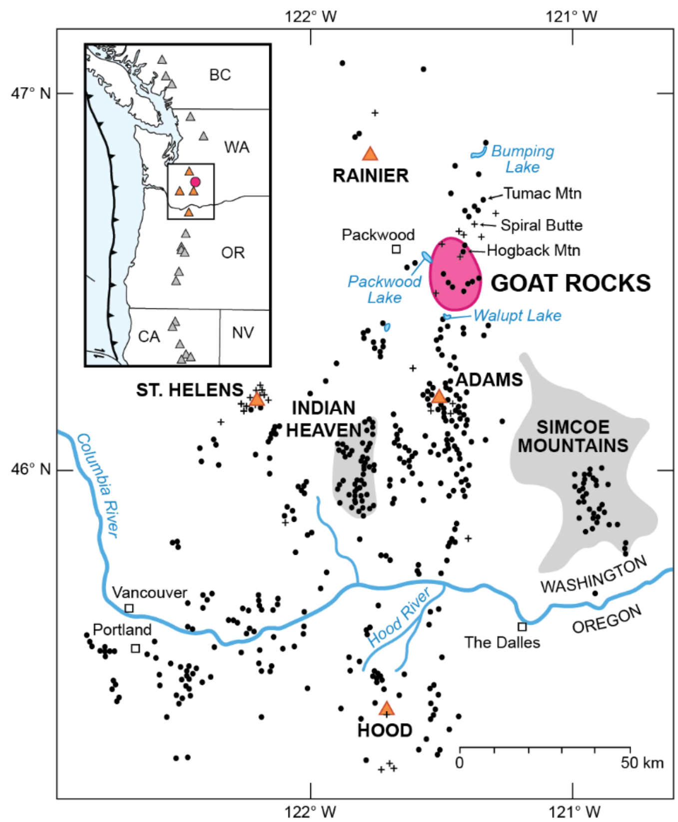

Figure 1.1. Map of the Mount Rainier to Mount Hood region of the Cascade arc. Inset shows location in the Cascade arc, which spans from British Columbia to California. Orange triangles are major Quaternary composite volcanoes Mount Rainier, Mount Adams, Mount St. Helens, and Mount Hood. The areal extent (andesitic footprint) of the Goat Rocks volcanic complex (including all Pliocene to Pleistocene andesite-dacite vents) is shown by the pink field (pink circle on inset map). Gray triangles on inset map are other major Quaternary edifi ces after Hildreth (2007). Gray fi elds show extent of distributed Indian Heaven and Simcoe Mountains mafi c fi elds. Black dots are locations of Quaternary basaltic to andesitic vents; crosses are dacitic to rhyolitic vents. The Goat Rocks fi eld includes two extinct Pliocene vents at Tieton Peak and Devils Washbasin. Figure is modifi ed from Hildreth (2007) with updated locations of vents in Goat Rocks volcanic complex. BC—British Columbia, WA—Washington, OR—Oregon, CA—California, NV—Nevada.

Figure 1.2. Generalized geologic map of the Goat Rocks volcanic complex.
Mapping and unit descriptions are compiled and modifi ed from Swanson (1996a, 1996b) and Swanson and Clayton (1983). Numbered sample locations correspond to numbered geochemical analyses presented in Table 2 and Table DR2 (see text footnote 1). The color scheme used on this map is also adopted for Figures 6, 7, 8, and 9. FT—fission track; MIS—marine oxygen isotope stage.

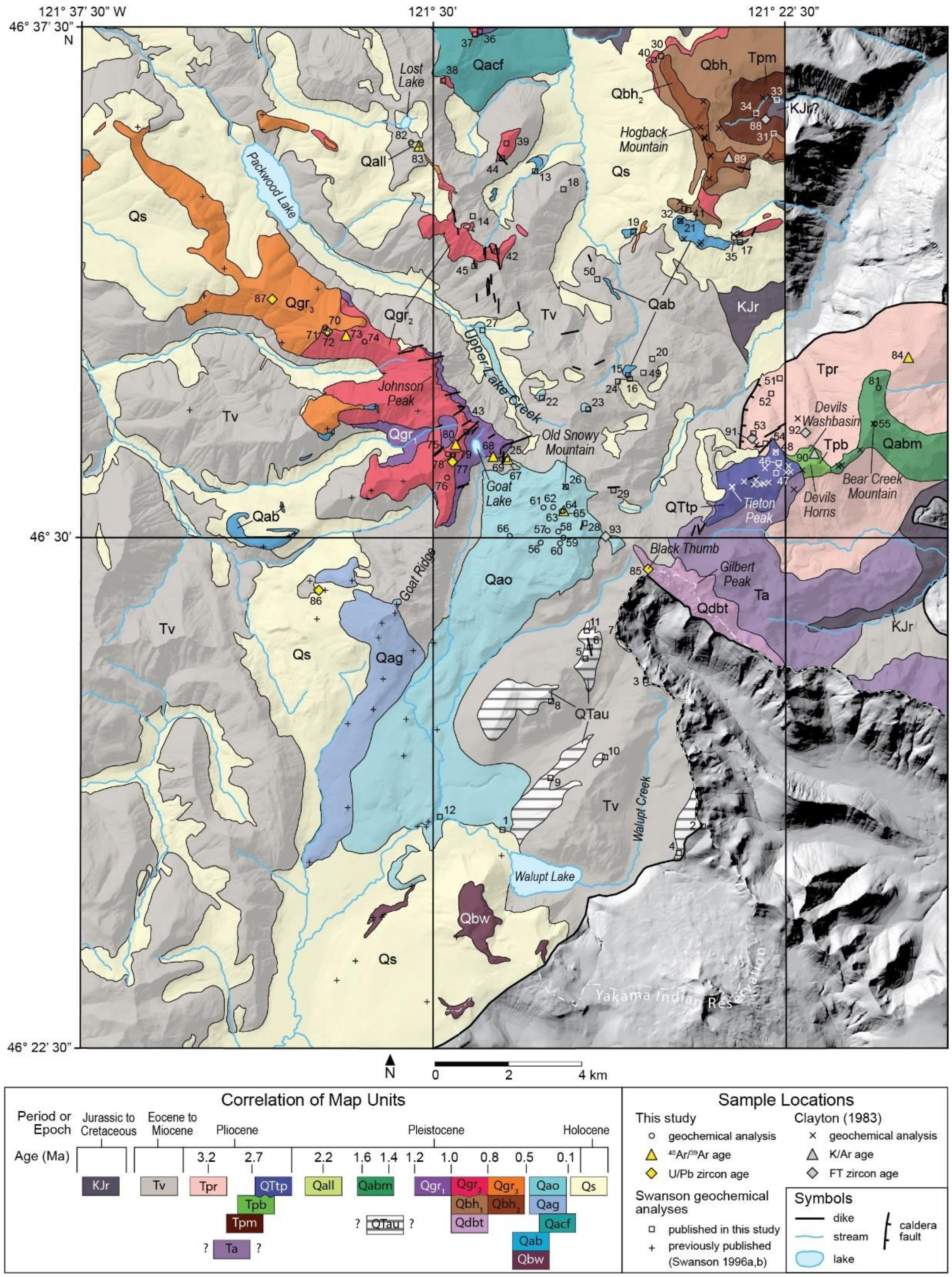

121° 37' 30" W
121° 30'
121° 22' 30"
46° 37' 30"
46° 30'
46° 22' 30"
Lost Lake
Packwood Lake
Hogback Mountain
Johnson Peak
Upper Lake Creek
Old Snowy Mountain
Goat Lake
Goat Ridge
Devils Washbasin
Bear Creek Mountain
Devils Horns
Tieton Peak
Black Thumb
Gilbert Peak
Walupt Creek
Walupt Lake
Yakama Indian Reservation
0 2 4 km
Correlation of Map Units
Period or Epoch
Jurassic to Cretaceous
Eocene to Miocene
Pliocene
Pleistocene
Holocene
Age (Ma)
3.2 2.7 2.2 1.6 1.4 1.2 1.0 0.8 0.5 0.1
KJr Tv Tpr QTtp Qall Qabm Qgr1 Qgr2 Qgr3 Qao Qs
Tpb Qbh1 Qbh2 Qag
Tpm QTau Qdbt Qacf
Ta Qab Qbw
Sample Locations
This study
geochemical analysis
40Ar/39Ar age
U/Pb zircon age
Clayton (1983)
geochemical analysis
K/Ar age
FT zircon age
Swanson geochemical analyses
published in this study
previously published (Swanson 1996a,b)
Symbols
dike
stream
lake
caldera fault

Figure 1.2.

Map unit descriptions

SURFICIAL DEPOSITS

Qs: Quaternary surficial deposits (Pleistocene to Holocene)— Undifferentiated alluvium, colluvium, alluvial fan deposits, and landslide deposits, plus glacial deposits of Evans Creek and possibly Hayden Creek age.

OLD SNOWY MOUNTAIN STAGE

Qao: Andesite of Old Snowy Mountain (Pleistocene)—Light gray, sparsely and finely hornblende-two pyroxene-plagioclase-phyric andesite flows erupted from Old Snowy Mountain-Ives Peak area. Typically fine-grained and pilotaxitic. Glomerocrysts of plagioclase and one or two pyroxenes are common. Occupies modern river valleys and so probably younger than Hayden Creek Drift. $^{40}Ar/^{39}Ar$ age of flow near Old Snowy Mountain is 210.9±3.8 ka. For simplicity, some overlying deposits of Evans Creek Drift are not shown on map.

Qag: Andesite of Goat Ridge (Pleistocene)—Sparsely to moderately but finely two-pyroxene-plagioclase andesite on south end of Goat Ridge. Some flows are hornblende-bearing. Also includes minor dacite and rhyolite flows (sub-units Qdg and Qrg, Swanson, 1996b). Erupted from southern crest of Goat Ridge, but glaciation has removed all trace of cones. For simplicity, some overlying deposits of Evans Creek Drift are not shown on map.

Qacf: Andesite of Clear Fork Cowlitz River (Pleistocene)—Gray, fine-grained, sparsely hornblende-phyric andesite flow erupted from vent on ridge just north of Coyote Lake (northern margin of map; small lake not shown). Flowed along ancestral Clear Fork Cowlitz River and ponded to form thick, strikingly columnar outcrop visible from Palisades Viewpoint on Highway 12. Occupies U-shaped valley probably carved by glacier of Hayden Creek age.

Qab: Andesite of Brunhes Chron (Pleistocene)—Undifferentiated late-stage andesites cropping out west-southwest, north, northeast, and east of Upper Lake Creek basin. Plugs and perched intracanyon flows, most amphibole-bearing. Includes Swanson's (1996a, 1996b, and unpublished) map units Qdj, Qgrh, Qac, and Qah. Mostly normal magnetic polarity, but a few reversed; some may be late Matuyama though most are likely of Brunhes age, postdating unit Qgr_3.

Qbw: Basalt of Walupt Lake Volcano (Pleistocene)—Hyaloclastic deposits of bedded sideromelane sand containing blocks of glassy olivine-bearing basalt, and hackly-jointed pillow-like masses of quenched basalt. Part of a large subglacial volcano (tuya) recognized by Hammond (1980), probably formed during Hayden Creek time. For simplicity, mapped extent also includes nearby outcrops of other young basaltic andesites (Qbt and Qba of Swanson, 1996a).

LAKE CREEK STAGE

Qgr_3: Upper normally-magnetized lava flows of Lake Creek Volcano (Pleistocene)—More than 450 m of dominantly vitrophyric, cognate-inclusion-bearing andesite and dacite flows filling canyons incised into older units, including older flows from Lake Creek Volcano. Flows follow paleovalleys but not modern valleys and so are older than Hayden Creek Drift. This in addition to normal magnetic polarity constrains eruptive duration to between ~0.8 and ~0.3 Ma.

Qbh_2: Normally-magnetized basalt of Hogback Mountain (Pleistocene)—Thin flows of basalt, often olivine-bearing, capping and erupted from Hogback Mountain shield volcano. Overlies unit Qbh_1.

Qgr_2: Reversely-magnetized lava flows of Lake Creek Volcano (Pleistocene)—Valley-filling flows totaling more than 500 m thick, dominantly vitrophyric, inclusion-bearing, and, except for reversed magnetic polarity, indistinguishable physically and chemically from older and younger flows from Lake Creek Volcano. Erupted during late Matuyama chron between ~1 and ~0.8 Ma; zircon age from andesite flow low in section is 0.97±0.16 Ma.

Qbh_1: Reversely-magnetized basalt of Hogback Mountain (Pleistocene)—Thin flows of basalt, often olivine-bearing, erupted from Hogback Mountain shield volcano and located stratigraphically between units Tpm and Qbh_2. Lower flows in section are interbedded with reversely-magnetized andesites probably from Lake Creek Volcano. $^{40}Ar/^{39}Ar$ age for a basalt north of the map area but probably from this unit is 0.893±0.006 Ma (Sisson and Calvert, 2017 written communication).

Qgr_1: Lower normally-magnetized lava flows of Lake Creek Volcano (Pleistocene)—Valley-filling vitrophyric andesite and dacite flows and laharic breccia erosionally overlying Tertiary rocks. Occurs on ridges above Upper Lake Creek basin; Goat Lake cirque is eroded into this unit. Normal magnetic polarity suggests eruptive pulse during Jaramillo subchron, and age of basal flow is 1.15±0.01 Ma.

BEAR CREEK MOUNTAIN STAGE

Qabm: Andesite of Bear Creek Mountain (Pleistocene)—Plagioclase- and pyroxene-phyric andesite lava flows capping and flanking the east side of Bear Creek Mountain. Some flows contain olivine phenocrysts. Included and not distinguished on map are zones of dikes and agglomerate inferred to be vents for Tieton andesite flows (see Gusey, this volume, for details).

Qall: Andesite of Lost Lake (Pleistocene)—Reversely-magnetized, isolated ridge-capping andesite flow remnants ~0.5 km southeast of Lost Lake. Upper flow is 2.17±0.01 Ma. Vent location uncertain.

STAGE UNCERTAIN

QTau: Undifferentiated andesites (Pliocene and/or Pleistocene)— Andesitic to dacitic lava flows, dikes, plugs, and lahar deposits in Walupt Lake quadrangle of uncertain age. Probably older than Old Snowy Mountain Stage, given exposure. Some or all postdate Tieton Peak andesites, as shown by stratigraphic relation at Gilbert Peak. Includes rocks of both normal and reversed magnetic polarity.

TIETON PEAK STAGE

QTa: Andesite of Tieton Peak (Pliocene and maybe Pleistocene)— Andesite, basaltic andesite, dacite, trachyte, and rhyolite flows and pyroclastic deposits overlying unit Tpr and intercalated with unit Tbw. Includes Swanson's (unpublished) units QTa, QTah, Qr, Qgrp, and tentatively assigned Qgr_1. These uppermost "Qgr_1" flows of andesite and dacite are similar to Qgr_1 lavas erupted from Lake Creek Volcano, but we infer the vent to be Tieton Peak.

Tpb: Basalt of Devils Washbasin (Pliocene)—Thin flows, bedded pyroclastic rocks, and narrow dikes of olivine basalt erupted from a vent near Devils Washbasin and comprising the spires of Devils Horns. Interbedded with pyroxene andesite flows low in unit QTa and overlies unit Tpr. Normal magnetic polarity suggests Gauss chron, and $^{40}Ar/^{39}Ar$ age for a basalt flow northeast of Bear Creek Mountain, interpreted to be from this unit, is 2.78±0.01 Ma.

Tpm: Basalt and andesite of Miriam Creek (Pliocene)—Basaltic and andesitic lava flows of normal magnetic polarity underlying unit Qbh_1 east of Hogback Mountain. Includes Swanson's (unpublished) units Qbm, basalt of Miriam Creek (probably Pliocene but possibly Eocene), and Qahm, hornblende andesite of Miriam Lake. A zircon FT age of 3.1±0.3 Ma was determined by Clayton (1983) for tephra between basalt flows midway up this section (low in Qahm).

DEVILS HORNS CALDERA

Tpr: Rhyolite of Devils Horns (Pliocene)—Thick deposits of domes, ash-flow tuff, air-fall tuff, and breccia of high-silica rhyolite beneath Devils Horns. Probably related to caldera-forming eruption (note caldera fault mapped north of Tieton Peak). Radiometric ages ~3.2 Ma.

BASEMENT

Tv: Undifferentiated Tertiary intrusive rocks and volcanic deposits (Eocene to Miocene)—Plutons, plugs, dikes, lava flows, and volcaniclastic and epiclastic rocks of mafic to silicic composition. Some units possibly related to the Ohanapecosh Formation (Eocene and Oligocene).

KJr: Russell Ranch Formation (Jurassic to Cretaceous)—Graywacke, argillite, and less abundant basaltic flows, most of which are pillowed. Sheared in most places. Most flows metamorphosed to greenstone.

Figure 1.2 (continued).

Figure 1.3. 40Ar/39Ar age spectra and inverse isochrons for seven samples from Goat Rocks volcanic complex and vicinity.
The preferred age for each groundmass or mineral separate is in bold. Heating steps included in the plateau age are white boxes used to fi t black and gray inverse isochrons. The black inverse isochron line is fi t to the intercept value of air; the calculated intercept for the gray line is in the upper-right corner of the plot. Calculated 40Ar/36Ar intercept values are shown in bold when not within error of the standard value for air (295.5) and when used in the plateau calculation. Total fusion data are indicated by gray circles with bold outlines on inverse isochron diagrams. For full data sets for each sample, see Supplementary Information DR1 (text footnote 1). MSWD—mean square of weighted deviates.

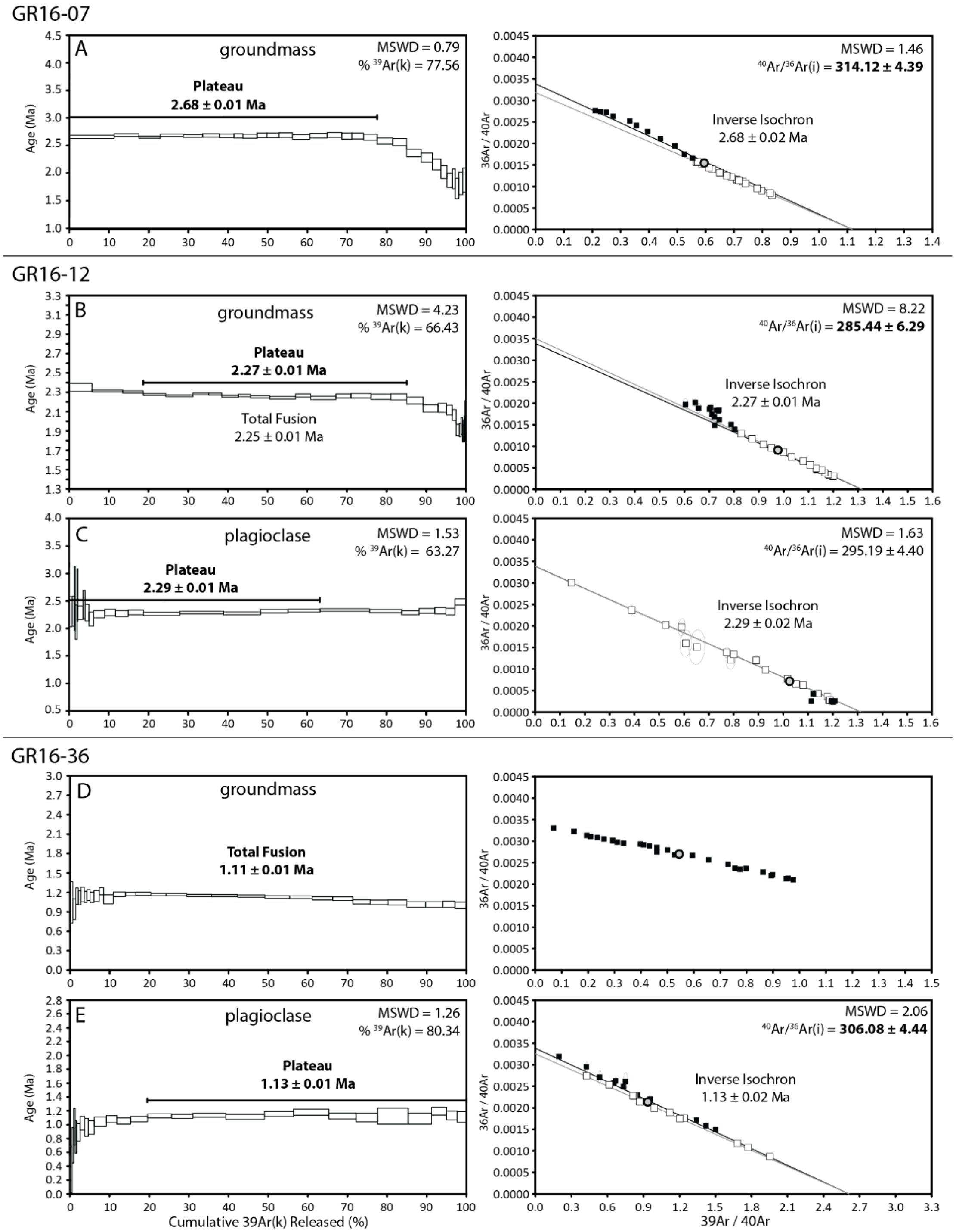

GR16-07
A
groundmass
MSWD = 0.79
% ^{39}Ar(k) = 77.56
Plateau
2.68 ± 0.01 Ma
Age (Ma)
MSWD = 1.46
^{40}Ar/^{36}Ar(i) = 314.12 ± 4.39
Inverse Isochron
2.68 ± 0.02 Ma
36Ar / 40Ar
GR16-12
B
groundmass
MSWD = 4.23
% ^{39}Ar(k) = 66.43
Plateau
2.27 ± 0.01 Ma
Total Fusion
2.25 ± 0.01 Ma
MSWD = 8.22
^{40}Ar/^{36}Ar(i) = 285.44 ± 6.29
Inverse Isochron
2.27 ± 0.01 Ma
C
plagioclase
MSWD = 1.53
% ^{39}Ar(k) = 63.27
Plateau
2.29 ± 0.01 Ma
MSWD = 1.63
^{40}Ar/^{36}Ar(i) = 295.19 ± 4.40
Inverse Isochron
2.29 ± 0.02 Ma
GR16-36
D
groundmass
Total Fusion
1.11 ± 0.01 Ma
E
plagioclase
MSWD = 1.26
% ^{39}Ar(k) = 80.34
Plateau
1.13 ± 0.01 Ma
MSWD = 2.06
^{40}Ar/^{36}Ar(i) = 306.08 ± 4.44
Inverse Isochron
1.13 ± 0.02 Ma
Cumulative 39Ar(k) Released (%)
39Ar / 40Ar

Figure 1.3.

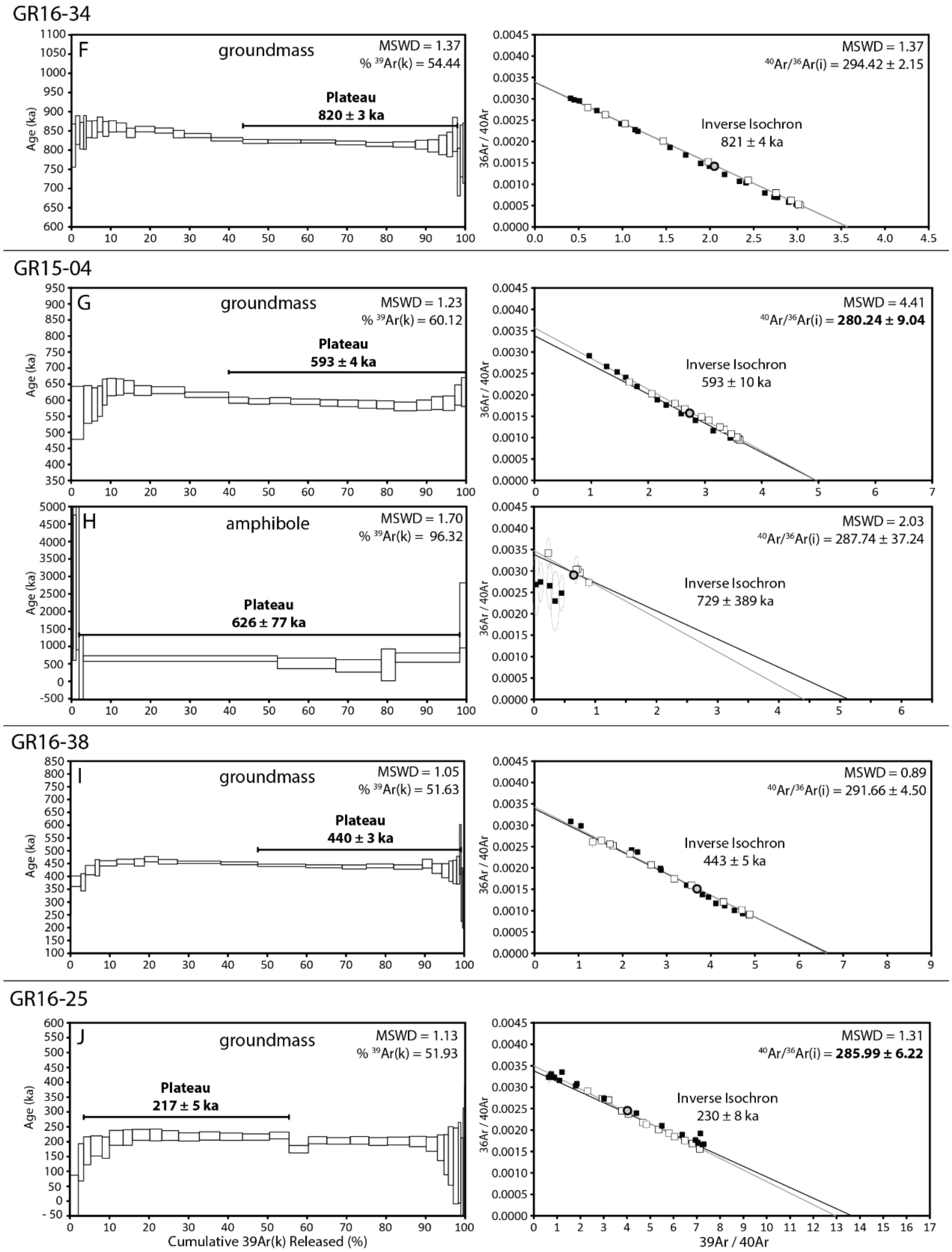

Figure 1.3 (continued).

Figure 1.4. 230Th-corrected 206Pb/238U ages of zircons from nine samples from Goat Rocks volcanic complex.
Individual spot ages are shown as 1σ error bars and are arranged in order from youngest to oldest, left to right, for each subsample (e.g., surfaces of crystals, polished interiors of crystals). Spot analyses included in weighted mean age(s) are black; those not included are gray. Weighted mean ages are shown with 2σ standard error and are represented by a light-gray bar centered on the mean; bar height is ±2σ error. For full data sets, refer to Supplementary Information DR1 (text footnote 1). MSWD—mean square of weighted deviates.

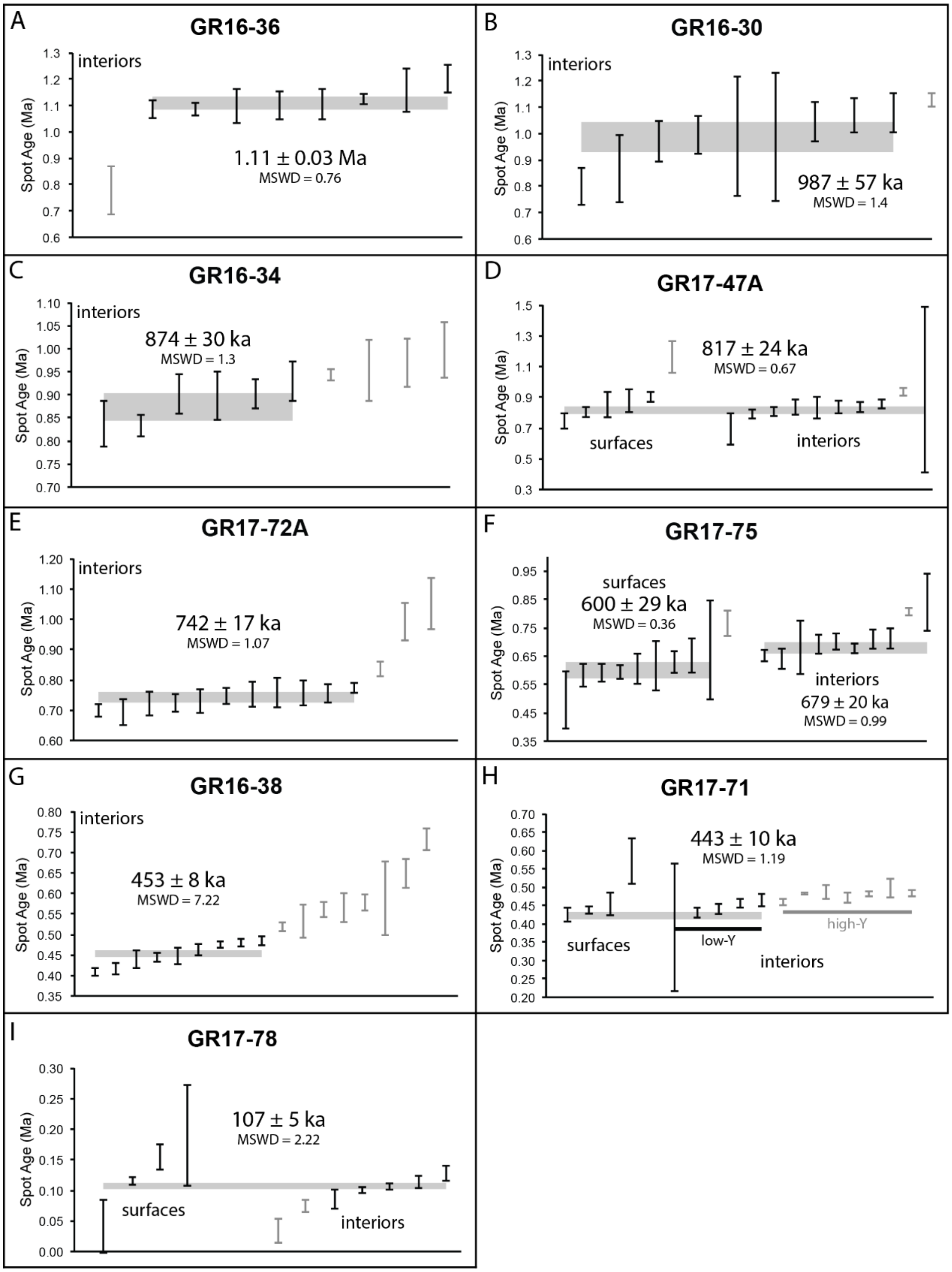
A
GR16-36
interiors
1.11 ± 0.03 Ma
MSWD = 0.76
Spot Age (Ma)
B
GR16-30
interiors
987 ± 57 ka
MSWD = 1.4
Spot Age (Ma)
C
GR16-34
interiors
874 ± 30 ka
MSWD = 1.3
Spot Age (Ma)
D
GR17-47A
817 ± 24 ka
MSWD = 0.67
surfaces
interiors
Spot Age (Ma)
E
GR17-72A
interiors
742 ± 17 ka
MSWD = 1.07
Spot Age (Ma)
F
GR17-75
surfaces
600 ± 29 ka
MSWD = 0.36
interiors
679 ± 20 ka
MSWD = 0.99
Spot Age (Ma)
G
GR16-38
interiors
453 ± 8 ka
MSWD = 7.22
Spot Age (Ma)
H
GR17-71
443 ± 10 ka
MSWD = 1.19
surfaces
low-Y
high-Y
interiors
Spot Age (Ma)
I
GR17-78
107 ± 5 ka
MSWD = 2.22
surfaces
interiors
Spot Age (Ma)

Figure 1.4.

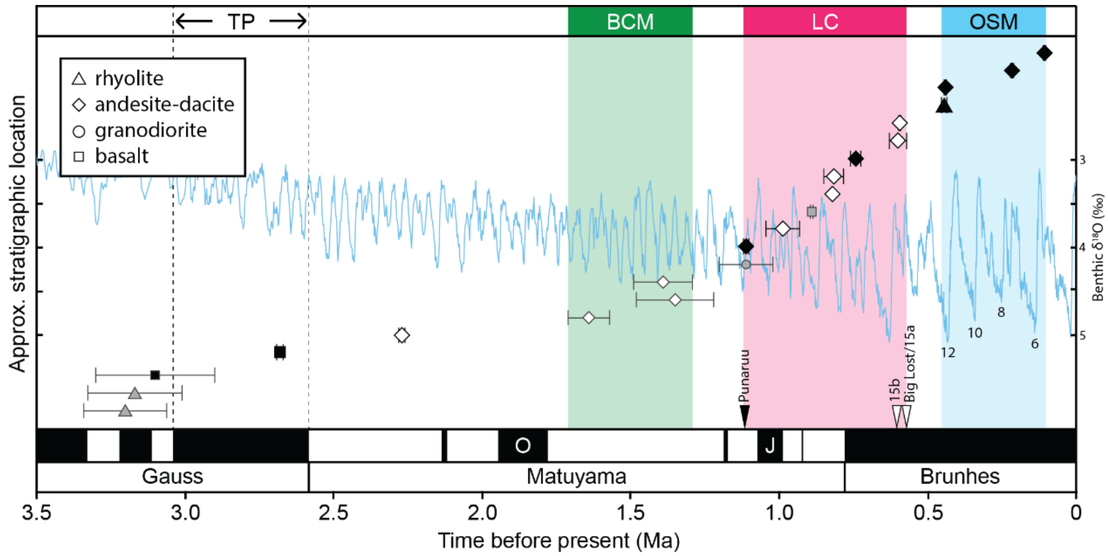

Figure 1.5. Eruptive timeline of the Goat Rocks volcanic complex.
Timeline is based on eruption ages from this study (large symbols) and ages from other studies (small symbols). Two erroneously old K/Ar ages for Devils Washbasin basalt and Hogback Mountain basalt by Clayton (1983) are excluded. Ages are arranged in stratigraphic order where stratigraphic relations are known and, otherwise, from oldest (bottom) to youngest (top). Error bars for each symbol show 2σ error. Symbol color indicates magnetic polarity: normal (black), reversed (white), or undefi ned (gray). Note that for tuff along Miriam Creek and tuff below Tieton andesite (the sources of which are uncertain), the symbol used is for the overlying lava fl ow. Magnetic polarity time scale is compiled from Horng et al. (2002; <2.13 Ma) and Cande and Kent (1995; >2.13 Ma). O and J—Olduvai and Jaramillo subchrons, respectively. Labeled triangles indicate ages of brief magnetic excursions as reported by Channell et al. (2002), Lund et al. (2006), and Laj and Channell (2007). Colored columns show duration of major eruptive stages (BCM—Bear Creek Mountain, LC—Lake Creek, OSM—Old Snowy Mountain). The tentative duration of Tieton Peak stage (TP) is shown with dotted lines and is based on normal magnetic polarity and possible coevolution with Devils Washbasin basalt. Ages are overlain on the benthic δ18O record determined by Lisiecki and Raymo (2005). Select glacial marine isotope stages (MIS) are numbered; MIS 6 possibly corresponds to Hayden Creek Drift.

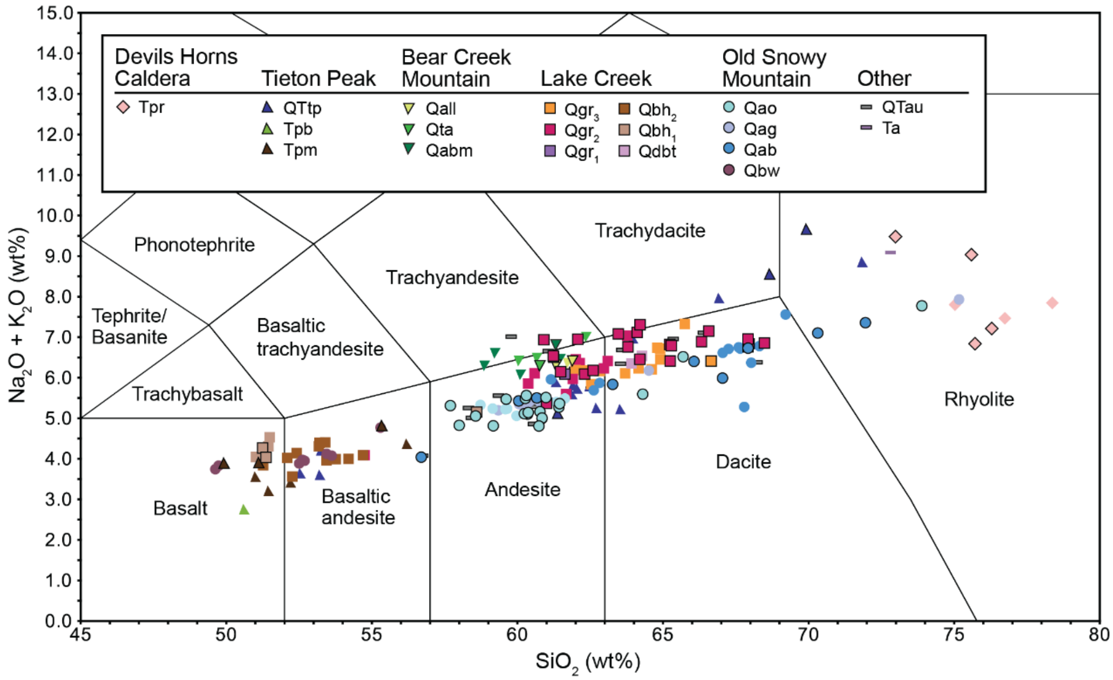

Figure 1.6. Total alkali-silica diagram for volcanic and shallow intrusive rocks of the Goat Rocks volcanic complex.

Compositional fields are after Le Bas et al. (1986). Compositions of Devils Horns caldera (pre–Goat Rocks; pink diamonds) are included for reference. Symbol colors follow map unit colors in Figure 2. Symbols with black outlines are data newly presented in this paper; symbols with no outline include data from Swanson (1996a, 1996b), Clayton (1983), and Gusey et al. (this volume). For all composition data used in this fi gure and in Figures 7, 8, and 9, refer to Table DR2 (text footnote 1).

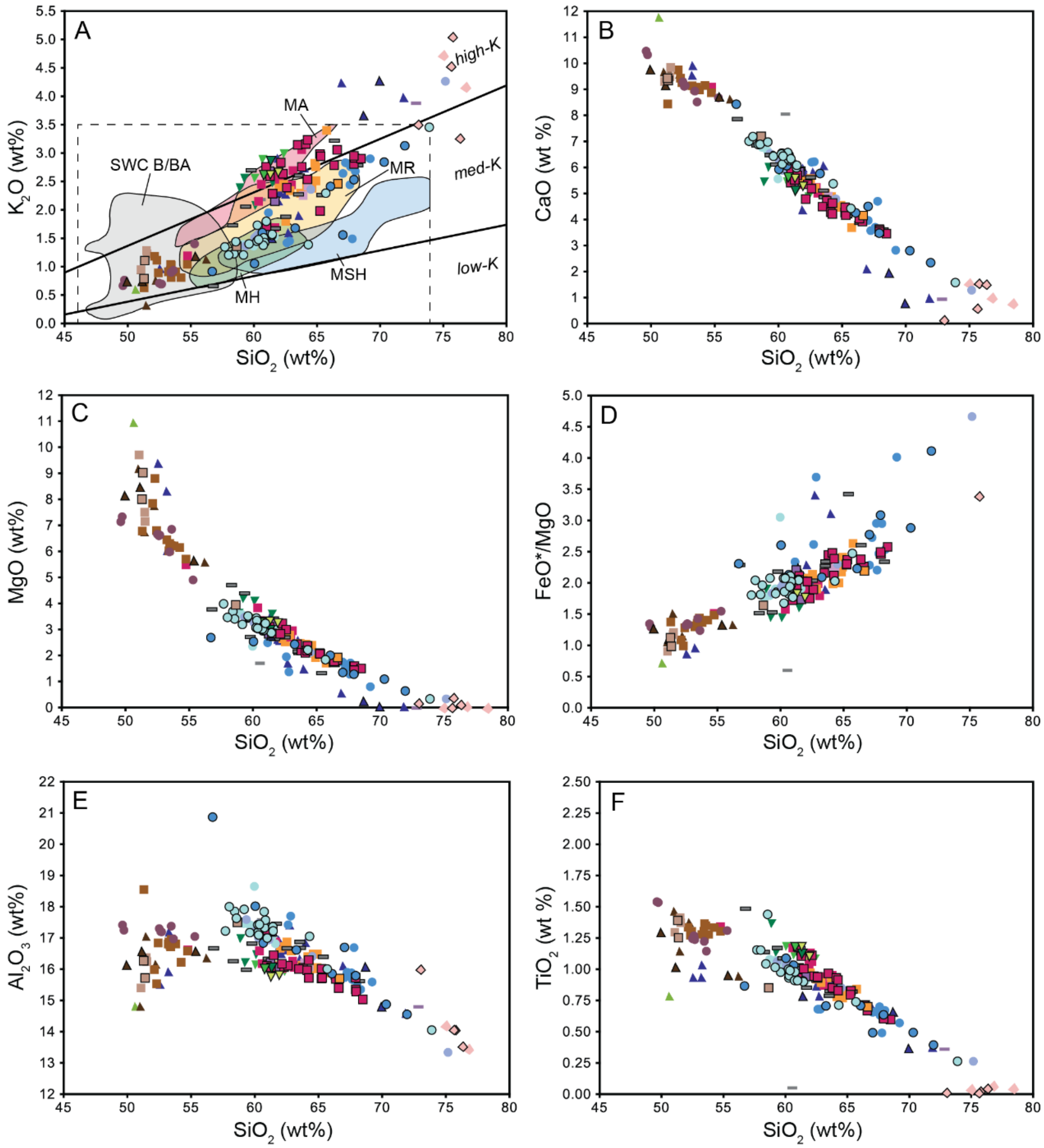

Figure 1.7. Major-element variation diagrams for volcanic and shallow intrusive rocks of the Goat Rocks volcanic complex.
Colors and symbols are as in Figure 6. Dashed inset shows boundary of K2O diagram in Sisson et al. (2014). Fields for Mount Rainier (MR), Mount Adams (MA), Mount St. Helens (MSH), and Southern Washington Cascades basalt/basaltic andesite (SWC B/BA) are from data compiled by Sisson et al. (2014). K2O-SiO2 fi eld for Mount Hood (MH) was drafted from data presented in Scott et al. (1997).

Figure 1.8. K2O vs. SiO2 for samples from each eruptive stage of the Goat Rocks volcanic complex.
(A) Old Snowy Mountain stage, (B) Lake Creek stage, (C) Bear Creek Mountain stage (plus Lost Lake andesite, though source of that lava fl ow is unknown), and (D) Tieton Peak stage. Age range of samples is shown at the top of each panel. Colors and symbols are as in Figure 6. Dashed inset and colored fi elds
are as in Figure 7.

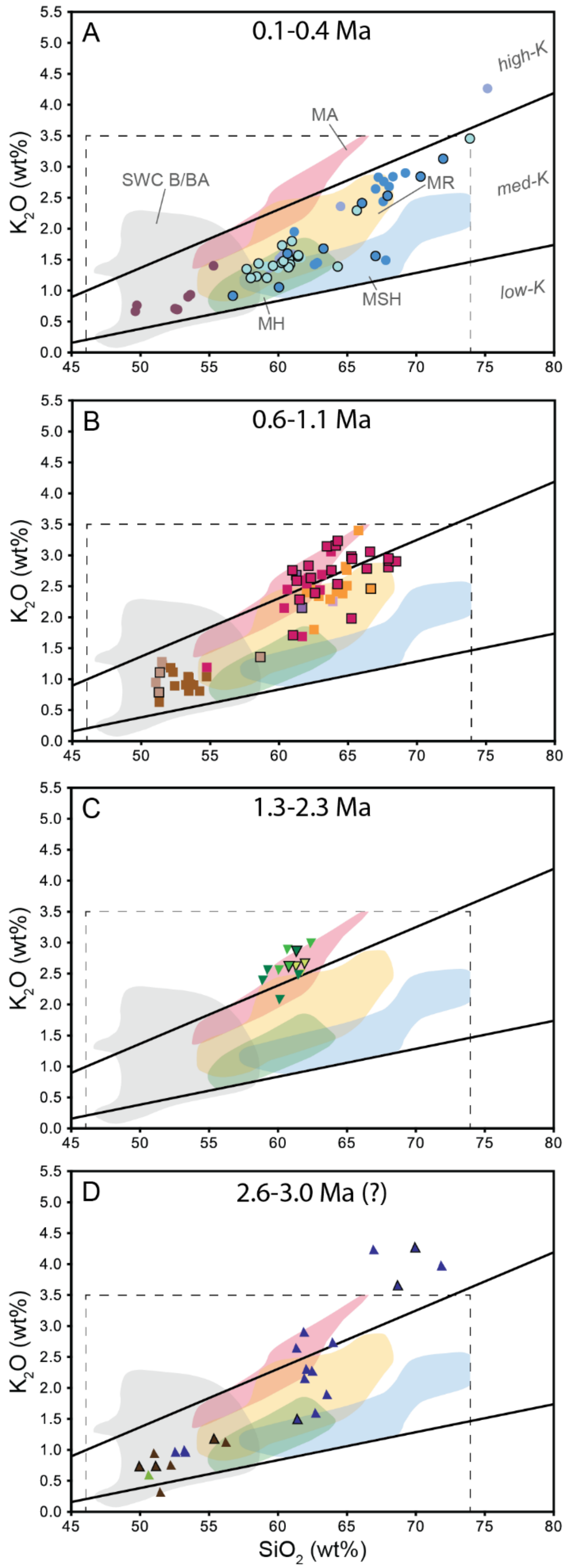
A
0.1-0.4 Ma
B
0.6-1.1 Ma
C
1.3-2.3 Ma
D
2.6-3.0 Ma (?)
high-K
med-K
low-K
MA
SWC B/BA
MR
MSH
MH
K_2O (wt%)
SiO_2 (wt%)

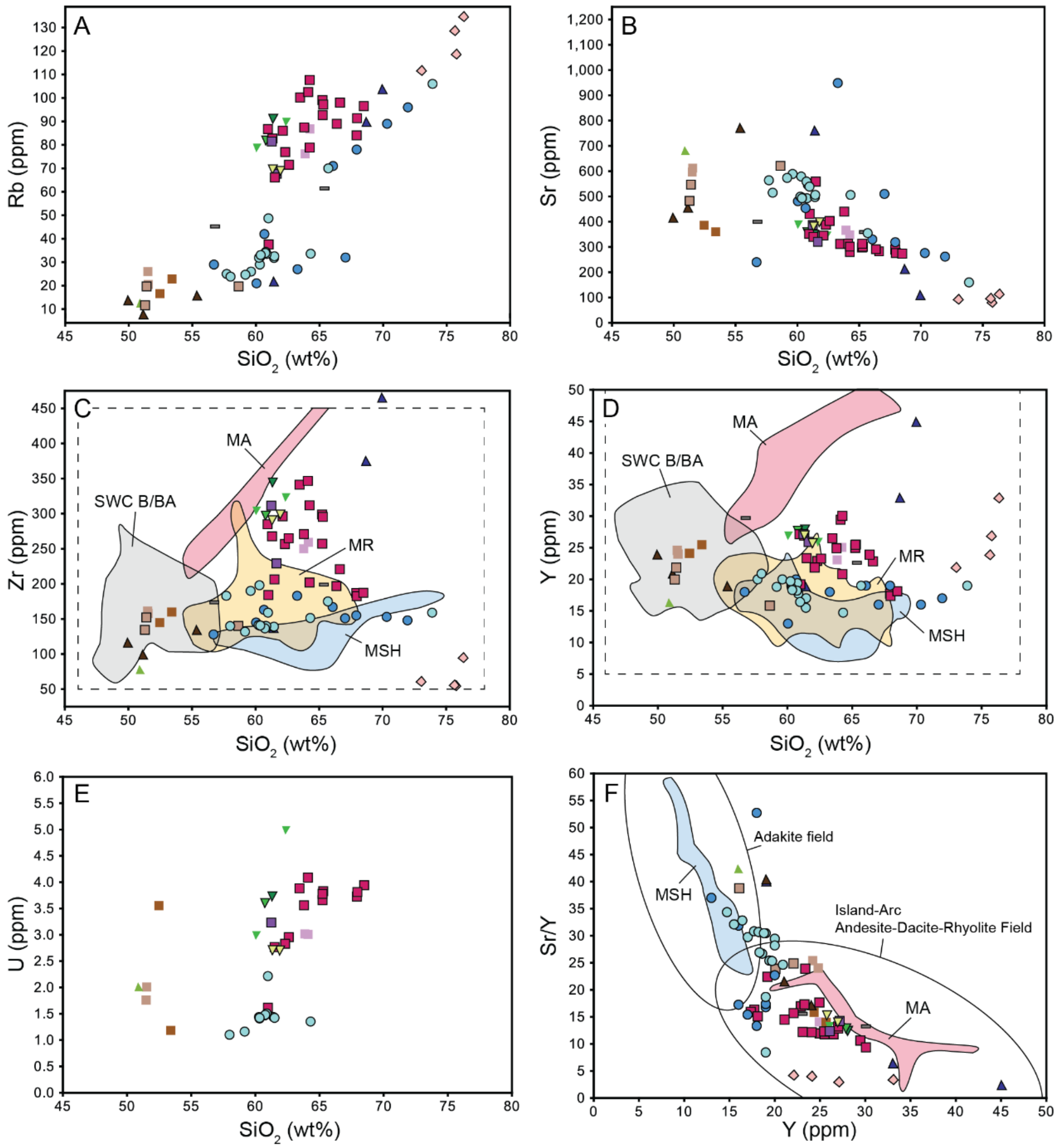

Figure 1.9. Trace-element variation diagrams for volcanic and shallow intrusive rocks of the Goat Rocks volcanic complex.
Colors and symbols are as in Figure 6. All data shown are X-ray fl uorescence (XRF) analyses, except for U (panel E), where inductively coupled plasma–
mass spectrometry (ICP-MS) data are shown for our new data (black outlines). Fields for Mount Rainier (MR), Mount Adams (MA), Mount St. Helens (MSH), and Southern Washington Cascades basalt/basaltic andesite (SWC B/BA) in panels C and D were drafted from data compiled by Sisson et al. (2014). Dashed insets in panels C and D show boundary of diagrams in Sisson et al. (2014). Fields for MSH and MA in panel F were drafted from data presented in Defant and Drummond (1993).

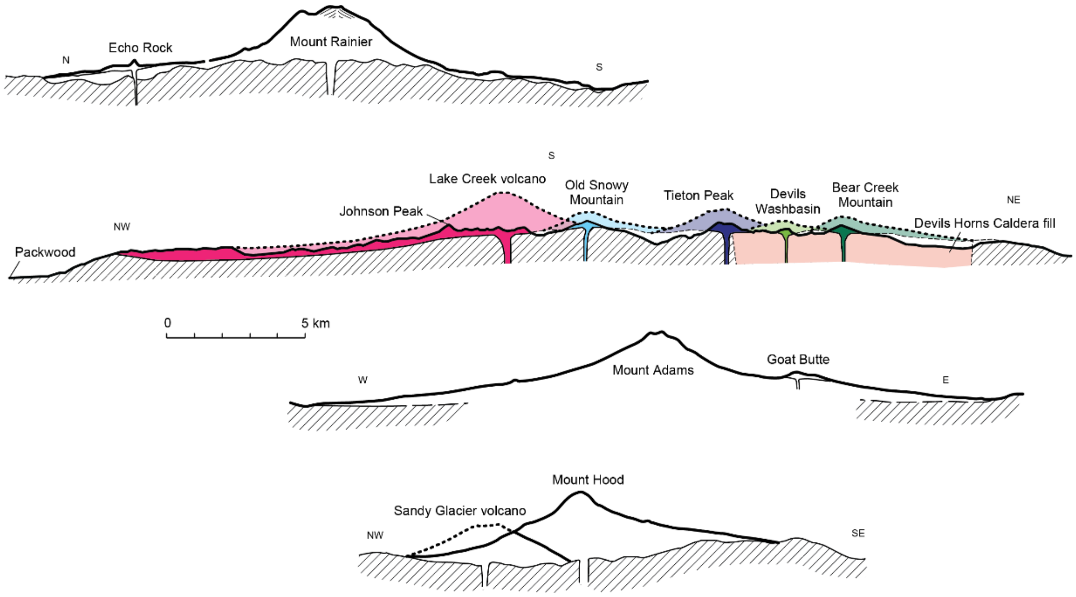

Figure 1.10. Schematic cross sections through major vents of the Goat Rocks volcanic complex.
Note that cross section is bent ~90° near Old Snowy Mountain to capture existing deposits from each of the four main andesitic vents, so distance shown between nonadjacent vents may be greater than true distance (e.g., true distance between hypothesized Lake Creek volcano and Bear Creek Mountain summits is ~10 km). Bold solid line denotes present-day topography. Solid colors represent present-day thickness and extent of volcanic deposits interpreted from geologic maps, with conduits shown schematically. Diagonal stripes indicate basement rock. Original topography for each vent is projected schematically with dashed bold lines and pale colors. Note overlay between projected Old Snowy Mountain and Lake Creek volcanoes and between Bear Creek Mountain and Devils Washbasin, where younger eruptive products may have covered eroded surfaces where older deposits were once present (no crosscutting relations were observed in the fi eld). The Devils Horns caldera ring fracture is fairly well constrained on the west side by a fault mapped north of Tieton Peak (Fig. 2; Swanson, 2017, written commun.), but its eastern extent is not well constrained, and the location shown here is for illustrative purpose only. Also included are profi les through nearby Mount Rainier, Mount Adams, and Mount Hood, after Hildreth (2007), all at the same scale with no vertical exaggeration.

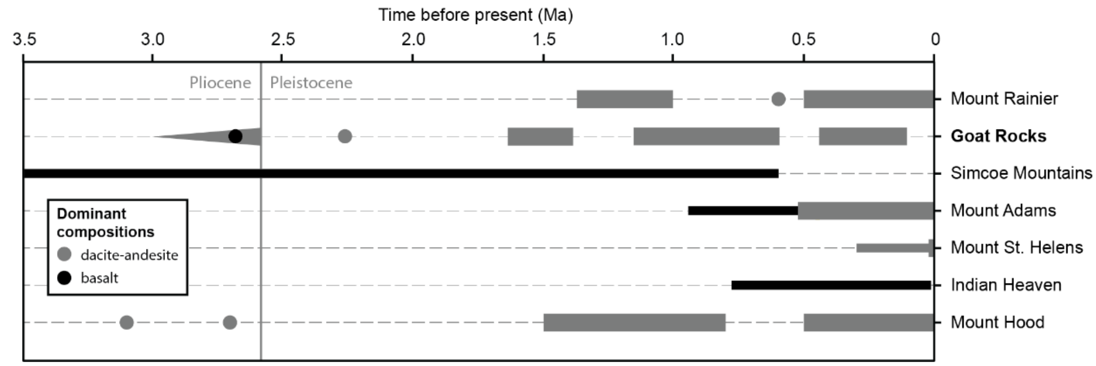

Figure 1.11. Eruptive history of Goat Rocks volcanic complex in context with regional volcanic activity.
Eruptive history of an extinct volcano is included with an active volcano if it is located within ~15 km (approximate diameter of the Goat Rocks volcanic complex) of the modern edifi ce. Circles represent single eruptive events or separate deposits with statistically equivalent ages. Bars show extended periods of eruptive activity. Thick bars represent focused activity at a major edifi ce, while narrow bars show activity across a distributed area. Tapered bar on Goat Rocks timeline represents Tieton Peak stage, for which eruptive duration is tentatively constrained by Devils Washbasin basalt (black circle; see text) and magnetic polarity. Eruptive history sources are: Mount Rainier—Sisson et al. (2001) and Sisson and Calvert (2017, written commun.); Simcoe Mountains—Hildreth and Fierstein (2015); Mount Adams—Hildreth and Lanphere (1994); Mount St. Helens—Mullineaux and Crandell (1981) and Clynne et al. (2008); Indian Heaven—Mitchell et al. (1989) and Korosec (1989); and Mount Hood—Sherrod and Scott (1995) and Scott et al. (1997).

TABLES.

Table 1.1

TABLE 1. AGES OF PLIOCENE TO PLEISTOCENE VOLCANIC DEPOSITS NEAR GOAT ROCKS VOLCANIC COMPLEX

Sample ID[*]	Map no.[†]	Map unit[§]	Location[#]		Magnetic polarity[**]	Age ± 2σ error (ka or Ma)[††]	Phase analyzed[§§]	Dating technique	Details[##]	Age Interpretation	Reference[***]
			Longitude	Latitude							
<u>Old Snowy Mountain Stage</u>											
GR17-78	N.A.	Qacf	-121.5480	46.6791	N	**107 ± 5 (ka)**	Zrn	U/Pb	Surfaces (n=4) and interiors (n=5), MSWD=2.22	Youngest zircon population	This study
GR16-25	65	Qao	-121.4549	46.5065	N	**217 ± 5**	Gm	$^{40}Ar/^{39}Ar$	Plateau, 52% $^{39}Ar(k)$, MSWD=1.13	Groundmass crystallization	This study
GR16-38	67	Qao	-121.4747	46.5188	N	**440 ± 3**	Gm	$^{40}Ar/^{39}Ar$	Plateau, 52% $^{39}Ar(k)$, MSWD=1.05	Groundmass crystallization	This study
						453 ± 8	Zrn	U/Pb	Interiors (n=9), MSWD=7.22	Youngest zircon population	This study
GR17-71	86	Qag	-121.5400	46.4866	N	**443 ± 10**	Zrn	U/Pb	Surfaces (n=4) and low-Y interiors (n=5), MSWD=1.19	Youngest zircon population	This study
<u>Lake Creek Stage</u>											
GR15-04	73	Qgr_2	-121.5322	46.5492	R	**593 ± 4**	Gm	$^{40}Ar/^{39}Ar$	Plateau, 60% $^{39}Ar(k)$, MSWD=1.23	Groundmass crystallization	This study
						626 ± 77	Am	$^{40}Ar/^{39}Ar$	Plateau, 96% $^{39}Ar(k)$, MSWD=1.70	Amphibole crystallization	This study
GR17-75 (GR15-02)	71	Qgr_2	-121.5388	46.5501	R	**600 ± 29**	Zrn	U/Pb	Surfaces (n=9), MSWD=0.36	Youngest zircon population	This study
GR17-72A	87	Qgr_3	-121.5572	46.5574	N	**742 ± 17**	Zrn	U/Pb	Interiors (n=11), MSWD=1.07	Youngest zircon population	This study
GR17-47A	85	Qdbt	-121.4241	46.4916	R	**817 ± 24**	Zrn	U/Pb	Surfaces (n=5) and interiors (n=9), MSWD=0.67	Youngest zircon population	This study
GR16-34	80	Qgr_2	-121.4932	46.5224	R	**820 ± 3**	Gm	$^{40}Ar/^{39}Ar$	Plateau, 54% $^{39}Ar(k)$, MSWD=1.37	Groundmass crystallization	This study
						874 ± 30	Zrn	U/Pb	Interiors (n=6), MSWD=1.3	Youngest zircon population	This study
08WP1019	N.A.	Qbh_1[†††]	-121.4297	46.6483	N.D.	***891 ± 7***	Gm	$^{40}Ar/^{39}Ar$	Plateau		1
GR16-30	77	Qgr_2	-121.4944	46.5184	R	**987 ± 57**	Zrn	U/Pb	Interiors (n=9), MSWD=1.4	Youngest zircon population	This study
N.G.	93	Un.[§§§]	-121.4390	46.4990	N.D.	***1.11 ± 0.09 (Ma)***	Zrn	Fission track			2, 3
GR16-36	68	Qgr_1	-121.4799	46.5198	N	1.11 ± 0.03	Zrn	U/Pb	Interiors (n=8), MSWD=0.76	Youngest zircon population	This study
						1.11 ± 0.01	Gm	$^{40}Ar/^{39}Ar$	Total fusion	Groundmass crystallization	This study
						1.13 ± 0.01	Pl	$^{40}Ar/^{39}Ar$	Plateau, 80% $^{39}Ar(k)$, MSWD=1.26	Plagioclase cooling age	This study
HM-SP-1	89	Qbh_2	-121.3961	46.5930	N	*1.53 ± 0.18*	WR	K/Ar			2, 3
<u>Bear Creek Mountain Stage</u>											
N.G.	N.A.	Qta_2	-121.1833	46.6320	R	***1.35 ± 0.13***	Zrn	Fission track			2, 4
07114	N.A.	Qta_2	-120.8169	46.7194	R	***1.39 ± 0.10***	Pl	$^{40}Ar/^{39}Ar$			5
04162	N.A.	Qta_1	-121.1515	46.6786	R	***1.64 ± 0.07***	Gm	$^{40}Ar/^{39}Ar$			5
<u>Tieton Peak Stage</u>											

Table 1.1 (continued).

Table 1.2

GR16-07	84	Tpb	-121.3324	46.5439	N	**2.68 ± 0.01**	Gm	$^{40}Ar/^{39}Ar$	Plateau, 76% $^{39}Ar(k)$, MSWD=0.79	Groundmass crystallization	This study
GRDH-2	90	Tpb	-121.3659	46.5205	N	*3.80 ± 0.31*	WR	K/Ar			2, 3
Unassigned Stage											
GR16-12	83	Qall	-121.5063	46.5957	R	**2.27 ± 0.01**	Gm	$^{40}Ar/^{39}Ar$	Plateau, 66% $^{39}Ar(k)$, MSWD=4.23	Groundmass crystallization	This study
						2.29 ± 0.01	Pl	$^{40}Ar/^{39}Ar$	Plateau, 63% $^{39}Ar(k)$, MSWD=1.53	Plagioclase cooling age	This study
HMMCSP-2	88	Tpm	-121.3831	46.6025	N	***3.1 ± 0.2***	Zrn	Fission track			2, 3
Pre-Goat Rocks											
GRTPC-9	91	Tpr	-121.3880	46.5241	N.D.	***3.17 ± 0.16***	Zrn	Fission track			2, 3
GRDH-3	92	Tpr	-121.3690	46.5255	N.D.	***3.20 ± 0.14***	Zrn	Fission track			2, 3

Note: plagioclase ages for samples GR15-04, GR16-07, and GR16-25 are in Appendix 1.

[*]N.G.=no sample ID given.

[†]N.A.=not applicable (location is outside of Figure 2 boundary).

[§]Map units as in Figure 2, except for Qta_1 and Qta_2 (older and younger Tieton andesite flows; Gusey et al., this volume).

[#]Longitude and latitude measured by GPS (coordinate reference system WGS84; this study, refs. 1, 4, 5), or approximated from sample locations in Clayton (1980).

[**]Measured by portable fluxgate magnetometer or inferred from map units by Swanson (1996a,b, unpublished). N=normal, R=reversed, N.D.=not determined (or no magnetic signal).

[††]Non-italic font=age from this study; italic font=age from a previous study (see Reference column). Bold font identifies the preferred eruption ages included on Figure 5. Non-bold font indicates an age that is not interpreted as the eruption age (e.g. phenocryst age older than groundmass from the same sample), or is considered a less reliable age (e.g. previously-published age that does not agree with stratigraphic relations).

[§§]Zrn=zircon, Gm=groundmass, Pl=plagioclase, Am=amphibole, WR=whole-rock.

[##]For zircon ages, n=(x) gives the number of spot analyses on crystal surfaces or polished interiors that are included in the weighted mean age.

[***]1. Sisson and Calvert, written communication; 2. Clayton (1983); 3. Clayton (1980); 4. Gusey et al., this volume; 5. Hammond (2017).

[†††]Map unit is interpreted from age, but not confirmed.

[§§§]Un.=unassigned. Sample is identified as part of the Cispus Pass pluton, but mapping of this pluton is unresolved.

TABLE 2. REPRESENTATIVE XRF MAJOR AND TRACE ELEMENT BULK COMPOSITIONS OF THE GOAT ROCKS VOLCANIC COMPLEX

Map no.		15	19	27	30	31	33	34	36	39
Sample ID[*]		81-35	96-17	96-23	96-27	96-55	96-29	96-54	82-83	82-105
Map unit[†]		Qab	Qab	Qao	Qbh_1	Qbh_1	Tpm	Tpm	Qgr_1	Qgr_2
Rock type[§]		pl	lf	lf	lf	pl	lf	lf	lf	lf
Classification[#]		rhy	rhyodac	and	bas	gab	bas	bas and	dac	and
Mineral assemblage[**]		NR	am, pl	px, pl, oxyhbl	ol	cpx, opx	ol	ol	NR	NR
Major element concentration, normalized volatile-free to 100 percent (wt %)										
	Uncertainty (%)[††]									
SiO_2	0.19	71.95	70.31	60.31	51.34	58.58	49.91	55.33	66.30	61.25
Al_2O_3	0.50	14.55	14.88	17.09	15.72	17.53	16.14	16.59	15.67	16.07
TiO_2	0.92	0.39	0.49	0.95	1.26	0.85	1.30	0.95	0.72	1.10
FeO*	1.17	2.61	3.14	6.22	8.82	6.44	10.41	7.57	4.32	6.11
MnO	0.68	0.05	0.06	0.10	0.15	0.11	0.16	0.13	0.07	0.10
CaO	0.69	2.34	2.80	6.13	9.36	7.18	9.78	8.73	4.05	5.53
MgO	1.33	0.64	1.09	3.34	9.00	3.98	8.16	5.66	1.83	3.08
K_2O	0.71	3.13	2.84	1.46	1.11	1.37	0.75	1.19	2.79	2.61
Na_2O	1.34	4.23	4.26	4.10	2.93	3.79	3.16	3.64	4.09	3.92
P_2O_5	2.16	0.10	0.12	0.30	0.32	0.18	0.24	0.21	0.16	0.23
Unnorm. total		99.08	99.97	100.50	99.80	99.91	99.29	99.10	98.55	98.73
Trace element concentration (ppm)										
	Uncertainty (%)[††]									
Ni	6.61	8	8	28	129	6	104	21	13	17
Cr	5.05	7	6	52	368	35	310	129	17	43
Sc	5.34	5	8	17	30	24	28	28	12	14
V	2.60	35	55	121	187	166	207	178	89	136
Ba	1.57	637	531	443	442	297	218	249	499	431
Rb	2.71	96	89	29	20	20	14	16	89	83
Sr	0.73	262	276	579	550	623	418	773	295	347
Zr	0.90	148	153	198	153	141	117	135	198	269
Y	3.01	17	16	19	22	16	24	19	24	27
Nb	5.23	11	11	14	12	6	12	5	15	19
Ga	3.82	18	19	21	17	20	20	18	19	21
Cu	3.63	10	27	45	22	30	42	30	16	16
Zn	1.98	41	48	84	77	69	80	70	56	65
Pb	8.71	11	9	5	1	4	0	0	10	4
La	8.71	26	32	19	27	17	5	23	30	25
Ce	6.48	54	48	49	58	40	39	39	65	73
Th	10.34	12	11	4	6	2	4	3	10	11
Nd	6.94									

Note: Additional XRF analyses, location data for all samples, and ICP-MS data for samples with prefix GR are in appendix Table A2.

[*](*) in GR16-08* and GR16-09* is part of sample name. Note that sample GR15-02 is from the same outcrop as GR17-75 (age presented in Table 1).

[†]Map units as in Figure 2, except unit Qta_2 (Gusey et al., this volume) not shown in Figure 2.

[§]lf=lava flow, dk=dike, pl=plug, fr=fragmental deposit, en=enclave separated from host lava.

[#]and=andesite, bas=basalt, bas and=basaltic andesite, dac=dacite, rhy=rhyolite, rhyodac=rhyodacite.

[**]Mineral assemblages from unpublished Swanson notes, hand sample characterization, and preliminary petrography. NR=not reported, pl=plagioclase, ol=olivine, am=amphibole, opx=orthopyroxene, cpx=clinopyroxene, px=undifferentiated pyroxene, oxyhbl=oxyhornblende, gloms=glomerocrysts.

[††]Analytical uncertainty for 2016 and 2017 analyses (samples with prefix GR) is based on the mean relative percent absolute difference (RPAD) reported for each element by Kelly (2016); see Methods.

40	42	46	47	48	51	55	59	60	62	65
96-28	81-25	96-52	96-51	96-50	96-45	GR16-09*	GR16-19	GR16-20	GR16-22	GR16-25
Qgr_2	Qgr_3	QTtp	QTtp	QTtp	Tpr	Qabm	Qao	Qao	Qao	Qao
lf	dk	lf	lf	lf	fr	lf	lf	lf(?)	fr	lf
and	dac	rhyodac	rhyodac	and	rhy	and	and	and	and	dac
pl, cpx, opx	NR	pl, cpx, am	pl, cpx, am	oxyhbl(?)	pl	pl, cpx, ol	pl, cpx(?)	pl	pl	am, pl, pl-cpx gloms
62.06	66.55	68.65	69.91	61.36	75.70	61.31	61.45	58.00	60.74	64.30
16.20	15.41	16.09	14.81	17.21	14.07	16.07	17.22	18.00	17.84	17.05
1.12	0.67	0.66	0.37	0.79	0.03	1.13	0.90	1.15	0.91	0.71
5.76	4.19	3.60	4.29	6.25	1.32	6.18	5.86	7.07	5.86	4.50
0.09	0.07	0.04	0.03	0.09	0.05	0.10	0.10	0.13	0.10	0.08
4.77	3.95	1.96	0.80	6.13	1.56	5.13	6.08	7.19	6.57	5.37
2.84	1.85	0.26	0.05	2.78	0.39	3.01	2.87	3.46	3.02	2.22
2.84	3.05	3.67	4.28	1.51	5.05	2.87	1.57	1.20	1.38	1.39
4.09	4.09	4.90	5.40	3.63	1.80	3.95	3.79	3.62	3.43	4.21
0.24	0.16	0.17	0.07	0.25	0.03	0.25	0.16	0.18	0.16	0.17
100.72	97.26	98.94	99.30	98.12	97.58	99.51	99.35	99.44	98.16	99.36
27	13	5	5	8	13	31	16	18	19	12
51	19	3	0	18	0	51	34	33	31	21
15	8	4	4	15	8	15	15	20	16	11
122	78	39	23	80	4	117	128	167	129	91
511	505	697	815	341	430	465	324	270	312	334
86	98	90	104	22	119	91	33	24	34	34
348	284	215	112	763	84	352	506	515	559	506
296	222	376	466	138	56	346	139	140	137	151
22	23	33	45	19	27	28	17	21	18	15
22	15	33	45	7	14	24	7	8	7	7
20	19	24	26	25	24	19	19	20	20	21
29	11	0	7	18	6	23	42	45	45	32
61	55	84	91	71	53	70	67	74	63	68
5	8	13	10	3	17	9	7	6	6	8
44	21	40	52	10	16	31	19	17	18	17
74	57	77	97	50	31	68	34	33	39	36
8	10	12	7	3	6	11	5	4	4	4
						31.0	14.8	17.2	18.8	15.6

67	68	70	70	72	73	77	81	82	83
GR16-38	GR16-36	GR15-01B	GR15-01C	GR15-03	GR15-04	GR16-30	GR16-08*	GR16-10	GR16-12
Qao	Qgr$_1$	Qgr$_2$	Qgr$_2$	Qgr$_2$	Qgr$_2$	Qgr$_2$	Qta2	Qall	Qall
lf	lf	en	dk	lf	lf	lf	lf	lf	lf
and	and	and	dac	and	rhyodac	dac	and	and	and
pl, am, cpx, opx	pl, cpx	pl, am	pl, am, cpx-opx-pl gloms	pl, cpx	pl, am	pl, cpx	pl, cpx	pl	pl, pl-px gloms
60.98	61.24	61.00	67.92	61.48	68.48	64.11	60.75	61.33	61.90
17.00	16.21	17.20	15.35	16.45	15.03	15.97	16.03	15.75	15.83
0.91	1.15	0.93	0.61	1.00	0.60	0.93	1.18	1.19	1.10
5.72	6.25	6.06	3.92	6.03	3.87	5.20	6.45	6.14	5.81
0.10	0.11	0.10	0.07	0.09	0.07	0.09	0.11	0.10	0.10
6.34	5.44	5.94	3.63	5.69	3.46	4.28	5.65	5.59	5.31
3.23	2.83	3.15	1.59	2.85	1.50	2.10	3.28	3.33	3.27
1.80	2.68	1.71	2.81	2.29	2.90	3.16	2.63	2.64	2.67
3.71	3.83	3.66	3.96	3.86	3.95	3.96	3.68	3.69	3.77
0.22	0.26	0.24	0.14	0.25	0.14	0.21	0.24	0.25	0.24
99.11	98.36	98.97	99.27	99.30	99.48	98.55	99.05	98.45	98.38
26	24	29	13	21	11	16	32	28	41
35	39	55	19	31	19	28	63	68	63
16	16	16	9	17	9	11	17	16	16
138	121	123	69	136	64	89	146	132	121
443	461	410	544	500	544	503	424	474	477
49	81	38	84	66	97	103	82	70	69
539	387	431	289	559	274	313	362	385	401
159	312	184	187	206	187	347	298	292	299
16	27	19	18	23	18	29	28	27	26
10	22	12	12	12	12	21	21	20	20
20	20	20	17	20	18	19	20	19	20
35	23	20	16	28	15	23	39	28	24
68	70	91	55	72	54	67	70	74	72
6	8	17	11	8	10	9	8	10	10
23	30	23	28	27	26	35	32	30	30
52	72	49	48	63	49	67	59	65	63
7	9	6	11	9	13	12	10	8	8
23.0	30.2	24.0	19.9	29.0	21.3	30.4	29.2	28.8	29.0

APPENDICES

Appendix A1. Argon isotope datasets.

Table A1. Zircon compositions.

Table A2. Compilation of bulk composition data.

ACKNOWLEDGEMENTS

This work was supported by National Science Foundation Graduate Research Fellowship Grant No. 1314109-DGE, and also by Grant Nos. EAR-1358514, 1358554, 1358401, 1358443, and 1101100 (Earthscope National Office). Any opinions, findings, and conclusions or recommendations expressed in this material are those of the authors and do not necessarily reflect the views of the National Science Foundation. Thanks to the Earthscope AGeS program for its support. A Geological Society of America graduate student research grant also supported this work. We deeply thank Don Swanson for providing his mapping and analytical data for inclusion in this project, and for discussion, guidance, and inspiration. We are grateful to reviewers Brian Jicha and Gary Michelfelder, whose insights improved this manuscript, and to Mike Garcia for attentive editorial handling. Thanks to the Washington State University GeoAnalytical Lab and Nansen Olson for support in sample preparation and data interpretation. We appreciate discussions and coordination with Daryl Gusey, including a tour of the Tieton andesite in summer 2016. We also appreciate discussions with Tom Sisson, Andy Calvert, Judy Fierstein, Wes Hildreth, and Daniel Heaton. William Otto, Nathan Van Cleave, Tommy Moore, Peter Davidson, Zoe Dilles, Marina Marcelli, and Nansen Olson provided essential support during field work in 2016 and 2017.

REFERENCES CITED

Bacon, C.R., Bruggman, P.E., Christiansen, R.L., Clynne, M.A., Donnelly-Nolan, J.M., and Hildreth, W., 1997, Primitive magmas at five Cascade volcanic fields: melts from hot, heterogeneous sub-arc mantle: The Canadian Mineralogist, v. 35, p. 397-423.

Barth, A.P., and Wooden, J.L., 2010, Coupled elemental and isotopic analyses of polygenetic zircons from granitic rocks by ion microprobe, with implications for melt evolution and the sources of granitic magmas: Chemical Geology, v. 277, no. 1, p.149-159.

Black, L.P., Kamo, S.L., Allen, C.M., Davis, D.W., Aleinikoff, J.N., Valley, J.W., Mundil, R., Campbell, I.H., Korsch, R.J., Williams, I.S., and Foudoulis, C., 2004, Improved 206Pb/238U microprobe geochronology by the monitoring of a trace-element-related matrix effect; SHRIMP, ID-TIMS, ELA-ICP-MS and oxygen isotope documentation for a series of zircon standards: Chemical Geology, v. 205, p. 115-140.

Bowles-Martinez, E., Bedrosian, P., Schultz, A., Hill, G.J., and Peacock, J., 2016, The Southern Washington Cascades magmatic system imaged with magnetotellurics: American Geophysical Union 2016 Fall Meeting, abstract GP41A-01.

Cande, S.C., and Kent, D.V., 1995, Revised calibration of the geomagnetic polarity timescale for the Late Cretaceous and Cenozoic: Journal of Geophysical Research, v. 100, no. B4, p. 6093-6095.

Channell, J.E.T., Mazaud, A., Sullivan, P., Turner, S., and Raymo, M.E., 2002, Geomagnetic excursions and paleointensities in the Matuyama Chron at Ocean Drilling Program Sites 983 and 984 (Iceland Basin): Journal of Geophysical Research, v. 107, no. B6, doi: 10.1029/2001JB000491

Claiborne, L.L., Miller, C.F., Flanagan, D.M., Clynne, M.A., and Wooden, J.L., 2010, Zircon reveals protracted magma storage and recycling beneath Mount St. Helens: Geology, v. 28, no. 11, p. 1011-1014, doi: 10.1130/G31285.1.

Clayton, G., 1980, Geology of the White Pass-Tumac Mountain Area, Washington: Washington Division of Geology and Earth Resources Open File Report no. 80-8.

Clayton, G., 1983, Geology of the White Pass Area, South-Central Cascade Range, Washington [M.S. thesis]: Seattle, University of Washington, 212 pp.

Clynne, M.A., Calvert, A.T., Edward, W.W., Evarts, R.C., Fleck, R.J., and Lanphere, M.A., 2008, The Pleistocene Eruptive History of Mount St. Helens, Washington, from 300,000 to 12,800 Years Before Present, *in* Sherrod, D., Scott, W.E., and Stauffer, P.H., eds., A Volcano Rekindled: The Renewed Eruption of Mount St. Helens, 2004-2006: U.S. Geological Survey Professional Paper 1750, p. 593-627.

Coble, M.A., Burgess, S.D., and Klemetti, E.W., 2017, New zircon (U-Th)/He and U/Pb eruption age for the Rockland tephra, western USA: Quaternary Science Reviews, v. 172, p. 109-117.

Colman, S.M., and Pierce, K.L., 1981, Weathering rinds on andesitic and basaltic stones as a Quaternary age indicator, western United States: U.S. Geological Survey Professional Paper 1210, 56 pp.

Conrey, R.M., Sherrod, D.R., Hooper, P.R., and Swanson, D.A., 1997, Diverse primitive magmas in the Cascade arc, northern Oregon and southern Washington: The Canadian Mineralogist, v. 35, p. 367-396.

Conrey, R.M., Hooper, P.R., Larson, P.B., Chesley, J., and Ruiz, J., 2001, Trace-element and isotopic evidence for two kinds of crustal melting beneath a high Cascades volcanic center: Contributions to Mineralogy and Petrology, v. 141, p. 710-732.

Conrey, R.M., Taylor, E.M., Donnelly-Nolan, J.M., and Sherrod, D.R., 2002, North-central Oregon Cascades: Exploring petrologic and tectonic intimacy in a propagating intra-arc rift: Field Guide to geologic processes in Cascadia: Oregon Department of Geology and Mineral Industries Special Paper 36.

Conrey, R.M., Grunder, A.L., and Schmidt, M.E., 2004, SOTA Field trip guide—State of the Cascade Arc: Stratocone persistence, mafic lava shields, and pyroclastic volcanism associated with intra-arc rift propagation: Oregon Department of Geology and Mineral Industries Open-File Report O-04-04, 40 p.

Crandell, D.R., 1987, Deposits of pre-1980 pyroclastic flows and lahars from Mount St. Helens, Washington: U.S. Geological Survey Professional Paper 1444, 91 p.

Crowley, J.L., Schoene, B., and Bowring, S.A., 2007, U-Pb dating of zircon in the Bishop Tuff at the millennial scale: Geology, v. 35, no. 12, p. 1123-1126, doi: 10.1130/G24017A.1

de Bremond d'Ars, Jaupart, C., and Sparks, R.S.J., 1995, Distribution of volcanoes in active margins: Journal of Geophysical Research, v. 100, p. 20421–20432, doi: 10.1029/95JB02153

Defant, M.J., and Drummond, M.S., 1993, Mount St. Helens: Potential example of the partial melting of the subducted lithosphere in a volcanic arc: Geology, v. 21, p. 547-550.

Dethier, D.P., 1988, The soil chronosequence along the Cowlitz River, Washington: U.S. Geological Survey Bulletin 1590-F, p. F1-F47.

DiGiulio, J., 2016, Reconstructing the physical record of a four-million-year volcanic system: Geochemistry, thermobarometery and geologic map of the Mount Jeffereson area, Oregon [M.S. thesis]: Oregon State University, 119 p.

Ellingson, J.A., 1968, Late Cenozoic Volcanic Geology of the White Pass–Goat Rocks area, Cascade Mountains, Washington [Ph.D. dissertation]: Pullman, Washington State University, 112 p.

Evarts, R.C., Clynne, M.A., Fleck, R.J., Lanphere, M.A., Calvert, A.T., and Sarna-Wojcicki, A.M., 2003, The Antiquity of Mount St. Helens and Age of the Hayden Creek Drift, Geological Society of America 2003 Annual Meeting, paper no. 33-8.

Evarts, R.C., 2005, Geologic map of the Amboy quadrangle, Clark and Cowlitz counties, Washington: U.S. Geological Survey Scientific Investigations Map 2885, 1 sheet, 26 p. text.

Gans, P.B., Mahood, G.A., and Schermer, E., 1989, Synextensional magmatism in the Basin and Range Province; a case study from the eastern Great Basin: Geological Society of America Special Papers, v. 233, p. 1-53.

Gill, J. B., 1981, Orogenic andesites and plate tectonics: Berlin, Springer Verlag, 390p.

Grunder, A.L., Klemetti, E.W., Feeley, T.C., and McKee, C.M., 2006, Eleven million years of arc volcanism at the Aucanquilcha Volcanic Cluster, northern Chilean Andes: implications for the life span and emplacement of plutons: Transactions of the Royal Society of Edinburgh: Earth Sciences, v. 97, p. 415-436.

Guffanti, M., and Weaver, C.S., 1988, Distribution of late Cenozoic volcanic vents in the Cascade Range: Volcanic arc segmentation and regional tectonic considerations: Journal of Geophysical Research, v. 93, p. 6513-6529.

Gusey, D.L., Hammond, P.E., and Lasher, J.P., this volume, Field volcanology with geochemistry of Tieton Andesite and other Quaternary lavas, Bear Creek Mtn to Yakima, south-central Washington state. Geological Society of America Special Volume.

Hammond, P.E., 2017, Geologic map of the northern portions of the Rimrock Lake, Tieton Basin, and western two-thirds of the Weddle Canyon 7.5-minute quadrangles, Yakima County, Washington: Washington Geological Survey Map Series 2017-03, scale 1:24,000, 1 sheet, 19 p. text.

Hildreth, W., 2007, Quaternary Magmatism in the Cascades: Geologic Perspectives: U.S. Geological Survey Professional Paper 1744, 125 pp.

Hildreth, W., and Fierstein, J., 2015, Geologic Map of the Simcoe Mountains Volcanic Field, Main Central Segment, Yakama Nation, Washington: U.S. Geological Survey Scientific Investigations Map 3315, scale 1:24,000, 3 sheets, 76 p. text.

Hildreth, W., and Fierstein, J., 1997, Recent eruptions of Mount Adams, Washington Cascades, USA: Bulletin of Volcanology, v. 58, p. 472-490, doi:10.1007/s004450050156.

Hildreth, W., and Fierstein, J., 1995, Geologic map of the Mount Adams volcanic field, Cascade range of Southern Washington: U.S. Geological Survey Map I-2460, scale 1:50,000, 2 sheets, 39 p. text.

Hildreth, W., and Lanphere, M.A., 1994, Potassium-argon geochronology of a basalt-andesite-dacite arc system: The Mount Adams volcanic field, Cascade Range of southern Washington: Geological Society of America Bulletin, v. 106, p. 1413-1429.

Hildreth, W., and Moorbath, S., 1988, Crustal contributions to arc magmatism in the Andes of central Chile: Contributions to Mineralogy and Petrology, v. 98, p. 455-489.

Hill, G.J., Caldwell, T.G., Heise, W., Chertkoff, D.G., Bibby, H.M., Burgess, M.K., Cull, J.P., and Cas, R.A.F., 2009, Distribution of melt beneath Mount St Helens and Mount Adams inferred from magnetotelluric data: Nature Geoscience, v. 2, p. 785-789.

Horng, C.-S., Lee, M.-Y., Pälike, H., Wei, K.-Y., Liang, W.-T., Iizuka, Y., and Torii, M., 2002, Astronomically calibrated ages for geomagnetic reversals within the Matuyama chron: Earth Planets Space, v. 54, p. 679-690.

Hughes, S.S., and Taylor, E.M., 1986, Geochemistry, petrogenesis, and tectonic implications of central High Cascade mafic platform lavas: Geological Society of America Bulletin, v. 97, p. 1024-1036.

Ireland, T.R., and Williams, I.S., 2003, Considerations in zircon geochronology by SIMS: Reviews in Mineralogy and Geochemistry, v. 53, p. 215-241.

Jicha, B.R., Johnson, C.M., Hildreth, W., Beard, B.L., Hart, G.L., Shirey, S.B., and Singer, B.S., 2009, Discriminating assimilants and decoupling deep- vs. shallow-level crystal records at Mount Adams using 238U– 230Th disequilibria and Os isotopes: Earth and Planetary Science Letters, v. 277, no. 1, p. 38-49.

Jicha, B. R., and Singer, B.S., 2006, Volcanic history and magmatic evolution of Seguam Island, Aleutian Island arc, Alaska: GSA Bulletin, v. 118, no. 7-8, p. 805–822, doi: https://doi.org/10.1130/B25861.1.

Johnson, D.M., Hooper, P.R., and Conrey, R.M., 1999, XRF analysis of rocks and minerals for major and trace elements on a single low dilution Li-tetraborate fused bead: Advances in X-ray Analysis, v. 41, p. 843-867.

Kelly, D., 2016, Estimation of analytical error for major, minor and trace elements analyzed by X-ray fluorescence at the Peter Hooper GeoAnalytical Laboratory, Washington State University: Geological Society of America Abstracts with Programs, v. 48, no. 7, doi: 10.1130/abs/2016AM-284288.

Koppers, A. A. P., 2002, ArArCALC—Software for 40Ar/39Ar age calculations: Computers and Geosciences, v. 28, p. 605–619 (Available at http://earthref.org/tools/ararcalc.htm).

Koppers, A.A.P., Staudigel, H., Pringle, M.S. and Wijbrans, J.R., 2003, Short-lived and discontinuous intraplate volcanism in the South Pacific: Hot spots or extensional volcanism?: Geochemistry Geophysics Geosystems, v. 4, doi: 10.1029/2003GC000533.

Korosec, M.A., 1989, New K-Ar age dates, geochemistry, and stratigraphic data for the Indian Heaven Quaternary volcanic field, south Cascade Range, Washington: Washington Division of Geology and Earth Resources Open-File Report 89-3, 42 p.

Kuiper, K.F., Deino, A., Hilgen, F.J., Krijgsman, W., Renne, P.R., and Wijbrans, J.R., 2008, Synchronizing rock clocks of Earth history: Science, v. 320, p. 500-504.

Laj, C., and Channell, J.E.T., 2007, Geomagnetic excursions, *in* Kono, M., ed., Treatise on Geophysics, Volume 5, Geomagnetism: Amsterdam, Elsevier, p. 373-416.

LeBas, M.J., Lemaitre, R.W., Streckeisen, A., and Zanettin, B., 1986, A chemical classification of volcanic-rocks based on the total alkali silica diagram: Journal of Petrology, v. 27, no. 3, p. 745-750.

Leeman, W.P., Smith, D.R., Hildreth, W., and Palacz, Z., and Rogers, N., 1990, Compositional diversity of Late Cenozoic basalts in a transect across the southern Washington Cascades: Implications for subduction zone magmatism, J. Geophys. Res., 95(B12), 19561-19582, doi:10.1029/JB095iB12p19561.

Leeman, W.P., Lewis, J.F., Evarts, R.C., Conrey, R.M., and Streck, M.J., 2005, Petrologic constraints on the thermal structure of the Cascades arc: Journal of Volcanology and Geothermal Research, v. 140, p. 67-105.

Lisiecki, L.E., and Raymo, M.E., 2005, A Pliocene-Pleistocene stack of 57 globally distributed benthic $\delta^{18}O$ records: Paleoceanography, v. 20, PA1003, doi: 10.1029/2004PA001071

Longo, A.L., Dilles, J.H., Grunder, A.L., and Duncan, R., 2010, Evolution of Calc-Alkaline Volcanism and Associated Hydrothermal Gold Deposits at Yanacocha, Peru: Economic Geology, v. 105, no. 7, doi: 10.2113/econgeo.105.7.1191.

Lund, S.P., Stoner, J.S., Channell, J.E.T., and Acton, G., 2006, A summary of Brunhes paleomagnetic field variability recorded in ODP Cores: Physics of the Earth and Planetary Interiors, v. 156, p. 194-204.

Mahon, K.I., 1996, The new “York” regressions: applications of an improved statistical method to geochemistry: International Geology Review, v. 38, p. 293-303.

Matthews, N.E., Vazquez, J.A., and Calvert, A.T., 2015, Age of the Lava Creek supereruption and magma chamber assembly at Yellowstone based on $^{40}Ar/^{39}Ar$ and U-

Pb dating of sanidine and zircon crystals: Geochemistry, Geophysics, Geosystems, v. 16, p. 2508-2528, doi:10.1002/2015GC005881.

Michalk, D.M., Böhnel, H.N., Nowaczyk, N.R., Aguírre-Diaz, G.J., López-Martínez, M., Ownby, S., and Negendank, J.F.W., 2013, Evidence for geomagnetic excursions recorded in Brunhes and Matuyama Chron lavas from the trans-Mexican volcanic belt: Journal of Geophysical Research: Solid Earth, v. 118, p. 2648-2669, doi:10.1002/jgrb.50214.

Michelfelder, G.S., Feeley, T.C., Wilder, A.D., and Klemetti, E.W., 2013, Modification of the continental crust by subduction zone magmatism and vice-versa: Across-strike geochemical variations of silicic lavas from individual eruptive centers in the Andean Central Volcanic Zone: Geosciences, v. 3, no. 4, p. 633-667, doi:10.3390/geosciences3040633.

Miller, R.B., 1989, The Mesozoic Rimrock Lake inlier, southern Washington Cascades: Implications for the basement to the Columbia Embayment: Geological Society of America Bulletin, v. 101, p. 1289-1305.

Min, K.W., Mundil, R., Renne, P.R., and Ludwig, K.R., 2000, A test for systematic errors in Ar-40/Ar-39 geochronology through comparison with U/Pb analysis of a 1.1-Ga rhyolite: Geochimica et Cosmochimica Acta, v. 64, no. 1, p. 73-98, doi: 10.1016/S0016-7037(99)00204-5.

Mitchell, R.J., Jaeger, D.J., Diehl, J.F., and Hammond, P.E., 1989, Paleomagnetic results from the Indian Heaven volcanic field, south-central Washington: Geophysical Journal, v. 97, p. 381-390.

Mullen, E.K., Weis, D., Marsh, N.B., and Martindale, M., 2017, Primitive arc magma diversity: New geochemical insights in the Cascade Arc: Chemical Geology, v. 448, p. 43-70.

Mullineaux, D.R., and Crandell, D.R., 1981, The eruptive history of Mount St. Helens, *in* Lipman, P.W., and Mullineaux, D.R., eds., The 1980 eruptions of Mount St. Helens, Washington: Washington, D.C., U.S. Geological Survey Professional Paper 1250, p. 3-15.

Ownby, S., Granados, H.D., Lange, R.A., and Hall, C.M., 2007, Volcán Tancítaro, Michoacán, Mexico, $^{40}Ar/^{39}Ar$ constraints on its history of sector collapse: Journal of Volcanology and Geothermal Research, v. 161, p. 1-14, doi:10.1016/j.jvolgeores.2006.10.009.

Peter Hooper GeoAnalytical Lab, ICP-MS Method: Trace Element Analyses of Rocks and Minerals by ICP-MS: http://cahnrs.wsu.edu/soe/facilities/geolab/technotes/icp-ms_method/ (May 2017).

Russell, I.C., 1893, A geological reconnoissance in Central Washington: Bulletin of the United States Geological Survey, no. 108, 108 p.

Savant, S., and de Silva, S. L., 2005, A GIS-based spatial analysis of volcanoes in the Central Andes: Insights into factors controlling volcano spacing: American Geophysical Union 2005 Fall Meeting, abstract no. V21D-0648.

Sawlan, M.G., 2018, Alteration, mass analysis, and magmatic compositions of the Sentinel Bluffs Member, Columbia River flood basalt province: Geosphere, v. 14, no. 1, p. 286-303, doi:10.1130/GES01188.1.

Schaltegger, U., Schmitt, A.K., and Horstwood, M.S.A., 2015, U-Th-Pb zircon geochronology by ID-TIMS, SIMS, and laser ablation ICP-MS: Recipes, interpretations, and opportunities: Chemical Geology, v. 402, p. 89-110.

Schärer, U., 1984, The effect of initial ^{230}Th disequilibrium on young U-Pb ages: The Makalu case, Himalaya. Earth and Planetary Science Letters, v. 67, p. 191-204.

Schmidt, M.E., Grunder, A.L., and Rowe, M.C., 2008, Segmentation of the Cascade Arc as indicated by Sr and Nd isotopic variation among diverse primitive basalts: Earth and Planetary Science Letters, v. 266, p. 166–181, doi: 10.1016/j.epsl.2007.11.013.

Scott, W.E., and Gardner, C.A., 2017, Field-Trip Guide to Mount Hood, Oregon, Highlighting Eruptive History and Hazards: U.S. Geological Survey Scientific Investigations Report 2017-5022-G, 115 p.

Scott, W.E., Gardner, C.A., Sherrod, D.R., Tilling, R.I., Lanphere, M.A., and Conrey, R.M., 1997, Geologic History of Mount Hood Volcano, Oregon—A Field-trip Guidbook: U.S. Geological Survey Open-File Report 97-263, 36 p.

Shen W., M. H. Ritzwoller, and V. Schulte-Pelkum (2013), A 3-D model of the crust and uppermost mantle beneath the Central and Western US by joint inversion of receiver functions and surface wave dispersion, J. Geophys. Res. Solid Earth, 118, 262–276.

Sherrod, D.R., and Scott, W.E., 1995, Preliminary geologic map of the Mount Hood 30- by 60-minute quadrangle, Northern Cascade Range, Oregon: U.S. Geological Survey Open-File Report 95-219, 36 p., 1 plate.

Singer, B.S., Hoffman, K.A., Chauvin, A., Coe, R.S., and Pringle, M.S., 1999, Dating transitionally magnetized lavas of the late Matuyama Chron: Toward a new ^{40}Ar/^{39}Ar timescale of reversals and events: Journal of Geophysical Research, v. 104, no. B1, p. 679-693.

Singer, B.S., Hoffman, K.A., Schnepp, E., and Guillou, H., 2008, Multiple Brunhes Chron excursions recorded in the West Eifel (Germany) volcanics: Support for long-held mantle control over the non-axial dipole: Physics of the Earth and Planetary Interiors, v. 169, p. 28-40, doi:10.1016/j.pepi.2008.05.001.

Sisson, T.W., Salters, V.J.M., and Larson, P.B., 2014, Petrogenesis of Mount Rainier andesite: Magma flux and geologic controls on the contrasting differentiation styles at stratovolcanoes of the southern Washington Cascades: GSA Bulletin, v. 126, no. ½, p. 122-144, doi: 10.1130/B30852.1.

Sisson, T.W., Vallance, J.W., and Pringle, P.T., 2001, Progress made in understanding Mount Rainier's hazards: Eos, v. 82, no. 9, p. 113, 118-120.

Smith, G.O., 1903, Description of the Ellensburg Quadrangle, Washington: U.S. Geological Survey Atlas, Folio 86, 7 p.

Smith, D., and Leeman, W., 1987, Petrogenesis of Mount St. Helens dacitic magmas: Journal of Geophysical Research, v. 92, no. 10, p. 10,313-10,334.

Stacey, J., and Kramers, J.D., 1975, Approximation of terrestrial lead isotope evolution by a two-stage model: Earth and Planetary Science Letters, v. 26, p. 207–221.

Stanley, W.D., Mooney, W.D., and Fuis, G.S., 1990, Deep crustal structure of the Cascade range and surrounding regions from seismic refraction and magnetotelluric data: Journal of Geophysical Research, v. 95, no. B12, p. 19,419-19,438.

Steenberg, L., Boroughs, S., and Knaack, C., 2017, Estimation of accuracy and precision for trace elements analyzed by inductively coupled plasma mass spectrometry (ICP-MS) at the Peter Hooper GeoAnalytical Laboratory, Washington State University: Geological Society of America Abstracts with Programs, v. 49, no. 6, doi: 10.1130/abs/2017AM-307211.

Swanson, D.A., 1966, Tieton Volcano, a Miocene Eruptive Center in the Southern Cascade Mountains, Washington: Geological Society of America Bulletin, v. 77, p. 1293-1314.

Swanson, D.A., 1978, Geologic map of the Tieton River area, Yakima County, south-central Washington: U.S. Geological Survey Miscellaneous Field Studies Map 968, scale 1:48,000.

Swanson, D.A., 1996a, Geologic map of the Hamilton Buttes quadrangle, southern Cascade Range, Washington: U.S. Geological Survey Open File Report 96-0016, 29 p., 2 plates.

Swanson, D.A., 1996b, Geologic map of the Packwood Lake quadrangle, southern Cascade Range, Washington: U.S. Geological Survey Open File Report 96-704, 25 p., 2 plates.

Swanson, D.A., and Clayton, G.A., 1983, Generalized geologic map of the Goat Rocks Wilderness and Roadless Areas (6036, Parts A, C, and D), Lewis and Yakima Counties, Washington: U.S. Geological Survey Open-File Report 83-357.

Tamura, Y., Tatsumi, Y., Zhao, D. Kido, Y and Shukuno, H., 2001, Distribution of Quaternary volcanoes in the Northeast Japan arc; geologic and geophysical evidence of hot fingers in the mantle wedge: Proceedings of the Japanese Academy, v. 77, p. 135-139.

Taylor, J. R., 1997, An Introduction to Error Analysis: The Study of Uncertainties in Physical Measurements, 2nd edition: Sausalito, California, Univ. Sci. Books, 327 p.

Trehu, A.M., Asudeh, I., Brocher, T.M., Luetgert, J.H., Mooney, W.D., Nabelek, J.L., and Nakamura, Y., 1994, Crustal architecture of the Cascadia forearc: Science, v. 266, p. 237-243.

Vazquez, J.A., and Lidzbarski, M.I., 2012, High-resolution tephrochronology of the Wilson Creek Formation (Mono Lake, California) and Laschamp event using ^{238}U-^{230}Th SIMS dating of accessory mineral rims: Earth and Planetary Science Letters, v. 357-358, p. 54-67.

Walker, B.A., Klemetti, E.W., Grunder, A.L., Dilles, J.H., Tepley, F.J., and Giles, D., 2012, Crystal reaming during the assembly, maturation, and waning of an eleven-million-year crustal magma cycle: thermobarometry of the Aucanquilcha Volcanic Cluster: Contributions to Mineralogy and Petrology, v. 165, no. 4, p. 663-682.

Walker, G.P.L., 2000, Basaltic volcanoes and volcanic systems *in* Sigurdsson, H., Houghton, B.F., McNutt, S.R., Rymer, H., and Stix, J., eds., Encyclopedia of Volcanoes: San Diego, California, Academic Press, p. 283-289.

Wells, R., Bukry, D., Friedman, R., Pyle, D., Duncan, R., Haeussler, P., and Wooden, J., 2014, Geologic history of Siletzia, a large igneous province in the Oregon and Washington Coast Range: Correlation to the geomagnetic polarity time scale and implications for a long-lived Yellowstone hotspot: *Geosphere*, v. 10, no. 4, p. 692-719, doi: https://doi.org/10.1130/GES01018.1

Wells, R.E., and McCaffrey, R., 2013, Steady rotation of the Cascade arc: Geology, v. 41, n. 9, p. 1027-1030.

Wells, R.E., Weaver, C.S., and Blakely, R.J., 1998, Forearc migration in Cascadia and its neotectonic significance: Geology, v. 26, p. 758-762.

Wise, W.S., 1969, Geology and petrology of the Mt. Hood area: A study of High Cascade volcanism: Geological Society of America Bulletin, v. 80, p. 969-1006.

York, D., 1969, Least squares fitting of a straight line with correlated errors: Earth and Planetary Science Letters, v. 5, p. 320–324.

CHAPTER 2 - LOCATION, DURATION, AND COMPOSITION OF VOLCANISM OVER THE THREE MILLION YEAR LIFESPAN OF THE GOAT ROCKS VOLCANIC COMPLEX, SOUTHERN WASHINGTON CASCADES

ABSTRACT

The Goat Rocks volcanic complex is a long-lived, dominantly andesitic to dacitic major arc volcanic center that was active between 3.1 Ma and 0.1 Ma—predating and overlapping the lifespans of nearby stratovolcanoes of the Cascade Arc. New $^{40}Ar/^{39}Ar$ ages confirm that the first composite volcano of the complex, the Tieton Peak volcano, began erupting at 3.1 Ma (shortly following the 3.2 Ma Devils Horns rhyolite eruption) and was active until at least 2.7 Ma. An early Pleistocene (2.1 Ma) lava and tephra sequence is identified on the ridge dividing Walupt Creek and Huckleberry Creek; like the andesite of Lost Lake (2.3 Ma), its source is not known, but a vent is suspected near the Huckleberry Creek drainage. New ages indicate overlap between the subsequent eruptive periods of Bear Creek Mountain, Lake Creek volcano, and Old Snowy Mountain. Compositional trends suggest that the several volcanoes built during that ~1.5 m.y. period were fed by one continuously active magma reservoir complex. New paleomagnetic (ChRM) analyses for lava flow sequences near Tieton Peak, Goat Lake, and Hogback Mountain help to clarify the ages and eruption frequency of those units. The longevity of this volcanic system brings perspective to the potential lifespans and life cycles of major arc volcanoes, the plutonic-volcanic connection, and the flux and distribution of melt at volcanic arcs.

INTRODUCTION

Timescales of volcanic activity are an integral component to understanding magmatic processes, mantle and crustal dynamics, and predicting future eruptive behavior. It is well documented that individual arc volcanoes have a common life cycle on the order of 10^5-10^6 years (see for example geochronologic data for the Cascade Arc, Hildreth, 2007; the Lesser Antilles Arc, Hatter et al., 2018; or the Central Andes, Grunder et al., 2008). Various mechanisms have been proposed to explain this observation, including “bottom-up” controls such as diapiric ascent of partially molten material through the mantle wedge (e.g. Hall and Kincaid, 2001), and “top-down” controls such as magma reservoir size and depth or edifice size on capturing dikes, stabilizing magma residence, or preventing eruption of magma (Muller et al., 2001; Karlstrom et al., 2009, 2010; Pinel et al., 2010; Roman and Jaupart, 2014; Pansino and Taisne, 2019). However, questions remain regarding the longer term periodicity of activity at volcanic arcs.

Intermediate magmas tend to focus at nodes along an arc, building new volcanoes in close proximity to extinct edifices, rather than distributing randomly along the arc. This indicates development of preferred transcrustal pathways for magma. For many arc volcanoes, ancestral precursors to the modern edifice are poorly dated due to lack of exposure (cover by the more recent deposits) or erosion, or perhaps because the history of those ancestral volcanoes is not as directly relevant to eruption forecasting. The work presented here on the Goat Rocks volcanic complex is an attempt to characterize the complete long-term lifespan of andesitic activity which recurred in the same area through several stages and multiple edifices. In a similar case study, Grunder and others (2008) showed that the Aucanquilcha Volcanic Complex in the Central Andes, which consists of at least 19 volcanoes within a ~700 km^2 area, was frequently active over 11 million years. Several unique factors may have contributed to that exceedingly long episode of volcanism, but it begs the question, what is the range of lifespans for major arc volcanic loci?

In the Cascade Volcanic Arc, several active volcanoes are built atop or very close to precursor volcanoes. In the Mount Hood area, the extinct andesite volcano of Lookout Mountain is approximately 14 km east of the modern edifice and was active at ~3.1 Ma (Wise, 1969; Sherrod and Scott, 1995), and potentially several other pre-Hood vents including the Sandy Glacier volcano were located within a few km of the present summit and active between 1.5 and 0.6 Ma (Keith et al., 1985; Sherrod and Scott, 1995; Scott et al., 1997; Hildreth, 2007; Scott and Gardner, 2017). Near Mount Rainier, possibly juvenile clasts in the Lily Creek formation and lava flows at Panhandle Gap and Glacier Basin have ages between 1.4-1.0 Ma, while construction of the modern edifice began at around 600 ka (Sisson and Calvert, 2017, written communication). In the Goat Rocks area, previous workers documented that several episodes of andesitic-dacitic activity followed a major rhyolitic eruption at 3.2 Ma and continued into the Pleistocene (Ellingson, 1968; Clayton, 1983; Swanson and Clayton, 1983; Swanson, 1996a,b). Owing to a delicate balance of vent migration and enough-but-not-too-much erosion, much of the Goat Rocks eruptive history is accessible for reconstruction.

For this dissertation, I dated 39 samples from at least 13 vents in the Goat Rocks area (including the andesitic complex as well as peripheral mafic centers) in hopes of answering questions like: What was the total duration of andesitic activity? For how long was each individual volcano active? Were the volcanoes distributed periodically in time, or did coeval activity occur at multiple vents? The answers to these questions bear weight on our understanding of the structure and longevity of transcrustal magmatic systems. Geochronology also provides the temporal framework for understanding how (and why) compositions of volcanic products evolved over time (addressed in more detail in chapters 3 and 4).

Select geochronological (and geochemical) results were presented in Chapter 1 and published in Wall et al. (2018), laying the groundwork for the definition of the volcanic complex and eruptive stages. A more detailed chronology is presented here and is intended to support a U.S. Geological Survey map and report (to be drafted with Donald Swanson). In Chapter 1, the duration of activity comprising the Goat Rocks volcanic complex was estimated at ~2.5 to 2.9 million years, based on radiometric ages of thirteen samples (dominantly from the younger eruptive stages) and the magnetic polarity of the Tieton Peak lava flows (normal polarity, so presumed late Gauss chron; Swanson, unpublished field notes; Wall et al., 2018). Here, I confirm the Gauss chron age of Tieton Peak and Devils Washbasin lava flows as well as the Miriam Creek basalts underlying the Hogback Mountain volcano. While the sequence of andesitic lava flows in the Conrad Creek basin south of Tieton Peak were previously of uncertain age and relation to the local Tieton Peak pile, a new age of 3.08 ± 0.01 Ma on a lava flow from that area suggests that all were emplaced following the 3.2 Ma Devils Horns rhyolite eruption. More work could be done between Tieton Peak and Gilbert Peak to better unravel that stratigraphy. Regardless, the oldest Tieton Peak andesite (~3.1 Ma) and the Clear Fork Lava Flow (~100 ka) span approximately three million years of intermediate volcanism. An early Pleistocene age (~2.1 Ma) was determined for an olivine andesite lava flow on the ridge north of Lakeview Mountain that separates Lewis County and Yakima County (here referred to as “Countyline Ridge”), similar to the ~2.3 Ma Lost Lake andesite. Importantly, new ages from Bear Creek Mountain and the southwestern flank of the Lake Creek volcano narrow the gaps between the Bear Creek Mountain, Lake Creek, and Old Snowy Mountain eruptive stages. Thus, I interpret the volcanoes of these eruptive stages as migrating vents connected to one long-lived (~1.5 m.y.), complex magmatic system, as opposed to distinct magmatic episodes, as was assumed based on the limited dating in Chapter 1.

Whether the ~3 m.y. life cycle of the Goat Rocks volcanic complex may be considered representative of other Cascade (or other arc) volcanoes, or stands out as an uncommonly persistent magmatic locus, remains to be determined. This author hopes that more research will be conducted on the deeper histories of neighboring Cascade volcanoes to reach a more complete understanding of the spectrum of behavior of arc volcanoes and the inner workings of volcanic arcs.

In following sections, I present a summary of the geologic history of the Goat Rocks/White Pass area, an updated volcanic timeline for the Goat Rocks volcanic complex based on new $^{40}Ar/^{39}Ar$ age determinations and paleomagnetic analyses, and will describe how compositions evolved through time (with detailed investigations on that matter to follow in Chapters 3 and 4).

GEOLOGIC SETTING

The Goat Rocks volcanic complex, and nearby Pleistocene volcanoes of the White Pass area, are the latest installment of a ~55-million-year saga of volcanism in southwestern Washington. Atop Mesozoic accreted terranes, basaltic volcanism related to the Challis magmatic episode formed the sequence of Summit Creek basalts from ~55 to 42 Ma. Volcanic quiescence, subsidence, and sedimentary deposition dominated for ~10 m.y., then volcanic activity resumed by ~32 Ma to mark the beginning of the Cascade Arc. The earliest arc products, erupted in a dominantly subaqueous environment, generated the Ohanapecosh Formation (~32-26 Ma). The Fifes Peak stage followed, which included the caldera-forming eruption of Mount Aix north of White Pass, the construction of the andesitic Tieton Volcano east of Rimrock Lake, and the andesitic to basaltic Angry Mountain volcano, remnants of which underlie the western flanks of the Goat Rocks complex. Interestingly, there are few examples of magmatism in the Goat Rocks area between the end of the Fifes Peak Formation (early to mid Miocene) and the onset of Goat Rocks-era volcanism in the late Pliocene. These geologic periods are described in more detail below.

Rimrock Lake inlier (Mesozoic)

The Rimrock Lake inlier is a ~260 km^2 dome-like uplift of north-northwest-trending belts of metamorphosed plutonic rocks and mélange, separated by steep faults, that crops out in the White Pass-Rimrock Lake area, underlying the eastern side of the Goat Rocks volcanic complex (Miller, 1989; Clayton, 1983; Swanson and Clayton, 1983; Gusey et al., 2018). The two units that comprise the inlier are: 1) the Late Jurassic Indian Creek complex, consisting of trondhjemitic to gabbroic rocks that probably represent the roots of an ancient volcanic arc, and 2) the Late Jurassic to Early Cretaceous Russell Ranch complex, a tectonic mélange consisting of mainly arkose and mudstone, with subordinate chert, conglomerate, pillowed greenstone (compositionally like MORB or within-plate-tholeiite), and tuff (Miller, 1989).

Based on steep, likely strike-slip faulting bounding the units in the inlier, and tectonic reconstructions suggesting major dextral translation during the Late Cretaceous and early Cenozoic, it is interpreted that considerable tectonic displacement occurred to bring the Indian Creek and Russell Ranch complexes together, as opposed to the Indian Creek representing the basement beneath or the source of Russell Ranch sediments (Engebretson et al., 1985; Miller, 1989). The two complexes are broadly age correlative and from similar settings as other arc plutonic rocks and mélange belts exposed in the northern Cascades and Puget sound areas, as well as units in the Klamath Mountains and California Coast Ranges (Miller, 1989).

Summit Creek basalt (Eocene)

Stratigraphically overlying the Rimrock Lake inlier basement rocks are the Eocene Summit Creek basalts. Vance et al. (1987) describe a 2000-m-thick unit cropping out in the canyon of Summit Creek, northwest of White Pass, consisting of dense, sparsely phyric subaerial basalt flows and lesser interbeds of silicic tuff and clastic/volcaniclastic sediments. A correlating sequence about 450 m thick occurs within the footprint of the Goat Rocks volcanic complex, in the vicinity of Tieton Pass and the headwaters of the North Fork Tieton River (Vance et al., 1987; Swanson, unpublished mapping).

Vance et al. (1987) report the following ages for the Summit Creek basalt unit: 1) 55 ± 3 Ma, U-Pb model age, for zircon from an ash-flow tuff interbed near the base of the Summit Creek section; 2) Fission-track ages of ~46 Ma and ~44 Ma for two silicic ash-flow tuffs south of Summit Creek and on strike with the upper part of the basalt section; and 3) Fission-track age of ~42 Ma for a thin, quartz-phyric vitric tuff immediately above the basalt section near Tieton Pass. In summary, the Summit Creek basalts were erupted between approximately 55 and 42 Ma. These basalts are associated with strike-slip faulting and other regional magmatism during the Eocene that predates initiation of the Cascade volcanic arc (Tabor et al., 2000). Specifically, Vance et al. (1987) consider the Summit Creek episode, as well as other age-correlative Eocene volcanism in Washington (including the Puget Group, Taneum, Teanaway, and Naches volcanism), to be the westernmost expression of Challis magmatism (~53-42 Ma; Armstrong, 1978) which produced scattered calc-alkaline volcanic and shallow plutonic activity across southern British Columbia, Washington, Idaho, and northeastern Oregon.

Summit Creek and Chambers Creek sandstone (Eocene)

Following the Summit Creek basalt episode, local volcanism was apparently quiescent for as long as ~10 m.y. while fluvial and lacustrine sediments were deposited in a subsiding basin. In Summit Creek Canyon, a 750-m-thick unit of fluvial arenites (called “Summit Creek sandstone” by Ellingson, 1959, 1972) conformably overlies the basalt pile there (Vance et al., 1987). The sandstone thins rapidly south of Summit Creek and is absent in the Eocene section near Tieton Pass, but correlative sedimentary deposits, the Chambers Creek beds, comprise much of the basement on the southwest side of Goat Rocks (e.g. along Johnson Creek and namesake Chambers Creek, Winters, 1984; Vance et al., 1987; Swanson, 1996a). In the Summit Creek section, the top of this sedimentary unit grades conformably upward into andesitic and dacitic volcaniclastic sediments that mark the onset of the Cascade Arc (Vance et al., 1987).

Ohanapecosh Formation (Oligocene)

By ~32 Ma, Cascade Arc volcanism had commenced with the accumulation of the extensive and voluminous Ohanapecosh Formation. The Ohanapecosh deposits are dominantly intermediate (andesitic and dacitic, lesser basalt, rare rhyolite) and volcaniclastic (lesser lava flows, shallow intrusions, scoria, and sedimentary interbeds; Fiske et al., 1963; Jutzeler et al., 2014). The Ohanapecosh Formation was first described by Fiske et al. (1963) as comprising much of the basement beneath Mount Rainier and in the vicinity of Ohanapecosh Hot Springs. Later, researchers interpreted similar Oligocene volcaniclastic deposits occurring more distally, including in the Goat Rocks area, to be correlative with the Ohanapecosh Formation (e.g. Vance et al., 1987; Tabor et al., 2000; Swanson, 1996b).

The Ohanapecosh deposits were initially interpreted by Fiske et al. (1963) and Fiske (1963) as subaqueous explosive volcanic products. Some debate ensued about the depositional environment (see, for example, Vance et al., 1987), considering such factors as locally abundant andesitic lava flows without pillows, distribution of pumice throughout tuff beds rather than strong sorting or grading, and abundance of accretionary lapilli. Jutzeler et al. (2014) explain that many of these features do not preclude a subaqueous environment; for example, pumice can be quickly waterlogged or already denser than water, and accretionary lapilli formed in a subaerial environment can be robust enough to survive sedimentation in water. These authors argue that while many of the source volcanoes were likely subaerial (either occurring around the edges of a basin, or forming islands), the characteristics of the Ohanapecosh Formation *sensu stricto* (i.e. in the type locale between Mount Rainier and Goat Rocks) indicate a subaqueous, below wave base, low-energy environment, such as within a continental basin. The source vents remain largely elusive: Fiske et al. (1963) suppose that the Sarvent lava complex (including the spectacular South Cowlitz Chimney) may represent vent deposits; Jutzeler et al. (2014) do not address that idea, but suggest the pre-caldera Mount Aix volcano as a possible source. Near White Pass, remnants of a small basaltic scoria cone include shallow intrusions of vesicular basalt and beds of basaltic scoria breccia (Jutzeler et al., 2014).

U-Pb ages (by LA-ICP-MS) for zircons from the lowermost and uppermost beds exposed in the White Pass association are 31.9 ± 1.4 Ma and 25.94 ± 0.31 Ma, respectively (Jutzeler et al., 2014), and are the most appropriate age estimates for the Ohanapecosh Formation. Previously reported fission-track and U-Pb zircon ages (for Ohanapecosh Formation *sensu lato*, including more distal deposits) range from 36 to 28 Ma (Vance et al., 1987; Tabor et al., 2000).

Fifes Peak Formation (Oligocene to Miocene)

The period of subsidence that enabled accumulation of the Ohanapecosh Formation came to an end by ~26 Ma, giving way to regional folding and uplift and a new phase of subaerial arc volcanism (Vance et al., 1987). The Fifes Peak Formation consists of many silicic pyroclastic deposits, including the Stevens Ridge Member (formerly "Stevens Ridge Formation") near Mount Rainier, and widespread andesitic to basaltic lava flows from several composite volcanoes (Fiske et al., 1963; Vance et al., 1987; Jutzeler et al., 2014).

In the Goat Rocks area, the quartz-phyric rhyolitic ash-flow tuff of Purcell Creek crops out in the Packwood, Packwood Lake, and Ohanapecosh Hot Springs quadrangles, and is probably equivalent to the rhyolite tuff of Bumping River, which erupted from Mount Aix caldera north of White Pass (Schreiber, 1981; Vance et al., 1987; Swanson, 1996b, 1997; Hammond, 2005). The ages determined for this unit are 24.8 ± 0.3 Ma (U-Pb) and 26.5 ± 2.1 Ma (zircon fission-track), closely following the end of the Ohanapecosh eruptive stage (Swanson, 1996b, 1997; Vance et al., 1987).

Andesitic volcanism occurred northeast of Goat Rocks, centered east of Rimrock Lake between the Tieton River and the headwaters of Oak Creek (Swanson, 1964, 1966). In that area two andesitic composite volcanoes were built. The younger was named Tieton Volcano by Swanson (1964, 1966) and is not to be confused with the late Pliocene Tieton Peak volcano of the Goat Rocks complex. A pumice flow interbedded with distal lavas of the Tieton Volcano yielded a zircon fission-track age of 23.3 ± 2.0 Ma (Vance et al., 1987). More locally, an andesitic to basaltic composite volcano was constructed at Angry Mountain, underlying the western side of the Goat Rocks volcanic complex (Swanson, 1996b). These lava flows have not yet been dated, but Swanson (1996b) interprets them as Oligocene, i.e. early Fifes Peak stage or possibly even late Ohanapecosh stage. Swanson (1996b) describes some lava flows of this unit Ta as interbedded with the volcaniclastic unit Ttv, which is associated with Ohanapecosh Formation). Numerous intrusions (plugs, sills, dikes) of Fifes Peak age (Oligocene to Miocene) occur throughout the Packwood Lake and Hamilton Buttes quadrangles, some of which may represent the roots of volcanic centers since eroded away (Swanson, 1996a, 1996b). The end of the Fifes Peak volcanic stage is not well defined, but it had ceased and undergone mild folding and erosion prior to the eruption of Columbia River Basalts (~16 Ma), which overlie the formation to the east (Vance et al., 1987).

Late Miocene to Early Pliocene quiescence (?)

Few late Miocene to early Pliocene volcanic or intrusive units are identified in the Goat Rocks area, which could be explained by 1) insufficient field work or dating, 2) lack of preservation owing to erosion, 3) cover by overlying younger units, or 4) a real quiescent period for this portion of the arc, which is intriguing given the coincidence of the Columbia River Basalt flare-up in the mid-Miocene. What volcanic and intrusive units are known from this time period occur outside of the footprint of the Goat Rocks volcanic complex. In the very southwestern corner of the Hamilton Buttes quadrangle, hornblende microdiorite and dacite sills associated with the intrusive suite of Kidd Creek are exposed (Swanson, 1996a). Zircon fission-track ages for that unit range from 13.4 ± 1.3 Ma to 10.4 ± 1.0 Ma (Swanson, 1991). At the general center of the radial swarm of dikes and sills comprising the Kidd Creek suite is the hydrothermally altered and mineralized McCoy Creek intrusion; this intrusion is interpreted as the root of a volcano which is now eroded away (Swanson, 1992). Further west and closer to Mount St. Helens, in the French Butte and Greenhorn Buttes quadrangles, several volcanic units are identified as Miocene but are not dated, and the Dacite of Bluff Mountain is dated at 15.7 ± 0.2 Ma (Swanson, 1989). North of the Goat Rocks area and White Pass, near Rattlesnake Peaks and Nelson Butte, Hammond (2005) describes several felsic shallow intrusions with ages between 5.13 ± 0.11 Ma ($^{40}Ar/^{39}Ar$, hornblende) and 3.82 ± 0.08 Ma ($^{40}Ar/^{39}Ar$, groundmass). Southeast of Goat Rocks and east of the Cascade Arc axis, the Simcoe Mountains volcanic field began erupting at ~4 Ma, continuing until ~0.6 Ma (Hildreth and Fierstein, 2015). Then construction of the Goat Rocks volcanic complex, subject of this dissertation, began at 3.1 Ma and persisted until as recently as ~100 ka.

Vents comprising the Goat Rocks volcanic complex

Chapter 1 defines the boundary of the Goat Rocks volcanic complex and which volcanoes are considered a part of its “andesite footprint.” Note that the updated age results presented in this chapter indicate that andesitic magmatism shortly followed (postdated by ~100 kyr) the eruption of the Devils Horns rhyolite at 3.2 Ma, and so perhaps the Devils Horns caldera should be reconsidered as part of the same magmatic system. Regardless, for the purpose of this dissertation, the Goat Rocks volcanic complex is defined as the cluster of dominantly andesitic-dacitic volcanoes that were built after the Devils Horns eruption. Adjacent mafic volcanoes such as the Hogback Mountain shield volcano and Walupt Lake tuya are not included in this definition, but clearly they are linked to the focus of magmatism in this area. Their ages are investigated in this study as well, and compositions are considered as a reflection of the mantle sources that potentially feed into the andesitic complex. More details about the peripheral mafic volcanoes are in Chapter 3. Also worth consideration are the andesitic and dacitic volcanoes just north of Goat Rocks along the White Pass corridor, including Spiral Butte and Round Mountain. Being geographically beyond the basaltic “shadow zone” as outlined in Chapter 1, these are not considered part of the Goat Rocks volcanic complex. However, the dacites of White Pass (e.g. products of Spiral Butte and Deer Lake Butte) are of similar age, composition, and mineralogy as the Clear Fork lava flow that erupted from the Coyote Lake volcano, which is included as a Goat Rocks center. Then again, many lava flows of the Old Snowy Mountain eruptive center have similar compositions as well. Additional dating of the Old Snowy Mountain stratigraphy and other young units (e.g. Qac, Qah; Figure 2.1), and petrologic/geochemical study of the White Pass dacites, may clarify the distinction or grouping of these units. While perhaps semantic or somewhat arbitrary, for consistency I continue to use the geographic designations of Chapter 1.

To summarize, the Goat Rocks volcanic complex includes, in age order: the Tieton Peak volcano, several(?) not-yet-located early Pleistocene volcanoes (one is possibly near the Lake Corral-Huckleberry Creek drainage, as discussed later in the text), Bear Creek Mountain, the Lake Creek volcano, a vent at Black Thumb, the Old Snowy Mountain-Ives Peak volcano, Goat Ridge, a small basaltic andesite vent near Chimney Rock, hornblende andesites southwest of Hogback Mountain (possibly domes, or intracanyon flows from a nearby unidentified vent), and the Coyote Lake volcano (Figure 2.1, Figure 2.2). Peripheral mafic volcanoes include the Miriam Creek volcano (which we now know predates the Devils Horns rhyolite; see Results), Devils Washbasin volcano, Hogback Mountain (built atop

Miriam Creek volcano), Lakeview Mountain, Walupt Lake volcano, and vents between Coleman Weedpatch and Two Lakes. Figure 2.1, Chapter 1, Clayton (1983), and Swanson (1996a, 1996b) can be consulted for additional details on the volcanic units and vent locations. New radiometric ages and compositional data for these units are presented below.

METHODS

Methods used in this chapter are as in Chapter 1, namely: mapping, petrography, $^{40}Ar/^{39}Ar$ dating (albeit no new U-Pb zircon dating), and major and trace element analysis. Additionally, oriented samples were collected for paleomagnetic analysis. Changes and additions to the methods are summarized below.

Field mapping and sampling

We conducted additional field work in 2018, 2019, and 2020 in Packwood Lake, Old Snowy Mountain, Pinegrass Ridge, Hamilton Buttes, and White Pass quadrangles. Samples for geochemical and geochronologic analysis were collected from outcrops or talus using a rock hammer. In 2018 we used a portable fluxgate magnetometer (MEDA µMAG-01) at selected outcrops, taking at least three readings per site to confirm whether the rock was magnetically normal or reversed. If the reading induced by the rock was indistinguishable from small movements of the handheld sensor probe during measurement (a common occurrence), we assigned an indeterminate magnetic polarity for the outcrop. Given the difficulty of field magnetometer measurements using our equipment, oriented samples were collected in the following years for more precise determination of characteristic remanent magnetization (ChRM). A sun compass was used when possible to orient samples (if cloudy, they were oriented by Brunton compass).

In total, from all field seasons (each year 2015-2020), approximately 300 samples were collected from the Goat Rocks volcanic complex. Thirty-nine of these samples were dated by either the $^{40}Ar/^{39}Ar$ or U/Pb methods (or both); the ages for thirteen samples were presented and published in Chapter 1, and $^{40}Ar/^{39}Ar$ ages for twenty-six additional samples are presented in this chapter. A total of 147 samples have been geochemically analyzed; thirty analyses were published in Chapter 1 alongside 54 analyses provided by Don Swanson, and the full dataset is presented here (Table A2.3) and discussed further in Chapters 3 and 4.

$^{40}Ar/^{39}Ar$ geochronology

Samples for $^{40}Ar/^{39}Ar$ dating were prepared at Oregon State University following the procedures outlined in Chapter 1. Most analyses were conducted at the Oregon State University Argon Geochronology Laboratory, but several samples were submitted to the U.S. Geological Survey Geochronology Laboratory in Menlo Park while the OSU argon laboratory recovered from a building fire (some of these samples were later analyzed in duplicate at OSU). Samples to be analyzed at the USGS lab were prepared using mostly the same procedures, except that a larger quantity (~60 to 120 mg) of groundmass grains were picked and packaged for irradiation. The samples (as well as a $KAlSiO_4$ glass and CaF_2 standard) were irradiated for 3 hours in the CLICIT-position at the TRIGA nuclear reactor at OSU (irradiation KW-OSU-20-01), then mailed directly from the radiation center to the USGS geochronology laboratory.

At the USGS laboratory, argon was extracted from samples in high vacuum by incremental heating, done by resistance-furnace heating of multigrain samples in copper packets. Isotopic analyses were made on a single-collector MAP216 gas mass spectrometer equipped with a Johnston MM1 electron multiplier. A linear correction for mass discrimination was made by measuring natural Ar from air after each sample loading. The $^{40}Ar/^{36}Ar$ value for air was assumed as 298.56 ± 0.31 after Lee et al. (2006). Procedural blanks were run after every third analysis. Analytical uncertainties were calculated by propagating errors from all measurements and corrections. Data was processed using an Excel plugin ("Argon reduction") developed and shared by Mark Stelten (personal communication).

The USGS laboratory customarily reports mean ages with one standard error, while OSU reports 2σ; in this dissertation all ages are presented with 2σ uncertainty for consistency.

Paleomagnetic analysis

Collection and analysis of paleomagnetic samples were assisted by Dr. Joe Biasi. When possible, block samples were oriented using a homemade sun compass tool designed for block sampling. Brunton compass measurements were used when a sun compass was not available, or during overcast periods or in shaded areas. After collection, two cores were drilled into each block sample to make any orientation errors easier to identify. Most lava flows were sampled twice, but in some cases only one sample could be collected or only one core could be drilled into a block sample.

All samples were measured on a 2G Enterprises vertical SQUID magnetometer with RAPID automatic sample changer at the California Institute of Technology (Kirschvink et al., 2008). Samples were demagnetized using a 20-step alternating field demagnetization protocol (1.6 – 90 mT). The magnetometer is housed in a shielded room with a background field of ~200 nT. Sample analysis was done using the DemagGUI program as part of the PmagPy software package (Tauxe et al., 2016). Principal component analysis (floating best-fit lines, no origin) was used to determine best-fit directions (Kirschvink, 1980). Maximum angle of deviation (MAD) statistics are reported to assess goodness of fit (Kirschvink, 1980).

Petrographic analysis

For most samples, a thin section was made for petrographic analysis. Billets were cut using a rock saw at Oregon State University and sent to Wagner Petrographic for thin section preparation. For most samples a standard thin section with cover glass was made, but for samples from key locations or with interesting mineralogy or textures observed in hand sample, a polished section was made for microprobe analysis (discussed in chapters 3 and 4). Thin sections were evaluated and imaged using petrographic microscopes equipped with cameras, and a select number were photographed at high resolution using a DSLR camera mounted on a stage.

Bulk rock major and trace element analysis

Samples for major and trace element analysis were prepared and analyzed via X-ray fluorescence (XRF) and inductively-coupled plasma mass spectrometry (ICP-MS) at the Peter Hooper GeoAnalytical Lab at Washington State University (WSU) following the methods described in Chapter 1. Note that a small number of analyses have erroneously high Pb concentrations; this is caused by contamination in the carbon crucibles used for fusing the glass beads (Ashley Steiner, personal communication). Other elements besides Pb are not known to be affected. Accuracy and precision of the WSU analyses are described in Chapter 1.

A subset of samples for isotopic analysis (discussed in Chapters 3 and 4) were also analyzed for trace elements at the Pacific Centre for Isotopic and Geochemical Research (PCIGR) at the University of British Columbia. The samples submitted to PCIGR were first crushed to <5 mm in a jaw crusher with alumina ceramic cheek plates at Oregon State University. At PCIGR, crushed samples were then pulverized into powder in a planetary mill with agate jars and milling balls. Aliquots of the powders were digested in an acid mixture, either in concentrated HF-HNO_3 (basaltic samples) or in concentrated HF-HNO_3-$HClO_4$ (more felsic rock types; Fourny et al., 2016). After digestion, a 5% aliquot of each sample was measured on an Element II High Resolution ICP-MS (HR-ICP-MS)(Thermo Scientific) for trace element concentrations, and the remaining 95% was subjected to ion exchange chromatography to separate Pb, Sr, Nd, and Hf (Fourny et al., 2016; Weis et al., 2006). Lead, Nd, and Hf separates were measured for isotopic compositions on three different Nu instruments MC-ICP-MS (Nu 021, NPII 214, Nu1700), and Sr isotopic ratios were measured by thermal ionization mass spectrometer (TIMS), a Thermo Scientific Triton and (or?) a Nu Instruments TIMS (Fourny et al., 2016). Detailed descriptions of PCIGR laboratory and analytical methods can be found in Weis et al. (2006) and Fourny et al. (2016).

RESULTS

Updated volcanic timeline based on new age and paleomagnetic data

Eruption and shallow intrusion of andesite, dacite, and rhyolite lavas persisted at the Goat Rocks volcanic complex for approximately 3 million years (from ~3.1 Ma to 0.1 Ma), based on the combination of $^{40}Ar/^{39}Ar$ ages and U/Pb ages for 39 samples from this study (26 new $^{40}Ar/^{39}Ar$ ages presented in this chapter), and ten previous ages (Table 2.1), in concert with field relations and paleomagnetic analyses. The ages and paleomagnetic data presented here constrain the Miriam Creek volcano, Devils Horns rhyolite, Devils Washbasin basalt, Tieton Peak volcano, Lost Lake andesite, andesite of Countyline Ridge, proximal eruptive products of Bear Creek Mountain, andesites and dacites from Lake Creek volcano, Hogback Mountain basalt, Black Thumb dacite, Old Snowy Mountain andesites, Goat Ridge rhyolite, Lakeview Mountain basaltic andesite, Clear Fork andesite, and Walupt Lake basalt. These data build upon previous ages (K/Ar, zircon fission-track, and $^{40}Ar/^{39}Ar$) determined for the Devils Horns rhyolite, Devils Washbasin basalt, a dacite tuff along Miriam Creek, Tieton andesite, Quaternary olivine basalt and basaltic andesite (Qob_1, Qob_2), Hogback Mountain basalt, and the Cispus Pass pluton (Table 2.1). Representative argon age spectra and ChRM analyses are included in Figure 2.3 and Figure 2.4, all previous and new radiometric ages are given in Table 2.1, and the eruptive timeline is summarized by Figure 2.5 (full datasets can be found in Appendix File A2.1 and Appendix Figure A2.1). Key results from these age and paleomagnetic data are presented below.

Miriam Creek volcano

The Miriam Creek basaltic volcano is the oldest studied, with groundmass $^{40}Ar/^{39}Ar$ ages of ~3.5 Ma for both a basalt lava flow and andesite plug. The dacite tuff of Miriam Creek, previously dated at 3.1 ± 0.2 Ma by Clayton (1983) using zircon fission-track analysis, was dated here using an amphibole separate and yielded an age of 4.16 ± 0.07 Ma. This age is derived from a somewhat discordant age spectrum and appears to be inconsistent with stratigraphy, since the basalt lava flow cropping out ~100 m beneath it yielded an age of 3.56 ± 0.02 Ma. Therefore, the age determined by Clayton (1983) should be used until further work can be done. The exact lower and upper age boundaries for the Miriam Creek volcano remain unconstrained, since the samples analyzed were midway through the stratigraphic section. The upper andesite unit (Swanson's Qahm) did not yield zircon for our U-Pb dating efforts, but could be a good candidate for future $^{40}Ar/^{39}Ar$ dating. Samples from that unit are geochemically and mineralogically similar to the prominent outcrop represented by sample GR20-30 (3.53 ± 0.02 Ma), and so the latter is grouped with Tahm on the map (Figure 2.1), though their age and genetic relation needs confirmation. Swanson (unpublished field notes) and Clayton (1983) sampled basalt farther down the Miriam Creek drainage than we accessed during field work, so the basal age of the Tbm unit is older than 3.56 ± 0.02 Ma (GR19-33) but not precisely known, and the contact between unit KJr and Tbm remains uncertain on the north side of Miriam Creek (it is approximated in Figure 2.1). In addition, the age and relation to other Miriam Creek volcanic deposits remain undefined for unit Tpd (Swanson and Clayton, 1983), an amphibole- and biotite-bearing diorite unit exposed further east along the Miriam Creek drainage and near Twin Peaks.

Devils Horns rhyolite

The Devils Horns rhyolite eruption is confirmed to have occurred at 3.2 Ma. The new plagioclase $^{40}Ar/^{39}Ar$ age of 3.19 ± 0.02 Ma aligns with (and is more precise than) previously determined zircon fission-track ages of 3.17 ± 0.16 Ma and 3.20 ± 0.14 Ma (Clayton, 1983; Figure 2.5). This is presumed a lower age boundary for the andesitic eruptive products of the Tieton Peak volcano, since Swanson (unpublished field notes) was convinced by his field observations that the mineralized andesite lava flows exposed around the headwaters of Conrad Creek were deposited on top of the Devils Horns rhyolite, as opposed to the rhyolite being faulted against the andesite.

Tieton Peak volcano and Devils Washbasin volcano

Eruption of andesite occurred a mere 100-150 kyr after the Devils Horns rhyolite eruption. The oldest Tieton Peak area andesite that we dated, sample TP19-06 (which directly overlies Devils Horns rhyolite), yielded analytically indistinguishable ages of 3.08 ± 0.01 Ma (OSU) and 3.05 ± 0.02 Ma (USGS). The Tieton Peak volcano and mafic Devils Washbasin volcano erupted coevally between ~3 Ma and ~2.6 Ma. The oldest Devils Washbasin basalt age is 3.01 ± 0.02 Ma, from a lava flow on the saddle between Tieton Peak and Devils Washbasin (sample TP19-17), although this may be slightly too old in context with nearby samples, and the age spectrum is somewhat discordant. Another proximal Devils Washbasin basalt is dated at 2.89 ± 0.08 Ma (GR20-14) and is normally magnetized. A distal basalt lava flow northeast of Bear Creek Mountain that is compositionally and mineralogically like other Devils Washbasin lavas (sample GR16-07) yielded an age of 2.68 ± 0.01 Ma (see Chapter 1).

North of the saddle between Tieton Peak and Devils Washbasin, a hornblende andesite unit (Swanson's QTah, unpublished) appears to be among the lowest in the stratigraphy, directly overlying Devils Horns rhyolite. The paleomagnetic orientation is reversed (the only reversed sample in the area), possibly corresponding to the reversed polarity interval between 3.04 and 3.11 Ma (Cande and Kent, 1995), which would align with its apparent stratigraphic position beneath the ~3.01 Ma Devils Washbasin basalt capping the ridge. However, the groundmass argon age for this unit is among the youngest in the stack at 2.71 ± 0.02 Ma (implications of these results are discussed below; see "Discussion"). Higher in the stratigraphy, a two-pyroxene andesite lava flow is magnetically normal and yields an age of 2.82 ± 0.01 Ma. The andesite capping the summit of Tieton Peak is also normally magnetized and is dated at 2.65 ± 0.04 Ma with an inverse isochron age using all heating steps (the age spectrum is discordant and a plateau could not be fit).

Early Pleistocene andesite of unknown source

Two andesite lava flow remnants with unknown vent locations yielded ages intermediate between the Tieton Peak lavas and older Bear Creek Mountain lavas (Tieton andesite). These are the andesite of Lost Lake, dated by groundmass at 2.27 ± 0.01 Ma (with a pseudo-plateau of 2.29 ± 0.01 Ma for plagioclase; see Chapter 1), and the andesite of Countyline Ridge (i.e. the next ridge east of Nannie Ridge that defines the boundary between Lewis County and Yakima County), which yielded a groundmass age of 2.09 ± 0.02 Ma.

Bear Creek Mountain

Two proximal eruptive products at Bear Creek Mountain yielded $^{40}Ar/^{39}Ar$ ages younger than the ages previously determined by Hammond (2017) for Tieton andesite. Sample 14432 was collected by Daryl Gusey from the northern agglomerate area on Bear Creek Mountain that he interprets based on geochemical composition to be the vent for the younger Tieton andesite lava flow (Gusey et al., 2018). The groundmass age newly determined for sample 14432 is 1.24 ± 0.01 Ma, which is younger than the Hammond (2017) plagioclase age of 1.39 ± 0.10 Ma for the younger Tieton andesite. In addition, groundmass from sample GR16-09-1, from the summit lava flow of Bear Creek Mountain, yielded an inverse isochron age of 1.10 ± 0.01 Ma. This age overlaps with that determined for the oldest lava flow from Lake Creek volcano (see below).

Lake Creek volcano

Construction of the Lake Creek volcano began at ~1.11 Ma and continued until at least ~456 ka. Sample GR16-36 (later re-sampled as GR19-02, Goat3, Goat4) is from the two-pyroxene andesite lava flow exposed atop Oligocene volcaniclastic basement along Trail 86 east of Goat Lake. This lava flow was mapped by Swanson (unpublished) as part of the lower normal unit in the Goat Lake-Snyder Mountain stratigraphy, but it is actually magnetically reversed (Figure 2.4). Sample GR16-36 from this flow yielded ages of 1.11 ± 0.03 Ma (zircon U-Pb), 1.11 ± 0.01 Ma (groundmass $^{40}Ar/^{39}Ar$ total fusion age), and 1.13 ± 0.02 Ma (plagioclase $^{40}Ar/^{39}Ar$ inverse isochron age; Chapter 1). The next lava flow above this (not dated) is also magnetically reversed, but all other samples analyzed within Swanson's (1996b) Qgr_1 unit have normal magnetic polarity. Sample GR19-09 is from the uppermost normal lava flow in that section and yielded a groundmass $^{40}Ar/^{39}Ar$ age of 1.01 ± 0.01 Ma.

Above the rubbly deposit that separates Swanson's lower normal (Qgr_1) from overlying reversed (Qgr_2) section, the next lava flow has reversed magnetic polarity (samples Goat21 and Goat22; Figure 2.4), confirming Swanson's field magnetometer measurements there. Sample GR16-30, from the next flow above, was dated by zircon U/Pb at 987 ± 57 ka and by groundmass $^{40}Ar/^{39}Ar$ at 969 ± 4 ka (see Chapter 1; Wall et al., 2018). Note that this second lava flow was dated, as opposed to the lowest, because during the 2016 field season I was wary about the latter outcrop being in place; after re-examination in 2019 I changed my mind, but I assume that the older flow would likely yield an age within uncertainty of the existing age. Another constraint on the base of that reversed unit is sample GR18-24, from the lava flow that forms the cliff below Heart Lake (the lowest reversely magnetized flow in that section; Swanson, 1996b), which yields a slightly older $^{40}Ar/^{39}Ar$ groundmass age of 993 ± 10 ka.

Notably, a lava flow on Snyder Mountain (sample GR15-04) that Swanson (1996b) mapped as part of the middle, reversely magnetized sequence yielded a $^{40}Ar/^{39}Ar$ groundmass age of 593 ± 4 ka, which is younger than other lava flows to the northwest that were mapped as the overlying upper normal sequence (Qgr_3). A nearby, previously unmapped dike exposed at the top of the ridge (sample GR17-75) also has a groundmass age of 559 ± 5 ka. Samples for ChRM analysis were not collected from these locations to confirm the reversed field magnetometer readings. Two lava flows exposed at lower elevation on the northern flank of Snyder Mountain gave ages of 735 ± 12 ka (GR17-77B, groundmass $^{40}Ar/^{39}Ar$) and 663 ± 3 ka (GR17-72A, groundmass $^{40}Ar/^{39}Ar$). The Jordan Creek dacite, an intracanyon flow southwest of the Lake Creek center, was dated at 580 ± 8 ka (GR18-27, groundmass $^{40}Ar/^{39}Ar$). Even younger is Swanson's (1996b) "late-stage hornblende andesite," exposed approximately 1 km west of Heart Lake, with a groundmass $^{40}Ar/^{39}Ar$ age of 456 ± 12 ka.

Hogback Mountain

Hogback Mountain was active between approximately 1.1 Ma and 900 ka. Swanson (unpublished) identified a change in paleomagnetic orientation (from reversed to normal) in the basalt lava flows that coincides with a hyaloclastic deposit exposed along the Pacific Crest Trail. Two basalt lava flows below this boundary have reversed ChRM orientations and groundmass $^{40}Ar/^{39}Ar$ ages of 1.10 ± 0.01 Ma (GR19-14) and 1.05 ± 0.01 Ma (GR20-02). Stratigraphically above these lava flows, the lowest normally magnetized lava flow that we sampled, GR19-15, yielded $^{40}Ar/^{39}Ar$ ages of 1.15 ± 0.02 Ma (OSU) and 1.14 ± 0.06 Ma (USGS). The OSU analysis produced a discordant age spectrum, so the total fusion age is used, and the USGS analysis produced a U-shaped age spectrum and so the younger inverse isochron age is used instead. However, based on the lava flow's normal magnetic polarity, and its superposition above the reversed lava flows, it is probably younger than 1.05 Ma and erupted during the Jaramillo Normal Polarity Subchron (lower boundary of 1.053 ± 0.006 Ma determined by Singer et al., 1999). The basalt lava flow at the summit of Hogback Mountain, which was mapped as part of the normal polarity sequence by Swanson (unpublished) but not analyzed for ChRM by us, yielded a U-shaped $^{40}Ar/^{39}Ar$ age spectrum and an imprecise inverse isochron age of 0.94 ± 0.26 Ma. A distal Hogback Mountain basalt north of White Pass was previously dated by Sisson (personal communication) at 891 ± 7 ka.

Old Snowy Mountain and Goat Ridge

The Old Snowy Mountain and Goat Ridge volcanoes began erupting at approximately the same time, between ~450-440 ka, shortly after the youngest dated Lake Creek stage lava flow. The zircon U/Pb age for sample GR17-71, from the rhyolite at the base of the Goat Ridge section, is 443 ± 10 ka (Chapter 1; Wall et al., 2018). Sample GR16-38, from the northwestern base of the Old Snowy Mountain pile, yielded similar ages of 453 ± 8 ka (zircon U/Pb) and 440 ± 3 ka (groundmass $^{40}Ar/^{39}Ar$; Chapter 1). An andesite lava flow high on Goat Ridge (sample GR17-68) is newly dated at 335 ± 13 ka (groundmass $^{40}Ar/^{39}Ar$), and an amphibole-bearing andesite lava flow high on the ridge between Old Snowy Mountain and Ives Peak (sample GR16-25) yielded a groundmass $^{40}Ar/^{39}Ar$ age of 217 ± 5 ka (Chapter 1).

Clear Fork Lava Flow

The Clear Fork Lava Flow, which forms the striking columnar cliff visible from the Palisades Viewpoint along Highway 12, erupted at approximately 110 ka. The zircon U/Pb age for this lava flow is 107 ± 5 ka, and the groundmass $^{40}Ar/^{39}Ar$ age is 115 ± 4 ka. These ages are also within uncertainty of the groundmass $^{40}Ar/^{39}Ar$ age of 113 ± 4 ka determined for nearby Spiral Butte north of White Pass (Tom Sisson, personal communication).

Late Pleistocene mafic volcanoes

The mafic volcanoes defining the southern margin of the Goat Rocks volcanic complex are young: Lakeview Mountain has a groundmass $^{40}Ar/^{39}Ar$ age of 194 ± 12 ka, and Walupt Lake, 65 ± 28 ka. The Coleman Weedpatch basalt was not dated, but given stratigraphic relations and textures described below, it is likely close in age to Walupt Lake volcano. Curiously, on this side of the Goat Rocks volcanic complex, in contrast to Hogback Mountain, the emergence of mafic lavas was scattered between more widely distributed vents over a shorter interval of time. (Yet similar to Hogback Mountain, a significant range of compositions is represented over this short interval; discussed further in Chapter 3).

The radiometric age for Walupt Lake basalt is well aligned with previous observations and interpretations. As Swanson (1996a) describes, the volcano consists of a thick (>500 m) deposit of dominantly hyaloclastic debris capped by basalt flows and cinders—classic evidence of a subglacial tuya emerging above the ice. The age of 65 ± 28 ka aligns with marine isotope stage (MIS) 4, which occurred between 71-57 ka (Lisiecki and Raymo, 2005).

While we have no radiometric age data on the Coleman Weedpatch basalt (which Swanson (1996a) equates to Hammond's (1980) Basalt of Two Lakes), it is likely close in age. The unit includes remnants of oxidized, agglutinated vent material near the Coleman Weedpatch trail and lavas that flowed around the southern base of the Walupt Lake volcano, therefore at least some of this unit overlies and is younger than Walupt Lake volcano (Swanson, 1996a). Note that these basalts are geochemically distinct from those erupted from Walupt Lake volcano (see Chapter 3). Swanson (1996a) describes quench textures including hackly jointing and pillow-like masses in one of the Coleman Weedpatch basalt flows, and therefore interprets that some ice or meltwater was present during its emplacement. Given the degree of erosion and mantling with glacial till (Evans Creek Drift; Swanson, 1996a), the Coleman Weedpatch vents were probably also active during MIS 4, rather than the most recent MIS 2 (29-14 ka; Lisiecki and Raymo, 2005).

Rock classification and major and trace element concentrations

Eruptive products of the Goat Rocks volcanic complex range from basaltic andesite to rhyolite in composition but are dominantly andesitic to dacitic (Figure 2.6). Earlier-erupted andesites (dominantly lava flows, but rare volcaniclastic deposits) are commonly highly porphyritic with plagioclase, clinopyroxene, and orthopyroxene phenocrysts, ± olivine (

Figure 2.7). Later products of the Lake Creek volcano are dominantly plagioclase-two-pyroxene-amphibole bearing dacites. Lava flows that erupted during Old Snowy Mountain stage are dominantly plagioclase-two-pyroxene-amphibole andesites and lesser dacites. The peripheral mafic volcanoes erupted basalt, basaltic andesite, and rare andesite (Figure 2.6, Chapter 3). Basalts are calc-alkaline and commonly their phase assemblage consists of olivine, plagioclase, and clinopyroxene (see Chapter 3 for further details on the local mafic compositions).

Thirty compositional analyses in addition to 54 previously unpublished Swanson analyses were presented and discussed in Chapter 1 (Wall et al., 2018). Here I present 89 additional analyses, including 15 new samples from the Tieton Peak unit, which was not addressed in Chapter 1. Compositions of peripheral mafic volcanoes are also included in Appendix Table A2.2, but discussion of those samples can be found in Chapter 3. Here I focus on the updated compositional data for the intermediate-felsic volcanic complex as well as a new Devils Horns rhyolite sample.

Devils Horns rhyolite

The Devils Horns rhyolite deposits were not a focus of this study, and only one compositional analysis is contributed here. That sample (T19-08, $^{40}Ar/^{39}Ar$ age presented above) consists of glassy rhyolite chips collected from a presumed lava flow or dome exposed on the ridge dividing Conrad Creek and South Fork Tieton River. The sample is a high-silica rhyolite (76 wt% SiO_2) with 4.5 wt% K_2O, similar to most previous analyses from this unit (Figure 2.6, Figure 2.8 Figure 2.9; Clayton, 1983; Swanson analyses published in Wall et al., 2018). Note that the suite of Devils Horns analyses spans a wide range of Na_2O, likely reflecting hydration and cryptic hydrothermal alteration. The new ICP-MS trace element data presented here (Figure 2.9, Appendix Table A2.2) agree with the previous XRF analyses by Swanson (Wall et al., 2018), for example, enriched Rb and depleted Zr.

Tieton Peak volcano

Tieton Peak lavas (and possible shallow intrusions) range in composition from andesite to rhyolite. Andesites commonly have a phase assemblage of plagioclase, clinopyroxene, and scarcer orthopyroxene. Lava flows and tuffs exposed on the saddle between Tieton Peak and Devils Horns have more varied compositions and mineral assemblages. One lava flow (TP19-24) is a nearly aphyric rhyolite, while another lava flow (GR20-21) is andesite with amphibole as the sole phenocryst. The Tieton Peak andesites are notably depleted in Na_2O (2.7-3.7 wt%) compared to the rest of the Goat Rocks suite. The amphibole-bearing lava flow mentioned above is also unusually low in K_2O (1.1 wt%). Another outcrop is a crystal-rich tuff (bulk composition silica-poor dacite) with dense, glassy sheared clasts of silica-rich dacite (69.2 wt% SiO_2); both dacite components are unusually enriched in P_2O_5 (0.32 and 0.23 ppm, respectively). Beneath that deposit, a pinkish tuff also has a dacitic bulk composition (less silicic than the glassy clasts in the above; 67.4 wt% SiO_2). An altered, spherulitic basaltic andesite with unusually high MgO (11.5 wt%) and K_2O (1.9 wt%) was also sampled on the southern flank of Tieton Peak. The felsic end of the Tieton Peak suite (compositions including dacite, trachyte, and rhyolite) is notably enriched in many high field strength elements (Nb, Ta, Hf) compared to other samples from the Goat Rocks area in this silica range (Figure 2.9).

Early Pleistocene andesites

The andesite of Lost Lake is compositionally similar to the Bear Creek Mountain suite and many lava flows from the Lake Creek volcano. Bulk rock compositions range from 61-62 wt% SiO_2, with K_2O 2.6-2.7 wt% (Figure 2.6, Figure 2.8). The texture is strikingly porphyritic with phenocrysts and glomerocrystic clots of plagioclase, clinopyroxene, and orthopyroxene (

Figure 2.7). In contrast, the andesite of Countyline Ridge is more mafic and occupies a unique compositional range. The phenocryst assemblage includes olivine, plagioclase, clinopyroxene, and orthopyroxene. Silica content is ~58 wt%, with K_2O on the lower side at 1.6-1.7 wt%, relatively high MgO (4.5-5 wt%), slightly enriched Ni (~40-60 ppm), slightly low Sr (~350 ppm)—in summary, a distinct cluster from other Goat Rocks compositions. Sample GR17-44 shares this composition, and it is from a sequence of pyroclastic beds (dense to scoriaceous blocks in ashy matrix, with thinner beds and lenses of lapilli-sized clasts) farther north along the ridge that dip generally south, so presumably the eruptive source of these pyroclastic deposits and lavas was nearby (warranting future field work in the adjacent Lake Corral-Huckleberry Creek basin).

Bear Creek Mountain stage

Bear Creek Mountain eruptive products have a relatively restricted range of compositions that straddles the andesite-trachyandesite boundary. Silica ranges from ~59-62 wt%, and K_2O is is high for this silica range of the Goat Rocks volcanic complex (~2-3 wt%; Figure 2.6, Figure 2.10; Gusey et al., 2018). Most lava flows have a phenocryst assemblage of plagioclase and two pyroxenes (

Figure 2.7), although the younger Tieton andesite lava flow and some of the andesite of Section 3 Lake contain olivine as well (Gusey et al., 2018). Note that the source and age of the andesite of Section 3 Lake need clarification according to Gusey et al. (2018), but based on its compositional similarity and proximity to the other units, I include this unit with the Bear Creek Mountain volcano. A more comprehensive description of the Bear Creek Mountain compositions can be found in Gusey et al. (2018), but here I contribute ICP-MS trace element results for four samples (older Tieton andesite, younger Tieton andesite, vent material related to the younger flow, and the lava flow at the summit of Bear Creek Mountain) to support the large suite of XRF results. The ICP-MS results include concentrations of additional high field strength elements (HFSE; e.g. Hf, Ta) and many more rare earth elements (REE; Appendix Table A2.2). Notably, the Bear Creek Mountain samples are enriched in HFSE (Nb, Ta, Hf, Zr, Th, U) compared to other andesites of the Goat Rocks suite (Figure 2.9). They are also among the most REE enriched in this silica range.

Lake Creek stage

Compositions that erupted during the Lake Creek stage are dominantly silicic andesite and dacite, with lesser trachyandesite, trachyte, and basaltic andesite (Figure 2.6). Notably, there is a general shift through time from less silicic to more silicic at a similar K_2O range (Figure 2.10, Figure 2.11; in Figure 2.10 note that the 1.5-1.0 Ma age bin also includes samples from Bear Creek Mountain).

The earliest eruptive products of the Lake Creek volcano—those erupted between ~1.1-1.0 Ma (dated by $^{40}Ar/^{39}Ar$ near Goat Lake, and by intercalation with Hogback Mountain lava flows in this age range)—overlap significantly with the compositions of Bear Creek Mountain and the andesite of Lost Lake. They occupy the boundary of trachyandesite-andesite-dacite and lie within the high-K field (Figure 2.6, Figure 2.10). They are enriched in HFSE (Nb, Ta, Hf, Zr, and especially Th and U) compared to other Goat Rocks andesites and dacites (Figure 2.9).

Lavas erupted between 1 Ma – 800 ka overlap in composition with those older Lake Creek stage samples agove and extend to more silicic compositions (trachyte and more dacite; Figure 2.6, Figure 2.10, Figure 2.11). A handful of samples from near Goat Lake, Heart Lake, and Coyote Lake form a more alkalic cluster (on the border of trachyte/dacite) that is more strongly enriched in HFSE (as above), while most other samples are less enriched. Samples from the coeval Black Thumb vent are like the less-enriched Lake Creek group. Two samples from the Black Thumb cliff and talus below are like those analyzed by

Gusey et al. (2018), while one sample from the breccia deposit beneath that massif is more enriched in K_2O and HFSE. A lava flow or dike on the ridge ~0.8 km south of Cispus Pass (GR17-51 and Swanson's 82-50) is close in composition to that breccia, while a dike farther south (GR17-54) is much like the former group. I also note that these compositions are relatively similar to the nearby sample of Cispus Pass pluton analyzed by Gusey et al. (2018; sample 14467, a quartz monzodiorite according to the classification of Enrique and Esteve, 2019). The implications of these Black Thumb and Cispus Pass area analyses are considered in more detail in the Discussion section.

Lake Creek eruptions between 800 – 600 ka, which mostly comprise the distal exposures on and northwest of Snyder Mountain, overlap the earlier compositional ranges but are generally less alkalic/potassic (no trachyandesite or trachyte and mostly in the medium-K field; Figure 2.10) and extend to higher silica, with dominantly dacite, but also two quenched magmatic inclusions with more mafic compositions (discussed below). They are less enriched in HFSE than the older Lake Creek compositions, having lower Nb, Ta, Hf, Zr, Th, and U.

Many Lake Creek lava flows have abundant quenched magmatic inclusions. For each of two samples collected from the Snyder Mountain area, the composition of a large inclusion was analyzed in addition to the host lava. One of these lava flows is a dacite (GR17-72A, 64.3 wt% SiO_2) and the inclusion is andesitic (GR17-72B, 59.4 wt% SiO_2) and somewhat low in Na_2O (3.3 wt%). The other lava flow is andesitic (GR17-77B, 62.4 wt% SiO_2) and the inclusion has a unique basaltic andesite composition (GR17-77A, 55.4 wt% SiO_2) with high Sr (852 ppm) and Ba (515 ppm), distinct from other Goat Rocks area basaltic andesites. Both of the inclusions are enriched in Al_2O_3 compared to most of the Goat Rocks suite (more like the lava flows of Old Snowy Mountain stage, although different in other element concentrations). Also, the compositions of inclusion and host are linked—for example, the more mafic inclusion (GR17-77A) that is enriched in P_2O_5, Sr, Ba, La, Ce, and Dy is carried by a lava flow that is also enriched in those elements, and vice versa for the more silicic inclusion.

The youngest (600 to ~456 ka) samples from the Lake Creek volcano occupy a range of compositions, from andesite to rhyodacite. Above I showed that the lava flows and dikes on Snyder Mountain are close in age to the intracanyon flows in the Middle Fork Johnson Creek and Jordan Creek drainages (Swanson's Qgrh and Qdj; Swanson, 1996b), and their compositions are similar, as well. Lava flows and dikes on Snyder Mountain range from andesite (61.5 wt% SiO_2) to dacite (68.5 wt% SiO_2) and are amphibole-bearing, unlike the two-pyroxene andesites and dacites erupted at earlier times. One dacitic lava flow (GR15-

01C, 67.9 wt% SiO_2) carried a quenched magmatic inclusion with a more mafic composition (GR15-01B, 61.0 wt% SiO_2), similar to that of the inclusion GR17-72B mentioned above. Like that inclusion from a slightly older lava flow, GR15-01B is less potassic and more aluminous, and significantly lower in U and Th, compared to the rest of the Lake Creek suite. On almost every plot, this sample lies within the range of compositions erupted later at Old Snowy Mountain. Similar in composition to GR15-01B are two exposures of the intracanyon lava flows along Middle Fork Johnson Creek (unit Qgrh; samples GR18-21 and Swanson's 82-100). These samples also contain ~61 wt% SiO_2 and 17.2 wt% Al_2O_3, and are near identical to the GR15-01B inclusion in most HFSE concentrations, but are slightly higher in K_2O, Rb, U, and Th (note that trace elements are only available for the new sample GR18-21). In contrast, two other samples of the same unit (GR18-20A and Swanson's 82-69; Swanson, 1996b) are rhyodacite with relatively high Na_2O (~4.7 wt%). Yet another exposure of this unit analyzed by Swanson (1996b) is dacitic and very similar in composition to the young dacites on Snyder Mountain as well as the dacite of Jordan Creek (GR18-27, -29, plus three samples analyzed by Swanson, 1996b). This group of dacites lies between 67-68.5 wt% SiO_2 and ~2.5-3 wt% K_2O. Despite their high Na_2O, the Qgrh rhyodacites are much like this dacite group in trace element concentrations: similar to the Qgrh andesite and the quenched inclusions in Snyder Mountain lava flows, they are depleted in most HFSE compared to the rest of the Lake Creek suite; however, their Th and U concentrations are within range of the more enriched Lake Creek suite.

Old Snowy Mountain stage

The shift to less potassic, more aluminous, amphibole-bearing magmas during the end of the Lake Creek stage is maintained during Old Snowy Mountain stage. The oldest lava flow sampled from Old Snowy Mountain (GR16-38 and Swanson's 82-80; Wall et al., 2018) is a medium-K andesite with low Rb, HFSE, and REE—very similar to the quenched inclusion GR15-01B. Other andesites from Old Snowy Mountain and Goat Ridge are even less potassic. Andesites of Goat Ridge occupy a narrow compositional range and tightly cluster between 60.1-60.3 wt% SiO_2, though older analyses from Swanson (1996a) record a broader range. The compositions mostly overlap with the Old Snowy Mountain suite, but they are distinctly high in P_2O_5, slightly more sodic, and more enriched in LREE. Note that with regard to P_2O_5 and LREE, GR16-38 and GR15-01B are intermediate between Goat Ridge and Old Snowy Mountain. Less commonly, dacite and rhyolite were also erupted from these volcanoes: five outcrops are known including a dacite lava flow northwest of Goat

Ridge (sample 82-100; Swanson, 1996a), a dacite lava flow proximal to Old Snowy Mountain (GR16-25; Wall et al., 2018), a distal Old Snowy Mountain dacite sampled by Swanson (81-34; Wall et al., 2018), rhyolite of Goat Ridge (93-052, Swanson, 1996a; GR17-71, Wall et al., 2018), and a distal rhyolite of Old Snowy Mountain (Swanson's 81-32, Wall et al., 2018). All but one (GR16-25) are significantly more potassic than the Old Snowy Mountain and Goat Ridge andesites. Like the andesites, they are somewhat depleted in most HFSE and REE compared to the rest of the Goat Rocks suite. Compositionally the rhyolites look more like Devils Horns rhyolite than the Tieton Peak rhyolite. However, the Goat Ridge rhyolite is distinctly high in Th and U (no U data exist for the Old Snowy Mountain rhyolite, 81-32, and the XRF analysis for Th is not nearly as enriched as the Goat Ridge sample).

The Clear Fork Lava Flow is compositionally similar to Old Snowy Mountain and Goat Ridge, but more felsic (silicic andesite to dacite, 62.2-63.1 wt% SiO_2; Figure 2.6), except for one near-vent exposure (agglutinated/welded spatter) on the northwest bank of Coyote Lake that is mafic andesite (CF19-04, 58.4 wt% SiO_2). Like the above, these amphibole-bearing rocks are medium-K (1.1-1.6 wt% K_2O) and aluminous (17.3-17.9 wt% Al_2O_3). Their P_2O_5 concentrations are intermediate between the main Goat Ridge and Old Snowy Mountain groups, like GR16-38, GR15-01B, and the rest of the Goat Rocks suite. They are similarly enriched in Sr and depleted in Rb, HFSE and REE as the aforementioned groups. The main cluster of silicic andesite-dacite samples is slightly more enriched in LREE than the near-vent andesite, more like the Goat Ridge andesites.

The hornblende-bearing lava flows or domes exposed along the Clear Fork Cowlitz River Basin south and southwest of Hogback Mountain (map unit Qah) are not yet dated, but presumed late Pleistocene, and their compositional alignment with the above units supports this. Most samples were collected and analyzed by Clayton (1983) and Swanson (included in Wall et al., 2018), but I add one sample (GR17-09) collected from an exposure ~0.9 km west of Hidden Spring. This outcrop and a lava flow sampled by Swanson (sample no. 96-8, Wall et al., 2018) and Clayton (1983; samples HMS-11 and HMS-12) are silicic andesite to mafic dacite (62.6-63.7 wt% SiO_2), very similar to the main cluster of Clear Fork Lava samples. My sample GR17-09 is less potassic and slightly less enriched in Rb, Ba, Th, U, La, and Ce than that group, but otherwise very similar in trace element concentrations. Clayton (1983) and Swanson (as published in Wall et al., 2018) also sampled dacite and rhyolite from outcrops further to the west (samples HMS-4 and -10, 96-58, and 96-17). One dome-like mass is compositionally on trend with the andesite-dacite (lower-K_2O and higher Al_2O_3, samples HMS-4 and 96-58), but the other dacite and the rhyolite are more potassic and less aluminous (samples HMS-10 and 96-17). The XRF trace element compositions for 96-17 are similar to Goat Ridge rhyolite, though the sample is less felsic.

The andesite of Chimney Creek is also not dated but presumed late Pleistocene in age; its compositions are similar to the above, with some slight differences. I did not sample this unit, so describe Swanson's analyses here (data included in Wall et al., 2018). The more distal sample (96-10) is an aluminous andesite very similar in composition to the Goat Ridge andesites. The other sample (96-30), nearer to the presumed vent area, is a basaltic andesite that is particularly high in Al_2O_3 (20.7 wt%) and low in P_2O_5 (0.13 wt%). Both samples are among the least potassic of the Goat Rocks suite. Their trace element concentrations are comparable to Old Snowy Mountain, Goat Ridge, and Qah andesites, though the basaltic andesite is notably low in Sr (Figure 2.9).

Nearby Late Pleistocene volcanoes of White Pass

Though not a focus of this study, for context I also sampled and analyzed lava flows from the late Pleistocene volcanoes north and northeast of the Goat Rocks volcanic complex along the White Pass corridor. Spiral Butte, Deer Lake Butte, and Round Mountain erupted compositions much like the volcanoes of Old Snowy Mountain stage described above. The eruptive products of Spiral Butte and Deer Lake Butte are grouped as Dacite of White Pass on the map (Figure 2.1; unit Qdwp), but Deer Lake Butte samples are actually silicic andesite (~62.7 wt% SiO_2) while those from Spiral Butte are dacite (65.4-65.7 wt% SiO_2; Appendix Table A2.2). They are medium-K and aluminous, and depleted in HFSE and REE, like the Clear Fork Lava and dacite of unit Qah. The andesite of Round Mountain is slightly more potassic and higher in P_2O_5, as well as more LILE-enriched, much like the andesite of Goat Ridge.

DISCUSSION

Pre-Goat Rocks volcanism and initiation of the andesitic volcanic complex

Previously, the Devils Horns rhyolite eruption was considered the oldest episode of Pliocene volcanism in the Goat Rocks area. Clayton (1983) had dated a dacite tuff along Miriam Creek at 3.10 ± 0.20 Ma, slightly postdating his ages for Devils Horns rhyolite (3.20 ± 0.14 Ma and 3.17 ± 0.16 Ma). However, the new age results place Miriam Creek basalts earlier on the timeline, at approximately 3.5-3.6 Ma, with Devils Horns rhyolite following at 3.2 Ma. The lifespan of the Miriam Creek volcano remains unconstrained, since the uppermost and lowermost units were not dated in this study. Most likely a long period of quiescence and erosion occurred between the waning of Miriam Creek volcano and the initiation of the much younger Hogback Mountain volcano. However, based on geochemistry and field relations, the ~1.4-Ma unit Qob_1 may have erupted from that area—perhaps an early Hogback Mountain eruption not preserved proximally (Gusey et al., 2018). Overall, the Miriam Creek-Hogback Mountain area was a major locus of dominantly mafic volcanism with recurring episodes of activity over a period of ~2.7 million years (youngest Hogback Mountain age is 891 ± 7 ka; Sisson, personal communication).

After the voluminous Devils Horns rhyolite was emplaced, only ~100 kyr passed before the Tieton Peak andesites and Devils Washbasin basalts began erupting. The Tieton Peak and Devils Washbasin volcanoes emerged along the western margin of the caldera, presuming a caldera was formed (there remains some uncertainty in the field observations; Clayton, 1983; Swanson, unpublished). For comparison, the Kulshan caldera in northern Washington (1.15 Ma) also preceded the growth of an andesitic composite volcano cluster, Mount Baker (0.5 Ma), but a longer time interval separates them, and the volcanic locus shifted southwestward by ~8-10 km (Hildreth et al., 2004). Similarly, the Gamma Ridge caldera (2-1.6 Ma) formed prior to the emergence of Glacier Peak at 0.6 Ma a few km to the southwest (Hildreth, 2007). The shorter distance and time interval between the Devils Horns caldera and Tieton Peak volcano, compared to the more northerly caldera-stratovolcano pairs, would seem to suggest a more likely genetic relation. Perhaps the shorter spatial and temporal separation are related to the Goat Rocks area's closer proximity to the axis of rotation of the arc (see Wells and McCaffrey, 2013, and discussion in Hildreth, 2007). The Devils Horns caldera could very well represent the initiation of the Goat Rocks volcanic complex, although for the purpose of this study, the complex is defined as those dominantly andesitic composite volcanoes that postdate Devils Horns rhyolite.

The duration of the Tieton Peak eruptive stage is now properly defined by radiometric ages, but some details of the stratigraphy remain uncertain. In particular, the age and stratigraphic position of the hornblende andesite northeast of Tieton Peak are unresolved. Clayton (1983) interpreted this unit as a dome on the flank of the Tieton Peak volcano, but without providing explanation. We did not observe evidence in the field that this unit was discordant with the adjacent stratigraphy, although it only occurs on the north side of the saddle, which may support such an interpretation. If true, and the new argon age of 2.71 ± 0.02 Ma is correct, then the reversed magnetic polarity could be attributed to an excursion during the late Gauss chron. The argon age aligns with the L7 excursion reported by Ohno et al. (2012) at 2.71 Ma (duration 2 kyr); however, that excursion only reached a minimum inclination of ~20°, whereas the hornblende andesite records a fully reversed orientation with inclination of -48 to -49°. While their ages are slightly outside of uncertainty of the argon age, the L6 (2.65 Ma) or L8 (2.75 Ma) excursions are full reversals and could be potential matches. More detailed field work and additional argon dating and paleomagnetic analysis are needed to clarify the age and stratigraphic relation of this unit. Based on the present data, the ambiguity does not affect the overall conclusions about the timing and duration of the Tieton Peak volcano.

Possible vent locations of early Pleistocene units

As described in the results section, several lava flows of olivine andesite are preserved on Countyline Ridge south of a sequence of pyroclastic beds (block-and-ash flows?) with the same bulk composition. These deposits vary in orientation from southward- to westward-dipping. An intrusive equivalent (dikes or plug) has not yet been identified, but given the southward dip of the pyroclastic beds, I suspect that the vent was nearby to the north, perhaps within the Lake Corral-Huckleberry Creek drainage. Future field work would be necessary in that area of the Yakama Indian Reservation to evaluate this speculation.

The source of the andesite above Lost Lake remains a mystery. Swanson (unpublished) mapped a swarm of dikes north of Old Snowy Mountain near Elk Pass that is presently assumed to be older Tertiary, likely associated with the many Oligocene to Miocene intrusions that comprise the basement beneath the Goat Rocks units (Swanson, 1996a, 1996b). However, the intrusive rocks near Cispus Pass that were previously mapped as Tertiary are most likely part of the feeder to the Pleistocene Black Thumb dacite (discussed further below), so the Elk Pass area seems a reasonable candidate for more detailed investigation.

In addition to their location, the size and duration of the early Pleistocene volcanoes remain to be determined. Given the degree of erosion and isolation of the two dated units, probably only a fragmented understanding can be reconstructed, but there are still potentially related deposits worth investigating in more detail. In particular, I suspect based on its outcrop description and composition that the andesite of Angry Mountain (Swanson, 1996b) may be close in age and from the same source as the andesite of Lost Lake. That unit consists of two isolated lava flow remnants on the western side of Angry Mountain, distal to the Lake Creek center (Swanson, 1996b; Figure 2.1). One outcrop is magnetically reversed, like the andesite of Lost Lake, as well as some lava flows from the Lake Creek volcano (Swanson, 1996b). The sample analyzed for major element concentrations (82-9; Swanson, 1996b) clusters with the andesite of Lost Lake (slightly more silicic) as well as some samples from the Lake Creek volcano (those two groups overlap significantly in trace elements as well, so the missing trace element data for the Angry Mountain andesite are not likely to be revealing). However, Swanson (1996b) points out that the outcrops are at quite high elevation (5200 feet) to be the downstream equivalent of the nearest reversed Lake Creek flows (5800 feet at nearly 4 km away). Therefore, I believe it most likely that those outcrops are early Pleistocene in age and from the same volcanic episode as the andesite of Lost Lake, not associated with the Lake Creek volcano. Future geochemical and geochronologic work on this and other distal lava flow remnants (e.g. presently unassigned units in Walupt Lake quadrangle) could help fill in the gap in the volcanic timeline between Tieton Peak and Bear Creek Mountain stages. One wonders, was magmatism essentially continuous through the ~3 m.y. lifespan of the Goat Rocks volcanic complex, or were there long periods of quiescence intercalated with the more productive periods? For the younger eruptive stages, at least, the new ages presented here indicate a continuation from one volcano to the next, rather than the previous model of punctuated activity (see discussion to follow).

No breaks between younger three eruptive stages

Based on the ages presented in Chapter 1, the activity of Bear Creek Mountain, Lake Creek volcano, and Old Snowy Mountain (and associated smaller volcanoes) were defined as three discrete eruptive stages. However, the new ages presented here indicate overlap between Bear Creek Mountain and Lake Creek volcano, and only a ~15 kyr gap between Lake Creek volcano and Old Snowy Mountain. Essentially, these eruptive stages represent a continuous ~1.5 Myr of volcanism. There is significant overlap between the compositions of Bear Creek Mountain andesites and Lake Creek andesites, which suggests that the same magmatic sources/reservoirs fed the migrating vents. The compositions of Old Snowy Mountain stage eruptive products are much different, which begs further investigation (see Chapter 4); however, the youngest Lake Creek eruptions are transitional in composition, suggesting a gradual change of input to one long-lived reservoir complex.

Stratigraphy of the Lake Creek volcano

Field magnetometer readings by Don Swanson guided his distinction of the Lake Creek eruptive products into three units: Qgr_1 (oldest and normally magnetized), Qgr_2 (reversely magnetized), and Qgr_3 (younger normally magnetized; Swanson, 1996b). The radiometric ages and paleomagnetic analyses presented in this and the previous chapter provide further understanding and open new questions. In Chapter 1, we noted that the 1.11-Ma age for the base of Qgr_1 possibly indicated that this entire normal unit was emplaced during the Punaruu excursion (ages for the excursion by previous authors include: 1.105 Ma, Singer et al., 1999; 1.115 Ma, Channel et al., 2002; 1.075 ± 0.032 Ma, Ownby et al., 2007; 1.095 ± 0.210, Michalk et al., 2013), or that the Jaramillo normal subchron (~1.05-0.99 Ma) is also represented. The new paleomagnetic data indicate that the basal Qgr_1 lava flow and next above are actually reversely magnetized, and so may slightly predate or postdate the Punaruu normal excursion. The highest normally magnetized lava flow in this section yielded a groundmass $^{40}Ar/^{39}Ar$ age of 1.013 ± 0.006 Ma, which is well within the Jaramillo subchron. The question remains whether the lower two flows predate, postdate, or bracket the Punaruu excursion. More than likely, the overlying normal sequence consists solely of Jaramillo aged lava flows, rather than sampling the Punaruu and then skipping the 50 kyr reversed period before the next eruption. Additional dating is needed to clarify this. Overall, the Qgr_1 unit spans approximately 100 kyr. We sampled 11 lava flows across the Goat Lake cirque within this unit, but may have missed a few owing to inconsistent exposure, so consider a range of 11-15 lava flows a reasonable guess. If eruption frequency was near regular (unlikely given magnetostratigraphy), then a lava flow occurred approximately every 7,000-9,000 years. If all (9 to 13) of the normally magnetized lava flows erupted during the Jaramillo subchron, then this shortens the average interval to ~3,000-4,000 years.

As documented in Chapter 1, two samples of hornblende dacite exposed on Snyder Mountain (one dike and one lava flow), mapped as Qgr_2 by Swanson (1996b), actually yielded among the youngest ages for the Lake Creek pile (559 ± 5 ka and 593 ± 4 ka). All samples of Qgr_3 lava flows yielded older ages, and these two unusual "Qgr_2" ages are far removed from the other Qgr_2 ages (~993-820 ka). Thus, there is an unmapped discontinuity between unit Qgr_2 and an upper reversed unit (I propose that they be designated Qgr_4). More detailed fieldwork (and perhaps geochronology and ChRM analysis) are required to place contacts on the map. Notably, the age of Jordan Creek dacite (580 ± 8 ka) falls between the above ages. Also hornblende-bearing, the Jordan Creek dacite is compositionally very similar to these Qgr_4 samples, so all signs point to them deriving from the same magmatic episode. One wonders whether other dikes mapped on the northwest flank of Johnson Peak, and those on the ridge southeast of Johnson Creek (see Swanson, 1996b), are also from the same time range, or whether flank eruptions were common throughout the lifespan of the Lake Creek volcano.

Interpretations about the Cispus Pass area: intrusive vs. extrusive and genetic relations

Characterizing the Cispus Pass pluton and its relation to overlying volcanic units was not a focus of this study, but it demands attention. Here I contribute my interpretations about the geology based on field observations, petrography, and a select few compositional analyses. My field work did not extend down into the Cispus River basin to sample the plutonic rocks there, so for those I rely on the descriptions and a small number of compositional analyses by previous workers (Ellingson, 1968; Clayton, 1983; Swanson, unpublished field notes; Gusey et al., 2018). My overall impression of the area aligns with Ellingson's (1968) model of an intrusive complex feeding into the Black Thumb dacite (Figure 2.1). The Black Thumb massif appears to be either a shallow plug or a dome/coulée based on its morphology and its proximity to pyroclastic breccia and a lava flow of similar composition. The deposits farther southeast along the ridge (including Gilbert Peak) require further work to determine their relation to the Black Thumb lava mass. From afar, that ridge appears to consist of pyroclastic rubble like the breccia observed near Black Thumb, and previously I had interpreted it as downflow rubble continuous with Black Thumb such that the entire package was essentially one massive coulee (Wall et al., 2018). However, based on several lines of evidence (described below), a more extensive composite cone was present here, into which the Black Thumb plug or dome intruded.

The major and trace element composition of a clast from the breccia outcrop below Black Thumb (GR17-46) differentiates it from the overlying lava, so this was probably not part of the same eruption. An outcrop ~0.5 km south of that rubble deposit is a devitrified lava flow with large sheared air pockets and autoliths that can be observed in both outcrop (photo) and in thin section at a smaller scale (sample GR17-49; Figure 2.12). The mineralogy and glomerocrystic clots in this lava are very much like those of the breccia clast (GR17-46; XRF and ICP-MS data for GR17-49 are not available for comparison). About 0.8 km south of Cispus Pass, there is a matrix-supported volcaniclastic deposit (block-and-ash flow or lahar?) overlain or intruded by a lava outcrop (unclear if flow or plug; Sample GR17-41) that has a very similar major and trace element composition to the breccia. The dike that forms the ridge south of this outcrop (including a distinctive columnarly jointed "postpile" outcrop above the Pacific Crest Trail) appears continuous with that flow or plug, although the sample analyzed (GR17-54) has a composition more like Black Thumb. In summary, between Black Thumb and the ridge overlooking the Walupt Creek valley are several pyroclastic deposits, lavas, and shallow intrusions, with a small range of dacitic compositions, above a complex of finely-holocrystalline to porphyritic and variably altered hypabyssal intrusions which presumably are part of the Cispus Pass pluton.

The extent of the Cispus Pass pluton and relation to the volcanic edifice requires deeper investigation. The Black Thumb-type dacite is relatively close in composition to a sample of Cispus Pass pluton from the Cispus River basin analyzed by Gusey et al. (2018), lending credence to Ellingson's (1968) interpretation that that intrusion was the feeder for Black Thumb. In addition, Clayton's (1983) zircon fission-track age of 1.11 ± 0.18 Ma aligns reasonably well with the age of Black Thumb; he acknowledges that it is probably too old due to the high uranium content of the zircons and consequent problems counting the induced tracks, so the true age could very well be ~ 815 ka. In the future, zircons from the intrusion could be dated more precisely by crystal surface analysis, as was performed for the Black Thumb sample (Chapter 1; Wall et al., 2018). It should be noted that the location of Clayton's sample is shown on the north side of the ridge connecting Ives Peak and Black Thumb (Clayton, 1980). Likewise, although he did not include them on his map, Ellingson (1968) describes numerous dikes in "Glacier Basin" on the north side of that ridge. Therefore it is apparent that the Cispus Pass intrusive complex extends over a broad area, both north and south of the Ives Peak-Black Thumb divide, but its precise boundary is not well defined. This author wonders whether it includes the intrusion identified by Swanson (unpublished), ~1.25 km north of Black Thumb, which is presently interpreted as an older Tertiary intrusion (Figure 2.1). However, Swanson's sample from that area (96-42, included in Appendix Table A2.2) is quite unlike Gusey's sample from the Cispus basin; it is significantly more alkalic and enriched in Ba and Zr. Interestingly, that composition is much like samples from the Tieton Peak area—could that more northern intrusion represent the underpinnings of the Tieton Peak volcano? Clearly, the greater Cispus Pass – Gilbert Peak – Conrad Basin area is promising for more detailed field study, petrographic and geochemical analysis, and dating (perhaps zircon U-Pb for plutonic rocks) to evaluate the extent of these intrusive units and their relation to overlying volcanic units.

Age and duration of Goat Ridge and Old Snowy Mountain volcanoes

Previously, Swanson (1996a) had interpreted that the lava flows of Old Snowy Mountain were younger than those of Goat Ridge, since the former occupy the Goat Creek-Cispus River valley, which has been eroded into the Goat Ridge flows. No samples from the downvalley extents of these units were dated, so Swanson's interpretation of emplacement order there remains plausible. However, given that each vent's proximal deposits overlap in age, it also seems plausible that the more far-travelled lava flows were coeval and banked against each other (or intercalated to some degree), rather than having been emplaced in sequence. Between 450-200 ka there were several glacial periods (MIS 12, 478-424 ka; MIS 10, 374-337 ka; MIS 8, 300-243 ka; Lisiecki and Raymo, 2005), and so the erosion observed in Goat Ridge lava flows on the valley wall more than likely represents a complex interplay of ice and volcanoes, rather than a simple sequence of events.

Longevity of Goat Rocks volcanic complex vs. other arc andesite centers

The new geochronology results contribute to our understanding of the persistence of andesitic volcanism at focal points along an arc. At Goat Rocks, andesite and dacite eruptions recurred over a period of about 3 million years following the 3.2-Ma Devils Horns rhyolite eruption. This is a much longer record of recent volcanism than is known in the Mount Rainier, Mount Adams, or Mount St. Helens areas (Figure 2.13). It is comparable to the history of the Mount Hood area, where andesite lava flows have been dated at 3.1 ± 0.2 Ma and 2.74 ± 0.03 Ma in the vicinity of Lookout Mountain, and where the Sandy Glacier volcano (and probably several other vents) was active between ~1.8 and 0.6 Ma, prior to the onset of the modern edifice at ~0.5 Ma (Sherrod and Scott, 1995; Scott and Gardner, 2017). One wonders whether andesite eruptions in the Mount Hood area also occurred in the early Pleistocene, where there is presently a gap in the geochronologic record. As more dating in the Goat Rocks area has revealed longer eruptive stages and less time between them, so it seems likely that other major arc centers represent sustained activity over millions of years. This was shown to be true by Hatter et al. (2018) for the volcanic complex of Montserrat, where the sequence of volcanoes spans ~2.2 million years of activity, with coeval periods of waxing and waning vents.

Further geochronologic study on the deeper histories of Cascade volcanoes (and indeed those of other arcs) is promising for new insights into the flux and distribution of melt delivery throughout the arc over time. The present data for the Rainier-to-Hood section of the Cascades indicate that magma genesis was focused at Goat Rocks, Simcoe Mountains, Boring Volcanic Field, and Mount Hood in the late Pliocene and early Pleistocene (Figure 2.13). By mid-Pleistocene, andesitic volcanism had begun in the Rainier area, and then by late Pleistocene, as activity at the Simcoe Mountains volcanic field was extinguished, new volcanoes were built to the west at Mount Adams, Mount St. Helens, and Indian Heaven (Figure 2.13). Is this transition a coincidence, or does it provide meaningful information about such things as a "budget" of mantle melt or a change in tectonics? Looking further back in time, the distribution and longevity of major Cascade andesite centers (such as the Miocene or Oligocene Angry Mountain and Tieton Volcano, near Goat Rocks) are not understood in detail. Decades of valuable work have clarified the broad evolution of the arc through time (e.g. du Bray and John, 2011), but at present our understanding of individual volcano lifespans is heavily weighted toward the recent, with much scarcer age data for most of the arc's history. Many units in the Goat Rocks area, for example, are identified as "Oligocene to Miocene" with no radiometric age constraints. Many of the ages that do exist are K-Ar or zircon fission-track and could likely be improved with modern techniques. Factors such as erosion, alteration, and increasing uncertainty with older ages pose significant challenges, but this author sees hope for a movement from staccato snapshots to a 4D perspective of the arc's dance in time.

Recommendations for future work

The evolutionary story of the Goat Rocks volcanic complex would benefit from additional mapping and geochronology in numerous locations. Several of these are compiled here from sections above, alongside several additional recommendations.

1) Perhaps most importantly, the Conrad Basin – Gilbert Peak – Cispus Pass area requires significant additional field investigation, petrography, geochemistry, and geochronology to evaluate the relations between intrusive and volcanic units. Not often can geologists observe the subvolcanic and extrusive components of a volcano together—what can this joint evidence reveal about the volcanic construction process?
2) The Walupt Lake quadrangle in general needs attention: intrusive and volcanic units farther southeast along Countyline Ridge are of unknown age, presently presumed older Tertiary, but like the intrusive suite at Cispus Pass, could be Goat Rocks-era after all. The apparently Quaternary andesitic units mapped preliminarily along the Cispus River drainage need further characterization to determine their source(s) and ages. In addition, the contacts and stratigraphy between the Coleman Weedpatch area (south of Walupt Lake) and Lakeview Mountain are not clearly defined; and while the Coleman Weedpatch/Two Lakes basalts are presumably close in age to the Walupt Lake volcano, this could be quantified (with implications for the production of distinct basalt compositions in a geographically confined area; discussed further in Chapter 3).

3) Radiometric ages for the following units in other areas are also desirable: the andesite of Angry Mountain, to confirm (or deny) relation to the Lost Lake andesite; the andesite along the upper Miriam Creek drainage, to evaluate whether related to underlying Miriam Creek basalts or overlying Hogback Mountain volcano (or whether its own isolated volcanic episode); the diorite intrusions between Miriam Creek and Round Mountain, which are suspected to be late Pliocene by Swanson and Clayton (1983); and Swanson's units Qah and Qac in Old Snowy Mountain quadrangle, which are presumed young, but how young? As well, more ages for the Old Snowy Mountain volcano (e.g. higher in stratigraphy/near summit, further east near Ives Peak vent area, and distal lava flows) could better constrain its end-of-life. The youngest age determined (for a lava flow on the proximal flank) is ~217 ka, ~100 ka before the Clear Fork Lava. One wonders: was there actually a short period of quiescence between these episodes, or was activity continuous as between Bear Creek Mountain, Lake Creek volcano, and Old Snowy Mountain?

CONCLUSIONS

Broadly andesitic, calcalkaline volcanism persisted at the Goat Rocks volcanic complex for nearly 3 million years. The earliest intermediate lava flows were erupted at ~3.1 Ma, shortly postdating the 3.2 Ma Devils Horns rhyolite eruption. Activity continued until nearly 100 ka when the Clear Fork Lava Flow was erupted. Early eruptive products from the Tieton Peak volcano represent a broad range of compositions, from two-pyroxene andesite to dacite, trachydacite, and rhyolite. The middle eruptive stages were dominated by two-pyroxene andesite, trachyandesite, and dacite, becoming gradually more silicic with time. Near the end of the Lake Creek stage, those magmas were replaced by amphibole-bearing andesites and dacites, and the youngest Old Snowy Mountain stage was dominated by similarly less potassic, more aluminous, amphibole-bearing andesites and lesser dacites.

The new ages reported in this chapter reveal that the three younger eruptive stages (Bear Creek Mountain, Lake Creek, Old Snowy Mountain) represent essentially a continuous sequence of volcanic activity. A younger eruption from Bear Creek Mountain overlaps with the onset of the Lake Creek volcano at ~1.1 Ma. A hornblende andesite on the western flank of the Lake Creek volcano was dated at 456 ± 12 ka, predating the earliest known Old Snowy Mountain eruption (440 ± 3 ka) by only ~16 kyr. Thus, volcanic eruptions occurred at a relatively steady pace between ~1.6 and 0.1 Ma, and were likely fed by a continuous magmatic system rather than discrete magmatic episodes. However, the distinction of eruptive stages as outlined in Chapter 1 is maintained due to the relocation of volcanic centers and changes in mineralogy and composition (especially between Lake Creek and Old Snowy Mountain stage). Given the dearth of dated samples between Tieton Peak and the early Pleistocene andesites from unidentified vents, and between the latter and Bear Creek Mountain, it remains unknown whether long periods of quiescence truly occurred or whether andesitic volcanism was essentially continuous from 3.1 Ma on.

The longevity of the Goat Rocks locus is comparable to the well-dated nearby mafic fields Simcoe Mountains (~3.4 m.y.) and the Boring Volcanic Field (~2.7 m.y.). Persistent andesitic volcanism is also indicated at the Mount Hood locus, where the Lookout Mountain volcano was coeval with Tieton Peak volcano, and Sandy Glacier volcano with the Bear Creek Mountain and Lake Creek volcanoes. The Goat Rocks volcanic complex, with its extended eruptive periods and overlapping activity of migrating vents, is unlikely to be anomalous for arc andesite centers. Lifespans of individual composite volcanoes are well documented at ~10^5-10^6 years, but with future more detailed geochronology on older Cascades volcanic units, the Goat Rocks example of sustained magmatism over millions of years may be revealed to be typical.

FIGURES

Figure 2.1. Simplified geologic map of the Goat Rocks volcanic complex and nearby vents. A-A' and B-B'-B" indicate cross sections shown on following page. Legend with unit descriptions follows cross sections. On map, quaternary sedimentary cover is removed for clarity where underlying unit relations are straightforward. Square markers indicate samples collected by this author between 2015 and 2020. Triangles indicate dated samples, and they are shaded light to dark from old to young. Map unit colors approximately correspond to colorways in other diagrams. Most map contacts are as determined previously by Clayton (1980, 1983), Swanson and Clayton (1983), Swanson (1996a, 1996b, and unpublished field maps), and Gusey et al. (2018). Minor modifications have been made considering new observations and results from recent field work, compositional analyses, and geochronology. Contacts are dashed where less confident. The extent of the Cispus Pass pluton is approximated based on descriptions by Ellingson (1968) and the boundary an intrusive body (formerly presumed Tertiary) mapped by Swanson and Clayton (1983). Lakes and waterways are from the U.S. Geological Survey National Hydrography Dataset. Note that glaciers are excluded for clarity. The DEM hillshade baselayer is from the Esri World Hillshade server. Map was compiled using QGIS Desktop v. 3.16.1.

Cross sections are highly schematic to emphasize geologic relations. Dashed lines in unit Tv represent generalized bedding and structure. The representation of the Cispus Pass pluton (unit Qicp) is inspired by the model of Ellingson (1968). Thickness of dikes above the pluton and feeding the Lake Creek volcano, and feeders for other volcanoes, are schematic and/or enlarged for emphasis. Tertiary intrusions (Ti) are highly simplified and projected from outcrops that are nearby but not intersecting cross sections. Dropped blocks of a caldera roof are assumed beneath the Devils Horns rhyolite (unit Tpr; Swanson, unpublished field notes), but this is not yet confirmed.

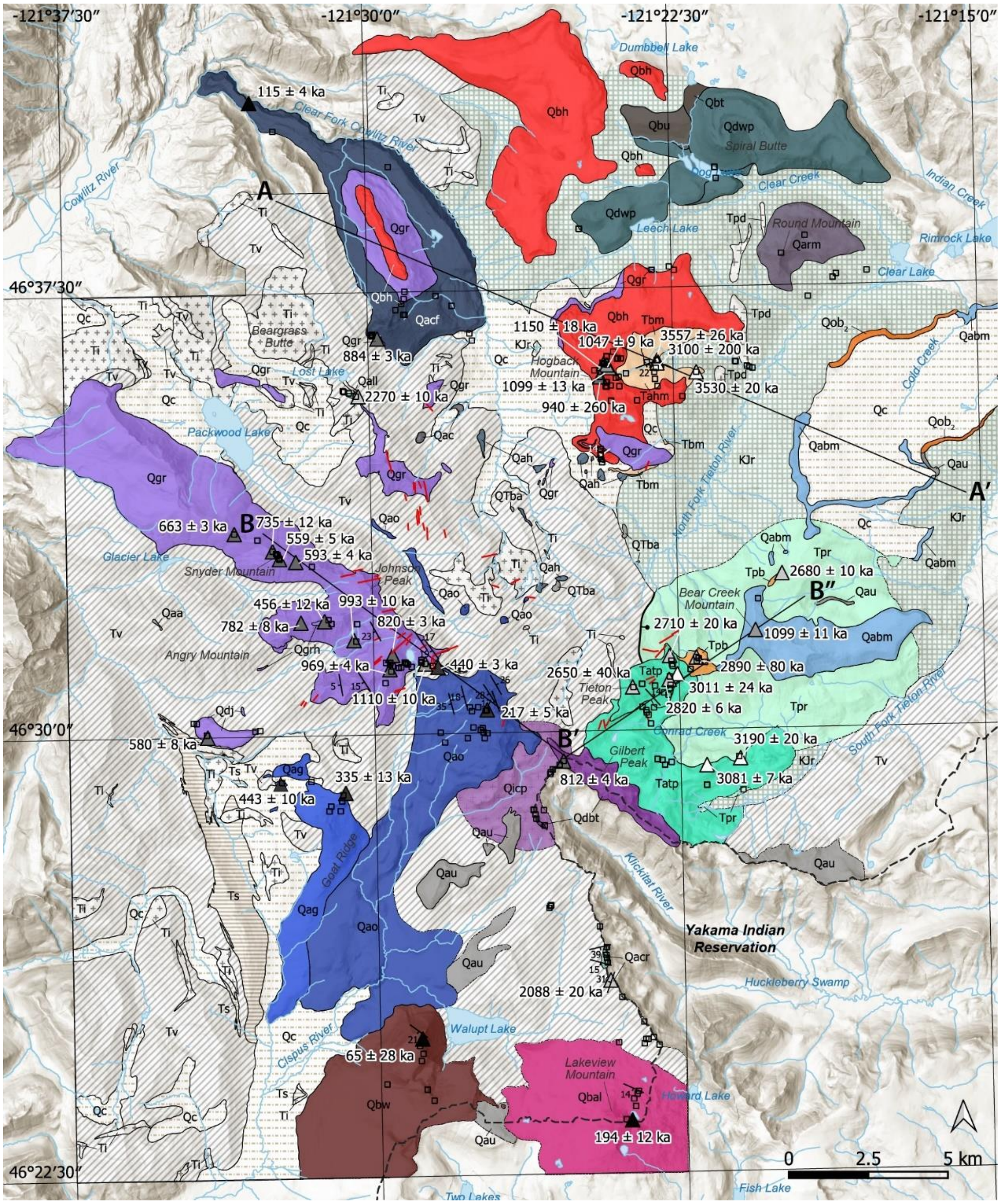
-121°37′30″
-121°30′0″
-121°22′30″
-121°15′0″
46°37′30″
46°30′0″
46°22′30″
115 ± 4 ka
1150 ± 18 ka
1047 ± 9 ka
3557 ± 26 ka
3100 ± 200 ka
884 ± 3 ka
1099 ± 13 ka
3530 ± 20 ka
2270 ± 10 ka
940 ± 260 ka
663 ± 3 ka
735 ± 12 ka
559 ± 5 ka
593 ± 4 ka
2680 ± 10 ka
456 ± 12 ka
993 ± 10 ka
782 ± 8 ka
820 ± 3 ka
2710 ± 20 ka
1099 ± 11 ka
969 ± 4 ka
440 ± 3 ka
2890 ± 80 ka
2650 ± 40 ka
1110 ± 10 ka
3011 ± 24 ka
217 ± 5 ka
2820 ± 6 ka
580 ± 8 ka
3190 ± 20 ka
335 ± 13 ka
3081 ± 7 ka
812 ± 4 ka
443 ± 10 ka
2088 ± 20 ka
65 ± 28 ka
194 ± 12 ka
A
A′
B
B′
B″
Dumbbell Lake
Clear Fork Cowlitz River
Cowlitz River
Spiral Butte
Clear Creek
Indian Creek
Leech Lake
Round Mountain
Rimrock Lake
Clear Lake
Beargrass Butte
Lost Lake
Hogback Mountain
Packwood Lake
Cold Creek
North Fork Tieton River
Glacier Lake
Snyder Mountain
Johnson Peak
Bear Creek Mountain
Angry Mountain
Tieton Peak
Conrad Creek
Gilbert Peak
South Fork Tieton River
Goat Ridge
Klickitat River
Yakama Indian Reservation
Huckleberry Swamp
Walupt Lake
Cispus River
Lakeview Mountain
Howard Lake
Two Lakes
Fish Lake
0
2.5
5 km

Figure 2.1.

Legend

Geologic Units

Qc — **Quaternary cover.** Undifferentiated alluvium, colluvium, alluvial fan deposits, landslides, and glacial deposits. Unit is removed in some areas to better show underlying volcanic units.

Qbt — **Basalt of Tumac Mountain.** Olivine-bearing basaltic andesite lava flows of the Tumac Mountain shield volcano.

Qbu — **Basalt, undifferentiated**, distinguished from Basalt of Tumac Mountain by Clayton (1980) near Spiral Butte.

Qbw — **Basalt of Walupt Lake volcano.** Hyaloclastic deposits, scoria, and lava flows of olivine basalt comprising the Walupt Lake subglacial volcano (tuya). For simplicity, unit includes basalts and basaltic andesites of Coleman Weedpatch and Two Lakes areas (Qbt and Qba of Swanson, 1996a).

Qacf — **Andesite of Clear Fork Cowlitz River.** Fine-grained, sparsely hornblende-phyric andesitic to dacitic lava flow erupted from vent near Coyote Lake. Flowed along ancestral Clear Fork Cowlitz River and ponded to form thick columnar outcrop visible from Palisades viewpoint on Highway 12.

Qdwp — **Dacite of White Pass.** Dacite and silicic andesite erupted from small vents near White Pass, including Spiral Butte. Commonly hornblende-bearing.

Qarm — **Andesite of Round Mountain**. Fine-grained, sparsely hornblende-phyric andesite from Round Mountain volcano.

Qbal — **Basaltic andesite of Lakeview Mountain.** Lava flows and pyroclastic deposits of the Lakeview Mountain volcano. Fine-grained, commonly glassy, olivine-phyric basaltic andesite.

Qao — **Andesite of Old Snowy Mountain**. Light gray, sparsely and finely hornblende-two-pyroxene-plagioclase-phyric andesite flows erupted from Old Snowy Mountain-Ives Peak area.

Qag — **Andesite of Goat Ridge.** Sparsely to moderately but finely two-pyroxene-plagioclase(±hornblende) andesite on southern end of Goat Ridge. Includes lesser dacite and rhyolite flows (Qdg and Qrg of Swanson, 1996b). Erupted from southern crest of Goat Ridge, but glaciation has removed all trace of cone(s).

Qac — **Andesite of Chimney Creek**. Basaltic andesite to andesite lava flow(s) that probably erupted from a vent ~1.5 km north of Chimney Rock, identified by Swanson (unpublished field notes). Age is uncertain, but probably post-Lake Creek stage.

Qah — **Quaternary hornblende andesite.** Light grey to beige, fine-grained, hornblende-bearing andesite to rhyolite flows or domes exposed along valley walls of the Clear Fork Cowlitz River basin southwest of Hogback Mountain. Age is uncertain, but probably post-Lake Creek stage.

Qgr Qdj Qgrh — **Andesite and dacite of Lake Creek volcano**. Unit Qgr combines Swanson's (1996b) Qgr_1, Qgr_2, and Qgr_3 of main stage Lake Creek volcano. Lava flows are dominantly two-pyroxene andesite, though amphibole is common in younger lava flows (including dacite of Jordan Creek (Qdj) and late-stage hornblende andesite (Qgrh)). Quaquaversal dips and radial dikes suggest a vent within the basin of Upper Lake Creek.

Qdbt — **Dacite of Black Thumb.** Pyroclastic deposits, lava flows and thick dome/plug of dacite from a vent centered near Black Thumb and forming the ridge northeast of Klickitat River headwaters that includes Gilbert Peak.

Qicp — **Cispus Pass pluton**. Complex of shallow intrusions of granodiorite or quartz monzonite near Cispuss Pass described by Ellingson (1968) and Clayton (1983). Presumed to be the intrusive equivalent of, and feeder for, dacite of Black Thumb.

Qbh — **Basalt of Hogback Mountain**. Thin flows of basalt or basaltic andesite, often olivine-bearing, erupted from Hogback Mountain shield volcano. Lower flows in section are interbedded with andesite lavas probably from Lake Creek volcano.

Qabm — **Andesite of Bear Creek Mountain.** Plagioclase-two-pyroxene (±olivine)-andesite lava flows, agglomerate, and dikes comprising Bear Creek Mountain and including the two far-travelled Tieton Andesite lava flows (Gusey et al., 2018).

Qob_2 — **Olivine basaltic andesite.** At least three flows of basaltic andesite that crop out on Pinegrass Ridge and near the confluence of the Tieton River and Naches River. Phenocrysts are olivine, clinopyroxene, and plagioclase (Hammond, 2017).

Qau Qaa QTba — **Basaltic andesite and andesite of uncertain source and age.** Includes basaltic andesite near Tieton Pass (QTba), undifferentiated andesite in Walupt Lake quadrangle (Qau), and andesite of Angry Mountain (Qaa; Swanson, 1996b and unpublished).

Qacr Qall — **Early Pleistocene andesite.** Includes plagioclase-two-pyroxene-andesite of Lost Lake (Qall, 2.3 Ma), and olivine andesite on Countyline Ridge (Qacr, 2.1 Ma).

Tatp — **Andesite of Tieton Peak.** Plagioclase-two-pyroxene-andesite and dacite (plus lesser rhyolite and trachyte) lava flows and dikes comprising Tieton Peak and upper Conrad Creek basin. Lava flows (or possible shallow intrusions) lower in stratigraphy are mineralized and often bleached or colored green or purple.

Tpb — **Basalt of Devils Washbasin.** Olivine-clinopyroxene-plagioclase basalt from a vent near Devils Washbasin marked by thin lava flows and bedded pyroclastic rocks crosscut by dikes.

Tpr — **Rhyolite of Devils Horns.** Thick accumulation of ignimbrites, tephra fall deposits, breccia, and possible domes of high-silica rhyolite beneath Devils Horns. Deposits probably represent a caldera-forming eruption (note fault north of Tieton Peak).

Tahm Tbm — **Basalt and andesite of Miriam Creek.** Lower section of sparsely olivine-phyric basaltic lava flows, scoria, and tephra comprise the ~3.5-Ma Miriam Creek volcano. Overlying andesitic to dacitic lava flows or intrusions are of uncertain age (late-stage Miriam Creek, early Hogback Mountain, or intermediate?).

Tpd — **Late Tertiary dacite intrusions.** Light-colored, coarsely porphyritic, fine-grained dacite. Phenocrysts are dominantly plagioclase and hornblende; some rocks also contain biotite and quartz. Occurs as dikelike bodies between Miriam Creek and Twin Peaks (Swanson and Clayton, 1983). Includes coarser-grained granodiorite along Miriam Creek.

Ti — **Tertiary intrusions.** Sills, dikes, and complex intrusions emplaced over numerous episodes. Dominantly intermediate compositions (andesite-dacite, or diorite), but gabbro and rhyodacite also occur. Oligocene to Miocene (Swanson, 1996a, 1996b).

Tv — **Tertiary volcanic deposits.** Lava flows, domes, and volcaniclastic rocks ranging from basalt to rhyolite in composition. Includes units correlative to Summit Creek basalts, Ohanapecosh Formation, and Fifes Peak Formation, including remnants of the Angry Mountain composite volcano. Eocene to Oligocene (Swanson, 1996a, 1996b).

Ts — **Tertiary sedimentary deposits**, i.e. Arkose of Chambers Creek (Winters, 1984; Swanson, 1996b). Well-bedded, typically micaceous arkose and lesser pebble conglomerate, siltstone, and mudstone. Complex interbedding with volcanic sandstone of unit Tv is greatly simplified on map. Eocene and Oligocene.

KJr — **Russell Ranch formation.** Graywacke, argillite, and less abundant basalt flows, most of which are pillowed and metamorphosed to greenstone. Sheared in most places. Constitutes part of the Rimrock Lake Inlier, an accreted Cretaceous to Jurassic arc terrane (Swanson and Clayton, 1983; Miller, 1989).

Samples

▫ Sample collected for thin section or geochemistry

Dated samples:

- ▲ 0 - 200 ka
- ▲ 200 - 450 ka
- ▲ 450 ka - 1 Ma
- ▲ 1 - 2 Ma
- ▲ 2 - 3 Ma
- △ > 3 Ma

Geologic Symbols

- Dike
- Fault
- 14 Strike and dip measurement
- Lake/Pond
- Stream

Figure 2.1 (continued)

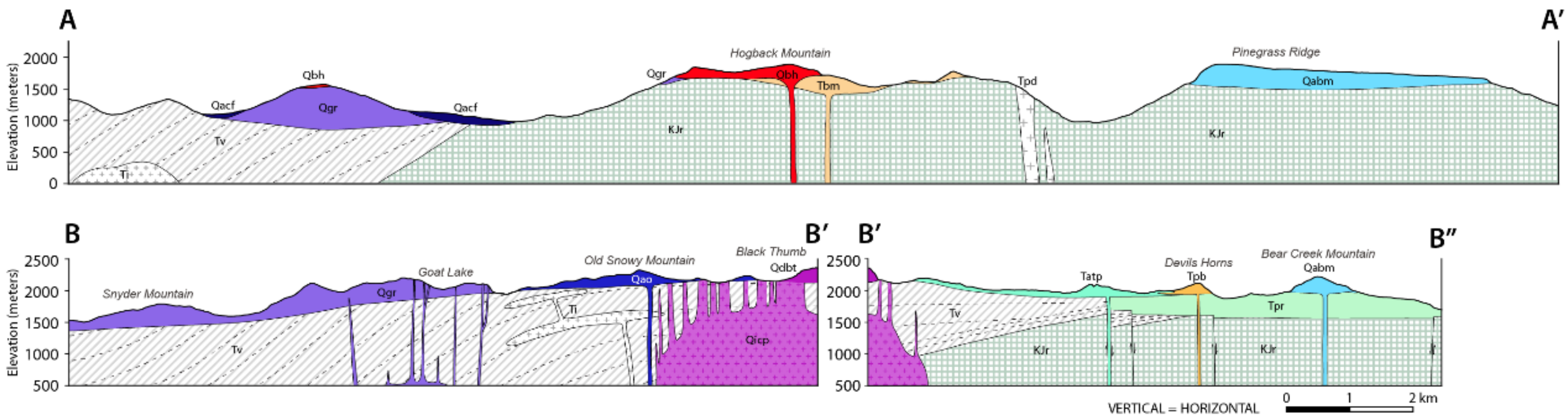

Figure 2.1 (continued).

Figure 2.2. Geographic evolution of the Goat Rocks volcanic complex and peripheral mafic volcanoes.
In each panel, for a given time period, locations of active vents are shown with interpreted approximate extent of lava flows. **a)** Includes pre-GRVC volcanoes of Miriam Creek and Devils Horns; the first Goat Rocks eruptive stage, Tieton Peak (includes Tieton Peak and Devils Washbasin volcanoes); and early Pleistocene andesites. Inset map shows location of Goat Rocks volcanic complex (GRVC) on the Cascade Arc. **b)** Proximal lava flows of Bear Creek Mountain and the two far-travelled Tieton andesite lavas (see inset) erupted from vents near Bear Creek Mountain (Gusey et al., 2018). Basalt and basaltic andesite (Qob_1 and Qob_2) also erupted during this period, but their source is uncertain. **c)** Lake Creek stage includes the Lake Creek volcano, the Cispus Pass volcano (including Black Thumb plug or dome), and Hogback Mountain shield volcano (two vents active there). **d)** Old Snowy Mountain stage includes the volcanoes of Old Snowy Mountain-Ives Peak, Goat Ridge, and Coyote Lake (source of the Clear Fork lava flow). The mafic Lakeview Mountain volcano also erupted during this time, and Walupt Lake volcano and vents near Coleman Weedpatch postdate it. Also shown are the young andesite and dacite volcanoes of White Pass and the Tumac Mountain shield volcano (see Clayton, 1980). **e)** Simplified volcanic timeline; see Figure 2.5 for more details.

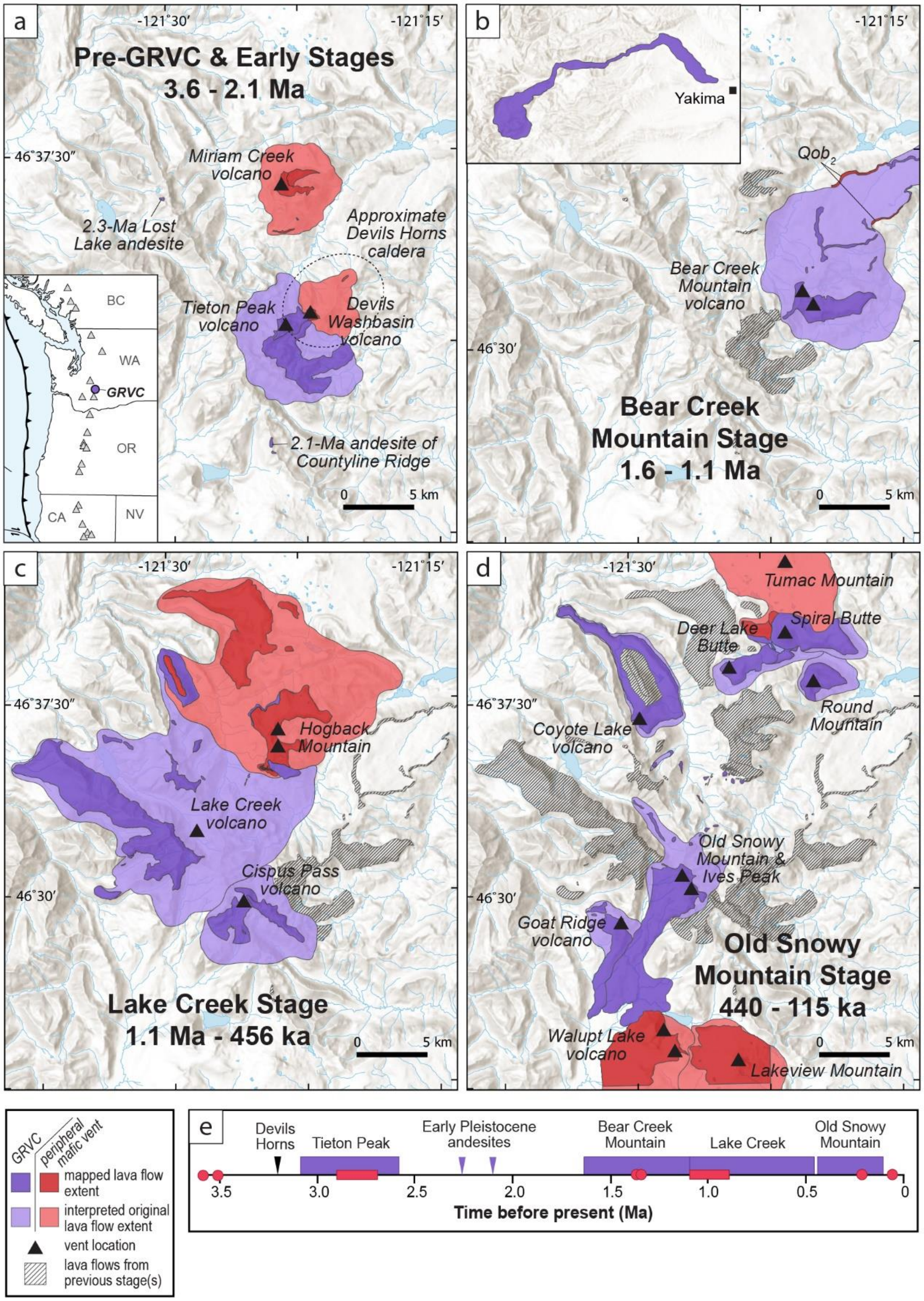
a
-121°30′
-121°15′
Pre-GRVC & Early Stages
3.6 - 2.1 Ma
46°37′30″
Miriam Creek
volcano
2.3-Ma Lost
Lake andesite
Approximate
Devils Horns
caldera
Tieton Peak
volcano
Devils
Washbasin
volcano
BC
WA
GRVC
OR
CA
NV
2.1-Ma andesite of
Countyline Ridge
0
5 km
b
-121°15′
Yakima
Qob2
Bear Creek
Mountain
volcano
46°30′
Bear Creek
Mountain Stage
1.6 - 1.1 Ma
c
Hogback
Mountain
Lake Creek
volcano
Cispus Pass
volcano
Lake Creek Stage
1.1 Ma - 456 ka
d
Tumac Mountain
Deer Lake
Butte
Spiral Butte
Round
Mountain
Coyote Lake
volcano
Old Snowy
Mountain &
Ives Peak
Goat Ridge
volcano
Old Snowy
Mountain Stage
440 - 115 ka
Walupt Lake
volcano
Lakeview Mountain
GRVC
peripheral
mafic vent
mapped lava flow
extent
interpreted original
lava flow extent
vent location
lava flows from
previous stage(s)
e
Devils
Horns
Tieton Peak
Early Pleistocene
andesites
Bear Creek
Mountain
Lake Creek
Old Snowy
Mountain
3.5
3.0
2.5
2.0
1.5
1.0
0.5
0
Time before present (Ma)

Figure 2.2.

Figure 2.3. Representative argon isotope data.
For each sample, the age spectrum and inverse isochron plot are shown. Samples GR16-09-1, GR20-15, and TP19-06 (a, c, d) were analyzed at Oregon State University (OSU), and GR17-38 (b) was analyzed at the USGS Argon Geochronology Laboratory. On age spectra diagrams, black bars (OSU) or blue boxes (USGS) indicate those temperature steps that are included in the weighted mean. On inverse isochron diagrams, the selected temperature steps are marked in pink (OSU) or with black boxes (USGS).

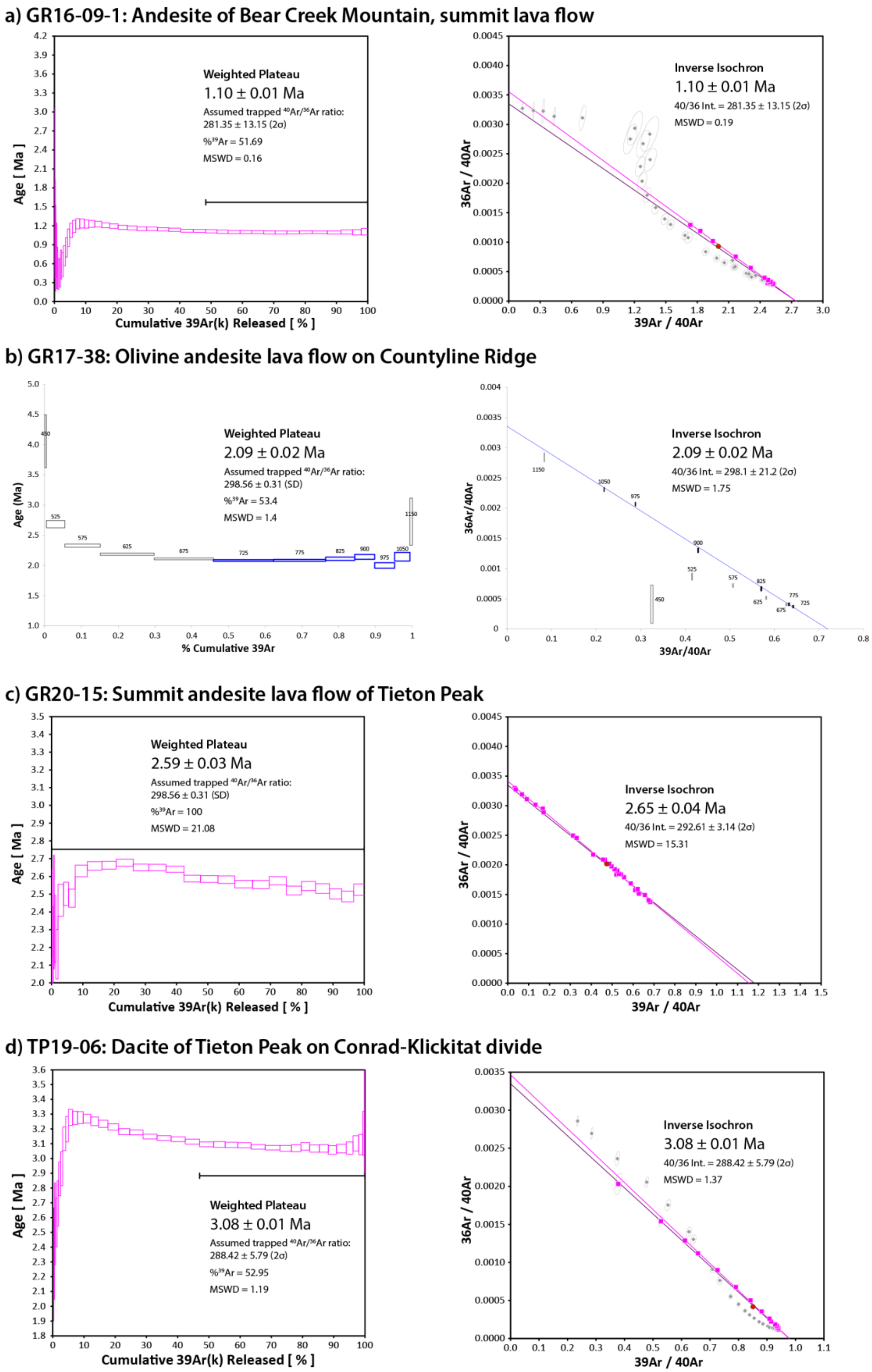
a) GR16-09-1: Andesite of Bear Creek Mountain, summit lava flow
Weighted Plateau
1.10 ± 0.01 Ma
Assumed trapped 40Ar/36Ar ratio:
281.35 ± 13.15 (2σ)
%39Ar = 51.69
MSWD = 0.16
Age [Ma]
Cumulative 39Ar(k) Released [%]
Inverse Isochron
1.10 ± 0.01 Ma
40/36 Int. = 281.35 ± 13.15 (2σ)
MSWD = 0.19
36Ar / 40Ar
39Ar / 40Ar
b) GR17-38: Olivine andesite lava flow on Countyline Ridge
Weighted Plateau
2.09 ± 0.02 Ma
Assumed trapped 40Ar/36Ar ratio:
298.56 ± 0.31 (SD)
%39Ar = 53.4
MSWD = 1.4
Age (Ma)
% Cumulative 39Ar
Inverse Isochron
2.09 ± 0.02 Ma
40/36 Int. = 298.1 ± 21.2 (2σ)
MSWD = 1.75
36Ar/40Ar
39Ar/40Ar
c) GR20-15: Summit andesite lava flow of Tieton Peak
Weighted Plateau
2.59 ± 0.03 Ma
Assumed trapped 40Ar/36Ar ratio:
298.56 ± 0.31 (SD)
%39Ar = 100
MSWD = 21.08
Age [Ma]
Cumulative 39Ar(k) Released [%]
Inverse Isochron
2.65 ± 0.04 Ma
40/36 Int. = 292.61 ± 3.14 (2σ)
MSWD = 15.31
36Ar / 40Ar
39Ar / 40Ar
d) TP19-06: Dacite of Tieton Peak on Conrad-Klickitat divide
Weighted Plateau
3.08 ± 0.01 Ma
Assumed trapped 40Ar/36Ar ratio:
288.42 ± 5.79 (2σ)
%39Ar = 52.95
MSWD = 1.19
Age [Ma]
Cumulative 39Ar(k) Released [%]
Inverse Isochron
3.08 ± 0.01 Ma
40/36 Int. = 288.42 ± 5.79 (2σ)
MSWD = 1.37
36Ar / 40Ar
39Ar / 40Ar

Figure 2.3.

Figure 2.4. Characteristic remanent magnetization (ChRM) of Goat Rocks area lava flows. **a)** Representative Zjiderfeld plots showing examples of normal and reversed magnetization. **b)** Equal area plots for each area studied. **c)** Interpretation of stratigraphy at each location, showing magnetic reversals.

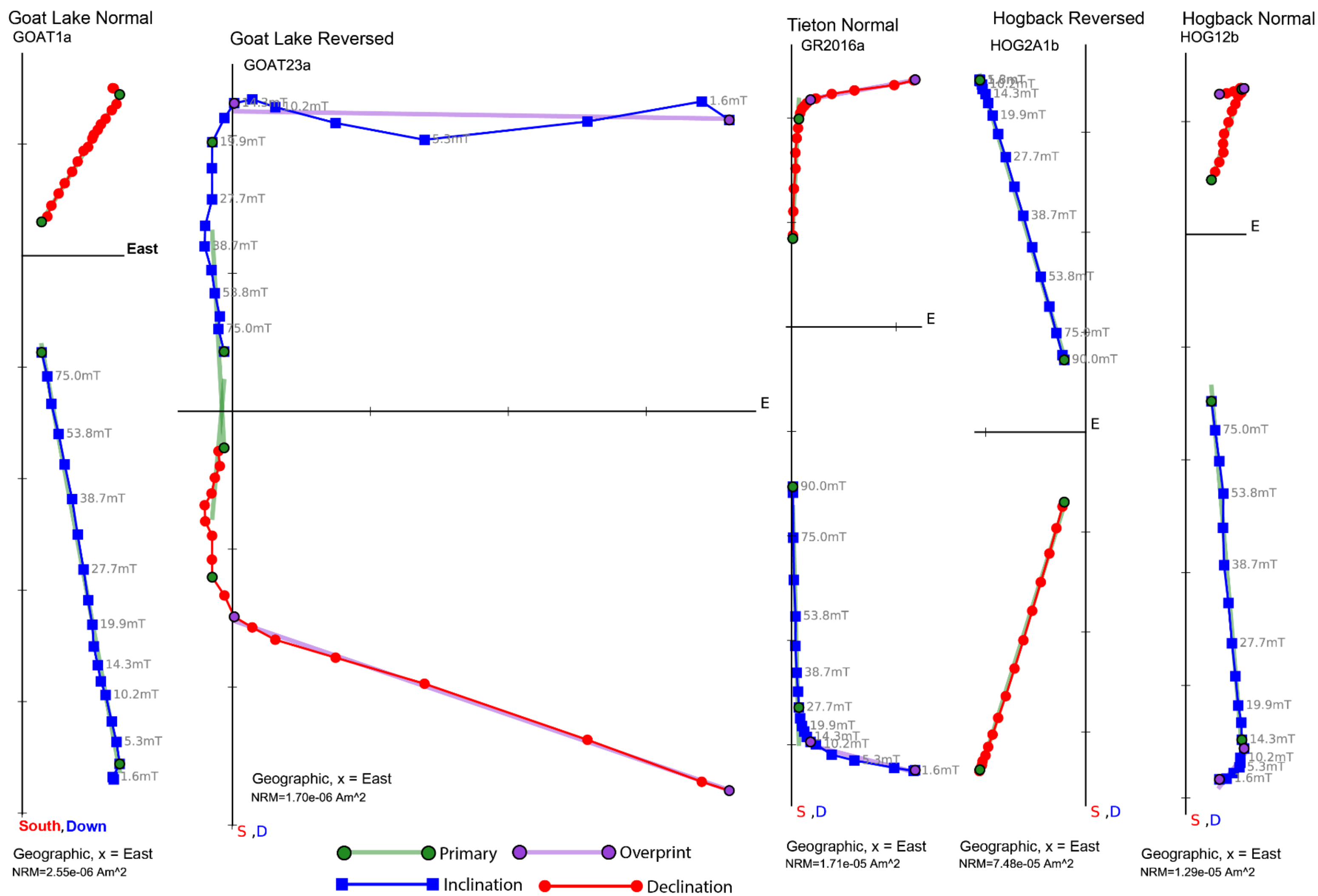

Goat Lake Normal
GOAT1a
East
75.0mT
53.8mT
38.7mT
27.7mT
19.9mT
14.3mT
10.2mT
5.3mT
1.6mT
South, Down
Geographic, x = East
NRM=2.55e-06 Am^2
Goat Lake Reversed
GOAT23a
1.6mT
5.3mT
10.2mT
19.9mT
27.7mT
38.7mT
53.8mT
75.0mT
E
Geographic, x = East
NRM=1.70e-06 Am^2
S ,D
Primary
Overprint
Inclination
Declination
Tieton Normal
GR2016a
E
90.0mT
75.0mT
53.8mT
38.7mT
27.7mT
19.9mT
14.3mT
10.2mT
5.3mT
1.6mT
S ,D
Geographic, x = East
NRM=1.71e-05 Am^2
Hogback Reversed
HOG2A1b
10.2mT
14.3mT
19.9mT
27.7mT
38.7mT
53.8mT
75.0mT
90.0mT
E
S ,D
Geographic, x = East
NRM=7.48e-05 Am^2
Hogback Normal
HOG12b
E
75.0mT
53.8mT
38.7mT
27.7mT
19.9mT
14.3mT
10.2mT
5.3mT
1.6mT
S ,D
Geographic, x = East
NRM=1.29e-05 Am^2

Figure 2.4a.

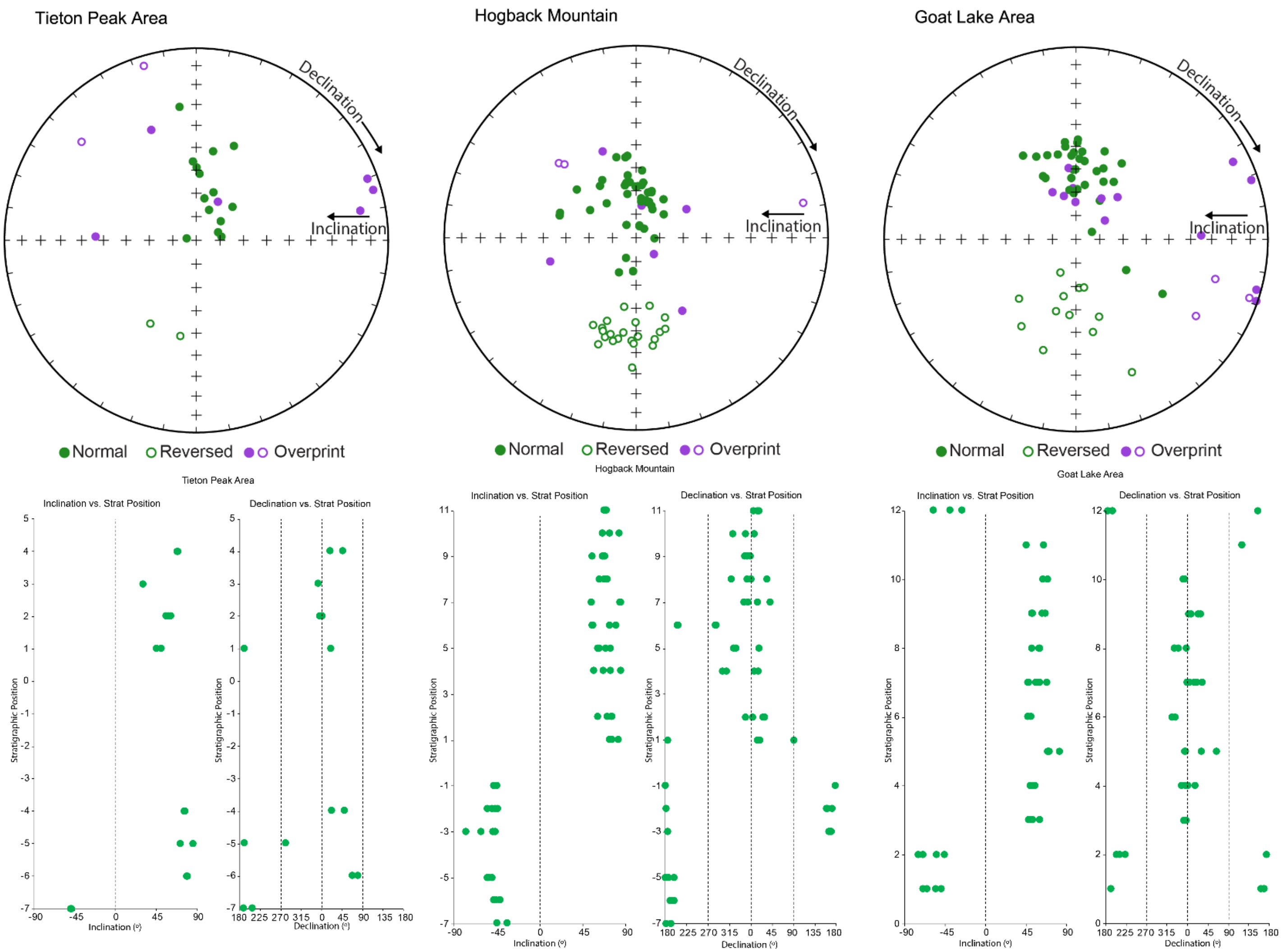

Figure 2.4b (top) and c (bottom).

Figure 2.5. Timeline of eruptive activity at the Goat Rocks volcanic complex and peripheral mafic volcanoes.
In upper panels, bars represent duration of each volcano (bars with arrows where age boundaries are not well defined), and triangles mark individual ages of units. In upper panels and on timeline, the ages of the intermediate to felsic Goat Rocks volcanic complex are separated from the ages of mafic volcanoes/units. On the age timeline, sample ages are stacked in order from oldest to youngest (bottom to top), or by stratigraphy where known. For example, one lava flow analyzed at Hogback Mountain is normally magnetized and stratigraphically above two reversed lava flows, but it yielded an older $^{40}Ar/^{39}Ar$ age. For some samples, multiple ages were determined (e.g. groundmass and plagioclase or hornblende for $^{40}Ar/^{39}Ar$ dating, or both $^{40}Ar/^{39}Ar$ and U/Pb zircon ages); these are plotted together horizontally. The Cispus Pass pluton is presumed to be coeval with Black Thumb, so its age is in line with the new Black Thumb age. New ages from this study are marked with circular symbols and represent both $^{40}Ar/^{39}Ar$ and U/Pb zircon ages. Ages from previous studies are marked with squares and represent K/Ar, $^{40}Ar/^{39}Ar$, and zircon fission-track ages. See Table 2.1 for these age data. Error bars indicate 2σ uncertainty. Black bars on the x-axis (projected to gray bars behind age data) represent periods of normal magnetic polarity. The geomagnetic polarity timescale combines those of Cande and Kent (1995), Singer et al. (1999), and Singer et al. (2008). I include the more detailed paleomagnetic data for late Matuyama and Brunhes chron to emphasize the good correspondence between ChRM results and ages. Note that additional young Lake Creek samples have field-measured reversed magnetic polarity, aligning with Brunhes-age excursions (see Chapter 1 for discussion about these samples), but on this plot I indicate magnetic polarity only for those samples with ChRM analyses presented in this chapter.

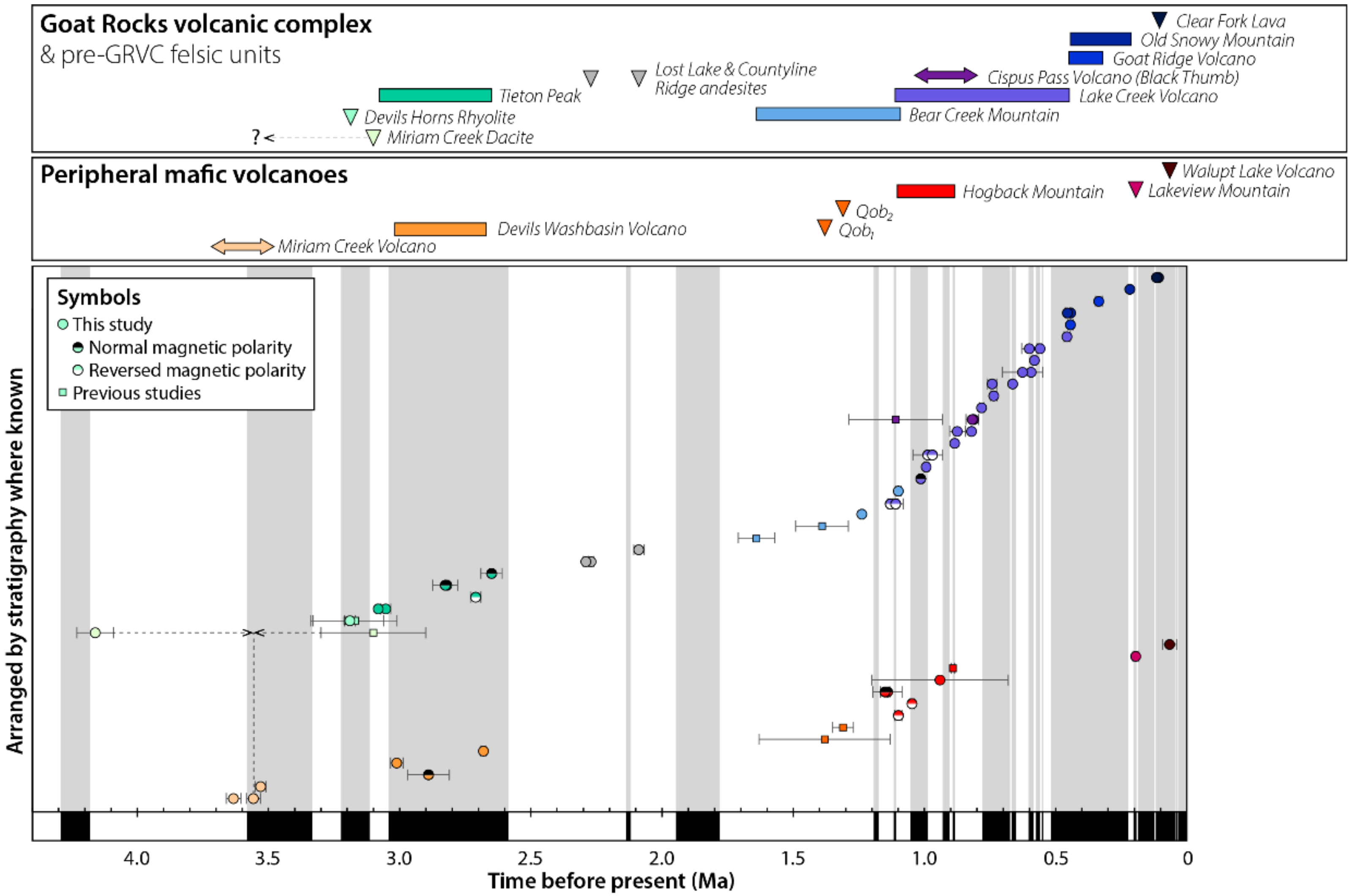

Goat Rocks volcanic complex
& pre-GRVC felsic units
Clear Fork Lava
Old Snowy Mountain
Goat Ridge Volcano
Lost Lake & Countyline Ridge andesites
Cispus Pass Volcano (Black Thumb)
Tieton Peak
Lake Creek Volcano
Bear Creek Mountain
Devils Horns Rhyolite
Miriam Creek Dacite
Peripheral mafic volcanoes
Walupt Lake Volcano
Hogback Mountain
Lakeview Mountain
Qob₂
Devils Washbasin Volcano
Qob₁
Miriam Creek Volcano
Symbols
This study
Normal magnetic polarity
Reversed magnetic polarity
Previous studies
Arranged by stratigraphy where known
4.0
3.5
3.0
2.5
2.0
1.5
1.0
0.5
0
Time before present (Ma)

Figure 2.5.

Figure 2.6. Total alkali silica (TAS) classification diagram for samples from the Goat Rocks volcanic complex and nearby volcanoes.
Includes samples presented in this dissertation and by Clayton (1983), Swanson (1996a,b), and Gusey et al. (2018). Sample locations are identified on index map in lower left panel. In legend, intermediate to felsic volcanoes/units (left side) are distinguished from peripheral mafic volcanoes (right side). Note that samples from peripheral mafic volcanoes are not represented in major and trace element diagrams in this chapter (Figures 2.9, 2.10), but these samples are discussed in detail in Chapter 3.

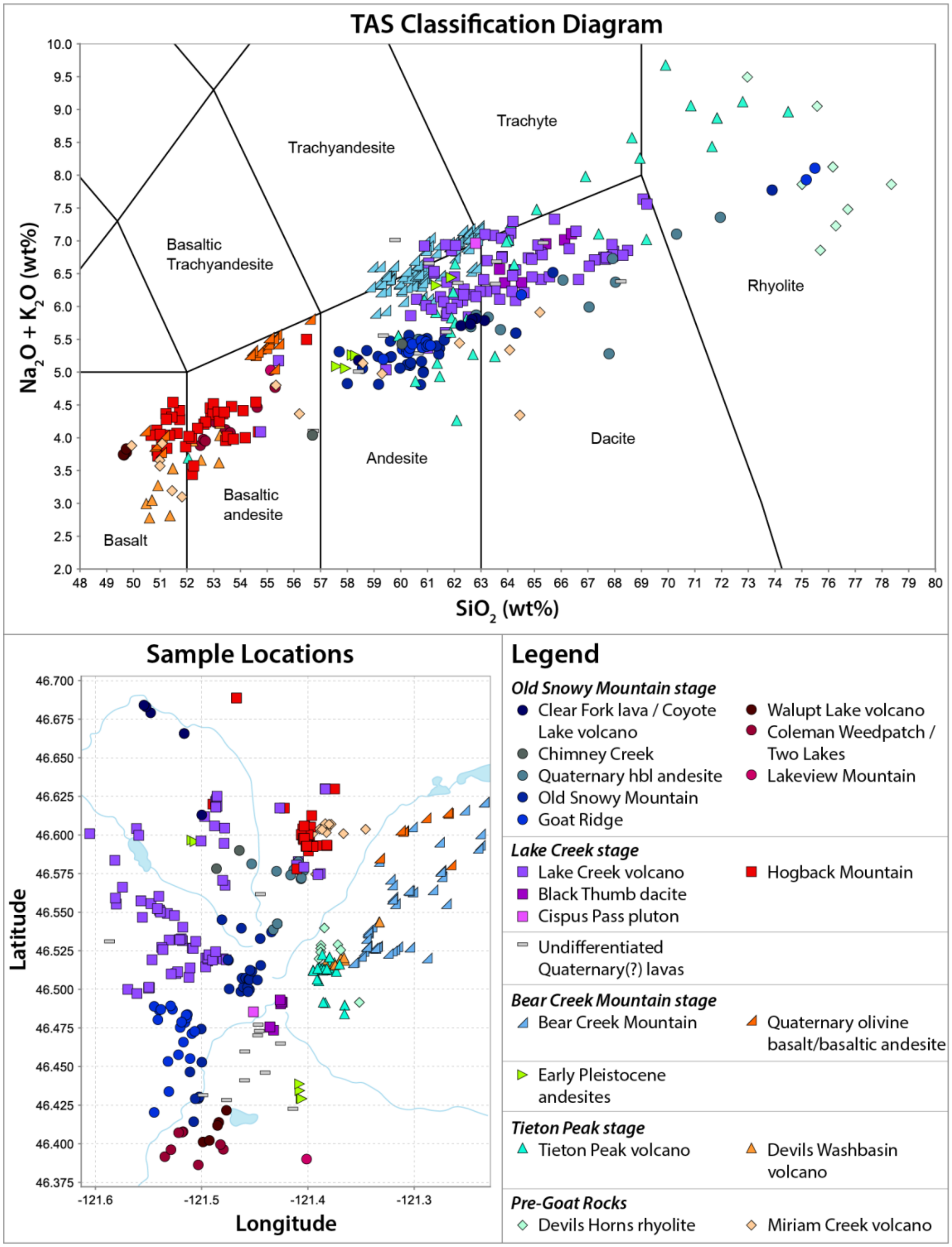

TAS Classification Diagram
Trachyte
Trachyandesite
Basaltic
Trachyandesite
Rhyolite
Andesite
Dacite
Basaltic
andesite
Basalt
$Na_2O + K_2O$ (wt%)
SiO_2 (wt%)
Sample Locations
Latitude
Longitude
Legend
Old Snowy Mountain stage
Clear Fork lava / Coyote Lake volcano
Chimney Creek
Quaternary hbl andesite
Old Snowy Mountain
Goat Ridge
Walupt Lake volcano
Coleman Weedpatch / Two Lakes
Lakeview Mountain
Lake Creek stage
Lake Creek volcano
Black Thumb dacite
Cispus Pass pluton
Hogback Mountain
Undifferentiated Quaternary(?) lavas
Bear Creek Mountain stage
Bear Creek Mountain
Quaternary olivine basalt/basaltic andesite
Early Pleistocene andesites
Tieton Peak stage
Tieton Peak volcano
Devils Washbasin volcano
Pre-Goat Rocks
Devils Horns rhyolite
Miriam Creek volcano

Figure 2.6.

Figure 2.7. Representative petrographic images of samples from the Goat Rocks volcanic complex.
Thin sections are viewed in plane polarized light on the left **(a, c, e, g)** and cross-polarized light on the right **(b, d, f, h)**. Scale bar in image **(a)** is the same for all photos. **a, b)** the andesite of Lost Lake contains phenocrysts and glomerocrystic clots of plagioclase, clinopyroxene, and orthopyroxene. **c, d)** The older Tieton andesite lava flow (unit Qta_1, Gusey et al., 2018) contains large sieve-textured and resorbed plagioclase phenocrysts and smaller clinopyroxene and orthopyroxene. Glomerocrysts of these phases also occur. **e, f)** This lava flow from the Lake Creek volcano contains abundant quenched magmatic inclusions that are light gray in color and mostly fine grained, with similar but less abundant phenocrysts compared to the host lava. Plagioclase is the dominant phenocryst, with lesser clinopyroxene and orthopyroxene. **g, h)** The Clear Fork lava flow contains amphibole pseudomorphs that are nearly all completely opacitized. The formerly-amphibole crystals range from large phenocrysts several mm across to fine microlite laths. Plagioclase also occurs, in less abundance.

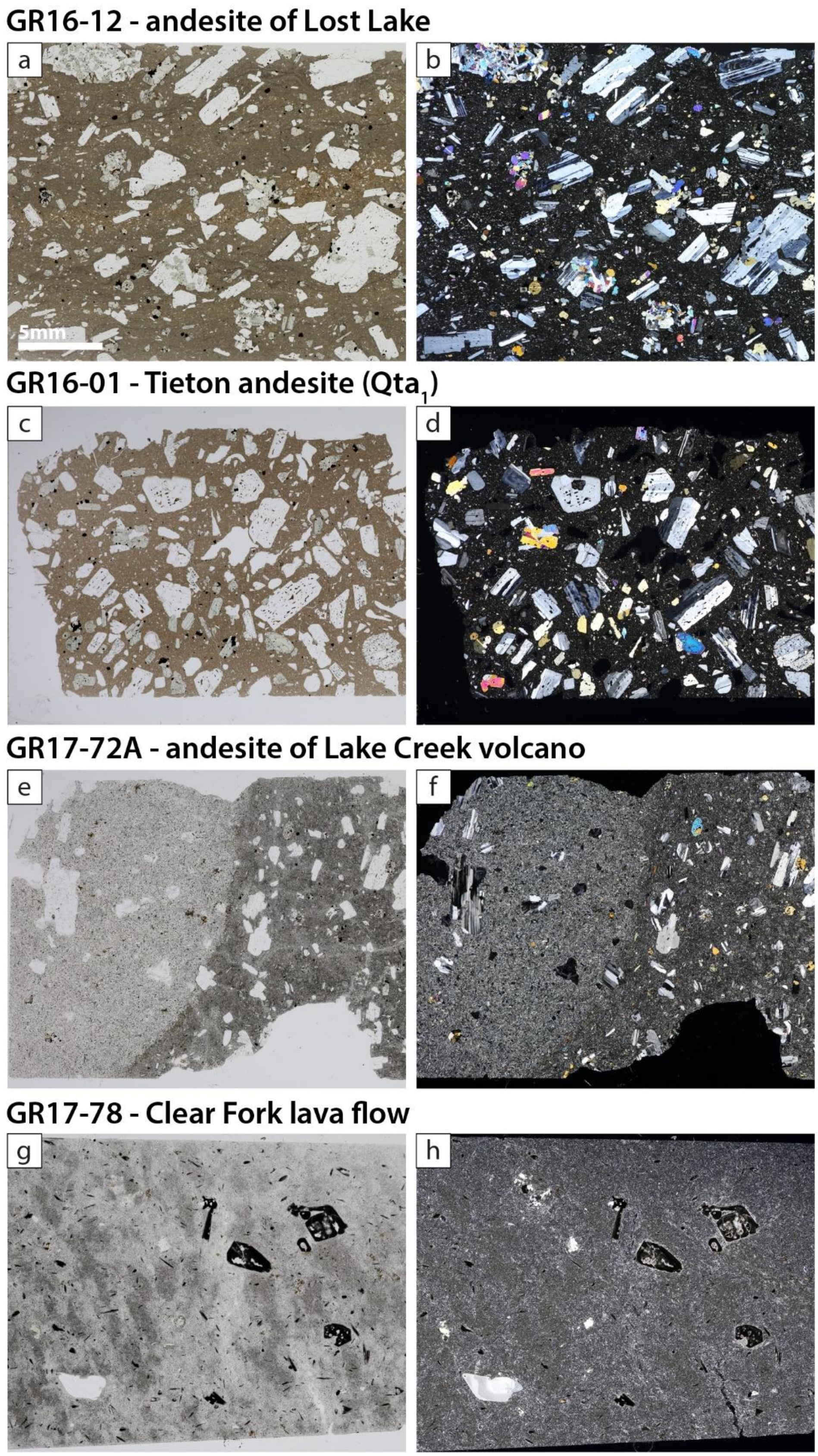
GR16-12 - andesite of Lost Lake
a
b
5mm
GR16-01 - Tieton andesite (Qta1)
c
d
GR17-72A - andesite of Lake Creek volcano
e
f
GR17-78 - Clear Fork lava flow
g
h

Figure 2.11.

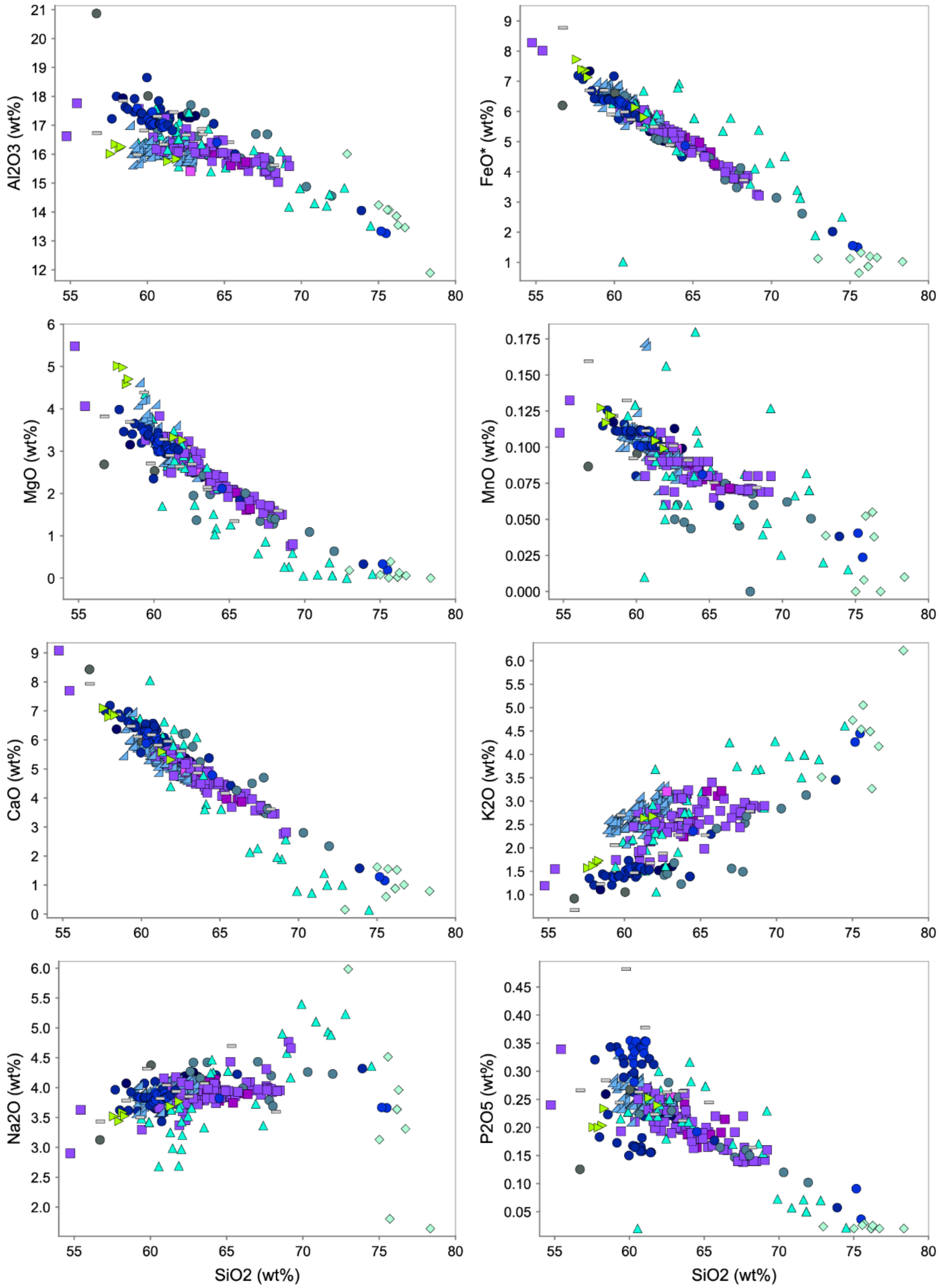

Figure 2.8. Major element variation diagrams.
Includes all samples shown in Figure 2.6 (refer to the legend on that figure). X-ray fluorescence analyses are from this dissertation (Appendix Table A2.2), and from Clayton (1983), Swanson (1996a,b), and Gusey et al. (2018). Element oxides are normalized to 100 percent volatile-free.

Figure 2.9. Trace element variation diagrams.
Refer to Figure 2.6 for legend. Where available (this study only), ICP-MS data are plotted; otherwise, XRF data are used (Swanson, 1996a, 1996b; Gusey et al., 2018).

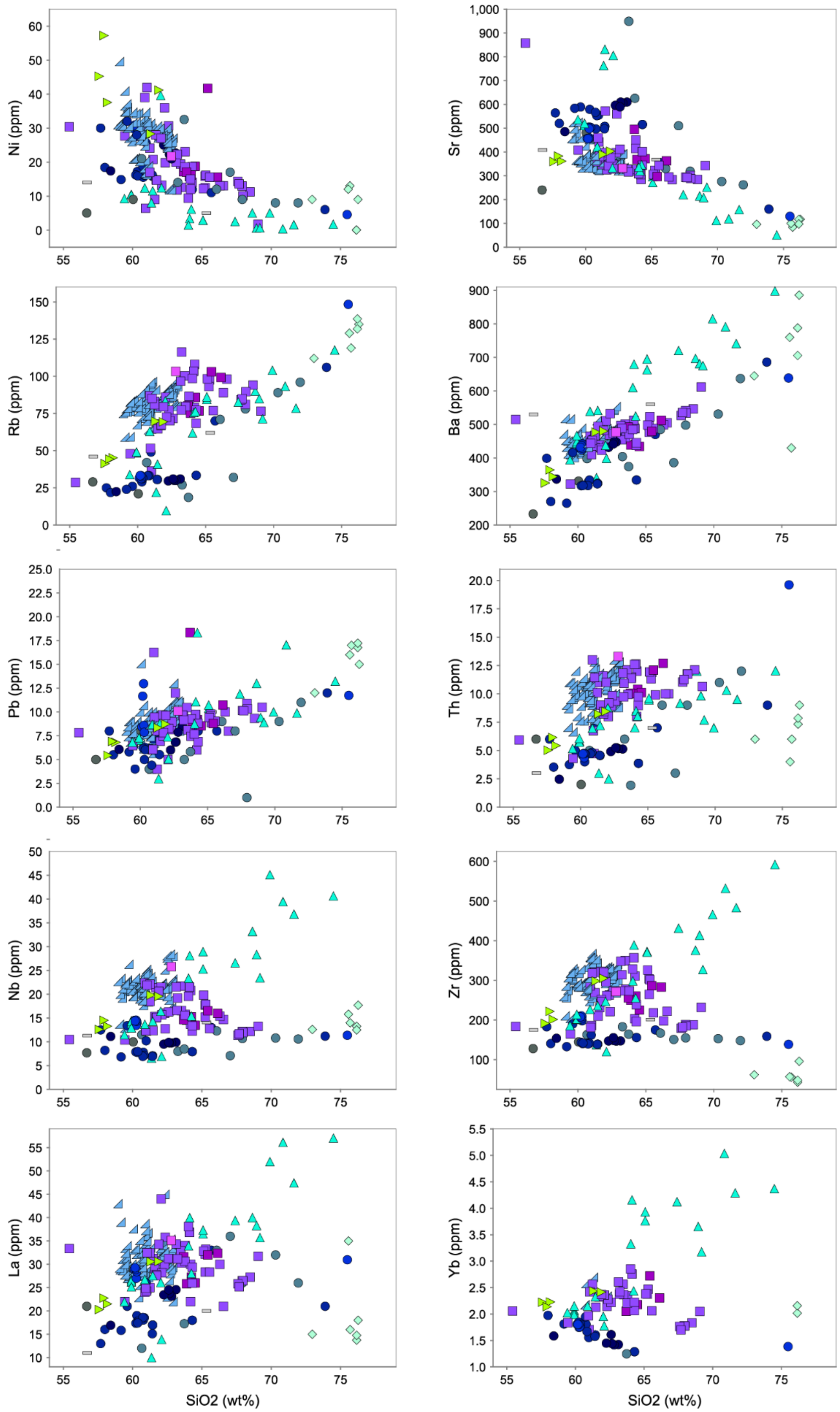
Ni (ppm)
Sr (ppm)
Rb (ppm)
Ba (ppm)
Pb (ppm)
Th (ppm)
Nb (ppm)
Zr (ppm)
La (ppm)
Yb (ppm)
SiO2 (wt%)
SiO2 (wt%)

Figure 2.10.

Figure 2.10. K_2O concentrations of samples from the Goat Rocks volcanic complex, peripheral mafic volcanoes, and Devils Horns rhyolite.
In top panel, Goat Rocks area compositions are compared to compositional ranges from Mount Rainier, Mount St. Helens, Mount Adams, and Mount Hood (update with citations). In middle panel, the Devils Horns rhyolite and four main eruptive stages are distinguished. Bottom panel highlights the general increase in SiO_2 at a similar K_2O range for samples erupted between 1.5 Ma and ~450 ka from the Bear Creek Mountain, Lake Creek, and Black Thumb eruptive centers. Includes data from Gusey et al. (2018), Swanson (1996a,b), and Clayton (1983). Note that some samples/units are excluded from these plots for simplicity, namely, the andesite of Chimney Creek, Quaternary hornblende andesite, early Pleistocene andesites, and other undifferentiated andesites of unknown age and source.

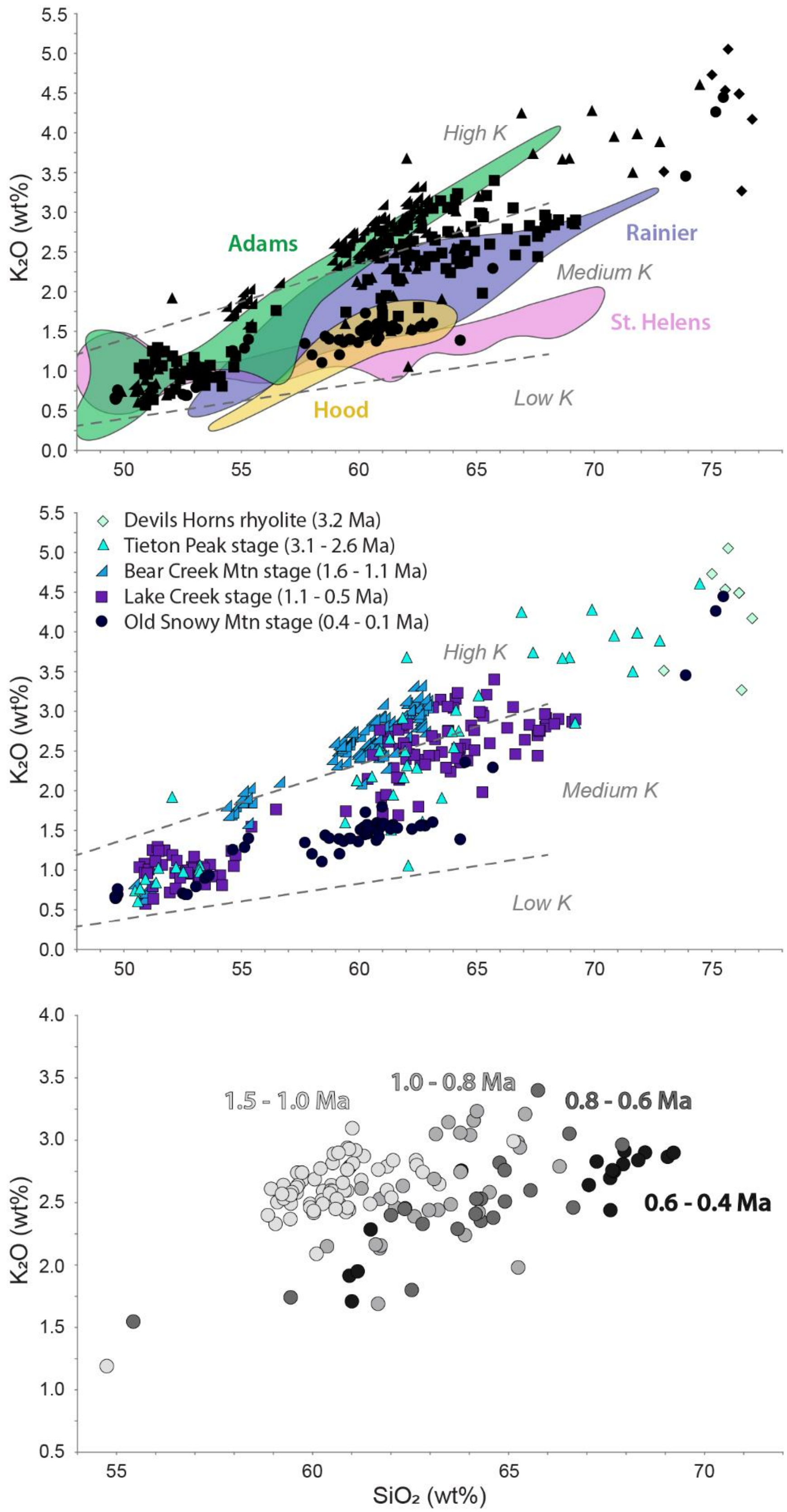

K₂O (wt%)
High K
Medium K
Low K
Adams
Rainier
St. Helens
Hood
Devils Horns rhyolite (3.2 Ma)
Tieton Peak stage (3.1 - 2.6 Ma)
Bear Creek Mtn stage (1.6 - 1.1 Ma)
Lake Creek stage (1.1 - 0.5 Ma)
Old Snowy Mtn stage (0.4 - 0.1 Ma)
1.5 - 1.0 Ma
1.0 - 0.8 Ma
0.8 - 0.6 Ma
0.6 - 0.4 Ma
SiO₂ (wt%)

Figure 2.7.

Figure 2.11. Silica concentration of Goat Rocks area magmas erupted over time. Includes samples from Devils Horns rhyolite and the Goat Rocks volcanic complex. Peripheral mafic volcanoes are excluded. Samples from White Pass area (Deer Lake Butte, Spiral Butte, Round Mountain) are included with Old Snowy Mountain stage for comparison. Histogram for each time period shows number of samples for each silica bin; note that sampling bias affects these distributions.

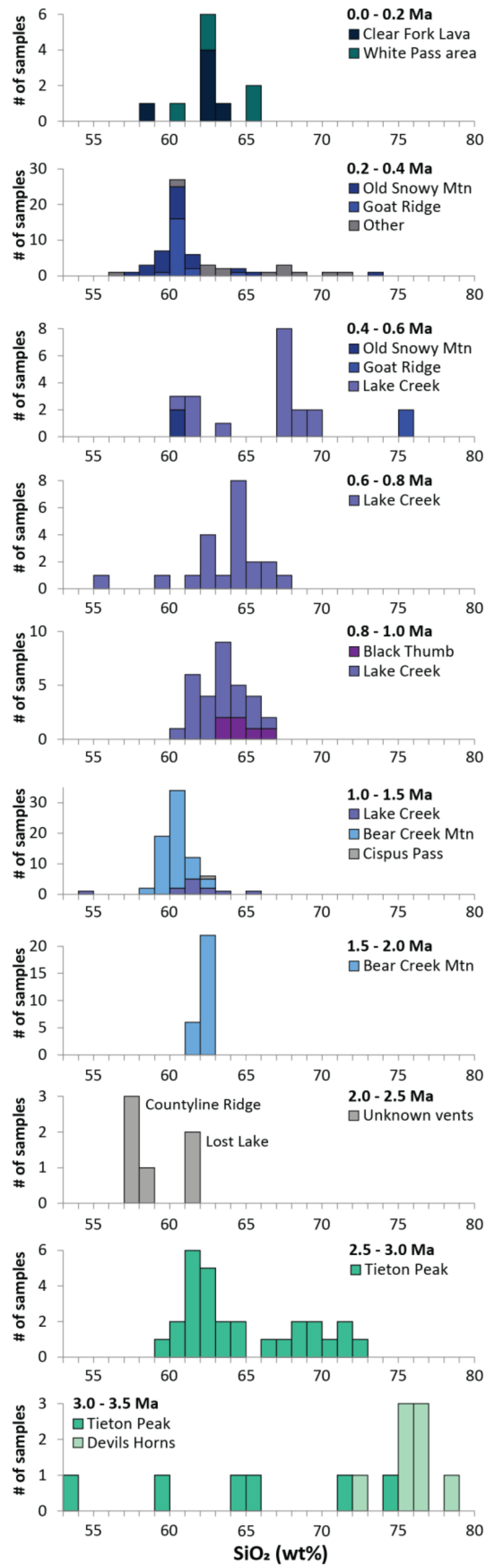
0.0 - 0.2 Ma
Clear Fork Lava
White Pass area
0.2 - 0.4 Ma
Old Snowy Mtn
Goat Ridge
Other
0.4 - 0.6 Ma
Old Snowy Mtn
Goat Ridge
Lake Creek
0.6 - 0.8 Ma
Lake Creek
0.8 - 1.0 Ma
Black Thumb
Lake Creek
1.0 - 1.5 Ma
Lake Creek
Bear Creek Mtn
Cispus Pass
1.5 - 2.0 Ma
Bear Creek Mtn
Countyline Ridge
Lost Lake
2.0 - 2.5 Ma
Unknown vents
2.5 - 3.0 Ma
Tieton Peak
3.0 - 3.5 Ma
Tieton Peak
Devils Horns
# of samples
SiO₂ (wt%)

Figure 2.8.

Figure 2.12. Photos from the Black Thumb – Cispus Pass area.
a) View looking toward northeast showing the Black Thumb plug/dome and pyroclastic rocks stratigraphically beneath it. Sample GR17-47A (dated by 40Ar/39Ar) was collected from the base of the Black Thumb cliff, and GR17-47B was taken from talus, presumably fallen from cliff above. **b)** View of pyroclastic breccia deposit (block and ash flow?). **c)** Closer view of outcrop in **(b)**. Note the angular clasts and their flow-banding, as visible in lower left. Sample GR17-46 was collected from this outcrop. **d)** Devitrified lava flow with large, sheared air pockets and xenoliths/autoliths (marked by tip of Sharpie), located on the ridge between Black Thumb and Cispus Pass. Sample GR17-49 was collected here. **e)** Sample GR17-49 viewed in thin section (plane polarized light). Note the subangular clasts (autoliths?) in fine-grained, devitrified groundmass. **f)** Block-and-ash flow deposit capping the ridge southwest of Cispus Pass. Field assistant Marina Marcelli for scale. **g)** Closer view of angular clasts in ashy matrix from outcrop near Marina in **(f). h)** Farther south along this ridge, a shallow plug or lava flow appears to be related to nearby dike fragments. Sample GR17-51 was collected from the plug or lava flow at the high point. **i)** Along the Pacific Crest trail, below and east of the vantage point in **(h)**, a columnar outcrop of glassy, porphyritic dacite is presumably associated with the dike above. Sample GR17-54 was collected from the talus beneath this cliff.

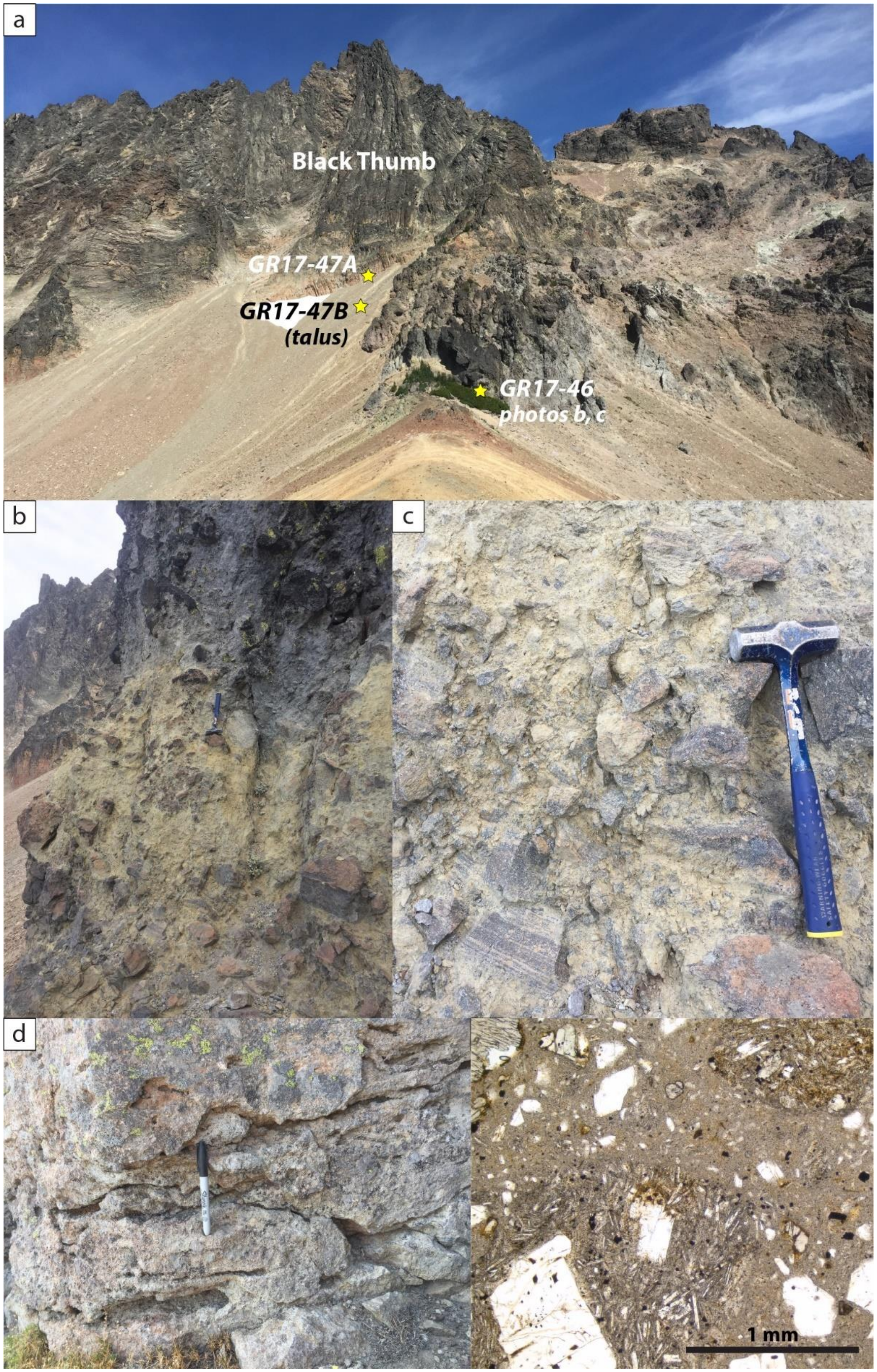
a
Black Thumb
GR17-47A
GR17-47B
(talus)
GR17-46
photos b, c
b
c
d
1 mm

Figure 2.12.

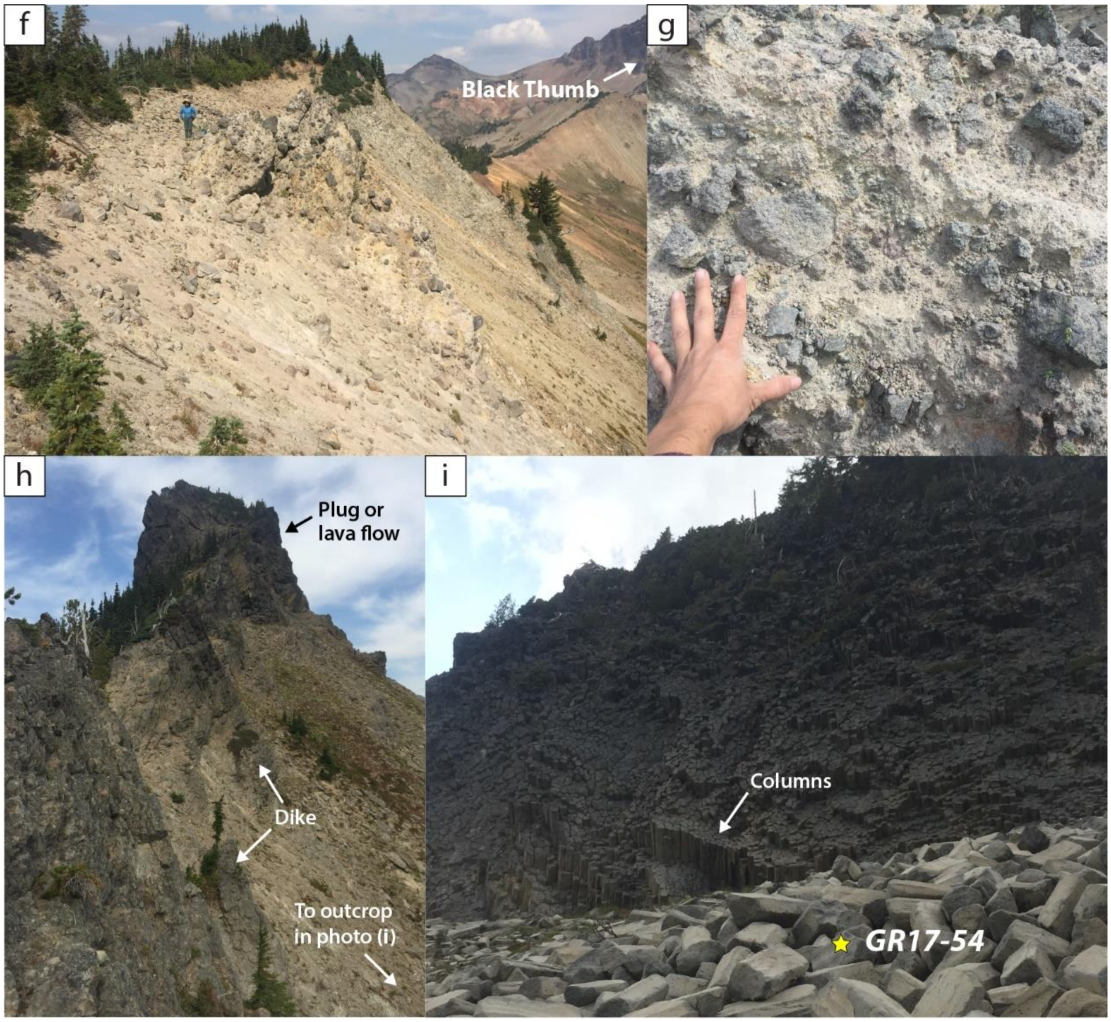

Figure 2.12 (continued).

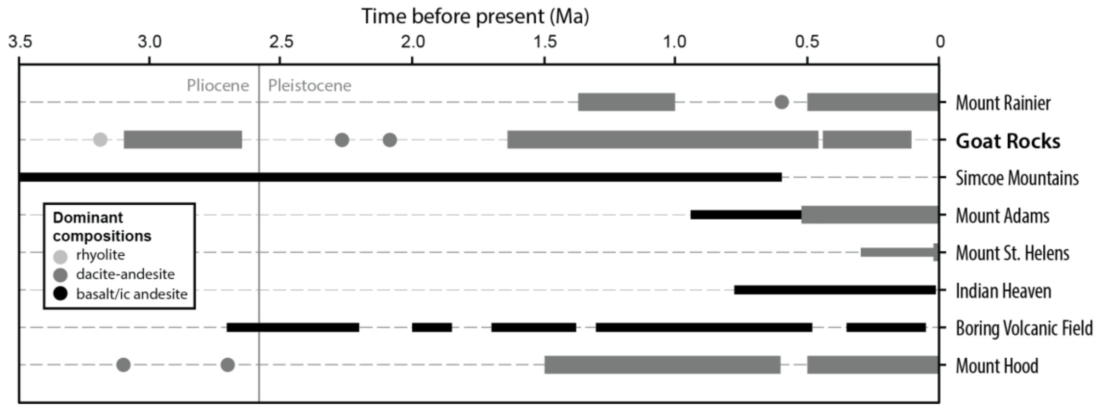

Figure 2.13. Comparison of the lifespan of the Goat Rocks volcanic complex and other recent major volcanic centers of the southern Washington and northern Oregon Cascades.
The eruptive history of an extinct volcano is included with an active volcano if it is located within ~15 km (the approximate diameter of the Goat Rocks volcanic complex) of the modern edifice. Circles represent ages of individual units (or of separate units with statistically equivalent ages). Bars show extended periods of eruptive activity. Thicker bars represent focused activity at a major edifice, while narrower bars represent distributed fields. Sources of ages include: Mount Rainier—Sisson et al. (2001) and Sisson and Calvert (2017, written communication); Simcoe Mountains—Hildreth and Fierstein (2015); Mount Adams—Hildreth and Lanphere (1994); Mount St. Helens—Mullineaux and Crandell (1981) and Clynne et al. (2008); Indian Heaven—Mitchell et al. (1989) and Korosec (1989); Boring Volcanic Field—Fleck et al. (2014); and Mount Hood—Keith et al. (1985), Sherrod and Scott (1995), Scott et al. (1997), and Scott and Gardner (2017).

TABLES

Table 2.1. Radiometric ages for the Goat Rocks volcanic complex and peripheral mafic volcanoes.

TABLE 1. AGES OF PLIOCENE TO PLEISTOCENE VOLCANIC DEPOSITS NEAR GOAT ROCKS VOLCANIC COMPLEX

Sample ID[*]	Map no.[†]	Map unit[§]	Location[#] Longitude	Latitude	Magnetic polarity[**]	Age ± 2σ error (ka or Ma)[††]	Phase analyzed[§§]	Dating technique	Details[##]	Age Interpretation	Reference[***]
Old Snowy Mountain Stage											
GR17-78	N.A.	Qacf	-121.5480	46.6791	N	**107 ± 5 (ka)**	Zrn	U/Pb	Surfaces (n=4) and interiors (n=5), MSWD=2.22	Youngest zircon population	This study
GR16-25	65	Qao	-121.4549	46.5065	N	**217 ± 5**	Gm	$^{40}Ar/^{39}Ar$	Plateau, 52% $^{39}Ar(k)$, MSWD=1.13	Groundmass crystallization	This study
GR16-38	67	Qao	-121.4747	46.5188	N	**440 ± 3**	Gm	$^{40}Ar/^{39}Ar$	Plateau, 52% $^{39}Ar(k)$, MSWD=1.05	Groundmass crystallization	This study
						453 ± 8	Zrn	U/Pb	Interiors (n=9), MSWD=7.22	Youngest zircon population	This study
GR17-71	86	Qag	-121.5400	46.4866	N	**443 ± 10**	Zrn	U/Pb	Surfaces (n=4) and low-Y interiors (n=5), MSWD=1.19	Youngest zircon population	This study
Lake Creek Stage											
GR15-04	73	Qgr_2	-121.5322	46.5492	R	**593 ± 4**	Gm	$^{40}Ar/^{39}Ar$	Plateau, 60% $^{39}Ar(k)$, MSWD=1.23	Groundmass crystallization	This study
						626 ± 77	Am	$^{40}Ar/^{39}Ar$	Plateau, 96% $^{39}Ar(k)$, MSWD=1.70	Amphibole crystallization	This study
GR17-75 (GR15-02)	71	Qgr_2	-121.5388	46.5501	R	**600 ± 29**	Zrn	U/Pb	Surfaces (n=9), MSWD=0.36	Youngest zircon population	This study
GR17-72A	87	Qgr_3	-121.5572	46.5574	N	**742 ± 17**	Zrn	U/Pb	Interiors (n=11), MSWD=1.07	Youngest zircon population	This study
GR17-47A	85	Qdbt	-121.4241	46.4916	R	**817 ± 24**	Zrn	U/Pb	Surfaces (n=5) and interiors (n=9), MSWD=0.67	Youngest zircon population	This study
GR16-34	80	Qgr_2	-121.4932	46.5224	R	**820 ± 3**	Gm	$^{40}Ar/^{39}Ar$	Plateau, 54% $^{39}Ar(k)$, MSWD=1.37	Groundmass crystallization	This study
						874 ± 30	Zrn	U/Pb	Interiors (n=6), MSWD=1.3	Youngest zircon population	This study
08WP1019	N.A.	Qbh_1[†††]	-121.4297	46.6483	N.D.	***891 ± 7***	Gm	$^{40}Ar/^{39}Ar$	Plateau		1
GR16-30	77	Qgr_2	-121.4944	46.5184	R	**987 ± 57**	Zrn	U/Pb	Interiors (n=9), MSWD=1.4	Youngest zircon population	This study
N.G.	93	Un.[§§§]	-121.4390	46.4990	N.D.	***1.11 ± 0.09 (Ma)***	Zrn	Fission track			2, 3
GR16-36	68	Qgr_1	-121.4799	46.5198	N	1.11 ± 0.03	Zrn	U/Pb	Interiors (n=8), MSWD=0.76	Youngest zircon population	This study
						1.11 ± 0.01	Gm	$^{40}Ar/^{39}Ar$	Total fusion	Groundmass crystallization	This study
						1.13 ± 0.01	Pl	$^{40}Ar/^{39}Ar$	Plateau, 80% $^{39}Ar(k)$, MSWD=1.26	Plagioclase cooling age	This study
HM-SP-1	89	Qbh_2	-121.3961	46.5930	N	*1.53 ± 0.18*	WR	K/Ar			2, 3
Bear Creek Mountain Stage											
N.G.	N.A.	Qta_2	-121.1833	46.6320	R	***1.35 ± 0.13***	Zrn	Fission track			2, 4
07114	N.A.	Qta_2	-120.8169	46.7194	R	***1.39 ± 0.10***	Pl	$^{40}Ar/^{39}Ar$			5
04162	N.A.	Qta_1	-121.1515	46.6786	R	***1.64 ± 0.07***	Gm	$^{40}Ar/^{39}Ar$			5
Tieton Peak Stage											

GR16-07	84	Tpb	-121.3324	46.5439	N	**2.68 ± 0.01**	Gm	$^{40}Ar/^{39}Ar$	Plateau, 76% $^{39}Ar(k)$, MSWD=0.79	Groundmass crystallization	This study
GRDH-2	90	Tpb	-121.3659	46.5205	N	*3.80 ± 0.31*	WR	K/Ar			2, 3
<u>Unassigned Stage</u>											
GR16-12	83	Qall	-121.5063	46.5957	R	**2.27 ± 0.01**	Gm	$^{40}Ar/^{39}Ar$	Plateau, 66% $^{39}Ar(k)$, MSWD=4.23	Groundmass crystallization	This study
						2.29 ± 0.01	Pl	$^{40}Ar/^{39}Ar$	Plateau, 63% $^{39}Ar(k)$, MSWD=1.53	Plagioclase cooling age	This study
HMMCSP-2	88	Tpm	-121.3831	46.6025	N	***3.1 ± 0.2***	Zrn	Fission track			2, 3
<u>Pre-Goat Rocks</u>											
GRTPC-9	91	Tpr	-121.3880	46.5241	N.D.	***3.17 ± 0.16***	Zrn	Fission track			2, 3
GRDH-3	92	Tpr	-121.3690	46.5255	N.D.	***3.20 ± 0.14***	Zrn	Fission track			2, 3

Note: plagioclase ages for samples GR15-04, GR16-07, and GR16-25 are in Appendix 1.

[*]N.G.=no sample ID given.

[†]N.A.=not applicable (location is outside of Figure 2 boundary).

[§]Map units as in Figure 2, except for Qta_1 and Qta_2 (older and younger Tieton andesite flows; Gusey et al., this volume).

[#]Longitude and latitude measured by GPS (coordinate reference system WGS84; this study, refs. 1, 4, 5), or approximated from sample locations in Clayton (1980).

[**]Measured by portable fluxgate magnetometer or inferred from map units by Swanson (1996a,b, unpublished). N=normal, R=reversed, N.D.=not determined (or no magnetic signal).

[††]Non-italic font=age from this study; italic font=age from a previous study (see Reference column). Bold font identifies the preferred eruption ages included on Figure 5. Non-bold font indicates an age that is not interpreted as the eruption age (e.g. phenocryst age older than groundmass from the same sample), or is considered a less reliable age (e.g. previously-published age that does not agree with stratigraphic relations).

[§§]Zrn=zircon, Gm=groundmass, Pl=plagioclase, Am=amphibole, WR=whole-rock.

[##]For zircon ages, n=(x) gives the number of spot analyses on crystal surfaces or polished interiors that are included in the weighted mean age.

[***]1. Sisson and Calvert, written communication; 2. Clayton (1983); 3. Clayton (1980); 4. Gusey et al., this volume; 5. Hammond (2017).

[†††]Map unit is interpreted from age, but not confirmed.

[§§§]Un.=unassigned. Sample is identified as part of the Cispus Pass pluton, but mapping of this pluton is unresolved.

APPENDICES

Table A2.1 Sample locations and descriptions

Table A2.2 Compilation of geochemical analyses

Folder A2.1 Argon isotope data for all dated samples

Folder A2.2 Zjiderfeld diagrams for all paleomagnetic analyses?

REFERENCES

Armstrong, R.L., 1978, Cenozoic igneous history of the U.S. cordillera from latitude 42° to 49° N, *in* Smith, R.B., Eaton, G.P., editors, 1978, Cenozoic tectonics and regional geophysics of the western cordillera: Geological Society of America Memoir, v. 152, p. 265-282.

Cande, S.C., and Kent, D.V., 1995, Revised calibration of the geomagnetic polarity timescale for the Late Cretaceous and Cenozoic: Journal of Geophysical Research, v. 100, no. B4, p. 6093-6095.

Channell, J.E.T., Mazaud, A., Sullivan, P., Turner, S., and Raymo, M.E., 2002, Geomagnetic excursions and paleointensities in the Matuyama Chron at Ocean Drilling Program Sites 983 and 984 (Iceland Basin): Journal of Geophysical Research, v. 107, no. B6, doi: 10.1029/2001JB000491

Clayton, G., 1983, Geology of the White Pass Area, South-Central Cascade Range, Washington: Unpublished M.S. thesis, University of Washington, 212 pp.

du Bray, E.A., and John, D.A., 2011, Petrologic, tectonic, and metallogenic evolution of the Ancestral Cascades magmatic arc, Washington, Oregon, and northern California: Geosphere, October 2011, v. 7, no. 5, p. 1102-1133, doi: 10.1130/GES00669.1.

Ellingson, J.A., 1959, General geology of the Cowlitz Pass area, central Cascade Mountains, Washington: University of Washington, Master of Science thesis, 60 p., 1 plate.

Ellingson, J.A., 1968, Late Cenozoic Volcanic Geology of the White Pass – Goat Rocks area, Cascade Mountains, Washington: Unpublished Ph.D. dissertation, Washington State University, 112 p.

Ellingson, J.A., 1972, The Rocks and Structure of the White Pass Area, Washington: Northwest Science, v. 46, n.1, p. 9-24.

Engebretson, D.C., Cox, A., and Gordon, R.G., 1985, Relative motions between oceanic and continental plates in the Pacific Basin: Geological Society of America Special Paper 206, 54 p.

Enrique, P., and Esteve, S., 2019, A chemical approximation to the modal QAPF and normative Q'(F')-ANOR classification of the igneous rocks based on their SiO_2-CaO-K_2O content: Geogaceta, v. 66, p. 91-94.

Fiske, R.S., 1963, Subaqueous pyroclastic flows in the Ohanapecosh Formation, Washington: Geological Society of America bulletin, v. 74, p. 391-406.

Fiske, R.S., Hopson, C.A., and Waters, A.C., 1963, Geology of Mount Rainier National Park Washington: Geological Survey Professional Paper 444, 93 p.

Fleck, R.J., Hagstrum, J.T., Calvert, A.T., Evarts, R.C., and Conrey, R.M., 2014, $^{40}Ar/^{39}Ar$ geochronology, paleomagnetism, and evolution of the Boring volcanic field, Oregon and Washington, USA: Geosphere, v. 10, no. 6, p. 1283-1314, doi:10.1130/GES00985.1.

Fourny, A., Weis, D., and Scoates, J.S., 2016, Comprehensive Pb-Sr-Nd-Hf isotopic, trace element, and mineralogical characterization of mafic to ultramafic rock reference materials: Geochemistry, Geophysics, Geosystems, v. 17, p. 739-773, doi:10.1002/2015GC006181.

Grunder, A.L., Klemetti, E.W., Feeley, T.C., and McKee, C.M., 2008, Eleven million years of arc volcanism at the Aucanquilcha Volcanic Cluster, northern Chilean Andes: implications for the life span and emplacement of plutons: Transactions of the Royal Society of Edinburgh: Earth Sciences, v. 97, p. 415-436.

Gusey, D.L., Hammond, P.E., and Lasher, J.P., 2018, Tieton andesite, south-central Washington Cascades: Two of the longest known andesite lava flows, *in* Poland, M.P., Garcia, M.O., Camp, V.E., and Grunder, A., editors, Field Volcanology: A Tribute to the Distinguished Career of Don Swanson: Geological Society of America Special Paper 538, p. 93-132, https://doi.org/10.1130/2018.2538(05).

Hall, P.S., and Kincaid, C., 2001, Diapiric flow at subduction zones: A recipe for rapid transport: Science, v. 292, p. 2472-2475, doi: 10.1126/science.1060488

Hammond, P.E., 1980, Reconnaissance geologic map and cross sections of southern Washington Cascade Range: Publications of Department of Earth Science, Portland State University, Portland, Oregon, scale 1:125,000.

Hammond, P.E., 2005, Geologic Map of the Timberwolf Mountain 7.5-minute Quadrangle, Yakima County, Washington: Washington State Department of Natural Resources, Division of Geology and Earth Resources, Geologic Map GM-60

Hammond, P.E., 2017, Geologic Map of the northern portions of the Rimrock Lake, Tieton Basin, and western two-thirds of the Weddle Canyon 7.5-minute quadrangles, Yakima county, Washington: Washington Geological Survey Map Series 2017-03, 19 p.

Hatter, S.J., Palmer, M.R., Gernon, T.M., Taylor, R.N., Cole, P.D., Barfod, D.N., and Coussens, M., 2018, The evolution of the Silver Hills volcanic center, and revised 40Ar/39Ar geochronology of Montserrat, Lesser Antilles, with implications for island arc volcanism: Geochemistry, Geophysics, Geosystems, v. 19, p. 427-452, https://doi.org/10.1002/2017GC007053.

Hildreth, W., 2007, Quaternary Magmatism in the Cascades: Geologic Perspectives: U.S. Geological Survey Professional Paper 1744, 125 pp.

Hildreth, W., and Fierstein, J., 2015, Geologic Map of the Simcoe Mountains Volcanic Field, Main Central Segment, Yakama Nation, Washington: U.S. Geological Survey Scientific Investigations Map 3315, scale 1:24 000, 3 sheets, 76 p. text.

Hildreth, W., Lanphere, M.A., Champion, D.E., and Fierstein, J., 2004, Rhyodacites of Kulshan caldera, North Cascades of Washington: Postcaldera lavas that span the Jaramillo: Journal of Volcanology and Geothermal Research, v. 130, p. 227-264, doi:10.1016/S0377-0273(03)00290-7.

Jutzeler, M., McPhie, J., and Allen, S.R., 2014, Facies architecture of a continental, below-wave-base volcaniclastic basin: The Ohanapecosh Formation, Ancestral Cascades arc (Washington, USA): GSA Bulletin, v. 126, no. 3/4, p. 352-376, doi: 10.1130/B30763.1.

Karlstrom, L., Dufek, J., and Manga, M., 2009, Organization of volcanic plumbing through magmatic lensing by magma chambers and volcanic loads: Journal of Geophysical Research, v. 114 (B10204), doi:10.1029/2009JB006339.

Karlstrom, L., Dufek, J., and Manga, M., 2010, Magma chamber stability in arc and continental crust: Journal of Volcanology and Geothermal Research, v. 190, p. 249-270, doi:10.1016/j.jvolgeores.2009.10.003.

Keith, T.E.C., Donnelly-Nolan, J.M., Markman, J.L., and Beeson, M.H., 1985, K-Ar ages of rocks in the Mount Hood area, Oregon: Isochron West, no. 42, p. 12-16.

Kirschvink, J.L., 1980, The least-squares line and plane and the analysis of palaeomagnetic data: Geophysical Journal International, v. 62, no. 3, p.699-718.

Kirschvink, J.L., Kopp, R.E., Raub, T.D., Baumgartner, C.T. and Holt, J.W., 2008, Rapid, precise, and high-sensitivity acquisition of paleomagnetic and rock-magnetic data: Development of a low-noise automatic sample changing system for superconducting rock magnetometers: Geochemistry, Geophysics, Geosystems, v. 9, no. 5.

Lisiecki, L.E., and Raymo, M.E., 2005, A Pliocene-Pleistocene stack of 57 globally distributed benthic $\delta^{18}O$ records: Paleoceanography, v. 20, PA1003, doi: 10.1029/2004PA001071

Michalk, D.M., Böhnel, H.N., Nowaczyk, N.R., Aguírre-Diaz, G.J., López-Martínez, M., Ownby, S., and Negendank, J.F.W., 2013, Evidence for geomagnetic excursions recorded in Brunhes and Matuyama Chron lavas from the trans-Mexican volcanic belt: Journal of Geophysical Research: Solid Earth, v. 118, p. 2648-2669, doi:10.1002/jgrb.50214.

Miller, R.B., 1989, The Mesozoic Rimrock Lake inlier, southern Washington Cascades: Implications for the basement to the Columbia Embayment: Geological Society of America Bulletin, v. 101, p. 1289–1305, doi: 10.1130/0016-7606(1989)101<1289:TMRLIS>2.3.CO;2.

Muller, J.R., Ito, G., and Martel, S.J., 2001, Effects of volcano loading on dike propagation in an elastic half-space: Journal of Geophysical Research, v. 106, no. B6, p. 11,101-11,113.

Ohno, M., Hayashi, T., Komatsu, F., Murakami, F., Zhao, M., Guyodo, Y., Acton, G., Evans, H.F., and Kanamatsu, T., 2012, A detailed paleomagnetic record between 2.1 and 2.75 Ma at IODP Site U1314 in the North Atlantic: Geomagnetic excursions and the Gauss-Matuyama transition: Geochemistry, Geophysics, Geosystems, v. 13, no. 1, doi:10.1029/2012GC004080.

Ownby, S., Granados, H.D., Lange, R.A., and Hall, C.M., 2007, Volcán Tancítaro, Michoacán, Mexico, $^{40}Ar/^{39}Ar$ constraints on its history of sector collapse: Journal of Volcanology and Geothermal Research, v. 161, p. 1-14, doi:10.1016/j.jvolgeores.2006.10.009.

Pansino, S., and Taisne, B., 2019, How magmatic storage regions attract and repel propagating dikes: Journal of Geophysical Research: Solid Earth, v. 124, p. 274-290, https://doi.org/10.1029/2018JB016311.

Pinel, V., Jaupart, C., and Albino, F., 2010, On the relationship between cycles of eruptive activity and growth of a volcanic edifice: Journal of Volcanology and Geothermal Research, v. 194, p. 150-164, doi:10.1016/j.jvolgeores.2010.05.006.

Roman, A., and Jaupart, C., 2014, The impact of a volcanic edifice on intrusive and eruptive activity: Earth and Planetary Science Letters, v. 408, p. 1-8, http://dx.doi.org/10.1016/j.epsl.2014.09.016.

Schreiber, S.A., 1981, Geology of the Nelson Butte area, south-central Cascade Range, Washington: University of Washington Master of Science thesis, 81 p., 1 pl.

Scott, W.E., Gardner, C.A., Sherrod, D.R., Tilling, R.I., Lanphere, M.A., and Conrey, R.M., 1997, Geologic History of Mount Hood Volcano, Oregon—A Field-trip Guidbook: U.S. Geological Survey Open-File Report 97-263, 36 pp.

Scott, W.E., and Gardner, C.A., 2017, Field-Trip Guide to Mount Hood, Oregon, Highlighting Eruptive History and Hazards: U.S. Geological Survey Scientific Investigations Report 2017-5022-G, 115 p.

Sherrod, D.R., and Scott, W.E., 1995, Preliminary geologic map of the Mount Hood 30- by 60-minute quadrangle, Northern Cascade Range, Oregon: U.S. Geological Survey Open-File Report 95-219, 36 p., 1 plate.

Singer, B.S., Hoffman, K.A., Chauvin, A., Coe, R.S., and Pringle, M.S., 1999, Dating transitionally magnetized lavas of the late Matuyama Chron: Toward a new $^{40}Ar/^{39}Ar$ timescale of reversals and events: Journal of Geophysical Research, v. 104, no. B1, p. 679-693.

Swanson, D.A., 1964, The middle and late Cenozoic volcanic rocks of the Tieton River area, south-central Washington: PhD dissertation, Johns Hopkins University, 329 p.

Swanson, D.A., 1966, Tieton Volcano, a Miocene Eruptive Center in the Southern Cascade Mountains, Washington: Geological Society of America Bulletin, v. 77, p. 1293-1314.

Swanson, D.A., 1989, Geologic Map of the French Butte and Greenhorn Buttes quadrangles, Washington: U.S. Geological Survey Open File Report 89-309, 25 p., 3 plates.

Swanson, D.A., 1991, Geologic map of the Tower Rock quadrangle, southern Cascade Range, Washington: U.S. Geological Survey Open File Report 91-314, 28 p., 2 plates.

Swanson, D.A., 1992, Geologic map of the McCoy Peak quadrangle, southern Cascade Range, Washington: U.S. Geological Survey Open File Report 92-336, 38 p., 2 plates.

Swanson, D.A., 1996a, Geologic map of the Hamilton Buttes quadrangle, southern Cascade Range, Washington: U.S. Geological Survey Open File Report 96-0016, 29 p., 2 plates.

Swanson, D.A., 1996b, Geologic map of the Packwood Lake quadrangle, southern Cascade Range, Washington: U.S. Geological Survey Open File Report 96-704, 25 p., 2 plates.

Swanson, D.A., and Clayton, G.A., 1983, Generalized geologic map of the Goat Rocks Wilderness and Roadless Areas (6036, Parts A, C, and D), Lewis and Yakima Counties, Washington: U.S. Geological Survey Open-File Report 83-357.

Tabor, R.W., Frizzell, V.A. Jr., Booth, D.B., and Waitt, R.B., 2000, Geologic map of the Snoqualmie Pass 30x60 minute quadrangle, Washington: U.S. Geological Survey Geologic Investigations Series Map I-2538, scale 1:100,000, 57 p., 1 plate.

Tauxe, L., Shaar, R., Jonestrask, L., Swanson-Hysell, N.L., Minnett, R., Koppers, A.A.P., Constable, C.G., Jarboe, N., Gaastra, K. and Fairchild, L., 2016, PmagPy: Software package for paleomagnetic data analysis and a bridge to the Magnetics Information

Consortium (MagIC) Database: Geochemistry, Geophysics, Geosystems, v. 17, no. 6, p.2450-2463.

Vance, J.A., Clayton, G.A., Mattinson, J.M., and Naeser, C.W., 1987, Early and Middle Cenozoic stratigraphy of the Mount Rainier-Tieton River area, southern Washington Cascades: Washington Division of Geology and Earth Resources Bulletin, v. 77, p. 269-290.

Wall, K.T., Grunder, A.L., Miggins, D.P., and Coble, M.A., 2018, Multistage growth and compositional change at the Goat Rocks volcanic complex, a major Pliocene-Pleistocene andesite center in the southern Washington Cascades, *in* Poland, M.P., Garcia, M.O., Camp, V.E., and Grunder, A., eds., Field Volcanology: A Tribute to the Distinguished Career of Don Swanson: Geological Society of America Special Paper 538, p. 63-91, https://doi.org/10.1130/2018.2538(04).

Wells, R.E., and McCaffrey, R., 2013, Steady rotation of the Cascade arc: Geology, v. 41, n. 9, p. 1027-1030.

Weis, D., et al., 2006, High-precision isotopic characterization of USGS reference materials by TIMS and MC-ICP-MS: Geochemistry, Geophysics, Geosystems, v. 7, Q08006, doi:10.1029/2006GC001283.

Winters, W.J., 1984, Stratigraphy and sedimentology of Paleogene arkosic and volcaniclastic strata, Johnson Creek-Chambers Creek area, southern Cascade Range, Washington, Portland State University Master of Science thesis, 162 p.

Wise, W.S., 1969, Geology and petrology of the Mt. Hood area: A study of High Cascade volcanism: Geological Society of America Bulletin, v. 80, p. 969-1006, 5 plates.

CHAPTER 3 - DIVERSE CALCALKALINE BASALTS IN THE GOAT ROCKS AREA: IMPLICATIONS FOR THE SUBARC MANTLE BENEATH THE SOUTHERN WASHINGTON CASCADES AND THE MAFIC UNDERPINNINGS OF THE GOAT ROCKS VOLCANIC COMPLEX

ABSTRACT

Throughout the construction of the intermediate to felsic Goat Rocks volcanic complex (3.1 Ma to 115 ka), several mafic volcanoes were active on its periphery. These include the overlapping Miriam Creek and Hogback Mountain volcanoes (3.6-3.1 Ma and 1.1-0.9 Ma, respectively), Devils Washbasin volcano (3.0-2.7 Ma), Lakeview Mountain (~194 ka), Walupt Lake volcano (~65 ka), and vents in the Coleman Weedpatch – Two Lakes region (probably <65 ka). All of the mafic lavas (and rarer scoria/tephra deposits) that erupted from these volcanoes are broadly classified as calc-alkaline, as can be readily observed from their elevated fluid-mobile element concentrations and Nb-Ta depletions on a spider diagram. While less extreme in variety than other Cascade volcanic centers such as Mount St. Helens or Mount Adams, which may erupt some combination of CAB, HAOT, and IPB-like magmas, the Goat Rocks basalt compositions point to a range of mantle sources and conditions, including a change with time. Between ~3.5-2.7 Ma, the Miriam Creek and Devils Washbasin volcanoes erupted basalts that were likely produced by higher degrees of melting of variably subduction-modified lithospheric mantle. Renewed mafic activity after ~1.5 Ma was likely driven by smaller degrees of melting of similar mantle sources. The variations in the relative subduction component or degree of mantle enrichment are represented across time and geographic space, supporting the concept of a heterogeneous distribution of mantle compositions beneath the arc. At several locations, distinct compositional suites erupted in close proximity (as at Hogback Mountain or the Walupt Lake-Coleman Weedpatch area), indicating that Goat Rocks mafic magmas occurred in discrete batches from multiple mantle domains, with limited opportunity for stalling and homogenizing beyond the "shadow zone" of the more felsic Goat Rocks transcrustal system.

INTRODUCTION

A diverse array of basalt compositions has erupted from the Cascade volcanic arc. The various classifications include calc-alkaline basalt (CAB), typical of volcanic arcs; high-alumina olivine tholeiite (HAOT; also called low-potassium (olivine) tholeiite, LKT/LKOT), intraplate-type basalt (IPB; or within-plate basalt, WPB), as well as high-Mg basaltic andesites erupted in the Shasta area, among others (Leeman et al., 1990, 2005; Bacon et al., 1997; Conrey et al., 1997; Schmidt et al., 2008; Mullen et al., 2017). Based on bulk major and trace element compositions discussed below, Goat Rocks basalts are all CAB, but distinct qualities indicate variable mantle melt sources and petrogenetic processes.

This chapter contributes new bulk rock and mineral compositional data for samples from several mafic volcanoes in the Goat Rocks area. These volcanoes span 3.5 million years of activity, from ~3.6 Ma to ~65 ka, coeval to (and slightly preceding and postdating) the long-lived andesitic Goat Rocks volcanic complex (~3.1 Ma to ~115 ka) and overlapping in age with the Simcoe Mountains volcanic field (~4 Ma to 0.6 Ma; Hildreth and Fierstein, 2015). This suite of mafic magmas gives insight into the compositions that may have been feeding into the Goat Rocks volcanic complex over time and potentially contributing to its compositional evolution (discussed in Chapters 1 and 2, and in more detail in Chapter 4). The primitive basalt compositions also yield insight into mantle melt sources in this region, complementing the numerous previous studies of Cascade Arc mafic rocks and their mantle sources (e.g. Leeman et al., 1990, 2005; Bacon et al., 1997; Conrey et al., 1997; Schmidt et al., 2008; Mullen et al., 2017; Pitcher and Kent, 2019).

Below I summarize previous discussions about Cascade Arc primitive magmas and mantle sources. I then describe each of the mafic volcanoes peripheral to the Goat Rocks volcanic complex to set the stage for new bulk rock and mineral composition results presented later in the chapter.

Diverse basalt types in the Cascades

The primitive input to arc volcanism is well characterized in the Cascade arc. Three major (and several minor) primitive basaltic components have been recognized in the Cascades, including calc-alkaline basalt (CAB), the typical arc signature; low-K tholeiitic/high aluminum olivine tholeiitic basalt (LKT/HAOT), a mid-ocean-ridge-like signature; and a high field strength element enriched basalt (HFSE-rich), which some call "intraplate" basalt (IPB) or oceanic island basalt-like (OIB-like; Bacon, 1990; Leeman et al., 1990, 2005; Bacon et al., 1997; Borg et al., 1997; Clynne and Borg, 1997; Conrey et al., 1997; Reiners et al., 2000; Grove et al., 2002; Smith and Leeman, 2005; Hildreth, 2007; Schmidt et al., 2008; Rowe et al., 2009; Moore and DeBari, 2012; Sisson et al., 2014; Mullen et al., 2017). Other less common mafic magma types include ultrapotassic shoshonites and absarokites as well as high-Mg andesites (Bacon, 1990; Baker et al., 1994; Clynne and Borg, 1997; Conrey et al., 1997; Grove et al., 2002; Schmidt et al., 2008; Sas et al., 2017; Streck and Leeman, 2018). Commonly, at least two of these primitive components have erupted at or near each major andesitic edifice (Leeman et al., 1990, 2005; Clynne, 1993), suggesting that individual volcanic systems may tap multiple mantle or crustal melt sources. At Mount St. Helens, for example, three different mafic magmas erupted during the relatively brief Castle Creek period (ca. 2025-1700 years BP; Pallister et al., 2017): HFSE-rich basalt, LKT, and calc-alkaline basaltic andesite (Wanke et al., 2018; Leeman and Smith, 2018).

Segmentation in the frequency of these primitive magma types and in isotopic compositions suggests that there are variable mantle sources along the arc and variable contributions from the subducting slab. Schmidt et al. (2008) proposed four arc segments based on composition and Sr and Nd isotope data: 1) the North segment from Mount Meager to Glacier Peak, 2) the Columbia segment from Mount Rainier to Mount Jefferson, 3) the Central segment from the Three Sisters to Medicine Lake, and 4) the South segment, which includes Mount Shasta and Lassen Peak. Using additional compositional data and a multivariate statistical approach, Pitcher and Kent (2019) modify this segmentation scheme: they distinguish Mount Baker and Glacier Peak from the rest of the North (Garibaldi) segment and from each other, split the Columbia segment into the Washington and Graben segments, and combine the Central and South segments into one South segment. As an another perspective, Mullen and Weis (2015) and Mullen et al. (2017) define three mantle domains based on high-precision Sr, Nd, Hf, and Pb isotope ratios and trace elements: 1) a distinct source for the Garibaldi Volcanic Belt from Mount Meager to Mount Baker, 2) a local anomaly feeding the the "Adams Array," which includes IPBs from Mount Adams and Simcoe volcanic field, and 3) a common source for CAB and HAOT magmas of the High Cascades from Mount Rainier to the Lassen area. In this view, factors other than mantle heterogeneity can explain much of the variation observed along the arc, such as variability in the composition and quantity of slab contributions (Mullen et al., 2017).

Compositions of the late Pliocene to Pleistocene mafic volcanoes of the Goat Rocks area contribute more spatial definition to the variations in primitive magma types along and across the arc. Goat Rocks lies near the northern end of the Washington segment of Pitcher and Kent (2019), and near Mount Adams, where the isotopically distinct IPB source is tapped (Mullen et al., 2017). As discussed further in the Results section, the Goat Rocks basalts are all CAB, are generally isotopically aligned with the High Cascades, and are similar to the basalts of nearby Mount St. Helens and the calcalkaline compositions erupted at Mount Adams.

Location and description of Goat Rocks area mafic volcanoes

Mafic volcanoes occur proximal to the Goat Rocks volcanic complex along the northeast, east, and southern margins. Although these volcanoes are defined as peripheral to the intermediate-felsic complex, and not a part of it (see Chapters 1 and 2), here I use shorthand such as "Goat Rocks basalts." Below I describe the location, size/extent, age (where known), and field description of each peripheral mafic volcano based on field work conducted as part of this dissertation, geochemical and age results from Chapters 1 and 2, and previous mapping and descriptions by Clayton (1983) and Swanson (unpublished field notes).

Miriam Creek volcano

Remains of the ~3.6-3 Ma Miriam Creek volcano occur beneath and to the east of Hogback Mountain, exposed in the valley of Miriam Creek and its tributaries. Outcrops of similar rock and presumed age were also identified near Hidden Spring by Clayton (1983) and Swanson (unpublished). The deposits include sandy basaltic tephra and scoria beds, basaltic lava flows that are 2 to 15 m thick (as estimated by Clayton, 1983), interbedded felsic tephra deposits, and a ~50 m thick hornblende dacite flow (or dome/coulée) in the upper part of the stratigraphy. Note that this upper hornblende dacite unit is not dated, and the temporal and petrologic association with either Miriam Creek volcano or Hogback Mountain remains to be determined, but here I tentatively include it with the Miriam Creek suite. I note also that an orange dacitic(?) welded tuff is present beneath the oldest dated Miriam Creek lava flow, and its age and relation to the overlying basalts also remains to be determined. Overall, the volcanic deposits appear to have banked against paleotopography of Jurassic-aged metasedimentary rocks (see map by Clayton, 1980; supported by my own field observations along the creek where samples GR19-33 and GR19-35 were sampled).

Ages for the Miriam Creek suite range from ~3.6 Ma to 3.1 Ma. The groundmass $^{40}Ar/^{39}Ar$ age for a basalt lava flow low in the stratigraphy near Miriam Creek (GR19-33) is 3.56 ± 0.03 Ma. Additional basalt lava flows were observed and sampled at even lower elevation along Miriam Creek by Clayton (1980, 1983) and Swanson (unpublished), so the maximum age of this unit remains unconstrained. A small andesite plug or flow remnant on the ridge south of Miriam Creek (GR20-30) has a similar age to the above basalt flow: 3.53 ± 0.02 Ma (see Chapter 2). In the creek bed above the basalt from which GR19-33 was sampled, a dacite tuff was dated by Clayton (1983) at 3.1 ± 0.2 Ma. The upper age of the Miriam Creek unit also remains unconstrained, and so further geochronology is required. Based on their composition (discussed further below), I suspect that the hornblende dacite below and east of Miriam Lake, and/or the ridge-forming holocrystalline andesite/diabase sampled by Swanson (unpublished; his sample 96-55), are petrologically related to the andesite represented by sample GR20-30, so I hypothesize that they are not significantly younger than 3.1 Ma.

The lower part of the Miriam Creek section consists of dominantly olivine basalt and basaltic andesite, while two-pyroxene andesite, hornblende andesite, and hornblende dacite are more common higher in the stratigraphy. Most basalts and basaltic andesites contain olivine as the sole phenocryst phase; less commonly, plagioclase or clinopyroxene are present. As with the other units described here, the bulk compositions of Miriam Creek samples are included in the Appendix table AX of Chapter 2, and these results are described in detail later in this chapter along with new mineral composition data.

Devils Washbasin volcano

The mafic lavas, dikes, and pyroclastic rocks that comprise the peaks of the Devils Horns and the basin surrounding Devils Washbasin represent the near-vent remains of a volcano that was active between ~3.0-2.7 Ma, overlying the 3.2 Ma Devils Horns rhyolite deposit (Chapter 2; Clayton, 1983). Products of the Devils Washbasin volcano range in composition from basalt to basaltic andesite and typically contain olivine, clinopyroxene, and plagioclase phenocrysts. Clayton (1983) also reported the occurrence of "rounded, less than 5-cm-diameter, xenoliths of mafic and ultramafic plutonic rocks," one example of which included mafic gabbro that graded into "cumulate textured, nearly mafic-free anorthosite or leuco-gabbro across a narrow, linear contact." No such spectacular xenoliths were found during my 2019 and 2020 field seasons, but one ~3 cm xenolith of fine-grained massive olivine (dunite?) was sampled, along with many large (~1-3 cm) glomerocrysts or oikocrysts of clinopyroxene. The occurrence of clinopyroxene and plagioclase as phenocrysts in addition to olivine makes the Devils Washbasin basalts distinct from the earlier Miriam Creek basalts.

Quaternary olivine basalt and basaltic andesite of unknown source(s)

Remnants of a Quaternary olivine basalt flow (map unit and shorthand Qob_1) are present along the Tieton River valley, occupying a channel eroded in the ~1.6 Ma Tieton andesite flow from Bear Creek Mountain (Swanson, 1964; Hammond, 2017; Gusey et al., 2018). The basalt is nearly aphyric, containing small phenocrysts of olivine (0-4.5%) and plagioclase (2.3-5.4%) in an intergranular, subophitic to diktytaxitic groundmass (Hammond, 2017; Gusey et al., 2018). The source of this lava flow remains unknown, but compositionally it is similar to basalts from Miriam Creek or Hogback Mountain, suggesting a source near there (Clayton, 1983; Gusey et al., 2018). Its age is 1.38 ± 0.25 Ma (Hammond, 2017), so possibly it was an early eruption from the Hogback Mountain volcano (the oldest age of which is 1.09 ± 0.1 Ma).

Not long after the eruption of the Qob_1 basalt and the second Tieton andesite lava flow, several basaltic andesite lava flows were emplaced along the Tieton Canyon. Hammond (2017) dated one of these flows at 1.31 ± 0.04 Ma ($^{40}Ar/^{39}Ar$). At least three flows of this unit Qob_2 occur on the west flank of Pinegrass Ridge, and an outcrop is located within the Oak Creek Wildlife Area (Gusey et al., 2018). Like the Qob_1 lava flow, the source of the Qob_2 basaltic andesites is uncertain, but it must be somewhere in the vicinity of the Goat Rocks area or Hogback Mountain (Gusey et al., 2018). The rock is a medium-gray to black basaltic andesite and contains phenocrysts of olivine (2.4-3.1%), clinopyroxene (3.8-8.4%), and plagioclase (13.7-14.7%) in an intergranular, subophitic to intersertal groundmass (Hammond, 2017; Gusey et al., 2018).

Hogback Mountain shield volcano

A Pleistocene shield volcano was built from two vents in the vicinity of Hogback Mountain, just south of the White Pass ski area. This volcano erupted more than 100 lava flows, some of which traveled at least 12 km from the summit (see Chapter 2, Figure 2.1, Figure 2.2). A lower sequence of several K-enriched olivine basalt lava flows erupted from the older vent about 0.5 km north of Miriam Lake, which is identified by a ~75-m-tall densely agglutinated plug surrounded by scoria and spatter deposits. A hyaloclastic deposit separates these older lava flows from overlying basalt and basaltic andesite flows that erupted from the younger vent to the south, 0.5 km northwest of Shoe Lake, which formed a shallow plug of fine-grained gabbroic rock. Approximately 100 lava flows, each typically 0.5-1.5 m thick, were erupted from this younger vent (Clayton, 1983). The older vent and lava flows are magnetically reversed and yielded ages ~1.10-1.05 Ma, and the younger vent and lava flows are normally magnetized and were erupted between ~1.05 and 0.89 Ma (Swanson, unpublished; Chapter 2).

Lakeview Mountain

Remnants of a young (194 ± 12 ka; Chapter 2) mafic volcano comprise Lakeview Mountain, ~4.5 km southeast of Walupt Lake. During the 2017 field season, we surveyed and sampled the eastern flank of the peak, near Gertrude Lake, and outcrops to the northeast along an unnamed trail that connects to the Pacific Crest Trail. Near Gertrude Lake, the volcanic pile consists of moderately welded, poorly sorted pyroclastic material (cobble-sized and smaller scoria in fine matrix), topped by rheomorphic lava (i.e. densely agglutinated material). A sample of the latter is basaltic andesite containing clinopyroxene and olivine phenocrysts with smaller plagioclase microphenocrysts. To the northeast, lava flows with similar phase assemblages but more silicic bulk composition (andesite) were likely erupted from this volcano as well, but field relations need further investigation.

Coleman Weedpatch-Two Lakes basalts

Hammond (1980) identified vents near the Two Lakes area of the Yakama Indian Reservation that likely sourced some of the basaltic andesite lava flows that crop out near and south of Walupt Lake. Swanson (1996a and unpublished field notes) and this author also recognized near-vent deposits (e.g. agglutinated scoria/spatter) near the Coleman Weedpatch trail on the ridge south of Walupt Lake. These rocks typically contain a few percent of olivine phenocrysts and small plagioclase phenocrysts (Swanson, 1996a). As Swanson (1996a) noted, these rocks can be difficult to distinguish from Walupt Lake basalt in hand sample, but their bulk compositions are distinct, as discussed further below.

Walupt Lake volcano

The remains of the Walupt Lake volcano (65 ± 28 ka; Chapter 2) comprise the steep mountain southwest of Walupt Lake (see Chapter 2 Figure 2.1). This volcano must have been constructed during a glacial period, as it formed a tuya with a nearly 500-m-thick hyaloclastic deposit capped by scoria and basaltic lava flows (Swanson, 1996a). The rocks include abundant plagioclase and olivine phenocrysts and glomerocrysts, and their bulk compositions represent a narrow, unique range, distinct from the nearby Coleman Weedpatch-Two Lakes and Lakeview Mountain units despite their geographic and temporal proximity (discussed further below).

METHODS

To investigate what magmatic conditions and petrogenetic processes may have contributed to the construction of the Goat Rocks area mafic volcanoes, a variety of methods were employed. Bulk major and trace element and isotope compositions were determined by X-ray fluorescence (XRF), inductively-coupled plasma mass spectrometry (ICP-MS), and thermal ionization mass spectrometry (TIMS). (Methods for major and trace element compositional analysis are described in Chapters 1 and 2, and the methods for isotopic analysis are described below.) Mineralogy and texture were evaluated in thin section under petrographic microscope (sample preparation is described in Chapter 2). Several mineral phases (olivine, spinel, and clinopyroxene) were imaged and analyzed via electron microprobe. Finally, various petrologic modelling tools were used to characterize the petrogenesis of these mafic magmas.

Bulk rock Sr, Nd, Pb, and Hf isotopic analysis

Crushed or powdered samples for isotopic analysis were submitted to the Pacific Centre for Isotopic and Geochemical Research (PCIGR) at the University of British Columbia (UBC). At least one sample was submitted for isotopic analysis from each mafic volcano or unit. The most primitive samples available for each volcano/unit were chosen based on highest MgO, Mg#, Cr, and Ni. Initially samples were crushed to <5 mm in a jaw crusher with steel plates and pulverized to powder in an alumina ceramic ring mill at OSU. To ensure minimal Pb contamination, later batches were crushed using alumina ceramic plates at OSU and then powdered at PCIGR in a planetary mill with agate jars and milling balls. Aliquots of the powders were then digested in a concentrated HF-HNO_3 acid mixture (see Fourny et al., 2016). For one batch analyzed in 2021, a 5% aliquot of each digested sample was measured on an Element II High Resolution ICP-MS (HR-ICP-MS)(Thermo Scientific) for trace element concentrations. Otherwise, ion exchange chromatography was performed to separate Pb, Sr, Nd, and Hf for isotopic analysis (Fourny et al., 2016; Weis et al., 2006). Lead, Nd, and Hf separates were measured for isotopic compositions on three different Nu instruments MC-ICP-MS (Nu 021, NPII 214, Nu1700), and Sr isotopic compositions were measured by thermal ionization mass spectrometer (TIMS), a Thermo Scientific Triton and (or?) a Nu Instruments TIMS (Fourny et al., 2016). Detailed descriptions of PCIGR laboratory and analytical methods can be found in Weis et al. (2006) and Fourny et al. (2016).

Microprobe analysis of olivine, spinel, and clinopyroxene

Minerals in polished thin sections were analyzed by electron microprobe over several sessions. Thin sections were prepared at Wagner Petrographic and were analyzed using the Cameca SX-100 Electron Microprobe at Oregon State University. Analytical procedures including spectrometer, crystal, and count time used for each element, and standard analyses and accepted values, are given in APPENDIX(?). During each analytical session, backscatter images were collected for each crystal/cluster to be analyzed. Locations of points were marked either physically on printouts or digitally on the images for later reference. The EDS detector was used to identify phases based on compositional indicators (e.g. high Cr distinguishes spinel from Fe-Ti oxides, high Ca distinguishes clinopyroxene from orthopyroxene). Typically, several points each were placed on rims and cores of crystals, and additional points were set on any notable intermediate zones visible in backscatter. Where equilibrium between phases was important, for example, evaluating co-crystallizing spinel and olivine, points were analyzed on each side of a touching crystal boundary.

Compositional data was filtered for quality by excluding any analyses that yielded excessively low or high totals; for example, <98 wt% or >101.5 wt% for silicate minerals, or for spinel a less restrictive range such as <90 wt%, since the total for that phase may be affected by Fe^{2+}/Fe^{3+} ratios. After more careful evaluation, analyses with questionable outlier compositions were culled, for example, high Si or Ti in what should be spinel (>2 wt% Ti is more likely titanomagnetite). Following this initial filtering, the geochemistry visualization software ioGAS was used to quickly plot and evaluate data.

For spinel, Fe^{2+} and Fe^{3+} proportions were approximated by assuming ideal stoichiometry (3 cations) and charge balancing. After Stormer (1983), molar proportions of cations were normalized to 3 cation sites, then the sum of charges was calculated assuming that all Fe has a 2+ charge. Subtracting that sum from 8 (the total negative charge from four O^{2-} anions) yields the charge deficiency that presumably comes from the extra 1+ charge on Fe^{3+}; as such, that number of Fe cations is assumed to be Fe^{3+}, and then the Fe^{2+}/Fe^{3+} and Fe^{3+}/Fe^{T} ratios can be calculated. However, it is important to note that this recalculation method alone does not yield a reliable Fe^{3+}/Fe^{T} value because errors on each measured oxide propagate into the calculation (Davis et al., 2017). To properly calculate Fe^{3+}/Fe^{T}, one would need to analyze spinel standards of similar composition during the same microprobe session that have had their Fe^{3+}/Fe^{T} ratios quantified by Mössbauer analysis, such that a correction factor could be applied to the unknown samples (e.g. Wood and Virgo, 1989; Davis et al., 2017). I did not analyze such standards, so the ferric/ferrous iron ratios I calculated are only rough estimates and cannot be used to reliably evaluate fO_2 of samples. However, for comparison to spinel compositions from Mount St. Helens basalts determined by Wanke et al. (2009), I calculate Mg#=Mg/(Mg + Fe^{2+}) as they do, using Fe^{2+} calculated by charge balancing as above. The unconstrained uncertainty in this Mg# calculation is not likely to affect the overall interpretations about spinel compositional groups, but the reader should be aware of it.

Petrologic modelling

Several petrologic modelling approaches were employed, from simple calculations to thermodynamic models. Calculations of liquid line of descent while fractionating a single mineral (olivine) were performed by assuming an initial equilibrium mineral composition, subtracting a small mass fraction (e.g. 1%) of that composition, re-normalizing the remaining 'liquid' composition, calculating a new equilibrium mineral composition, and repeating these steps to the desired degree of fractionation. An Excel version of XLFRAC (Stormer and Nichols, 1978) was used to perform least-squares regressions for simple tests of bulk crystal removal or mixing. Rhyolite-MELTS (Gualda et al., 2012; Gualda and Ghiorso, 2015) was used to quickly calculate Fe_2O_3 concentration from measured FeO^T based on a chosen oxygen fugacity (fO_2), to normalize compositions, and to determine liquidus (or solidus) temperatures at a given pressure and H_2O concentration; these parameters could then be input into the Magma Chamber Simulator (MCS) for more detailed modelling. MCS (Bohrson et al., 2014) was used to run fractional crystallization models and to test mixing, recharge, and assimilation of partial melts from country rock.

RESULTS

Bulk rock compositions

All of the basalts that erupted in the Goat Rocks area share elevated fluid-mobile element concentrations and Nb-Ta depletions on a "spider" diagram, and therefore can be classified as calc-alkaline basalt (CAB). Some of the volcanoes or units have their own unique compositional fingerprints (for example, unit Qob_2 has distinctly high K, while Walupt Lake basalts are uniquely enriched in Sc). Two main observations are: 1) the older basalts that erupted from Miriam Creek volcano and Devils Washbasin volcano are overall more depleted in incompatible trace elements than younger basalts; 2) two endmember groups can be defined based on trace element ratios and isotopic compositions, and these groups persist through time with no clear temporal or geographic trend.

The bulk rock compositions produced by each peripheral mafic volcano are described in detail below. Note that the major and trace element and isotopic data are included in the appendix dataset for Chapter 2 (Appendix 2.x). Isotope ratios are also given here in Table 3.x. Major element data are represented in Figure 3.1and Figure 3.2, trace element data are shown in Figure 3.3 and Figure 3.4, and isotope data are given in Figure 3.5 and Figure 3.6.

Miriam Creek volcano

The Miriam Creek section ranges in composition from basalt to dacite. Bulk compositions of the Miriam Creek basalts fall between 49.9-51.8 wt% SiO_2 and 9.3-6.8 wt% MgO, with somewhat low K_2O (0.3-1.0 wt%), and CaO comparable to compositions erupted later at Hogback Mountain (8.1-9.8 wt%; Figure 3.1, Figure 3.2). Their high FeO^T (9.4-10.5 wt%) distinguishes them from most other Goat Rocks area basalts, except for the Qob_1 lava flow (see below). The Miriam Creek basalts are among the least enriched in Ba and LREE, comparable to Qob_1 and some compositions from Upper Hogback Mountain and Coleman Weedpatch (Figure 3.3, Figure 3.4). They are also depleted in high field strength elements (HFSE) such as Nb, Ta, Zr, and Th (Figure 3.3, Figure 3.4). Isotope ratios were determined for one basalt sample, GR19-33. This sample is approximately in the middle of the Goat Rocks basalt array for $^{143}Nd/^{144}Nd$, $^{87}Sr/^{86}Sr$, and $^{176}Hf/^{177}Hf$ ratios, and is on the higher end for Pb isotope ratios ($^{206}Pb/^{204}Pb$, $^{207}Pb/^{204}Pb$, and $^{208}Pb/^{204}Pb$; Figure 3.5; Table 3.x; Appendix A3.x).

Basaltic andesite lava flows sampled by Clayton (1983; sample HMMLC-4) and Swanson (unpublished; sample 96-54) contain 55.3-56.2 wt% SiO_2, 5.7-5.6 wt% MgO, ~8.7 wt% CaO, and 1.2-1.1 wt% K_2O. Trace element data are available for sample 96-54 (Appendix x). Similar to the basalts described above, it is relatively depleted in HFSE compared to other basaltic andesites in the area. It is quite enriched in Sr (773 ppm), though not as enriched as andesite and dacite discussed below.

The andesitic point on the valley wall south of Miriam Creek (long/lat: -121.3655, 46.6014) is mineralogically and compositionally variable. The rock exposed in outcrop is a somewhat fine-grained hornblende andesite, but the surrounding talus commonly contains phenocrysts or glomerocrysts of olivine, clinopyroxene, orthopyroxene, and plagioclase, with an absence of amphibole. The amphibole-bearing rock is more felsic (62.2 wt% SiO_2, 3.4 wt% MgO) and the olivine-andesite is more mafic (59.3 wt% SiO_2, 5.8 wt% MgO). Both are strikingly enriched in Sr (1020-1115 ppm) and on the lower side in Y and HREE (e.g. ~15 ppm Y) compared to other Goat Rocks area andesites. Although not as enriched in Sr, the hornblende dacite (GR17-16) and two-pyroxene andesite/diabase (96-55) outcropping further west are mineralogically and chemically similar to the above two rock types, respectively (Figure 3.3).

The white hornblende dacite tuff (my GR19-35; Clayton's HMMCSP-2) dated at 3.1 ± 0.2 Ma (Clayton, 1983) is notably high in Al_2O_3 (21.3 wt%) and low in K_2O (0.4 wt%) and

FeO (2.6 wt%; Figure 3.2), perhaps a result of weathering/alteration (the rock was sampled in a creek bed and is clayey).

Overall: the high FeO concentrations of Miriam Creek basalts distinguish them from most other Goat Rocks area basalts, and the lower-K trend of the more evolved rocks is similar to the much younger andesites and dacites that erupted during Old Snowy Mountain stage (see Chapter 2, Figure 2.10).

Devils Washbasin

Bulk compositions of the Devils Washbasin basalts and basaltic andesites are similar in some ways to the basalts of Miriam Creek and in other ways to younger basalts. The most striking difference is that the Devils Washbasin suite includes compositions that are uniquely high in CaO (11.0-11.8 wt%; most others 9.0-9.8 wt%; Figure 3.2). These basalts are also the most depleted in FeO^T, in contrast to the Miriam Creek compositions. K_2O concentration rises with decreasing MgO approximately parallel to the younger Lower Hogback Mountain suite, with slight overlap (Figure 3.2). Incompatible trace element concentrations generally overlap with the Miriam Creek suite (on the depleted end of the spectrum), but Ba, Pb, Th, U, and La are slightly more enriched. Apart from one outlier composition (TP19-17, described below), the suite is the most depleted in several HFSE (e.g. Hf, Zr, Y) and the HREE (Figure 3.3, Figure 3.4). Ba/Nb and Pb/Ce values are among the highest determined for the Goat Rocks area mafic volcanoes, suggesting a significant fluid/subduction component. La/Sm and La/Yb are also on the higher end, reflecting the stronger depletion of HREE relative to LREE (or, LREE enrichment relative to very depleted HREE; Figure 3.4, Figure 3.6).

Interestingly, one basalt lava flow that caps the ridge between Tieton Peak and Devils Horns (sample TP19-17) is unique in composition from the rest of the Devils Washbasin basalts: at a given MgO range it is slightly more silicic (52.2-53.2 wt% SiO_2), with much lower CaO (9.3-9.6 wt%) and slightly high K_2O (~1.0 wt%; Figure 3.2). On many element diagrams, this sample plots with the Lower Hogback Mountain suite. However, it is not quite as enriched in Ba, HFSE, and LREE (Figure 3.3).

Two samples from Devils Washbasin were analyzed for their isotopic compositions: GR16-07, with MgO ~8.0 wt%, Mg# 67, 77 ppm Ni, and 242 ppm Cr; and the more primitive GR20-13, with MgO ~9.8 wt%, Mg# 71, 118 ppm Ni, and 352 ppm Cr. These samples are very close in Pb, Sr, and Nd isotope compositions (Figure 3.5): on the higher end of $^{87}Sr/^{86}Sr$ and on a steeper $^{208}Pb/^{204}Pb$ (or $^{207}Pb/^{204}Pb$) vs. $^{206}Pb/^{204}Pb$ trend compared to the rest of the Goat Rocks mafic suite. However, the samples are quite different from one another in

$^{176}Hf/^{177}Hf$ isotopes; the more evolved sample GR16-07 has a much lower ratio than GR20-13 (Figure 3.5).

Quaternary olivine basalt (Qob_1)

The Qob_1 lava flow is a relatively primitive basalt, with ~50.4-51.0 wt% SiO_2, 8.1-7.3 wt% MgO, Mg# 61-63, 236-270 ppm Cr, and 91-115 ppm Ni (Gusey et al., 2018; Figure 3.1, Figure 3.2, Figure 3.3). Its CaO concentration is like that of Miriam Creek and Hogback Mountain basalts (9.0-9.6 wt%), and K_2O is relatively low (0.6-0.8 wt%), like Miriam Creek and Upper Hogback Mountain compositions. FeO^T is also on the higher side at 9.3-10.4 wt%, similar to the Miriam Creek basalts.

For major element and more comprehensive (ICP-MS) trace element concentrations as well as isotopic ratios, I analyzed one sample of Qob_1 (16423) that was collected by Daryl Gusey but not previously analyzed. Fortuitously for the isotopic analysis, its composition represents the most primitive values of the above range. The sample is an endmember in $^{143}Nd/^{144}Nd$-$^{87}Sr/^{86}Sr$ space for the Goat Rocks mafic suite, with the highest $^{143}Nd/^{144}Nd$ and lowest $^{87}Sr/^{86}Sr$ measured (Table 3.x, Figure 3.5). Its Pb isotope ratios are comparable to samples from unit Qob_2 and Hogback Mountain.

Quaternary olivine basaltic andesite (Qob_2)

The compositional range of the Qob_2 suite is in many ways unique from the rest of the Goat Rocks mafic suite. These lava flows are basaltic andesite, with SiO_2 from 54.4-56.6 wt%, and MgO concentration is between 6.1-4.7 wt% (Gusey et al., 2018; Figure 3.1, Figure 3.2). They are relatively low in CaO (7.5-8.0 wt%) and Al_2O_3 (15.8-16.4 wt%). The lavas are much more enriched in K_2O (1.6-2.1 wt%), and HFSE (Nb, Ta, Hf, Zr, Th) than any other basaltic andesites in the Goat Rocks area (Figure 3.2, Figure 3.3). They are also typically enriched in TiO_2 (1.2-1.6 wt%), P_2O_5 (0.25-0.34 wt%), and LREE (e.g. La 22-34 ppm, Ce 47-68 ppm, Nd 24-33 ppm; Gusey et al., 2018; Figure 3.2, Figure 3.3). Sample GR16-06 has Pb isotope ratios close to those of Hogback Mountain and Qob_1 samples. $^{143}Nd/^{144}Nd$ and $^{87}Sr/^{86}Sr$ are like Upper Hogback Mountain and Walupt Lake basalts, and $^{176}Hf/^{177}Hf$ is close to Qob_1 (Figure 3.5, Table 3.x, Appendix X).

Hogback Mountain

The lava flows that erupted from the Hogback Mountain volcano can be split into two distinct compositional groups, here called Lower Hogback Mountain and Upper Hogback

Mountain. The two groups are separated in time and stratigraphy by the hyaloclastic deposit exposed near the Pacific Crest Trail.

The Lower Hogback Mountain suite comprises those olivine basalt lava flows that erupted from the older, northern vent. They are more primitive than the younger suite, with SiO_2 of 50.7-51.7 wt%, MgO between 6.8-9.7 wt%, and Mg# 62-68. Olivine is typically the only phenocryst phase, with rare clinopyroxene as phenocrysts or glomerocrysts. CaO content overlaps the range of Miriam Creek basalts and Qob_1, between 9.3-9.9 wt%. FeO^T is intermediate between the Devils Washbasin and Miriam Creek/Qob_1 ranges at 8.6-9.1 wt%. K_2O concentrations are among the highest of the Goat Rocks basalts (1.0-1.3 wt%), and Na_2O is also on the higher side (2.8-3.2 wt%, similar to Qob_1 and some Miriam Creek basalts). The Lower Hogback Mountain suite is generally the most enriched among the Goat Rocks basalts in fluid-mobile trace elements (Rb, Ba, Th, less so Sr), HFSE (Nb, Ta, Zr, less so Ti), and LREE-MREE. Note that Clayton's sample HMSP-3 is from an area that Swanson interpreted as Upper Hogback Mountain (his unit Qbh_2; unpublished field notes), but based on its elevated K_2O (1.2 wt%) and P_2O_5 (0.35), I include it with the Lower Hogback Mountain group (Appendix table 2.x, Figure 3.2).

The Upper Hogback Mountain suite consists of typically more evolved compositions. These basalts and basaltic andesites range from 51.2-54.7 wt% SiO_2 and 8.8-5.5 wt% MgO (Figure 3.1, Figure 3.2). The phenocryst assemblage of these rocks is commonly plagioclase, olivine, and clinopyroxene. Concentrations of CaO and FeO^T are of similar range as the Lower Hogback Mountain suite, but K_2O concentration is typically lower (0.6-1.3 wt%), along with other fluid-mobile elements (Ba, Sr, Th) and LREE (La, Ce), more akin to the basalts of Miriam Creek and Qob_1 (Figure 3.3).

The two Hogback Mountain suites share similar Pb isotope ratios to each other and to Qob_1 and Qob_2, plotting on the High Cascades Array (Figure 3.5b). They are close in $^{143}Nd/^{144}Nd$ ratios, but Upper Hogback Mountain samples are significantly higher in $^{87}Sr/^{86}Sr$ (Figure 3.5a). In $^{176}Hf/^{177}Hf$ ratios, the samples span nearly the full range of the Goat Rocks mafic suite (Figure 3.5c).

A dike (or plug) that crops out just above Miriam Lake is of uncertain age and has an intriguing composition. It was only identified in that location and not traced higher up in the Hogback Mountain stratigraphy, so it is not clear whether it is older than the Lower Hogback Mountain flows or did not erupt through them. Its composition is basaltic andesite (56.5 wt% SiO_2, 4.3 wt% MgO) with relatively high K_2O (1.8 wt%), enriched HFSE (e.g. 242 ppm Zr, 5.8 ppm Hf, 6.2 ppm Th), and moderately enriched LREE (e.g. 22 ppm La; Figure 3.1, Figure

3.2, Figure 3.3). In many ways it is closest to Qob_2 in composition, but in other ways more like the Upper Hogback Mountain suite.

Lakeview Mountain

One sample was analyzed from the agglutinated/rheomorphic lava on the eastern flank of Lakeview Mountain. This sample is a basaltic andesite, with 55.1 wt% SiO_2 and 5.6 wt% MgO, enriched Na_2O (3.7 wt%) and relatively enriched K_2O (1.3 wt%; not as high as unit Qob_2, Figure 3.2). Similar to basalts from Lower Hogback Mountain, it is enriched in fluid-mobile elements (Ba, Sr, Pb) and LREE (e.g. La concentration 27 ppm; Figure 3.3, Figure 3.4, Figure 3.5, Figure 3.6). Its $^{87}Sr/^{86}Sr$ ratio is the highest and $^{143}Nd/^{144}Nd$ the lowest measured for the Goat Rocks mafic suite (Table 3.x, Figure 3.5a). It is on the lower side for $^{176}Hf/^{177}Hf$, like Upper Hogback Mountain, Coleman Weedpatch, and the more evolved Devils Washbasin sample (Figure 3.5c). Its Pb isotope ratios are on the higher end of the suite, most similar to the Devils Washbasin samples (Figure 3.5b).

Basaltic andesites from Coleman Weedpatch and Two Lakes area

One lava flow and one agglutinated spatter deposit from the Coleman Weedpatch area were analyzed to complement previous analyses by Swanson (1996a). Major element concentrations of this unit largely overlap the range of the Upper Hogback Mountain suite, with 52.5-53.6 wt% SiO_2, 7.7-6.0 wt% MgO, and 0.7-1.3 wt% K_2O. New sample GR17-58 (the agglutinated spatter) stands out as being highest in K_2O. This sample and the lava flow (GR17-57) generally have similar HFSE concentrations (e.g. Nb, Ta, Hf, Zr, Y) and REE, but Pb, Th, and U are significantly higher in the spatter deposit. The lava flow is an outlier in Pb isotopes for the Goat Rocks mafic suite—significantly lower in $^{206}Pb/^{204}Pb$, $^{207}Pb/^{204}Pb$, and $^{208}Pb/^{204}Pb$, but still aligned with the High Cascades array (Figure 3.5b; Mullen et al., 2017). In $^{143}Nd/^{144}Nd$ and $^{87}Sr/^{86}Sr$ ratios, it is near the middle of the Goat Rocks range (Figure 3.5a). Its $^{176}Hf/^{177}Hf$ ratio is among the lowest measured, clustering with a Devils Washbasin sample and those from Lakeview Mountain and Upper Hogback Mountain (Figure 3.5c).

Walupt Lake

Walupt Lake basalts have similar mineralogy to the Coleman Weedpatch basaltic andesites, but their bulk compositions are unique. Olivine phenocrysts are commonly skeletal and plagioclase phenocrysts tend to be bladelike, and the two commonly occur together in glomerocrysts. The bulk compositions are depleted in SiO_2 compared to other Goat Rocks-area basalts at a given MgO range (~49.7 wt% SiO_2 at 6.7-7.3 wt% MgO). They are also relatively enriched in Al_2O_3 (17.2-17.7 wt%) and low in K_2O (0.64-0.76 wt%). Similar to Devils Washbasin basalts, they are enriched in CaO (10.3-10.5 wt%), but like Miriam Creek and Qob_1 they are enriched in FeO^T (9.5-10.0 wt%). These basalts have distinctly high Sc concentrations, higher than any other basalts in the area (36.8-38.4 wt%; Figure 3.3c). They are also enriched in Y and middle- to heavy-REE relative to other Goat Rocks area basalts, with among the lowest MREE/HREE ratios (e.g. Y = 28-30 ppm, Dy = 5.4-5.7 ppm, Dy/Yb = 1.9; Figure 3.3j, Figure 3.4).

The Walupt Lake basalt sample GR17-62 is very similar to Miriam Creek sample GR19-33 in Pb isotope ratios and $^{176}Hf/^{177}Hf$ (Figure 3.5b,c, Table 3.x). Its $^{143}Nd/^{144}Nd$ and $^{87}Sr/^{86}Sr$ ratios are like Upper Hogback Mountain and Qob_2 (Figure 3.5a).

Summary – two main compositional groups

Overall, the mafic magmas in the Goat Rocks area define two main groups in their major and trace element concentrations and isotopic ratios. There are variations and transitional compositions among them, but in general, the groups can be defined as: 1) Group 1: LILE- and LREE-enriched CAB with higher $^{87}Sr/^{86}Sr$, lower $^{143}Nd/^{144}Nd$, and Pb isotopes aligned with the High Cascades; 2) Group 2: CAB with lower LILE concentrations and LREE/HREE ratios, lower $^{87}Sr/^{86}Sr$, higher $^{143}Nd/^{144}Nd$, and Pb isotopes that extend slightly toward the Adams Array of Mullen et al. (2017; Figure 3.5, Figure 3.6). Both compositional groups are represented through time and across a geographically broad area. Both types are erupted in close proximity at the Hogback Mountain volcano within a narrow interval of time. Group 1 includes basalts from Devils Washbasin and Lower Hogback Mountain and the basaltic andesite of Lakeview Mountain, and Group 2 includes the basalts of Miriam Creek, Qob_1, Upper Hogback Mountain, Walupt Lake volcano, and Coleman Weedpatch. Basaltic andesite unit Qob_2 is compositionally unique, being enriched in LREE like Group 1, but is isotopically more like Group 2 (Figure 3.5, Figure 3.6).

Olivine compositions

Backscatter electron images and compositions were collected for olivine in eight samples representing all Goat Rocks area basalt groups but Qob_1 and Qob_2; that is, from Miriam Creek volcano (GR17-17), Devils Washbasin (GR16-07), Hogback Mountain (GR17-14 and GR17-19, Lower; and GR17-03, Upper), Lakeview Mountain (GR17-24), Coleman Weedpatch (GR17-58), and Walupt Lake volcano (GR17-62). For each olivine analyzed, several points were placed within the core and several near the rim. Representative backscatter electron images are presented in Figure 3.7, and a summary of compositions is given in Table 3.x, with the full dataset in Appendix X. Forsterite number (Fo) of olivine was calculated as Fo = molar Mg/(Fe+Mg)*100, assuming that all iron is present as Fe^{2+}.

Olivine among the different samples exhibits a range of textures. Some have skeletal to euhedral habits, while others have rounded or scalloped shapes or (rarely) what looks to be breakdown to orthopyroxene (Figure 3.7). Some euhedral crystals have crisp edges, while others show intergrowth with groundmass microlites, indicating rapid crystallization (e.g. Figure 3.7c,d). In most of the analyzed samples, spinel (chromite) inclusions are common, but they are rarer in some (GR16-07, GR17-62, GR17-03 interior). In a few samples, the olivine is pervasively riddled with tiny spinel or Fe-Ti oxides (e.g. Figure 3.7f,g,k) and yields abnormal compositions (for example, excessively high Fo or MnO concentration). Given the red oxidation of groundmass in some of these samples, the olivine is also interpreted as oxidized/altered. Most samples display simple, normal zoning (more magnesian core, darker in BSE; and less magnesian rim, brighter in BSE), and the zoning is diffuse rather than sharp (Figure 3.7).

The oxidized olivine (in samples GR17-19, GR17-58, and GR17-03) have distinctly high MnO concentrations for a given MgO range compared to the other samples which form a neat array (Figure 3.8b). These samples also tend to have lower CaO concentrations than the other samples (Figure 3.8c). The olivine in Lakeview Mountain sample GR17-24 shares a similar CaO range, but does not have the same oxidized texture. On a Rhodes diagram of olivine Fo# vs. whole-rock Mg# (Figure 3.8e), two of the samples with oxidized olivine plot above the equilibrium range, but the GR17-19 analyses fall below this range.

Among all samples, Fo# ranges from as high as 96 (oxidized olivine from GR17-03) to as low as 52 (groundmass olivine from GR17-62; Table 3.2). Most individual samples exhibit a broad range of Fo#, with core analyses at higher Fo# in (or close to) equilibrium with the whole-rock composition, and rims extending to much lower Fo# (Table 3.2, Figure 3.8).

A detailed description of the analyses for each volcano/unit is provided below. Note that to simplify the description of large olivine crystals (whether “phenocrysts,” “antecrysts,” or even “xenocrysts”), they are described here as “macrocrysts,” after Leeman and Smith (2018).

Miriam Creek

Olivine macrocrysts in sample GR17-17 from Miriam Creek volcano are commonly broken (the rock is a sandy basaltic tephra deposit), but the fragments tend to have euhedral facets (Figure 3.7a). Chromite inclusions are present in some olivines. One olivine macrocryst analyzed contains two melt inclusions, each with a vapor bubble (larger crystal in Figure 3.7a). Zoning in these olivines, if visible at all, is subtle and diffuse—i.e. their compositions are relatively homogenous from core to rim. Macrocryst cores have Fo between 85-80, and rims overlap this range, falling between Fo 83-75.

Devils Washbasin

Sample GR16-07, from a Devils Washbasin basalt lava flow northeast of Bear Creek Mountain, contains olivine macrocrysts and glomerocrysts that are rounded or irregularly shaped, suggestive of resorption. Chromite inclusions are present, but scarce. Several smaller olivines occur as inclusions within a large plagioclase crystal. Cores were measured to have Fo between 86-82, and rims are significantly less magnesian, at Fo 77-69.

Hogback Mountain

Olivine macrocrysts in sample GR17-14 (a Lower Hogback Mountain lava flow) are generally euhedral in shape, but some have slightly embayed textures, and all have rims that are intergrown with microlites of plagioclase, clinopyroxene, and oxides from the surrounding groundmass, suggesting rapid crystallization (Figure 3.7c,d). Chromite inclusions are common. Most crystals appear relatively homogeneous in BSE, although one large (~2mm) crystal in a glomerocryst has a notably darker core with diffuse zoning to a brighter rim. The latter has core Fo 87-86, but all other cores are much less magnesian, with Fo 77-66. Rims are Fo 72-65, and a groundmass olivine is Fo 64.

Olivines in sample GR17-19, from the vent plug of Lower Hogback Mountain, are similar to those of GR17-14. Their crystal habit is euhedral or sometimes embayed (Figure 3.7e,f). Intergrowth with surrounding groundmass microlites is also common, though at a smaller scale, and also some crystals appear to be either intergrown with or reacting into pyroxene (presumably orthopyroxene, but not analyzed; Figure 3.7f). Very small oxide inclusions are also abundant in the olivine crystals, commonly in linear trails that may represent annealed fractures. Larger macrocrysts have cores with Fo 84-81, while smaller macrocrysts are between Fo 80-78. Rim compositions are Fo 81-78. All of these olivines are enriched in Mn at a given Mg concentration compared to most other samples, which is similar to the other oxidized olivines analyzed in samples GR17-03 and GR17-58 (Figure 3.8). However, the Fo numbers and other compositional parameters do not seem to be compromised by alteration (i.e. they are not excessively high, as discussed further below).

Sample GR17-03 is from Upper Hogback Mountain. The rock from which it was sampled was a talus block with a lighter gray, dense zone in contact with an oxidized, vesicular zone. Presumably this talus block fell from one of the lava flows higher on the slope which have vesiculated flow tops and dense interiors, interpreted to be inflated flows. The olivine macrocrysts within the vesicular (exterior) zone are dark in BSE and riddled with inclusions, which may be fine grained and broadly distributed (similar to GR17-19), or concentrated along rims, or relatively coarse and "wormy" in texture (e.g. Figure 3.7g). Two of these crystals have cores with Fo 96-94, while another two are Fo 82-81 (81 at rim). In contrast, olivine macrocrysts within the dense (interior) zone are euhedral (Figure 3.7h), with more scarce (larger) inclusions, and display darker-grayscale (more magnesian) cores that grade diffusely into brighter rims, similar to the olivines observed in sample GR17-14. Cores of these olivines have Fo 82-77, with rims of Fo 73-66.

Lakeview Mountain

Olivine macrocrysts in sample GR17-24 (Lakeview Mountain basaltic andesite) have rims and fractures that are greenish-brown under plane polarized light and dark in BSE (iddingsite or perhaps magnesite alteration? Figure 3.7i,j). Some crystals are euhedral while others have irregular embayments that look like dissolution textures (Figure 3.7i). The cores have Fo 79-73, and rims overlap this range at Fo 78-73.

Coleman Weedpatch

Olivine in sample GR17-58, from an agglutinated vent deposit in the Coleman Weedpatch area, tends to be euhedral, with fine oxide crystals distributed throughout (similar to GR17-19) and also highly concentrated at the rim (Figure 3.7k). Like the oxidized olivines from the exterior zone of GR17-03, these are very dark in BSE. As discussed below, their compositions appear to be compromised by the oxidation/alteration (the rock as a whole is red with oxidation). Their measured Fo ranges from 89-87.

Walupt Lake

Sample GR17-62 contains olivine that is euhedral or skeletal and occurs in glomerocrysts with bladelike plagioclase crystals, where the plagioclase appears to have crystallized first, and the olivine crystallized around it and interstitially (Figure 3.7l). Aside from the intergrowth with plagioclase, inclusions are uncommon (rare spinel inclusions occur; see additional BSE images in Appendix X). Cores are darker in BSE, with Fo 84-82, grading to brighter, much less magnesian rims (Fo 73-58). Smaller phenocrysts (~100 micron) and groundmass microlites (<30 microns) are very bright in BSE, with Fo 67-52.

Equilibrium testing

For each sample, a model equilibrium olivine Fo was calculated from its bulk composition to evaluate whether the olivine macrocrysts are likely phenocrysts (in equilibrium) or entrained crystals. The equilibrium constant was assumed to be $K_{D,Fe2+\text{-}Mg}$ = $(FeO/MgO)^{ol}/(FeO/MgO)^{liq}$ = 0.3 (after Roeder and Emslie, 1970), and FeO of the bulk rock was considered to approximate FeO^{liq}. For two samples, GR17-14 and GR17-19, a model melt composition was also calculated assuming 5% olivine fractionation (as both samples have approximately 5% olivine), i.e. by subtracting 5% of a reasonable olivine composition (e.g. a megacryst core) from each bulk composition, in attempt to evaluate whether rim compositions are in equilibrium. The thermodynamic tool MELTS (Gualda et al., 2012; Gualda and Ghiorso, 2015) was utilized to estimate FeO of bulk rock (or calculated melt) compositions from FeO^T by setting the fO_2 constraint at the NNO buffer (which may be slightly too oxidized by about one log unit, as addressed on page 156, and could be recalculated at QFM for better accuracy). For both GR17-14 and GR17-19, the calculated melt composition yielded an equilibrium Fo of 4 units lower than the bulk rock composition (e.g. Fo 83 rather than Fo 87), so this deduction was extrapolated to the other equilibrium Fo calculations as an approximate lower estimate (this assumes also ~5% olivine crystallization, which is probably close for most samples, but a ballpark approximation).

A comparison of these equilibrium olivine Fo estimates vs. measured olivine Fo is presented in Table 3.2. Most of the samples contain olivine with measured core compositions that are within range of the equilibrium compositions, but two of the samples that contain olivine riddled with oxides (GR17-03 and GR17-58) have measured olivine Fo that are much higher than the calculated equilibrium compositions. These high-Fo olivines are also enriched in Mn, which could indicate hydrothermal alteration (e.g. Plechov et al., 2018). Olivine from sample GR17-19 has similar, but less extreme, oxidation textures and elevated Mn, but their measured Fo values do not exceed the calculated equilibrium values (rather, they are on the lower side, with only cores of large macrocrysts overlapping the estimated range). Crystal rims and groundmass olivines commonly have considerably lower Fo than megacryst cores and the calculated equilibrium ranges. For example, sample GR17-62 contains microphenocrysts and groundmass microlites with Fo between 67-58, compared to macrocryst core Fo between 82-84 and an equilibrium estimate of Fo 83-79.

Olivine equilibrium can be evaluated with a Rhodes diagram (Figure 3.8e). A typical Rhodes diagram (e.g. Putirka, 2008) uses $Fe^{2+}/Fe^{T}=1$ (i.e. considers all iron as Fe^{2+}) for the liquid Mg# calculation, but here I use $Fe^{2+}/Fe^{T}=0.85$, approximating the oxidation state at the QFM buffer, which simply shifts the equilibrium line and liquid compositions toward higher melt Mg# (their relative position remains the same). The maximum and minimum equilibrium range is represented using $K_D(\text{Fe-Mg})^{\text{ol-liq}} = 0.30 \pm 0.03$ after Roeder and Emslie (1970). As above, most samples have olivine with core compositions overlapping the equilibrium range, though samples GR17-24 (Lakeview Mountain) and GR17-19 (Lower Hogback Mountain) are slightly low, and the oxidized olivines from GR17-03 (Upper Hogback Mountain) and GR17-58 (Coleman Weedpatch) are clearly far above equilibrium. Interestingly, some olivine core compositions from GR17-14 (Lower Hogback Mountain) and GR17-62 (Walupt Lake) are portrayed on this diagram as slightly above the equilibrium range, which could indicate entrainment of more primitive antecrystic or cumulate material.

In summary, olivine core compositions are broadly within range of equilibrium with bulk rock compositions (with a few exceptions), but rim compositions and groundmass microlites tend to be much below the equilibrium range. A diffuse gradient from rim to core, ubiquitous across samples, is interpreted to reflect diffusive re-equilibration from originally sharper zone boundaries, as described by other authors (e.g. Kahl et al., 2011). However, maps of a slow-diffusing element such as phosphorus were not collected to confirm this. All of the olivine compositions for sample GR17-58 (Two Lakes basalt) have been reset by oxidation, as have some of the olivines in the oxidized flow exterior of sample GR17-03 (Hogback Mountain). Olivine core compositions from GR17-19 (Hogback Mountain) and GR17-24 (Lakeview Mountain) are slightly below the equilibrium range, and in sample GR17-14 (Hogback Mountain), except for one crystal, they are significantly low. Slightly low-Fo cores could be a result of analyzing surfaces that are oblique cuts through crystals rather than directly through the core. Alternatively, the three samples with systematically low-Fo populations may instead represent entrainment of crystals from slightly more evolved mush zones, and/or rapid disequilibrium crystallization. The latter process is invoked to explain the low-Fo rims that are present in all samples. “Supercooling” of basaltic magmas upon interaction with cooler, more evolved mush zones or crustal rocks may be a common process for all of the mafic volcanoes in this region. This process was described by Tamura et al. (2000) to explain iron-rich olivines (texturally similar to many olivines described here) in magnesian basalts from Daisen volcano in Japan. Abnormally iron-rich olivines are also observed by Leeman et al. (2018) in basalts from Mount St. Helens, but with evidence of re-equilibration and resorption (reversed zoning, orthopyroxene rims), which are rare or cryptic in the Goat Rocks area basalts and basaltic andesites. Perhaps the temperature contrast that these magmas experienced (10-30 °C is proposed for skeletal olivine textures; Donaldson, 1976, in Tamura et al., 2000) was more severe than at Mount St. Helens, causing the basalts to rapidly crystallize disequilibrium compositions rather than more slowly re-equilibrate.

Spinel compositions

Spinel was analyzed in four samples that span in age from ~3.5 Ma to ~200 ka: from oldest to youngest, GR17-17 from Miriam Creek volcano, GR16-07 from Devils Washbasin volcano, GR17-14 from lower Hogback Mountain, and GR17-24 from Lakeview Mountain (Figure 3.9). These samples were previously analyzed for their olivine compositions, and in each, spinel was observed as inclusions within the olivine (Figure 3.7a,b,c,d,j). The three older samples are basalts, and the sample from Lakeview Mountain is basaltic andesite. Certainly in the future more spinel-bearing basalts from this area could be analyzed (GR17-62, a Walupt Lake basalt, also contains spinel in lesser abundance.) These preliminary results give some insight into mantle melt sources and evolution processes, to complement results from olivine and bulk rock compositions. Compositional data are included in Appendix X and shown in Figure 3.9.

In general, the magnesium content of the spinels varies widely, from ~15 wt% MgO and Mg# 0.66 (Mg# = Mg/(Mg + Fe^{2+}); see Methods, p.140) to ~4 wt% MgO and Mg# 0.20. The most magnesian spinels were found in sample GR16-07, from Devils Washbasin volcano, falling between Mg# 0.66 and Mg# 0.38. A much more restricted range is represented by spinel crystals in GR17-17 (Miriam Creek basalt) from Mg# 0.55 to 0.47. Overlapping this range are the most magnesian spinels from GR17-14 (Lower Hogback Mountain basalt). However, most spinels in that sample are more evolved, extending to Mg# as low as 0.20. Sample GR17-24, from Lakeview Mountain, contains evolved spinels with Mg# 0.30 to 0.20. These spinels are unique in the suite for having the highest TiO_2 (~1.75-2 wt%), FeO (46-59 wt%), and NiO (0.16-0.24 wt%), indicating a more significant titanomagnetite component; ultimately, this evolved basaltic andesite does not appear to have preserved any relict primitive spinels.

In general, the suite of spinel displays a slightly negative correlation between spinel Mg# and Cr#: i.e. as spinel Mg# declines, Cr# increases (Figure 3.9g). Spinel in the Hogback Mountain sample yields a linear array in Mg#-Cr#, overlapping with the Miriam Creek and Lakeview Mountain spinels, that is slightly shallower than the vector defined by Dick and Bullen (1984) for decompression during crystallization (Figure 3.9g). Therefore, decompression during magma ascent plays a stronger role than crystal fractionation in the evolution of these spinel compositions. Most of the spinel analyzed in the Devils Washbasin basalt occupies a parallel trend, but offset at higher Cr#, indicating either a more refractory (less fertile) mantle source where Al is less abundant, or a higher degree of melting (Figure 3.9g). Overall, these Devils Washbasin spinels and the more magnesian/primitive spinels from Hogback Mountain and Miriam Creek are similar in composition to spinels from southern Washington Cascades CAB analyzed by Smith and Leeman (2005; Figure 3.9g). However, the Devils Washbasin sample also contains two resorbed-looking olivine megacrysts that each have spinel with much lower Cr# at high Mg#, overlapping spinel compositions from Mount St. Helens basalts as well as other HFSE-rich basalt and LKOT from the southern Washington Cascades (Figure 3.9g,h; Wanke et al., 2019; Smith and Leeman, 2005).

The concentration of Al was below detection limit for nearly all of these spinels (Appendix X), so the Wan et al. (2008) spinel-olivine thermometer (which relies on Al partitioning between these phases) could not be utilized.

Clinopyroxene compositions

Clinopyroxene was analyzed by electron microprobe in two samples: GR16-07 (Devils Washbasin) and GR17-03 (Upper Hogback Mountain). Their compositions with calculated endmembers are included in Appendix X, and backscatter electron (BSE) images are in Appendix X. Clinopyroxenes in GR16-07 are slightly more calcic, on the border of augite and diopside in composition, while those in GR17-03 are mostly augite. In both samples, the crystals are texturally variable, ranging from euhedral with neat zoning patterns to deeply resorbed or sieved. This suggests entrainment of different populations from mushy cumulate zones, and/or recharge by magmas in which clinopyroxene is not stable. Most of the clinopyroxene crystals in GR16-07 have “hopper” like texture that looks like melt embayments and/or intergrowth with groundmass microlites. This may indicate rapid crystal growth. Commonly the outer rims are brighter in BSE images and more Fe-rich, which perhaps indicates that they were mixed into a more evolved magma. GR16-07 is on the more evolved side of the Devils Washbasin suite, and in the future one could test for equilibrium between the clinopyroxenes and bulk rock. Crystals in GR17-03 commonly have subtle, fine-scale zoning, and non-systematic variations in Al concentration that suggest recharge (changing temperature, not pressure) as the cause. The compositions were not considered in further detail for this study but may complement future work.

Petrologic modelling

Petrologic modelling was employed to evaluate whether the varied compositions of Goat Rocks area mafic magmas were derived from a single mantle source and modified by variable differentiation and assimilation processes, or if unique mantle sources are required. Specific questions that were tested include:

- Did differentiation of the Devils Washbasin parent magma yield compositions that erupted from younger vents?
- Are the two compositional suites of Hogback Mountain genetically related, or were they derived from distinct parent magmas?

In the next sections I discuss the results of various XLFRAC and MCS models that were tested as solutions to these questions. Additional questions, listed below, are worth investigating but were not within the scope of my limited modeling work:

- Is the uniquely alkalic basaltic andesite suite, Qob_2, from a distinct source, or can it be explained by assimilation of a felsic component into one of the more mafic magmas represented in the area?
- Can the Sc- and HREE-enriched Walupt Lake compositions be products of the same parent as other Goat Rocks mafic magmas?

Primitive Devils Washbasin as a parent magma

The most primitive Devils Washbasin sample in my data collection was evaluated as a potential parent for other mafic rocks in the area. The rationale is that this suite was one of the earliest erupted (later it was determined that Miriam Creek basalts are older), and its compositions are among the most primitive (high MgO, Mg#, Ni, and Cr). The most primitive sample of the suite, GRDH-2, was collected and analyzed by Clayton (1983). Only major element concentrations for this sample are available, and unfortunately an equally primitive sample was not found during my field work. Trace element concentrations were estimated by projecting a line through more evolved samples to the MgO concentration of

GRDH-2 (11.0 wt%). The assumed trace element composition of GRDH-2 is included in Appendix X.

Various conditions for fractional crystallization were tested. The FeO/Fe_2O_3 ratio was assigned according to an oxygen fugacity at the quartz-fayalite-magnetite (QFM) buffer, since most arc basalts fall between QFM and a log unit below (Lee et al., 2005), and most Goat Rocks basalts have V/Sc ratios in the range of 6-7, which translates to an fO_2 of ~0.5 log unit below the QFM buffer according to the model of Lee et al. (2005). After assigning this initial FeO/Fe_2O_3 and normalizing to 100% in MELTS (Gualda et al., 2012; Gualda and Ghiorso, 2015), the input composition was entered into MCS where models were run with unconstrained fO_2. (To test the sensitivity of the initial fO_2 constraint, a few models were run with the same conditions except for fO_2 ranging between QFM-1 and QFM+1, and the difference was negligible.) Water was varied between 0.5 and 2 wt%, and pressure between 200 and 800 MPa (approximate depth of the Moho in the Cascades; Lee et al., 2009). All model run conditions are given in Appendix X. Select model runs are illustrated in Figure X.

Overall, the calculations indicate that GRDH-2 is *not* a suitable parent to other mafic magmas in the Goat Rocks area. For the Devils Washbasin suite alone, fractional crystallization (FC) plus recharge with the same parent is the best model, but the increase in K_2O is not suitably replicated and indicates an assimilant not accounted for.

The most significant barrier to GRDH-2 being a parent to the other mafic suites is its high CaO concentration. Regardless of input conditions, all of the MCS models yield a trend toward higher CaO as olivine crystallizes, then a decline as clinopyroxene crystallizes (Figure 3.x). The position (MgO concentration) of this transition from olivine to clinopyroxene crystallization changes with pressure (sooner at greater pressure), but the general trend is the same—nothing can achieve the drop from 11.8 wt% CaO to the ~9 wt% CaO of other basalts at 9-10 wt% MgO. Even a mixing line between GRDH-2 and a hypothetical composition with 0 wt% CaO and MgO would miss the primitive end of that suite. Therefore it is not easy to achieve the lower-CaO range by FC or mixing, and so these other basalts more likely have less calcic parent magmas.

The MCS FC model results also do not satisfactorily replicate the Devils Washbasin suite itself. The peaked trend in CaO-MgO caused by sequential olivine-clinopyroxene crystallization does not match the observed linear decline in CaO (Figure X). A select range of the same input conditions were run via Petrolog, and the results were the same: increasing CaO during olivine-only crystallization, then declining CaO during clinopyroxene-only crystallization. However, due to textural observations I am led to believe that the two phases were co-crystallizing in Devils Washbasin magmas: the samples contain macrocrysts of clinopyroxene and olivine of similar size, in similar proportions among variably evolved samples, and in particular, in one thin section a glomerocryst of both phases is present.

As a simple test, the program XLFRAC was used to calculate the mass-balance of observed phases clinopyroxene, olivine, and plagioclase between endmember GRDH-2 and a more evolved composition (GR20-20). For the clinopyroxene and olivine inputs, representative compositions from microprobe analyses of sample GR16-07 were used. For plagioclase, I tested an anorthite composition from the DHZ reference book (#7 in their Table 38; Howie et al., 1992) as well as both pure anorthite and pure albite (to let the program calculate the ideal plagioclase composition). Results from these input compositions can be found in Table 3.3. The XLFRAC model with anorthite yielded phase proportions of 48% clinopyroxene, 27% olivine, 25% plagioclase. This is very close to the phase proportions I estimated from observing thin sections from this suite: approximately 50% clinopyroxene, 25% olivine, 25% plagioclase. Interestingly, the two-plagioclase model has a better fit (lower ΣR^2), with *addition* of albite and subtraction of anorthite (-5.3%) in addition to the olivine and clinopyroxene fractionation. This suggests that assimilation of a felsic component like albite is important. Therefore several felsic volcanic rock compositions were tested as components in XLFRAC: Devils Horns rhyolite (TP19-08), Tieton Peak dacite (TP19-16), and Tieton Peak andesite (GR20-15).

All of the XLFRAC models with felsic components yield good fits with very low ΣR^2 (0.001-0.003; Table 3.x). These felsic compositions were then tested in MCS as assimilants in the approximate proportions indicated by XLFRAC. Devils Horns rhyolite (TP19-08) was tested as wall rock to be partially melted, but the results of those models do not accurately replicate the trends for several elements. Bulk assimilation via RFC mode (5 “recharge” events with small masses of felsic contaminant) was tested for this and the other felsic compositions. Details are given in Appendix X. These FC + mixing models are a reasonably good fit for some elements; however, they are all too enriched in silica. Notably, clinopyroxene was not calculated as a phenocryst phase for these runs, which does not align with the observed rocks.

The best-fitting MCS model involves recharge of the fractionating GRDH-2 with more GRDH-2—mixing back to the original composition at a suitable tie-point, i.e. 6 wt% MgO. Assuming that MCS accurately predicts the saturation of olivine vs. clinopyroxene during FC mode (i.e. that these phases do not co-crystallize), this model of cycling olivine-cpx-olivine-cpx saturation by recharge could explain the assemblage observed in the rocks.

Still, the recharge model does not yield the observed K_2O enrichment trend, so a potassic but low-silica contaminant must be required. The possible sources and compositions of this contaminant were not further investigated.

Distinct parent magmas for Lower and Upper Hogback Mountain suites

A primitive basalt composition from Lower Hogback Mountain was tested as a possible parent for both the Lower and Upper Hogback Mountain suites. Models of fractional crystallization of sample GR17-19 are good matches for the rest of the Lower Hogback Mountain suite. In XLFRAC, olivine, clinopyroxene, pure anorthite, and pure albite were input as potential mixing components between the most primitive Lower Hogback Mountain composition (GR17-19) and a more evolved composition from that suite (GR20-02). This combination yields a good fit (ΣR^2=0.048) with 7% olivine fractionation, negligible clinopyroxene and anorthite fractionation, and addition of ~1% albite (Table 3.4). The lack of clinopyroxene and anorthite fractionation agree with the mineralogy of the samples—most contain only olivine phenocrysts, rarely also clinopyroxene, and plagioclase only as groundmass microlites. The addition of albite in the XLFRAC model suggests minor assimilation of a felsic component. FC models in MCS yield only olivine crystallization for the MgO range represented by the Lower Hogback Mountain suite, and the FC paths align well with observed compositions. Felsic assimilants (via wall rock partial melting or mixing/RFC) were not tested in MCS given the close fit of FC models, but this could be further evaluated in future work. The FC models are slightly shallow in K_2O and P_2O_5 compared to the trend of real samples, so there is room for improvement (Figure X).

As discussed above, primitive Devils Washbasin basalt was also evaluated as a parent magma for the Lower Hogback Mountain suite, but it does not yield a good fit. An XLFRAC mixing model between GRDH-2 and GR17-19 has a reasonably low ΣR^2 of 0.157, but requires significant clinopyroxene and anorthite removal with little olivine crystallization (Table 3.4), which does not match the mineralogy observed in the rocks. The FC models of GRDH-2 in MCS do not trend in the appropriate direction, and assimilation of a very low-CaO composition would be required—nothing in my sample collection appears suitable. The possibility of a Devils Washbasin type magma being modified by an unidentified assimilant could be reevaluated in the future, but currently the most sensible model is fractional crystallization of a distinct parent magma like GR17-19, possibly with a minor felsic contaminant.

Fractional crystallization of primitive Lower Hogback Mountain magma is not a suitable means to achieve Upper Hogback Mountain compositions. An XLFRAC model with GR17-19 and GR17-05 (one of the least evolved Upper Hogback compositions) as endmembers has a much poorer fit than that for the Lower Hogback Mountain endmembers (Table 3.4). The FC models for GR17-19 described above are suitable for some elements, but not all—the liquid lines of descent are much too high in K_2O and P_2O_5 (Figure X). To replicate that trend, a contaminant depleted in those elements and enriched in silica would need to be involved. Recall also that samples from Upper Hogback Mountain are distinct in $^{87}Sr/^{86}Sr$ from those of Lower Hogback Mountain, so such a contaminant would need to have lower $^{87}Sr/^{86}Sr$.

Given similar compositional traits, primitive Miriam Creek basalt was evaluated as a potential parent for Upper Hogback Mountain. An XLFRAC model with GR17-17 as a primitive endmember has a poor fit (ΣR^2=0.953), but Clayton's (1983) sample HMMLC-6 (more calcic, lower FeO) yields a better fit (ΣR^2=0.112; Table 3.4). Still, this model requires significant addition of plagioclase (roughly equal proportions anorthite and albite, so ~andesine), meaning that assimilation of an intermediate to felsic component would be necessary. The possibility of Miriam Creek basalt as a parent alongside assimilation of a felsic component was not further evaluated but is worth future investigation. According to XLFRAC, fractional crystallization of the observed olivine-clinopyroxene-plagioclase assemblage does not well explain the range within the Upper Hogback Mountain suite (i.e. using less evolved and more evolved Upper Hogback Mountain compositions as endmembers); instead the model calculates addition of clinopyroxene and albite, but the fit could be improved (ΣR^2=0.271; Table 3.4). This result, and the steeper SiO_2-MgO trend than the FC models of Devils Washbasin or Upper Hogback Mountain, point to the involvement of an intermediate or felsic contaminant, but more testing is needed.

DISCUSSION

New insights into eruptive sources

New bulk composition data from this study may provide clues to the origin of lavas with unidentified vents. The sources of units Qob_2 and Qba are not yet confirmed, but new samples from the Hogback Mountain area and Lakeview Mountain are similar in composition, respectively, suggesting a possible link. In the future, additional field work, geochronology, and/or geochemical analysis are recommended to test these ideas.

Hogback Mountain a likely source for Qob_2 (and Qob_1)?

As discussed above and by Gusey et al. (2018), the compositions of the ~1.3-Ma Qob_2 lava flows are unique from other basaltic andesites in the Goat Rocks area. They are particularly enriched in K_2O and many of the high field strength elements (HFSE). Their outcrop locations and field relations indicate a source somewhere in the Goat Rocks or Hogback Mountain area (see Gusey et al., 2018, for details), but no previously determined compositions from these areas were a good match. However, the newly analyzed dike or plug near Miriam Lake (GR17-15) shares many similar qualities. It is slightly more silicic than the Qob_2 range but is similarly K_2O- and HFSE-enriched. In TiO_2, P_2O_5, Sr, and Ba, however, it is more like the basaltic andesites of Upper Hogback Mountain. So, the dike is not a smoking gun as the source of Qob_2, but the possibility remains open given its transitional composition between Qob_2 and more “typical” Hogback Mountain. An argon age on the dike would provide a critical piece of evidence to support or disprove this idea.

In addition, as noted by Gusey et al. (2018) and in results here, the composition of the Qob_1 lava flow is very much like the lava flows of Upper Hogback Mountain (though on the more magnesian end). Based on this compositional similarity alone, the Hogback Mountain area seems a likely eruptive source for that lava flow. However, near-vent or shallow intrusive material with the same composition has not yet been found. It may have been eroded away, or it may be hidden beneath the younger Hogback Mountain pile.

Qba a distal lava flow from Lakeview Mountain?

A sample from the young basaltic andesite unit Qba of Swanson (1996b) is included with the Coleman Weedpatch basalts on diagrams for simplicity, but its composition is actually distinct from that unit and the Walupt Lake basalt—more silicic with the phenocryst assemblage olivine-clinopyroxene-plagioclase. Swanson (1996b) interprets it as older than Walupt Lake volcano and some or all of the Coleman Weedpatch lavas. The mineral assemblage and composition are similar to the basaltic andesite that I sampled from Lakeview Mountain, which was dated at 194 ± 12 ka, older than Walupt Lake at 65 ± 28 (see Chapter 2). So, there is a strong possibility that Qba is a distal lava flow from Lakeview Mountain rather than a more proximal vent buried beneath Walupt Lake volcano and the Coleman Weedpatch lavas. More work in that region is required to clarify the unit contacts there.

Magmatic sources and modification processes

The variation in bulk major and trace elements and isotopic compositions of Goat Rocks area basalts, and preliminary petrologic modeling results described above, point to distinct mantle melt sources in close proximity that are tapped recurrently over time and even at the same volcano (Hogback Mountain). Below I consider the implications of various compositional indicators for the two main compositional groups and particularly unique suites.

Devils Washbasin – unique mantle source and higher degree of partial melting?

The Devils Washbasin basalts stand out from the rest with their high CaO content. Elevated CaO could indicate a more fertile (cpx-bearing, Ca-rich) mantle source—mineralogically distinct from but isotopically similar to the other Group 1 mantle source(s). Alternatively, a clinopyroxene or amphibole component could have been added to that mantle source by metasomatic enrichment (as suggested by McDonough and Frey, 1989, for a less common subset of peridotites with both enriched CaO and LREE). Concentrations of trace elements are generally among the lowest in the Goat Rocks suite, especially HFSE and HREE. This points to either a high degree of partial melting, or previous depletion of that mantle source by high-degree or numerous partial melting events. The high spinel Cr# (~0.5-0.65, Figure 3.9g) of the majority of spinels in sample GR16-07 supports that interpretation. Outlier low-Cr# spinels in that sample could represent relict olivine scavenged from smaller-degree melt pockets along the ascent pathway.

While Devils Washbasin samples do not have the highest concentrations of fluid-mobile elements compared to other Goat Rocks area basalts, they do have the highest Ba/Nb and Pb/Ce ratios, which suggest a significant fluid/subduction component. La/Sm ratios of Devils Washbasin basalts are as high as those of Lower Hogback Mountain (Figure 3.6b), and LREE enrichment is also linked to fluid/melt contribution to the mantle (McDonough and Frey, 1989). Significant fluid addition resulting in a higher degree of flux melting could explain the HFSE-depleted and LILE/LREE-enriched compositions of these basalts. Whether this fluid/subduction component is ancient or modern cannot be resolved with the present data, but it seems plausible that there was a direct cause and effect between fluid delivery and high-degree flux melting. Alternatively, perhaps a diapir of metasomatized mantle was melted at relatively high degree due to decompression.

Since the HREE are only slightly depleted in Devils Washbasin basalts (Figure 3.4), their higher LREE/HREE are unlikely to be caused by deep melting from a garnet-bearing source. More likely, HREE were depleted in the source by previous melting or were diluted by a higher degree of partial melting, and LREE were enriched by subduction fluids.

Lower Hogback Mountain: high subduction component, smaller degree melt?

The isotopic compositions of Lower Hogback Mountain basalts are very similar to those of Devils Washbasin, and trace element patterns on spider diagrams (Figure 3.5, Figure 3.4) are parallel, with similar trace element ratios such as La/Sm, La/Yb, and Ba/Nb not nearly as elevated but among the highest of the Goat Rocks suite (Figure 3.6). Considering their much lower CaO, like the other Goat Rocks basalts, I propose that they are from a similar melt source as Devils Washbasin that was less fertile or lacked clinopyroxene or amphibole addition by metasomatism. A similar subduction component is suggested by the elevated LILE and LREE, as well as the higher $^{87}Sr/^{86}Sr$. In addition, these basalts are among the most enriched in HFSE (e.g. Nb, Th, and especially Zr; Figure 3.3), which suggests that either their mantle source is more enriched in these elements, or it underwent a smaller degree of partial melting (or perhaps both).

Group 2 mantle source—less modified by subduction

Basalts and basaltic andesites of Miriam Creek, Qob_1, Upper Hogback Mountain, Coleman Weedpatch, and Walupt Lake are alike in having much lower LREE/MREE (or LREE/HREE) ratios and less enrichment in LILE such as Ba—an indication that their source was less modified by subduction fluids. The Miriam Creek suite is generally more depleted in trace elements than the rest, which may indicate a higher degree of melting, like the Devils Washbasin basalts. However, the Cr# of spinel from Miriam Creek basalt is like that of some Lower Hogback Mountain spinel, which possibly contradicts this (Figure 3.9g). No spinel were analyzed in other Group 2 lavas for comparison. It could be that the Miriam Creek mantle source was simply more depleted by prior melting events.

The Walupt Lake basalts stand out from this group as being particularly low in SiO_2 and enriched in Sc and HREE. On isotope and trace element plots it is usually among the closest of the Goat Rocks suite to the Adams-Simcoe IPB array (Figure 3.5, Figure 3.6). There are some Mount Adams basalts that are more magnesian than the Walupt Lake basalt but share similar characteristics such as low SiO_2 and elevated TiO_2. An invented mixture (50:50) of samples MA-696 (tholeiitic IPB) and MA-953 (CAB) from Mullen et al. (2017) was tested as a parent magma for an MCS FC run, and the results are remarkably close in major element compositions (Appendix X). The trace elements have not been evaluated, but this may indicate that there are transitional mantle domains or mixing of melts between the Adams-Simcoe IPB source and CAB mantle sources. It seems only reasonable that magmas from diverse sources should interact on their pathways to the surface, and that there is a continuum of compositions between endmembers as suggested by Bacon et al. (1997).

Implications for regional mantle composition and structure

Overall, the Goat Rocks area basalts are similar in composition to those from Mount St. Helens and the CABs from Mount Adams. On several isotopic and/or trace element diagrams, the trio of Goat Rocks, Mount St. Helens, and Mount Adams CAB span the range between the Adams-Simcoe IPB array and the High Cascades CAB-HAOT array (particularly in Ba vs. Nb, Mg# vs. La/Yb_N, and Ba/Nb vs. $^{87}Sr/^{86}Sr$, Figure 3.5g,h, Figure 3.6c). As suggested above to explain the Walupt Lake compositions in particular, this transitional array between the IPBs and other High Cascades compositions suggests a continuum between the Adams-Simcoe IPB source and more "typical" High Cascades mantle to the north and south, perhaps by physical mixing at its boundary, or a gradient of upwelling asthenospheric mantle through a slab gap in greater proportion proximal to Mount Adams and Simcoe and in smaller quantities further away. The distinctions of the local CABs and HAOTs from other compositions further north and south along the High Cascades support the classification of the southern Washington Cascades as a distinct "segment" with unique qualities (as in Pitcher and Kent, 2019).

While the variability in the Goat Rocks area is far less extreme than at other centers, where a combination of CAB or HAOT or IPB may erupt, the different CAB types represented at Goat Rocks indicate a sub-arc mantle that is heterogeneously modified by subduction processes. Since both Group 1 and Group 2 magmas are represented through time and space, including at a single center (Hogback Mountain), this suggests that the two mantle domains are either stratified in layers or intermixed at a relatively fine scale—perhaps in a web-like network of fluid ascent pathways.

CONCLUSIONS

Basalts and basaltic andesites erupted on the periphery of the Goat Rocks volcanic complex throughout its lifespan, from 3.6 Ma to 65 ka. The vents include Miriam Creek volcano, Devils Washbasin volcano, Hogback Mountain, Lakeview Mountain, Walupt Lake volcano, and vents between Coleman Weedpatch-Two Lakes. Based on compositional similarities, it is plausible that the Qob_1 basalt lava flow and Qob_2 basaltic andesite lava flows were also erupted from the Hogback Mountain area.

Each mafic volcano has a distinctive compositional personality, but all compositions classify as calcalkaline, with depletion in high field strength elements (HFSE) and enrichment in fluid-mobile large-ion lithophile elements (LILE) and light rare earth elements (LREE). Trace element and Sr, Nd, Hf, and Pb isotope characteristics define two compositional groups. Group 1 includes the basalts of Devils Washbasin and Lower Hogback Mountain and the basaltic andesite of Lakeview Mountain. These compositions are enriched in LILE (e.g. Ba/Nb) and LREE, and they have higher $^{87}Sr/^{86}Sr$ ratios. Group 2 includes compositions from Miriam Creek volcano, Qob_1, Upper Hogback Mountain, Walupt Lake volcano, and the Coleman Weedpatch vents. These are less enriched in LILE and LREE and lower in $^{87}Sr/^{86}Sr$. These differences are attributed to mantle sources that are variably modified by subduction processes. The different mantle domains must occur together over a relatively wide spatial scale—either in a vertically stratified manner, or as a fine network of fluid transport pathways through less metasomatized mantle—because both compositional groups are represented across the region and even at the same volcano (Hogback Mountain).

As a group, the Goat Rocks CABs, basalts of Mount St. Helens, and Mount Adams CABs share similar trace element and isotopic characteristics that make them intermediary between the rest of the High Cascades and the Mount Adams IPB-Simcoe IPB compositional array. This suggests a diffuse bleed of the IPB melt source (perhaps asthenospheric mantle through a slab gap, as Mullen et al., 2017, propose) more broadly across the southern Washington Cascades, and solidifies its distinction as a unique segment of the arc (as in Pitcher and Kent, 2019).

Importantly, the recurrence of Group 1 and Group 2 magmas across space and time in the Goat Rocks area means that the compositional evolution of the andesitic to dacitic Goat Rocks volcanic complex is not likely caused by a change in mantle input.

TABLES

Table 3.1. Sr, Nd, Hf, and Pb isotopic ratios for Goat Rocks area mafic magmas.

Sample ID	Analysis ID	Rock class.	Primitive?*	Latitude	Longitude	Unit	Age (ka) ±2σ	Age bin (Ma)	$^{87}Sr/^{86}Sr$ ± 2 SE	$^{143}Nd/^{144}Nd$ ± 2 SE	$^{176}Hf/^{177}Hf$ ± 2 SE	$^{208}Pb/^{204}Pb$ ± 2 SE	$^{207}Pb/^{204}Pb$ ± 2 SE	$^{206}Pb/^{204}Pb$ ± 2 SE
Late Pleistocene mafic volcanoes														
GR17-57	GR17-57 wt avg	Bas And	no	46.3964	-121.4795	Qbcw (Qbt)		0.0-0.2	0.703403 0.000010	0.512953 0.000007	0.282973 0.000004	38.4723 0.0018	15.5721 0.0007	18.8457 0.0009
GR17-62	GR17-62 wt avg	Basalt	no	46.4139	-121.4839	Qbw	65 ± 28	0.0-0.2	0.703251 0.000007	0.512965 0.000006	0.283023 0.000003	38.6186 0.0022	15.5879 0.0008	18.9949 0.0009
GR17-24	GR17-24	Bas And	no	46.3901	-121.4012	Qbal	194 ± 12	0.0-0.2	0.703645 0.000007	0.512922 0.000007	0.282980 0.000006	38.6450 0.0029	15.5952 0.0011	18.9621 0.0012
Hogback Mountain														
GR17-05	GR17-05 wt avg	Basalt	no	46.6000	-121.4061	Qbh2	940 ± 260	0.8-1.0	0.703270 0.000005	0.512966 0.000004	0.282986 0.000003	38.5707 0.0012	15.5851 0.0004	18.9388 0.0005
GR17-14	GR17-14 wt avg	Basalt	yes	46.5996	-121.3995	Qbh1		1.0-1.5	0.703587 0.000009	0.512955 0.000005	0.283080 0.000009	38.5634 0.0020	15.5840 0.0007	18.9282 0.0008
GR17-19	GR17-19	Basalt	yes	46.6052	-121.3986	Qbh1		1.0-1.5	0.703592 0.000007	0.512943 0.000006	0.283018 0.000008	38.5683 0.0021	15.5843 0.0008	18.9344 0.0010
Qob_1 and Qob_2														
16423	16423	Basalt	yes			Qob1	1380 ± 250	1.0-1.5	0.703088 0.000007	0.512975 0.000007	0.283044 0.000004	38.5531 0.0018	15.5798 0.0006	18.9307 0.0008
GR16-06	GR16-06	Bas And	no	46.6253	-121.1614	Qob2	1310 ± 40	1.0-1.5	0.703226 0.000009	0.512965 0.000008	0.283045 0.000005	38.5687 0.0021	15.5841 0.0009	18.9455 0.0010
GR16-06	GR16-06 re	Bas And	no	46.6253	-121.1614	Qob2	1310 ± 40	1.0-1.5	0.703226 0.000009	0.512965 0.000008	0.283045 0.000005	38.5687 0.0021	15.5841 0.0009	18.9455 0.0010
Devils Washbasin														
GR16-07	GR16-07 wt avg	Basalt	no	46.5436	-121.3331	Tpb	2680 ± 10	2.5-3.0	0.703559 0.000007	0.512940 0.000005	0.282971 0.000003	38.6320 0.0013	15.5944 0.0005	18.9502 0.0005
GR20-13	GR20-13	Basalt	yes	46.5203	-121.3688	Tpb	2890 ± 80	2.5-3.0	0.703558 0.000009	0.512942 0.000007	0.283068 0.000004	38.6248 0.0024	15.5923 0.0009	18.9488 0.0011
GR20-13	GR20-13 re	Basalt	yes	46.5203	-121.3688	Tpb	2890 ± 80	2.5-3.0	0.703558 0.000009	0.512944 0.000008	0.283069 0.000005	38.6271 0.0021	15.5930 0.0007	18.9497 0.0009
Miriam Creek volcano														
GR19-33	GR19-33	Basalt	no	46.6044	-121.3825	Tbm	3557 ± 26	3.5-4.0	0.703462 0.000009	0.512940 0.000006	0.283034 0.000005	38.6296 0.0020	15.5915 0.0007	18.9886 0.0008

Table 3.2. Comparison of measured olivine to calculated equilibrium Fo.

Sample	Volcano/unit	Whole-rock Mg#	Calculated equilibrium olivine Fo	Measured olivine Fo range	Within range of equilibrium?
GR17-58	Coleman Weedpatch	63	85	88	no
GR17-62	Walupt Lake	58	83	83-52	yes
GR17-24	Lakeview Mountain	60	84	79-73	no
GR17-03 exterior	Upper Hogback Mountain	61	84	94-96; 82-74	no; yes
GR17-03 interior	Upper Hogback Mountain	58	83	82-66	yes
GR17-19	Lower Hogback Mountain	69	89	84-78	no
GR17-14	Lower Hogback Mountain	68	88	87-63	yes
GR16-07	Devils Washbasin	67	88	86-69	yes
GR17-17	Miriam Creek	65	86	85-75	yes

Note: Sample GR17-03 is a small block sample that was not analyzed for major and trace element compositions. Bulk rock Mg# of the two domains represented thin section are estimated from analyses of similar rock in outcrop, GR17-02 (vesicular flow exterior) and GR17-01 (dense flow interior). Equilibrium Fo is calculated assuming $K_{D,Fe2+-Mg}$ = $(FeO/MgO)_{ol}/(FeO/MgO)_{liq}$ = 0.3 (after Roeder and Emslie, 1970).

Table 3.3. Results of least-squares mixing models for the Devils Washbasin suite.

Table 3.3. Results of least-squares mixing models for the Devils Washbasin suite.

	DW frac w/ anorthite	**DW frac, 2 plagioclase**	**DW frac + DH rhyolite**	**DW frac + TP dacite**	**DW frac + TP andesite**
Mafic endmember	GRDH-2	GRDH-2	GRDH-2	GRDH-2	GRDH-2
Evolved endmember	GR20-20	GR20-20	GR20-20	GR20-20	GR20-20
Component 1	DW cpx	DW cpx	DW cpx	DW cpx	DW cpx
% added/removed	-17.1	-14.7	-16.3	-15.3	-15.2
Component 2	DW olivine	DW olivine	DW olivine	DW olivine	DW olivine
% added/removed	-9.5	-8.5	-7.6	-7.6	-7.6
Component 3	natural anorthite	pure anorthite	natural anorthite	natural anorthite	natural anorthite
% added/removed	-8.8	-5.3	-3.7	-3.4	-2.9
Component 4	N/A	pure albite	TP19-08	TP19-16	GR20-15
% added/removed	N/A	4.8	5.3	11.08	19
ΣR^2	0.94	0.27	0.003	0.003	0.001

Table 3.4. Results of least-squares mixing models for the Hogback Mountain suite.

Table 3.4. Results of least-squares mixing models for the Hogback Mountain suite.

	DW to LHM	**LHM primitive to evolved**	**Primitive LHM to UHM**	**LHM to UHM + MC dacite**	**MC primitive-1 to UHM**	**MC primitive-2 to UHM**	**MC prim-2 to UHM + MC dacite**	**UHM less to more evolved**
Mafic endmember	GRDH-2	GR17-19	GR17-19	GR17-19	GR17-17	HMMLC-6	HMMLC-6	GR17-05
Evolved endmember	GR17-19	GR20-02	GR17-05	GR17-05	GR17-05	GR17-05	GR17-05	GR17-01
Component 1	olivine	olivine	olivine	olivine	olivine	olivine	olivine	olivine
% added/removed	-1.5	-7	-6.5	-6.1	-6	-3.2	-2.9	-2.9
Component 2	cpx	cpx	cpx	cpx	cpx	cpx	cpx	cpx
% added/removed	-18	-0.1	-5.8	-5.9	2.7	-7.4	-8.1	4
Component 3	pure anorthite	pure anorthite	pure anorthite	natural anorthite	pure anorthite	pure anorthite	natural anorthite	pure anorthite
% added/removed	-7.4	-0.18	0.4	0.5	6.4	5.6	5.1	-3.8
Component 4	pure albite	pure albite	pure albite	GR19-35	pure albite	pure albite	GR19-35	pure albite
% added/removed	-0.2	1.07	1.4	3.4	2.5	5.9	8.4	5.7
ΣR^2	0.157	0.048	0.434	0.318	0.953	0.112	0.137	0.271

Notes: DW=Devils Washbasin, LHM=Lower Hogback Mountain, UHM=Upper Hogback Mountain, MC=Miriam Creek.

FIGURES

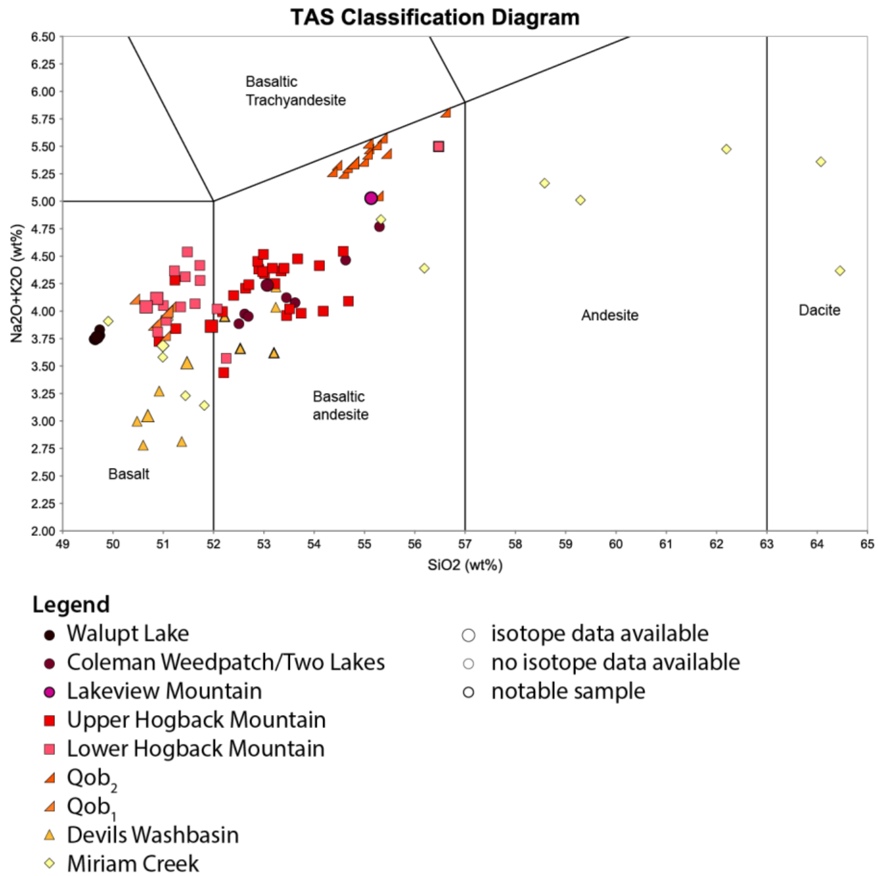

Figure 3.1. Total-alkali-silica (TAS) diagram of Goat Rocks area mafic volcanoes. Includes samples from this dissertation as well as Clayton (1983), Swanson (1996a), and Gusey et al. (2018). The legend also applies to Figures 3.2-3.6. Different symbol shapes indicate age relative to the andesitic Goat Rocks volcanic complex: diamond—pre-Goat Rocks, isosceles triangle—Tieton Peak stage, right triangle—Bear Creek Mountain stage, square—Lake Creek stage, and circle—Old Snowy Mountain stage (and slightly younger). A handful of samples are outlined in bold in this and other composition figures for more easy identification: samples from a ridge-capping lava flow west of Devils Washbasin with composition unique from the rest of the suite, sample GR17-24 from Lakeview Mountain, and sample GR17-15, a dike near Miriam Creek of uncertain age (here tentatively included with Lower Hogback Mountain).

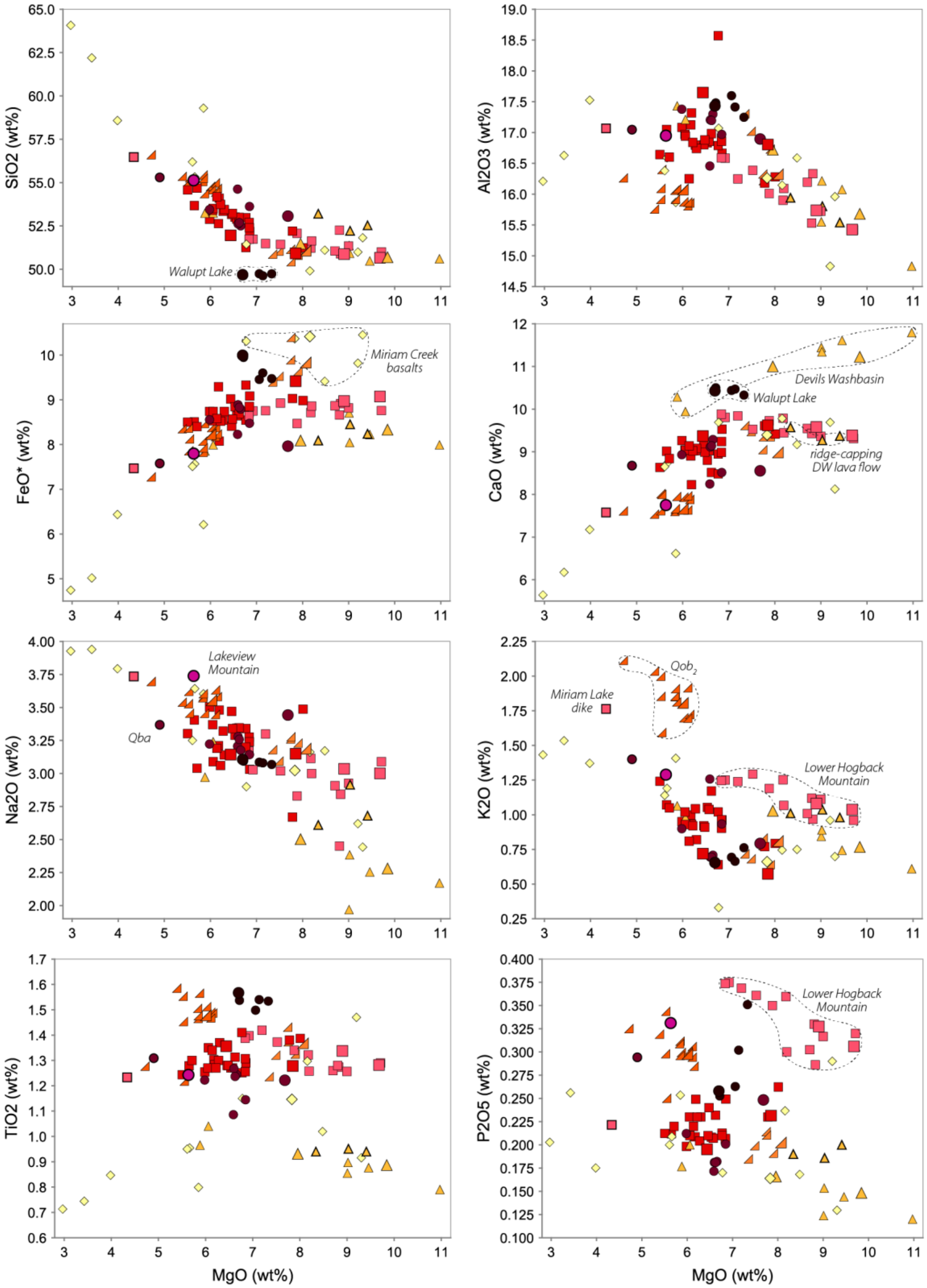

Figure 3.2. Major element variation diagrams.
Element oxides are normalized to 100% without volatiles. Dashed fields in some plots emphasize distinct compositional suites. Legend is as in figure 3.1.

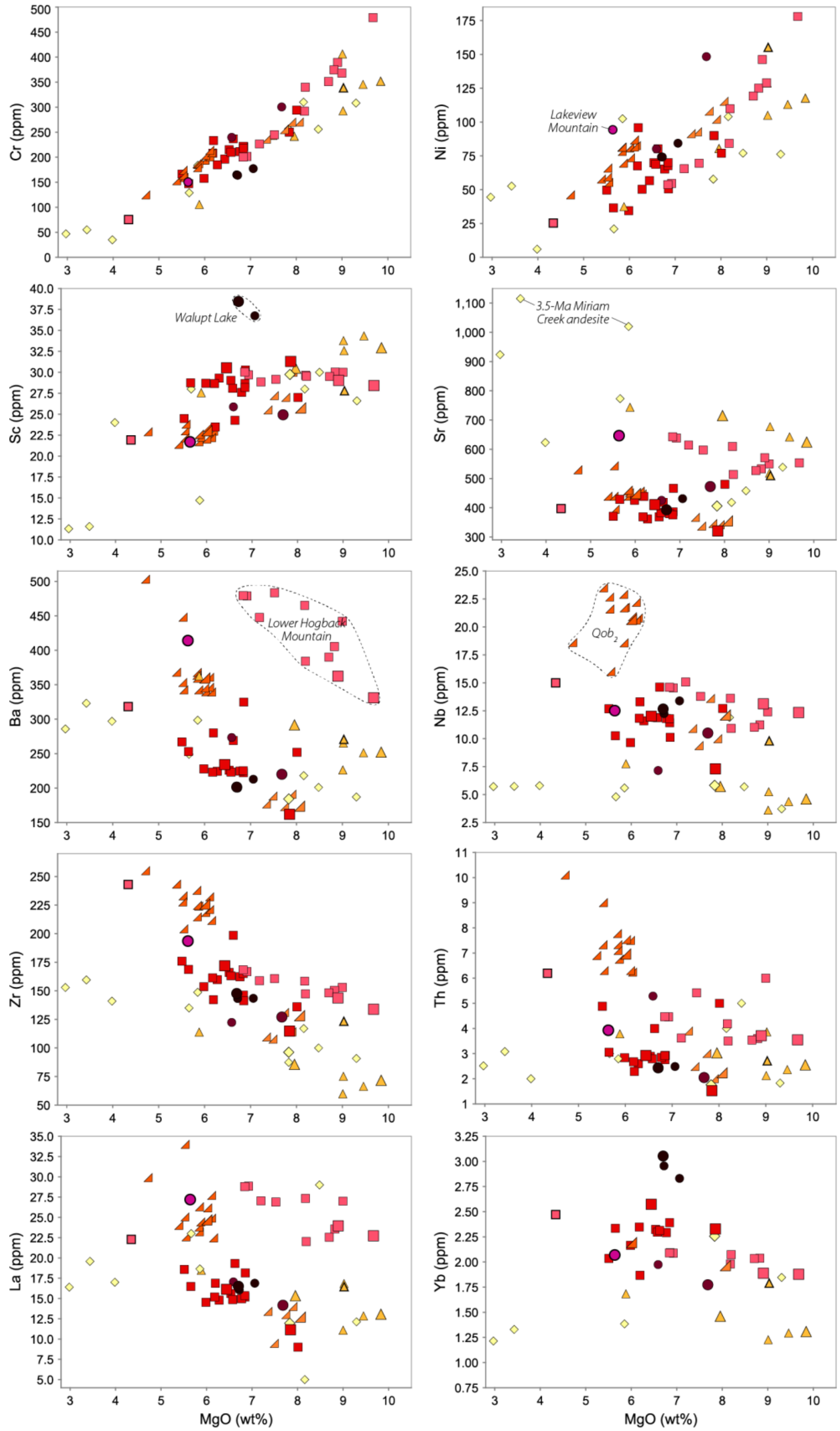

Figure 3.3. Trace element variation diagrams. Legend is as in Figure 3.1.

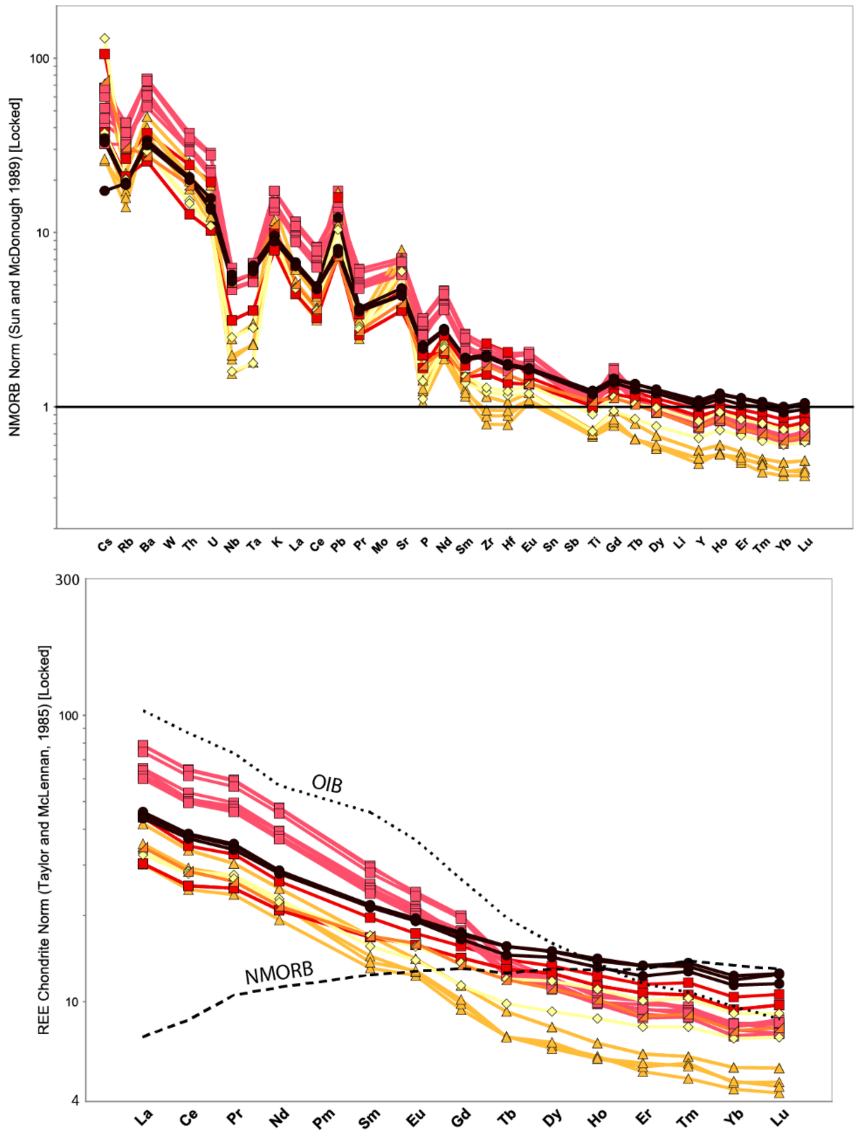

Figure 3.4. MORB-normalized spider diagram and chondrite-normalized REE diagram. Only samples from this study, with ICP-MS trace element concentrations, are shown. a) Compositions normalized to NMORB of Sun and McDonough (1989). b) Rare earth elements (REE) normalized to chondrite of Taylor and McLennan (1985). REE profiles of typical NMORB and OIB compositions (Sun and McDonough, 1989) are shown with dashed lines for reference.

Figure 3.5. Isotopic and trace element ratios of Goat Rocks area mafic magmas. Compositions of Group 1 (higher LILE, LREE, and $^{87}Sr/^{86}Sr$) are highlighted with bold outlines and a yellow field where compositional differences can be readily observed. a) $^{143}Nd/^{144}Nd$ vs $^{87}Sr/^{86}Sr$. For comparison I include compositions from Mount St. Helens (Leeman et al., 2018), Mount Adams (Mullen et al., 2017), and Simcoe volcanic field (Mullen et al., 2017). b) $^{208}Pb/^{204}Pb$ vs. $^{206}Pb/^{204}Pb$. Samples from Mount St. Helens, Mount Adams, and Simcoe are included as in (a), and samples from other volcanic centers of the High Cascades are also included with the regression lines for the High Cascades Array and Adams-Simcoe IPB Array ("Adams Array") of Mullen et al. (2017). A regression line is included for Goat Rocks-Mount St. Helens-Mount Adams IPB as well (fuchsia). Fields for north Cascadia sediment, Explorer MORB, and vectors toward Juan de Fuca (JdF) MORB and HIMU are taken from Mullen et al. (2017). c) $^{176}Hf/^{177}Hf$ vs $^{143}Nd/^{144}Nd$. For simplicity, High Cascades samples (overlapping ranges for HAOT and CAB) are shown with a blue field. Note the broad range in $^{176}Hf/^{177}Hf$ with little variation in $^{143}Nd/^{144}Nd$. d) $^{208}Pb/^{204}Pb$ vs. Hf/Pb. Samples from Group 1 have lower Hf/Pb due to higher Pb concentrations and are more like High Cascades CABs. Group 2 samples extend to higher Hf/Pb values, overlapping the field of High Cascades HAOTs. e) 1/Sr vs. $^{87}Sr/^{86}Sr$. The higher Sr concentration (lower $^{87}Sr/^{86}Sr$) in Group 1 samples is correlated with their higher $^{87}Sr/^{86}Sr$ ratios. Note the apparent array between High Cascades CAB and the Adams-Simcoe IPB array. f) Zr/Nb vs. La/Yb normalized to C1 chondrite of Taylor and McLennan (1985). Note that x-axis is on a logarithmic scale. Note that all analyses with Mg# > 60 are shown, not only those with isotopic data. Mg# is calculated as Mg/(Mg+Fe^{2+})*100, in atomic proportions and where Fe^{2+}=0.85*Fe^T, approximating fO_2 at the QFM buffer. Compositions are mostly within the field of High Cascades CAB. g) Ba (ppm) vs. Nb (ppm). All analyses with Mg# > 60 are shown. Slope indicates Ba/Nb ratio. Note that Group 1 samples mostly overlap the High Cascades CAB field, while many Group 2 samples fall between that and the Adams-Simcoe IPB array. h) Mg# vs. La/Yb_N. All samples with trace element data are shown, including less primitive samples with Mg# < 60. Note how compositions span between High Cascades CAB and the Adams-Simcoe IPB array.

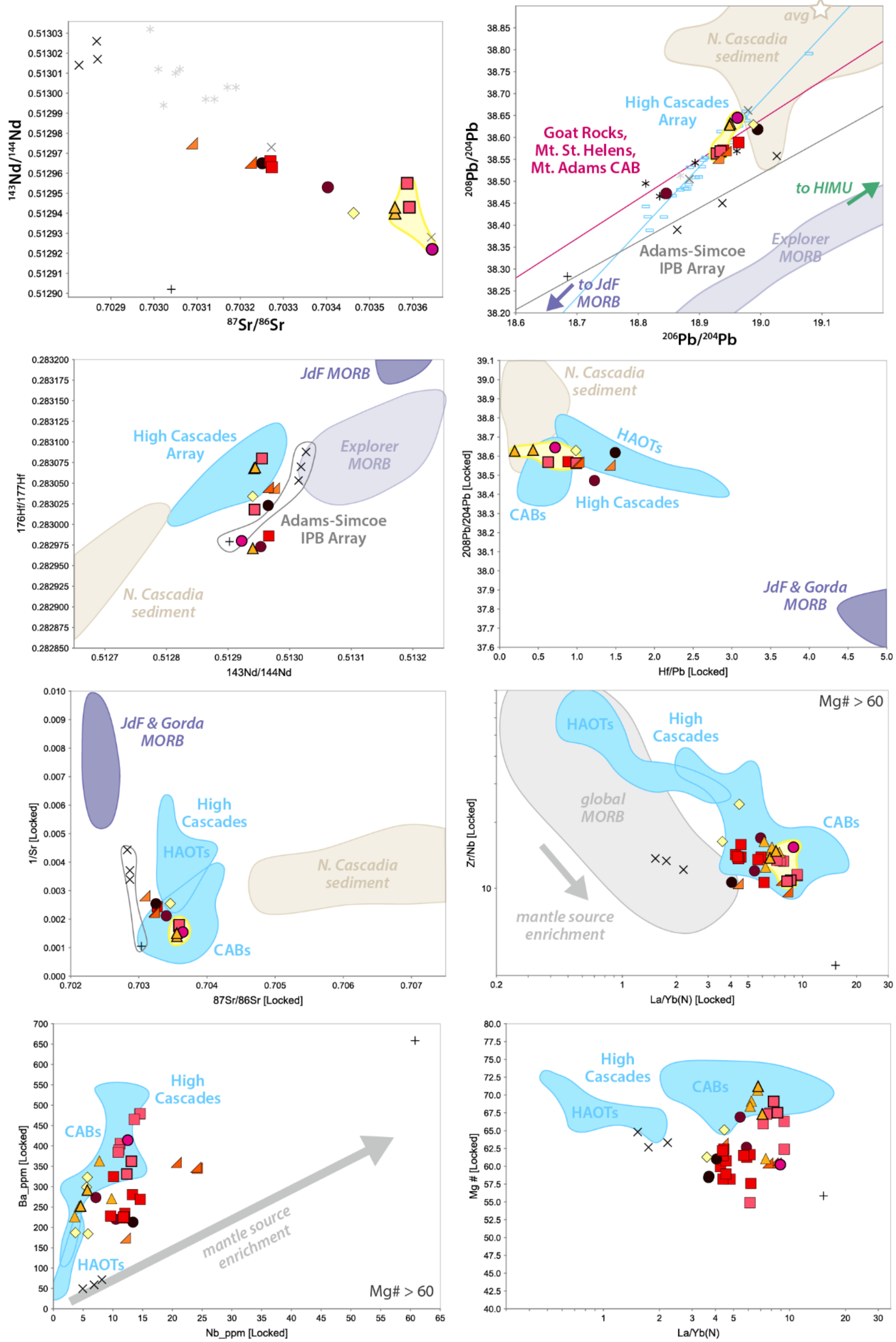

87Sr/86Sr
143Nd/144Nd
206Pb/204Pb
208Pb/204Pb
High Cascades Array
Goat Rocks, Mt. St. Helens, Mt. Adams CAB
N. Cascadia sediment
avg
to HIMU
Explorer MORB
Adams-Simcoe IPB Array
to JdF MORB
176Hf/177Hf
JdF MORB
208Pb/204Pb [Locked]
Hf/Pb [Locked]
HAOTs
High Cascades
CABs
JdF & Gorda MORB
1/Sr [Locked]
87Sr/86Sr [Locked]
Zr/Nb [Locked]
La/Yb(N) [Locked]
Mg# > 60
global MORB
mantle source enrichment
Ba_ppm [Locked]
Nb_ppm [Locked]
Mg # [Locked]
La/Yb(N)

Figure 3.5.

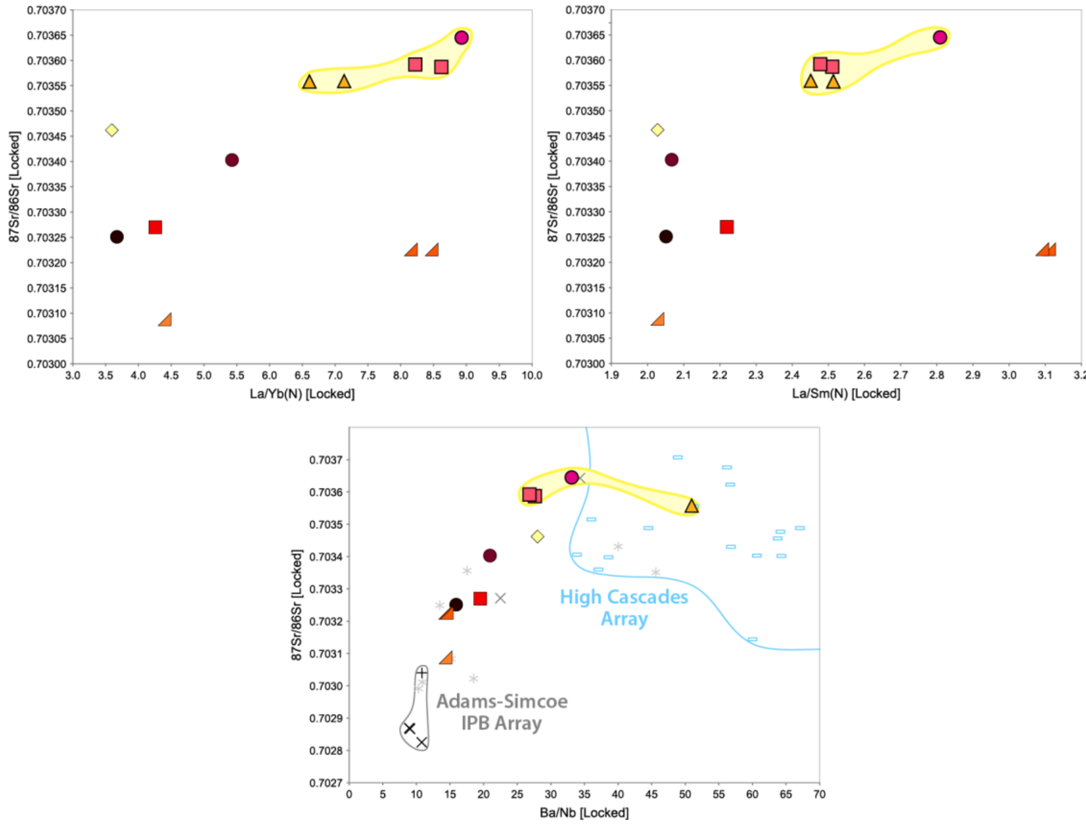

Figure 3.6. $^{87}Sr/^{86}Sr$ and trace element indicators of subduction.
a) $^{87}Sr/^{86}Sr$ vs La/Yb$_N$. Except for samples of Qob$_2$ (basaltic andesite, higher La/Yb corresponds tith higher $^{87}Sr/^{86}Sr$. b) $^{87}Sr/^{86}Sr$ vs. La/Sm$_N$. Samples with higher $^{87}Sr/^{86}Sr$ have significantly higher La/Sm. Qob$_2$ is an outlier with enriched LREE but not high $^{87}Sr/^{86}Sr$. c) Higher $^{87}Sr/^{86}Sr$ correlates with higher Ba/Nb. Note the array formed by Goat Rocks mafic magmas, Mount St. Helens basalts, and Mount Adams CABs between the High Cascades array and the Adams-Simcoe IPB array.

Figure 3.7. Representative backscatter electron images of olivine analyzed by electron microprobe.
Variations in grayscale between images/samples is more likely a result of brightness and contrast settings rather than compositional differences. Changes in brightness within individual images indicate compositional differences. Very bright inclusions in olivine are chromian spinel.

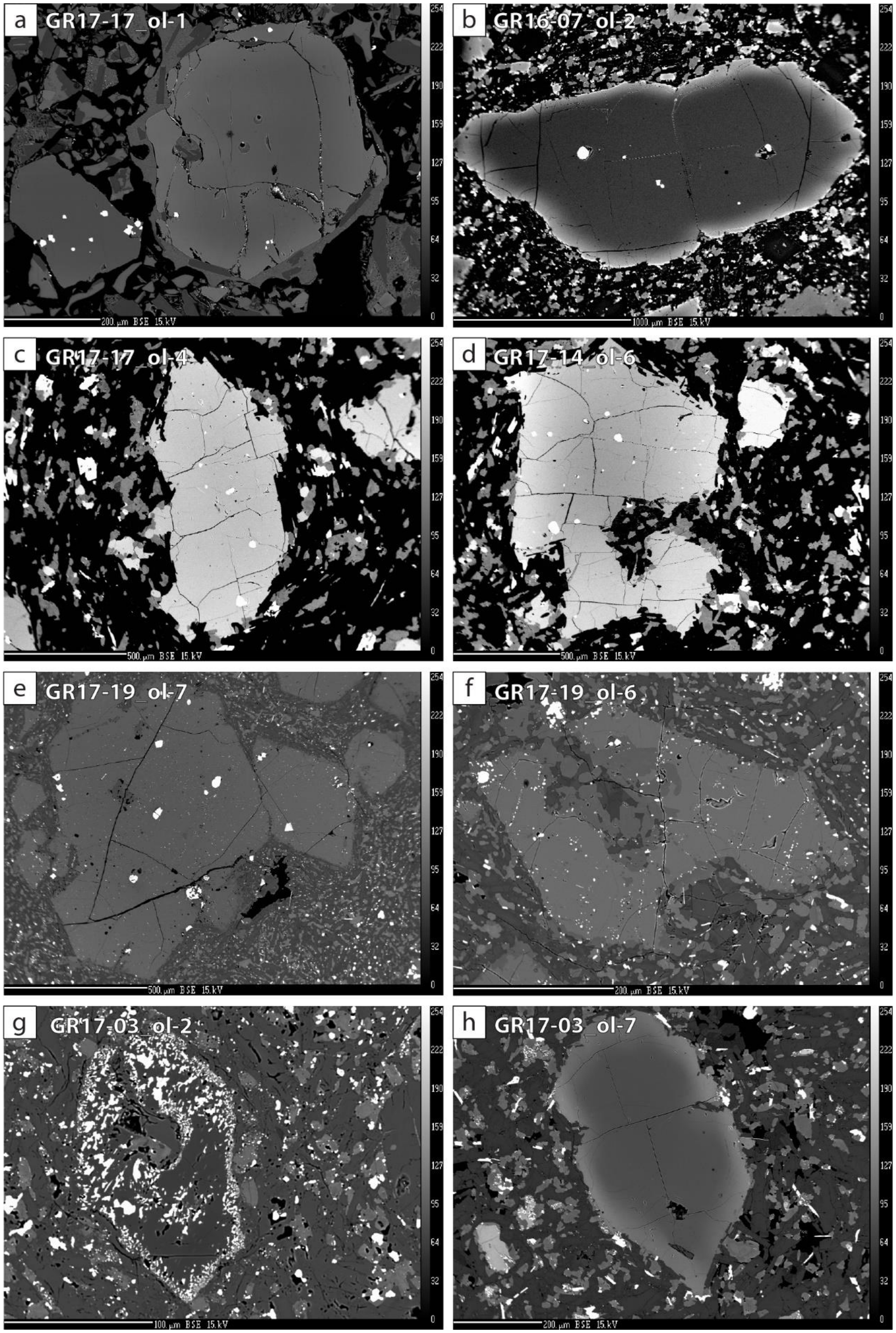
a GR17-17_ol-1
200 μm BSE 15 kV
b GR16-07_ol-2
1000 μm BSE 15 kV
c GR17-17_ol-4
500 μm BSE 15 kV
d GR17-14_ol-6
500 μm BSE 15 kV
e GR17-19_ol-7
500 μm BSE 15 kV
f GR17-19_ol-6
200 μm BSE 15 kV
g GR17-03_ol-2
100 μm BSE 15 kV
h GR17-03_ol-7
200 μm BSE 15 kV
254
222
190
159
127
95
64
32
0

Figure 3.7.

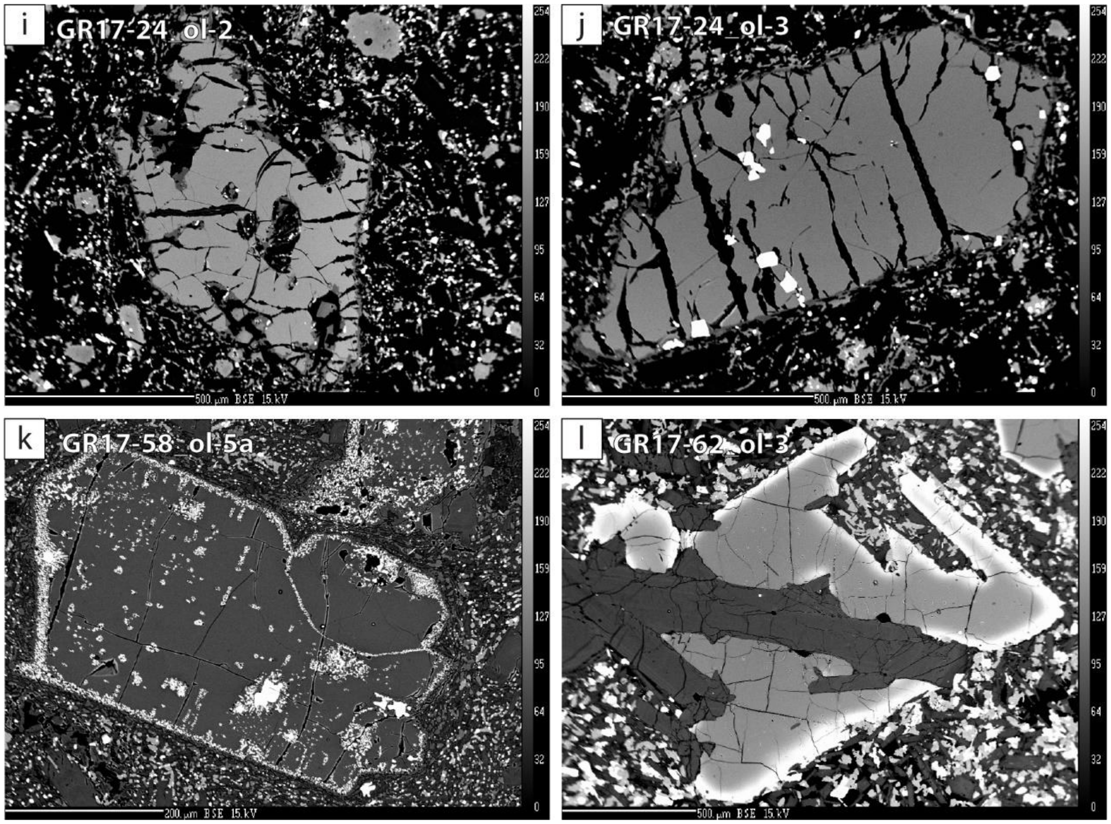

Figure 3.7 (continued).

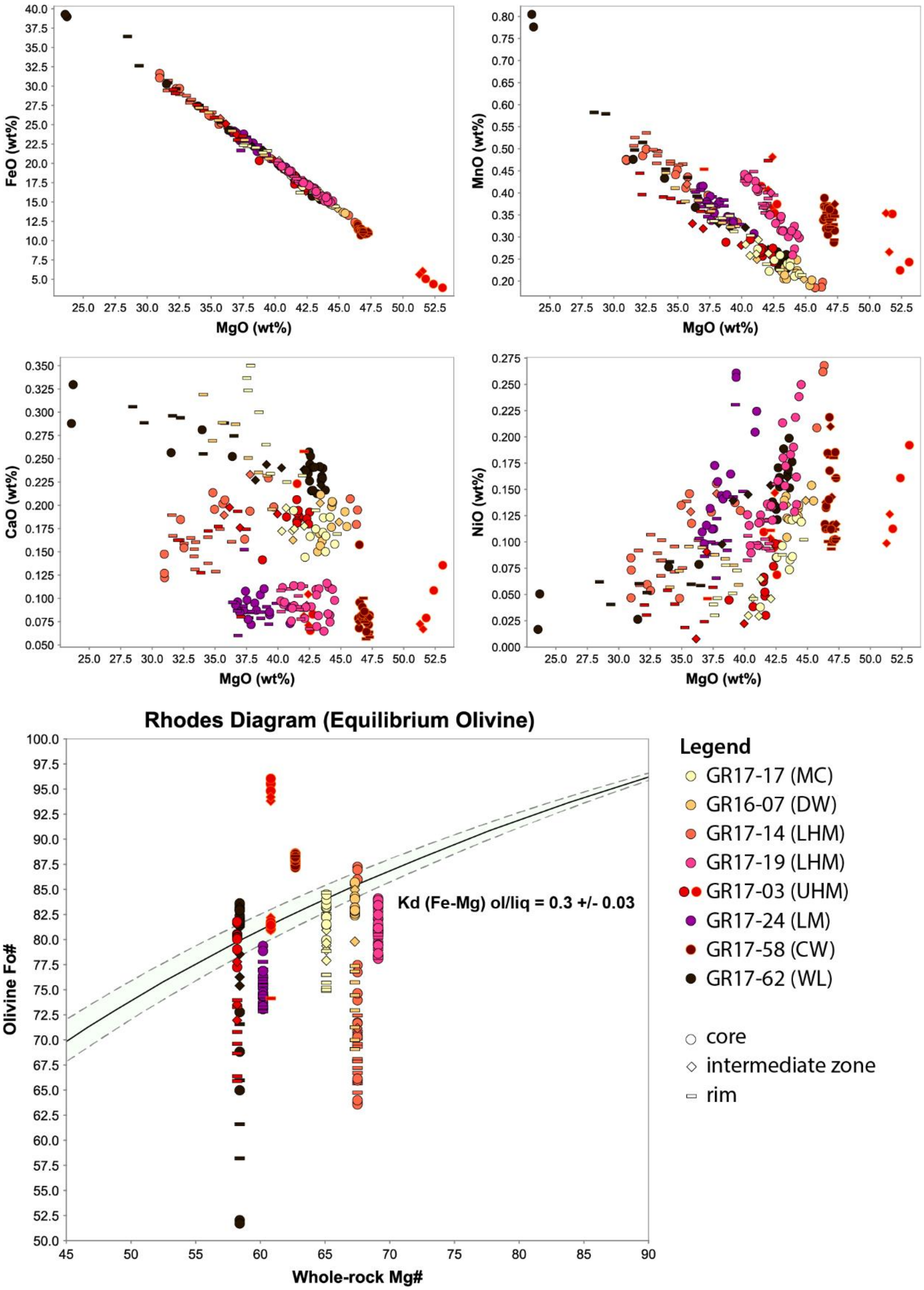

Figure 3.8. Compositions of olivine analyzed by electron microprobe.
Samples with oxidized textures and excessively high MgO/Fo in olivine are outlined in red. a, b, c, d) MgO vs. FeO, MnO, CaO, and NiO. e) Rhodes diagram (after Rhodes et al., 1979a) modified to calculate Mg# of whole rock using Fe^{2+}/Fe^{T}=0.85.

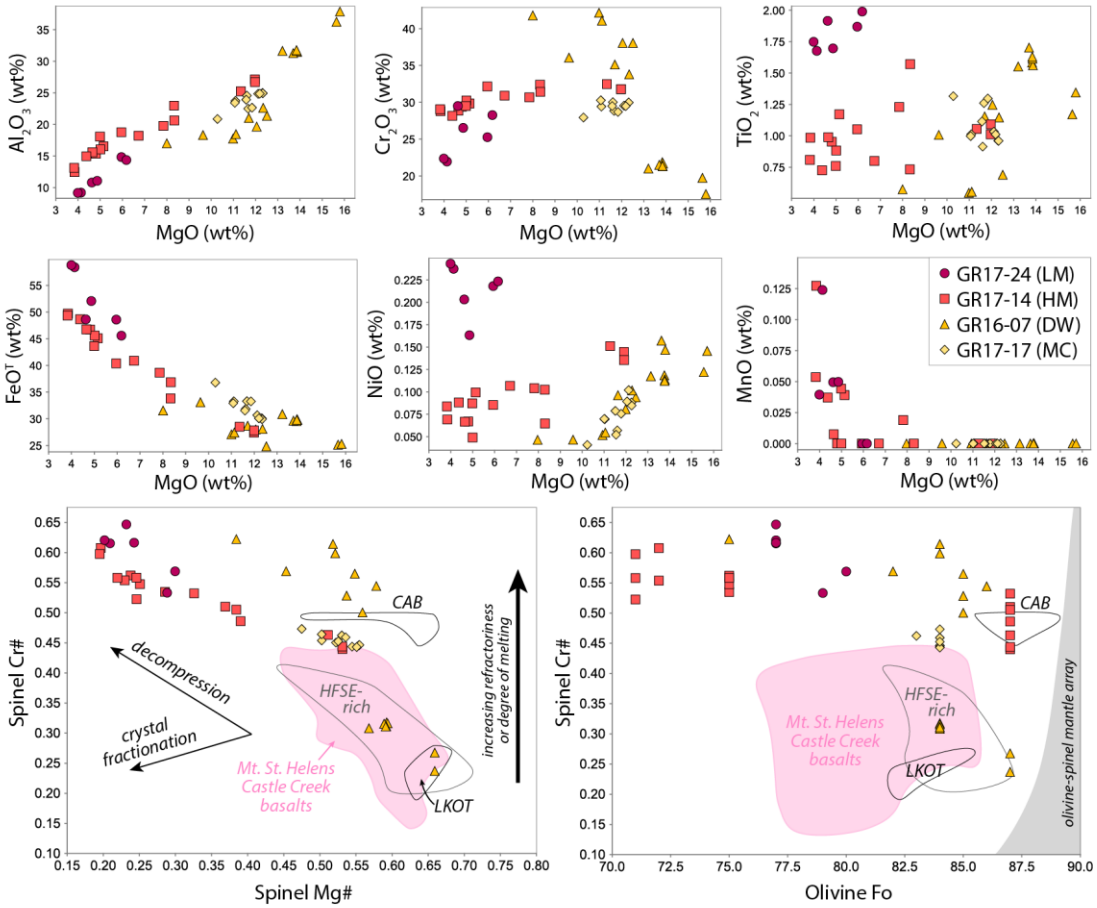

Figure 3.9. Compositions of spinel inclusions in olivine from Goat Rocks area basalts. LM = Lakeview Mountain, HM = Hogback Mountain, DW = Devils Washbasin, MC = Miriam Creek. Spinel Cr# = atomic Cr/(Cr+Al). Spinel Mg# = atomic Mg/(Mg+Fe^{2+}) (see text for discussion about iron oxidation). Olivine Fo = atomic Mg/(Mg+Fe)*100. Note that for some spinel crystals, composition of directly adjacent olivine was not determined (or did not yield usable data), in which case the maximum olivine core Fo content is used, hence the vertical arrays. Olivine-spinel mantle array is from Arai (1994). Field for Mount St. Helens Castle Creek basalts is from Wanke et al. (2019). Fields for LKOT, HFSE-rich basalt, and CAB from the southern Washington Cascades are from Smith and Leeman (2005; as plotted in Wanke et al., 2019, Fig. 9). Vectors for decompression and crystal fractionation without plagioclase are from Dick and Bullen (1984; as plotted in Clynne, 1993, Fig. 5).

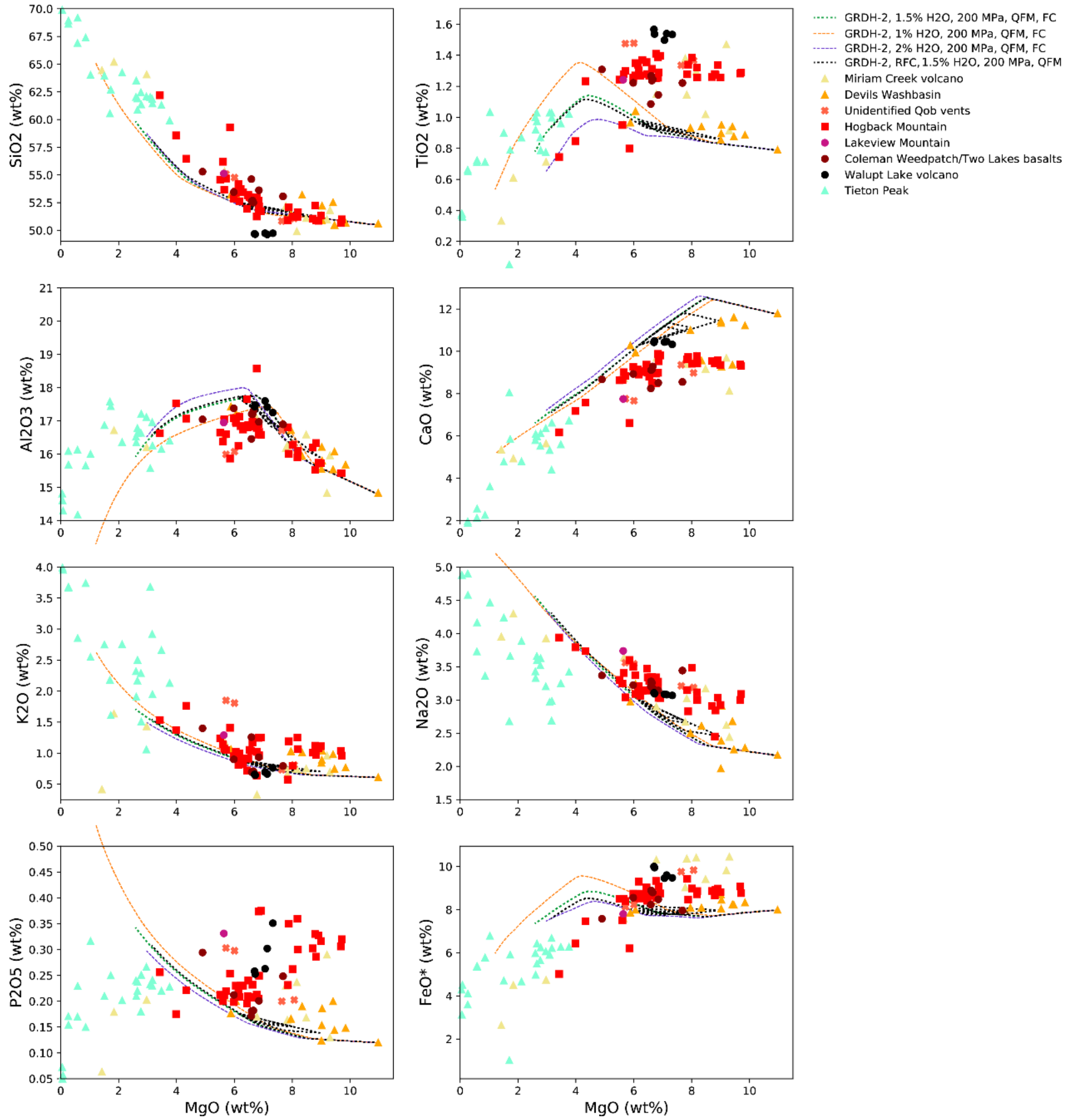

Figure 3.10. MCS models testing fractional crystallization and recharge for the Devils Washbasin suite.

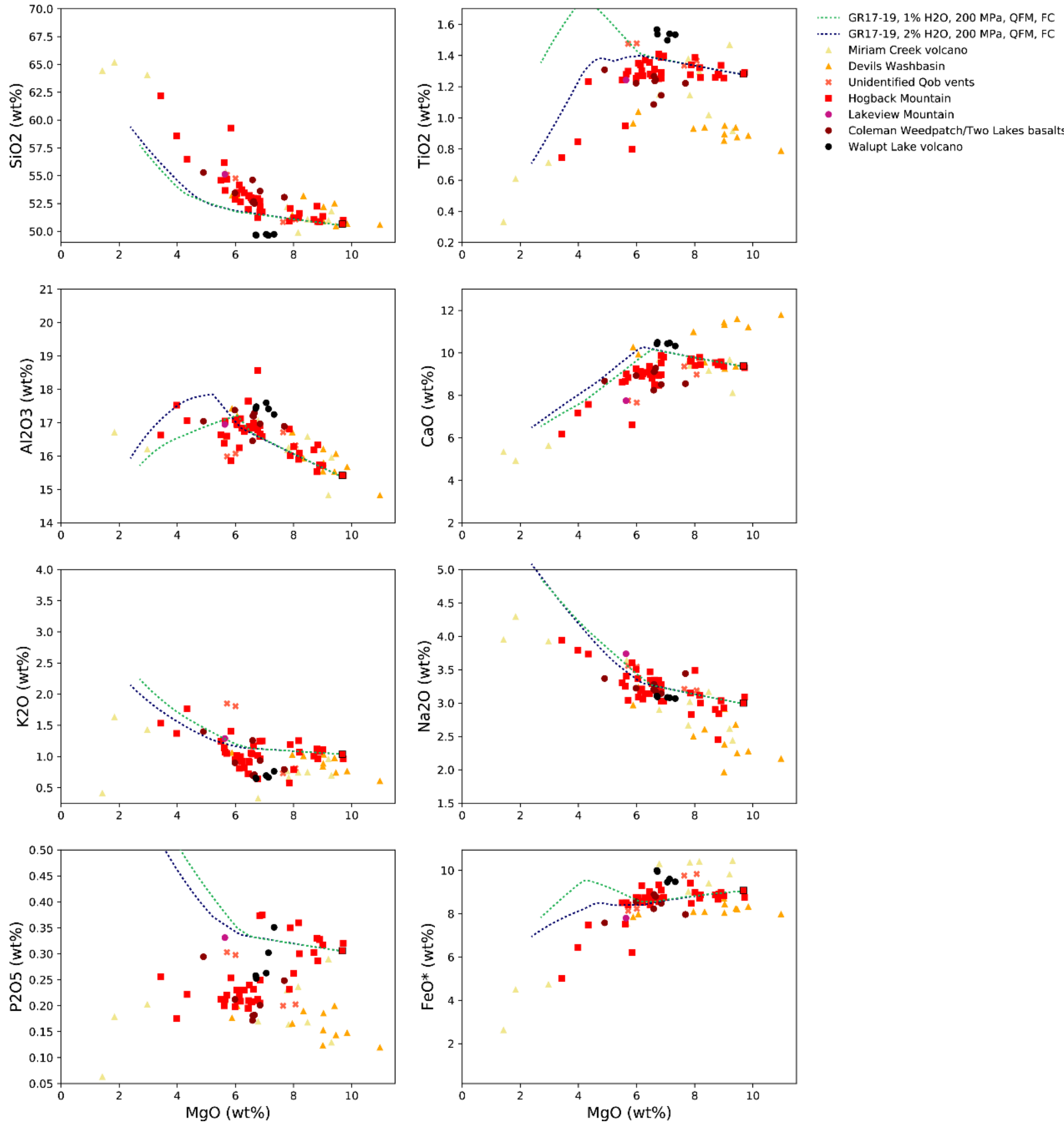

Figure 3.11. MCS models testing fractional crystallization within the Lower Hogback Mountain suite.

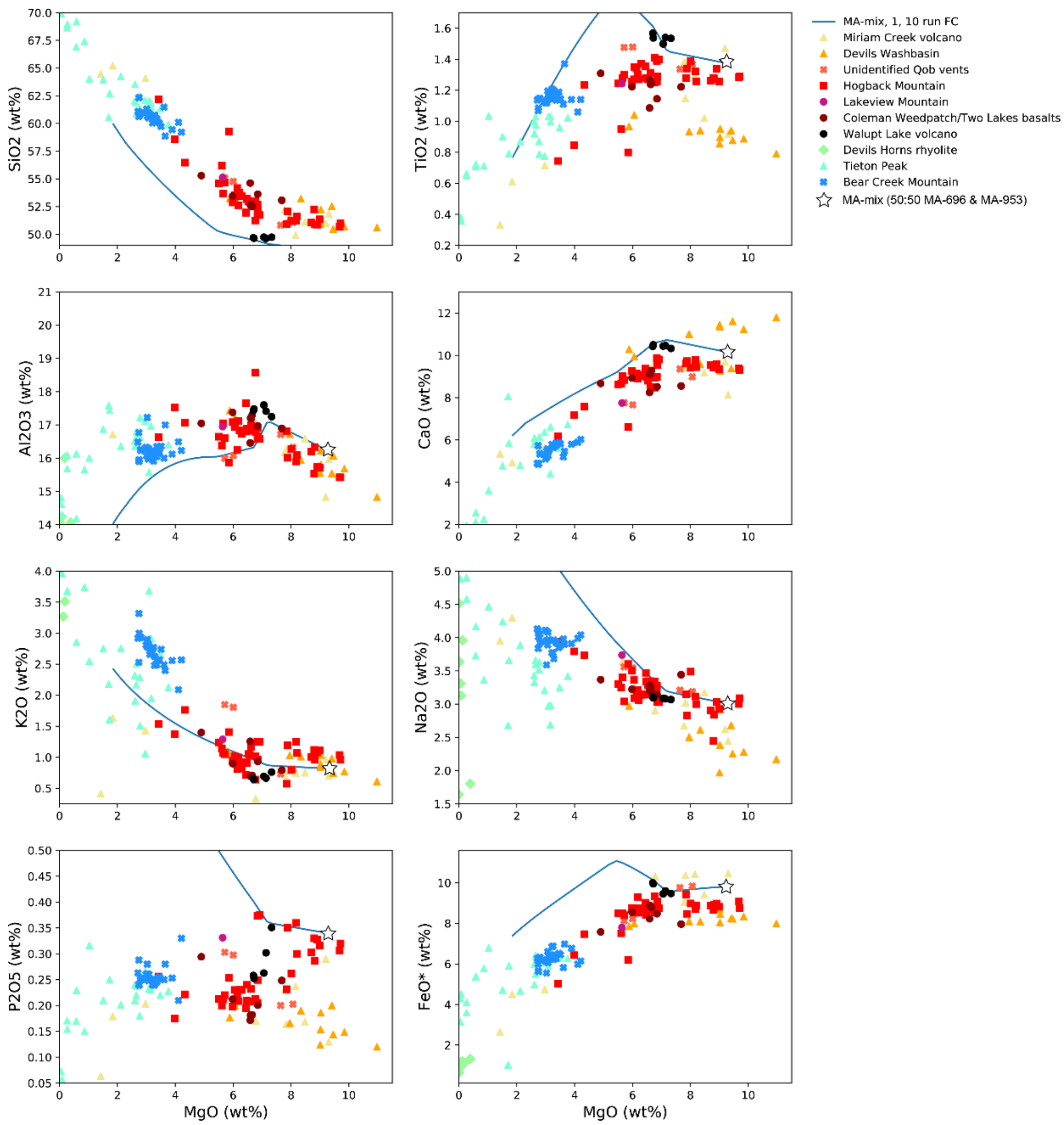

Figure 3.12. MCS model testing fractional crystallization of a synthetic Mount Adams parent for the Walupt Lake suite.

REFERENCES

Bohrson, W. A., Spera, F. J., Ghiorso, M. S., Brown, G. A., Creamer, J. B., and Mayfield, A., 2014, Thermodynamic model for energy-constrained open-system evolution of crustal magma bodies undergoing simultaneous recharge, assimilation and crystallization: The Magma Chamber Simulator: Journal of Petrology, v. 55, no. 9, p. 1685-1717.

Clayton, G., 1983, Geology of the White Pass Area, South-Central Cascade Range, Washington: Unpublished M.S. thesis, University of Washington, 212 pp.

Clynne 1993 dissertation

Davis, F.A., Cottrell, E., Birner, S.K., Warren, J.M. and Lopez, O.G., 2017. Revisiting the electron microprobe method of spinel-olivine-orthopyroxene oxybarometry applied to spinel peridotites. American Mineralogist, v. 102, no. 2, p.421-435.

Dick, H.J. and Bullen, T., 1984, Chromian spinel as a petrogenetic indicator in abyssal and alpine-type peridotites and spatially associated lavas: Contributions to Mineralogy and Petrology, v. 86, no. 1, p.54-76.

Donaldson, C.H., 1976, An experimental investigation of olivine morphology: Contributions to Mineralogy and Petrology, v. 57, no. 2, p.187-213.

Fourny, A., Weis, D., and Scoates, J.S., 2016, Comprehensive Pb-Sr-Nd-Hf isotopic, trace element, and mineralogical characterization of mafic to ultramafic rock reference materials: Geochemistry, Geophysics, Geosystems, v. 17, p. 739-773, doi:10.1002/2015GC006181.

Gualda, G. A., Ghiorso, M. S., Lemons, R. V., and Carley, T. L., 2012, Rhyolite-MELTS: a modified calibration of MELTS optimized for silica-rich, fluid-bearing magmatic systems. Journal of Petrology, v. 53, no. 5, p. 875-890.

Gualda, G. A., and Ghiorso, M. S., 2015, MELTS _ Excel: A Microsoft Excel-based MELTS interface for research and teaching of magma properties and evolution: Geochemistry, Geophysics, Geosystems, v. 16, no. 1, p. 315-324.

Gusey, D.L., Hammond, P.E., and Lasher, J.P., 2018, Tieton andesite, south-central Washington Cascades: Two of the longest known andesite lava flows, *in* Poland, M.P., Garcia, M.O., Camp, V.E., and Grunder, A., editors, Field Volcanology: A Tribute to the Distinguished Career of Don Swanson: Geological Society of America Special Paper 538, p. 93-132, https://doi.org/10.1130/2018.2538(05).

Hammond, P.E., 1980, Reconnaissance geologic map and cross sections of southern Washington Cascade Range: Publications of Department of Earth Science, Portland State University, Portland, Oregon, scale 1:125,000.

Hammond, P.E., 2017, Geologic Map of the northern portions of the Rimrock Lake, Tieton Basin, and western two-thirds of the Weddle Canyon 7.5-minute quadrangles, Yakima county, Washington: Washington Geological Survey Map Series 2017-03, 19 p.

Hildreth, W., and Fierstein, J., 2015, Geologic Map of the Simcoe Mountains Volcanic Field, Main Central Segment, Yakama Nation, Washington: U.S. Geological Survey Scientific Investigations Map 3315, scale 1:24 000, 3 sheets, 76 p. text.

Howie, R.A., Zussman, J. and Deer, W., 1992, An introduction to the rock-forming minerals, 696 p., London, UK: Longman.

Kahl, M., Chakraborty, S., Costa, F. and Pompilio, M., 2011, Dynamic plumbing system beneath volcanoes revealed by kinetic modeling, and the connection to monitoring data: An example from Mt. Etna: Earth and Planetary Science Letters, v. 308, no. 1-2, p.11-22.

Lee, C.T.A., Leeman, W.P., Canil, D. and Li, Z.X.A., 2005, Similar V/Sc systematics in MORB and arc basalts: implications for the oxygen fugacities of their mantle source regions: Journal of Petrology, v. 46, no. 11, p.2313-2336.

Lee et al., 2009, mafic thermobarometers

Leeman et al 1990

Leeman et al 2005

Leeman, W.P. and Smith, D.R., 2018, The role of magma mixing, identification of mafic magma inputs, and structure of the underlying magmatic system at Mount St. Helens: American Mineralogist: Journal of Earth and Planetary Materials, v. 103, no. 12, p.1925-1944, DOI: https://doi.org/10.2138/am-2018-6555

McDonough, W.F. and Frey, F.A., 1989, Rare earth elements in upper mantle rocks: Reviews in Mineralogy and Geochemistry, v. 21, no. 1, p.100-145.

Mullen, E.K., Weis, D., Marsh, N.B., and Martindale, M., 2017, Primitive arc magma diversity: New geochemical insights in the Cascade Arc: Chemical Geology, v. 448, p. 43-70, http://dx.doi.org/10.1016/j.chemgeo.2016.11.006

Pallister et al 2017

Pitcher, B.W., and Kent, A.J., 2019, Statistics and segmentation: using Big Data to assess Cascades Arc compositional variability: Geochimica et Cosmochimica Acta, v. 265, p.443-467, https://doi.org/10.1016/j.gca.2019.08.035.

Plechov, P.Yu., Shcherbakov, V.D., and Nekrylov, N.A., 2018, Extremely magnesian olivine in igneous rocks: Russian Geology and Geophysics, v. 59, no. 12, p. 1702-1717, https://doi.org/10.1016/j.rgg.2018.12.012.

Roeder and Emslie, 1970

Schmidt, M.E., Grunder, A.L., and Rowe, M.C., 2008, Segmentation of the Cascade Arc as indicated by Sr and Nd isotopic variation among diverse primitive basalts: Earth and Planetary Science Letters, v. 266, p. 166–181, doi: 10.1016/j.epsl.2007.11.013.

Smith, D.R. and Leeman, W.P., 2005, Chromian spinel–olivine phase chemistry and the origin of primitive basalts of the southern Washington Cascades: Journal of Volcanology and Geothermal Research, v. 140, no. 1-3, p.49-66.

Stormer Jr, J.C., and Nicholls, J., 1978, XLFRAC: a program for the interactive testing of magmatic differentiation models. Computers & Geosciences, v. 4, no. 2, p. 143-159.

Stormer, J.C., 1983, The effects of recalculation on estimates of temperature and oxygen fugacity from analyses of multicomponent iron-titanium oxides: American Mineralogist, v. 68, no. 5-6, p. 586-594.

Swanson, D.A., 1964, The middle and late Cenozoic volcanic rocks of the Tieton River area, south-central Washington: PhD dissertation, Johns Hopkins University, 329 p.

Swanson, D.A., 1996a, Geologic map of the Hamilton Buttes quadrangle, southern Cascade Range, Washington: U.S. Geological Survey Open File Report 96-0016, 29 p., 2 plates.

Tamura, Y., Yuhara, M. and Ishii, T., 2000, Primary arc basalts from Daisen volcano, Japan: equilibrium crystal fractionation versus disequilibrium fractionation during supercooling: Journal of Petrology, v. 41, no. 3, p.431-448.

Till, C.B., Kent, A.J.R., Abers, G.A., Janiszewski, H.A., Gaherty, J.B. and Pitcher, B.W., 2019, The causes of spatiotemporal variations in erupted fluxes and compositions along a volcanic arc: Nature communications, v. 10, no. 1, p.1-12.

Wan, Z., Coogan, L.A. and Canil, D., 2008, Experimental calibration of aluminum partitioning between olivine and spinel as a geothermometer: American Mineralogist, v. 93, no. 7, p.1142-1147.

Wanke, M., Clynne, M.A., von Quadt, A., Vennemann, T.W. and Bachmann, O., 2019, Geochemical and petrological diversity of mafic magmas from Mount St. Helens: Contributions to Mineralogy and Petrology, v. 174, no. 1, p.1-25, https://doi.org/10.1007/s00410-018-1544-4.

Weis, D., et al., 2006, High-precision isotopic characterization of USGS reference materials by TIMS and MC-ICP-MS: Geochemistry, Geophysics, Geosystems, v. 7, Q08006, doi:10.1029/2006GC001283.

Wood, B.J. and Virgo, D., 1989, Upper mantle oxidation state: Ferric iron contents of Iherzolite spinels by 57Fe Mössbauer spectroscopy and resultant oxygen fugacities: Geochimica et Cosmochimica Acta, v. 53, no. 6, p.1277-1291.

CHAPTER 4 – THERMAL MATURATION AND WANING OF THE GOAT ROCKS VOLCANIC COMPLEX

ABSTRACT

The Goat Rocks volcanic complex in the southern Washington Cascades was persistently active over ~3 million years and produced a broad array of compositions that follow a pattern in time. Early products from the Tieton Peak volcano range from andesite to rhyolite and are strikingly HFSE- and HREE-enriched compared to later compositions. Bear Creek Mountain and early Lake Creek volcano, which overlap in time, produced a narrow range of andesite and trachyandesite, the most alkalic of the suite. Compositions became more silicic through the Lake Creek stage, and then the Old Snowy Mountain suite introduced a new array of less potassic andesite to rhyolite. In this chapter, I use various mineral thermo(baro)meters (zircon, Fe-Ti oxides, amphibole), isotopic compositions, and petrologic modelling to explore the underlying causes of these compositional changes. Together, the mineral compositions indicate hotter conditions during Bear Creek to early Lake Creek time, a cooling magmatic system during the Lake Creek stage, and percolation of deeper, hotter magmas by the onset of Old Snowy Mountain stage. Isotopic ratios of Sr, Nd, Hf, and Pb in the intermediate to felsic magmas are well aligned with the local basalts, indicating that crustal assimilation was either minor or geochemically difficult to distinguish. Additional petrologic modelling is needed to confirm, but these mineralogical and geochemical data suggest that the changes observed at Goat Rocks represent a cycle of waxing and waning magmatism, controlled more by the mass flux and thermal state of the system than by different mantle or crustal inputs.

INTRODUCTION

The time-constrained compositions of the Goat Rocks volcanic complex serve as a natural laboratory for investigating the evolution of transcrustal magmatic systems. Schematic representations of sub-arc magma reservoirs typically depict a zone of melt differentiation and stagnation at the base of the crust and a distinct mid-to-upper-crustal, more felsic, melt-present zone. On the other hand, exhumed sections of arc crust are pervasively igneous, with the proportion of igneous rock increasing with crustal depth, implying wholesale magmatic remaking of the crust (e.g., Jagoutz and Behn, 2013; Otamendi et al., 2012; DeBari and Greene, 2011; Ducea et al., 2010; Miller et al., 2009). Perhaps a more accurate representation of the transcrustal magma factory was drafted by Cashman et al.

(2017, their Figure 1B), showing a continuous column of mush zones and interconnected melt pockets, broad at the base of the crust and focusing into a central volcanic conduit.

Studies of long-lived arc volcanic loci are limited. Research of arc volcanoes focuses largely on young, prominent volcanoes, with key applications to hazards assessment based on eruption frequency, explosivity, magma storage conditions and eruption triggers. Less common are investigations into the deeper histories of these centers for the sake of understanding the crustal modulation process. Brief summaries of comparable case studies are described below: Mount St. Helens (on the much shorter end of the timescale) and Aucanquilcha volcanic cluster (a long-lived endmember at ~11 million years duration).

Evolution of a shorter-lived arc volcano: Mount St. Helens

While representing a much shorter timescale, the volcanic and petrologic history of Mount St. Helens records changes through time that can serve as a comparison to other arc centers such as Goat Rocks. The eruptive record at Mount St. Helens spans from ~300 ka to the present, but zircons reveal a much more protracted history of plutonic construction prior to its surface expression, as old as 600 ka (Claiborne et al., 2010). The zircons, other minerals, and bulk compositions all point to an early period of cooler, wetter, and more silicic magmatism that has become more mafic with time (Clynne et al., 2008; Claiborne et al., 2010). Compositions of zircons with ages in the first several hundred years of the magmatic system record lower Ti concentrations, indicating cooler temperatures (Ferry and Watson, 2007), and higher Hf concentrations, suggesting more evolved melt compositions (Claiborne et al., 2006a, 2010). The amphibole mineral cummingtonite is present in rocks from Ape Canyon (300-35 ka) to early Swift Creek stage (16-12.8 ka), which indicates cooler and wetter conditions (Geschwind and Rutherford, 1992; Clynne et al., 2008). Most of the volcanic center's eruptive history consists of a long period of distributed dacite dome building, with only very recent (2.5 ka) construction of a stratovolcano (Clynne et al., 2008). The influence of a basaltic component has increased with time, as shown by the presence of olivine in some Cougar stage (28-18 ka) tephras, and in later stages, eruptions of andesite and basalt (Clynne et al., 2008). Around 16 ka (beginning of the Swift Creek stage), the volcano began demonstrating magmatic cycles that are characterized by an initial explosive phase, then dacite dome building with a gradually increasing mafic component (Clynne et al., 2008). Low mantle flux and a high degree of crustal interaction are proposed by Sisson et al. (2014) to explain the differentiation and mixing trends observed in the chemistry of Mount St. Helens deposits.

Large-scale, long-lived arc volcanic system: the Aucanquilcha volcanic cluster

In northern Chile, the Aucanquilcha volcanic cluster (AVC) was constructed between ~11 Ma to recent and consists of at least 19 volcanoes that have erupted dominantly andesite and dacite (Grunder et al., 2008). Four major pulses of volcanism are defined: the Alconcha Group (~11-8 Ma), the Gordo Group (~6-4 Ma), the Polan Group (~4-2 Ma), and the present pulse expressed as Volcan Aucanquilcha (1 Ma to recent; Grunder et al., 2008). The successive eruptive groups record several changes in time: 1) a spatial pattern of volcanism from peripheral to central, 2) a change from compositionally diverse andesite-dacite volcanism to increasingly restricted and more silicic compositions, 3) a change from anhydrous mafic silicate assemblages (pyroxene dominant) to biotite and amphibole assemblages, 4) an abrupt increase in eruption rate, and 5) later onset of pervasive hydrothermal alteration (Grunder et al., 2008). The lifespan and evolution of this system is compared by Grunder et al. (2008) to the voluminous magmatism in eastern Nevada at ~35 Ma (Gans et al., 1989; Grunder, 1995), Yanacocha, Peru (Longo, 2005), the San Juan Volcanic System (Lipman, 2007), and the Tuolumne Intrusive Suite (Coleman et al., 2004; Glazner et al., 2004). The authors suggest a common pattern of development of large-scale and long-lived volcanic complexes that represent protracted and fitful construction of underlying plutonic complexes (or batholiths).

In a later detailed study of the zircon crystal cargo erupted at AVC through time, Walker et al. (2010) demonstrate that age spectra (the range in zircon ages recorded by a sample) span more time among samples of the oldest (Alconcha) and youngest (Aucanquilcha) groups, compared to the eruptive flare-up between ~6-3 Ma when the age spectra are more restricted. Zircon crystallization temperatures are also higher during the flare-up. Interestingly, none of their analyzed zircons yield ages from the time gap in the AVC volcanic record (~7.5-6 Ma), which indicates reduced magmatic activity during this time, not just the surface expression of it. These data are interpreted to reflect a patchwork assembly of a batholith in discrete magmatic episodes linked to volcanism.

Petrologic evolution of the Goat Rocks magmatic system

On a timescale intermediate between the above examples is the Goat Rocks volcanic complex, spanning ~3 million years of activity (Chapters 1 and 2; Wall et al., 2018). The reader is referred to Chapters 1 and 2 of this dissertation for a summary of the local geologic setting and detailed descriptions of the eruptive stages and changes in bulk compositions over time. In this chapter, I am to explain why some of these changes occurred, by 1) probing the evolving magma reservoir with thermo(baro)meters such as Ti-in-zircon, magnetite-ilmenite pairs, and amphibole; 2) evaluating isotopic signatures in the context of local coeval basalts and potential crustal contaminants, and 3) testing petrogenetic models using tools such as the Magma Chamber Simulator (MCS; Bohrson et al., 2014). The thermobarometry results focus on the evolution from the Lake Creek to Old Snowy Mountain stages. The different mineral records corroborate each other to suggest a gradually cooling and waning magmatic system during the Lake Creek stage that is rejuvenated by a pulse from deeper-staged magmas during Old Snowy Mountain stage.

METHODS

Zircon compositional analysis by SHRIMP-RG

Zircon crystals from nine andesitic to rhyolitic Goat Rocks samples were analyzed on the USGS-Stanford SHRIMP-RG for U, Th, and Pb isotope ratios (for geochronology discussed in Chapter 1), as well as concentrations of ^{48}Ti, ^{49}Ti, Fe, Y, and rare earth elements (REE). Both polished interiors and crystal surfaces were analyzed. Details of the methods for sample preparation and analysis are described in Chapter 1 (Analytical Methods: U/Pb Geochronology). Trace element concentrations were standardized relative to sample MAD-559, a homogeneous zircon standard calibrated relative to MAD-green (Barth and Wooden, 2010). Spot analyses with anomalous compositions, such as high Fe (>5 ppm) or La (>0.1 ppm), likely indicate contamination from glass or a mineral inclusion and are excluded.

The Ti-in-zircon thermometer of Ferry and Watson (2007) was used to determine crystallization temperatures. The inputs to the thermometer are Ti concentration (ppm) in zircon, activity of TiO_2 (a_{TiO2}) in the rock, and activity of SiO_2 (a_{SiO2}) in the rock. Since the samples are andesite to rhyolite in composition (silica saturated), $a_{SiO2} = 1$. An activity of TiO_2 of 0.6 is used for all samples, based on a_{TiO2} calculations from paired Fe-Ti oxides using the model of Ghiorso and Evans (2008; see further details of Fe-Ti oxide compositions in the Results section).

Claiborne et al. (2018) presented a calibration for calculating trace element K_D's and equilibrium melt concentrations based on zircon compositions. This technique was applied to the Goat Rocks zircon samples for comparison to the whole-rock compositions erupted over time.

Compositional analysis and thermobarometry of pyroxene, amphibole, and Fe-Ti oxides

Sample selection and electron microprobe analysis

Polished thin sections were analyzed by electron microprobe to determine compositions of amphibole, paired clinopyroxene and orthopyroxene, and magnetite-ilmenite pairs. Polished thin sections were prepared at Wagner Petrographic. Minerals of interest were identified under petrographic microscope in order to select suitable samples for analysis. Whenever possible, the same sample was analyzed for multiple phases to allow for thermobarometry comparisons. For magnetite-ilmenite analysis, samples were selected within a limited range of SiO_2 to enable comparison of thermometry results between samples, while also aiming to include samples from all eruptive stages. Samples were analyzed using the Cameca SX-100 Electron Microprobe at Oregon State University. Analytical procedures including spectrometer, crystal, and count time used for each element, and standard analyses and accepted values, are given in APPENDIX(?).

During each analytical session, backscatter images were collected for each crystal/cluster to be analyzed. Locations of points were marked either physically on printouts or digitally on the images for later reference. The EDS detector was used to identify phases based on compositional indicators (e.g. a significant Ca peak on a pyroxene indicates clinopyroxene; high Ti distinguishes ilmenite from magnetite). Where mineral pairs were analyzed for thermo(baro)metry, several points were placed on either side of the touching crystal boundary. Only touching mineral pairs were analyzed and used for the pyroxene and oxide thermo(baro)metry calculations. Six samples were analyzed for pyroxene compositions, seven for amphibole, and eight for paired magnetite and ilmenite.

Data filtering

Electron microprobe results were checked for quality based on analytical totals and compositional indicators. Analyses were culled if they had unusually low or high totals, taking a more conservative approach (e.g. no lower than 90%) to Fe-Ti oxide totals which depend on iron oxidation state. Analyses with high concentrations of elements that should not be in the mineral of interest were also culled, for example, high SiO_2 in magnetite or ilmenite.

For clinopyroxene-orthopyroxene pairs and Fe-Ti oxide pairs, a “Pair ID” was manually assigned to analytical points on either side of a crystal boundary, then the compositions were joined by that ID using a script in Python. This hastened the matching of points and entry into thermobarometry engines.

Mineral formula and thermobarometry calculations

The calculators by Ridolfi et al. (2010), Putirka (2016), and Ridolfi (2021) were utilized to evaluate amphibole compositions and determine temperatures and pressures.

Compositions of clinopyroxene-orthopyroxene pairs were input into the Python tool Thermobar (Wieser et al., 2021) to evaluate compositions and test for equilibrium using the criteria defined by Putirka (2008). Nearly all clinopyroxenes analyzed have Mg# below 75, the lower limit of the compositional range used to calibrate the Putirka (2008) temperature and pressure regressions. Therefore, few pyroxene pairs are appropriate for the thermometer, and few data points do not lend much confidence, so they are not further discussed (compositions are presented in the Results section without thermobarometry calculations).

Paired magnetite and ilmenite compositions were entered into the ILMAT calculator (Lepage, 2003) for comparison of different stoichiometric formulations and thermometers (Carmichael, 1967; Anderson, 1968; Lindsley & Spencer, 1982; Stormer, 1983; Powell and Powell, 1977; Spencer and Lindsley, 1981; Andersen and Lindsley, 1985). The Ghiorso and Evans (2008) thermometer was also applied using the APP-Fe-Ti-Oxide-Geotherm (Ghiorso and Prissel, 2020).

Sr, Nd, Hf, and Pb isotopic analysis

Isotopic ratios of Sr, Nd, Hf, and Pb were determined for sixteen samples representing the four major eruptive stages of Goat Rocks (plus samples from Devils Horns rhyolite, Spiral Butte, and Round Mountain) and ranging in composition from basaltic andesite to rhyolite. One batch of samples was chipped in a jaw crusher with steel plates and powdered in an alumina ceramic ring mill at Oregon State University; a later batch was chipped with alumina ceramic plates, then submitted to the Pacific Centre for Isotopic and Geochemical Research (PCIGR) for powdering in agate planetary mills. Samples were analyzed for isotopic ratios at PCIGR using the methods described in Chapter 3. There is no systematic relationship between isotope compositions and sample preparation method, which lends confidence against sample contamination.

Geochemical and petrologic modelling

Several petrologic modelling approaches were employed. An Excel version of XLFRAC (Stormer and Nichols, 1978) was used to perform least-squares regressions for simple tests of bulk crystal removal or mixing. Rhyolite-MELTS (Gualda et al., 2012; Gualda and Ghiorso, 2015) was used to quickly calculate Fe_2O_3 concentration from measured FeO^T

based on a selected oxygen fugacity (fO_2), to normalize compositions, and to determine liquidus (or solidus) temperatures at a given pressure and H_2O concentration. These parameters could then be input into the Magma Chamber Simulator (MCS; Bohrson et al., 2014) to run fractional crystallization models and to test mixing, recharge, and assimilation of partial melts from country rock.

RESULTS

Zircon ages, compositions, and thermometry

In Chapter 1, $^{206}Pb/^{238}U$ ages of zircon rims and surfaces were used alongside $^{40}Ar/^{39}Ar$ ages to reconstruct the eruptive history of the Goat Rocks volcanic complex (Wall et al., 2018; the geochronology is updated with new $^{40}Ar/^{39}Ar$ ages in Chapter 2). Here I consider in more detail the ages of zircon antecrysts and xenocrysts that extend on the order of hundreds of thousands of years to tens of millions of years older than the samples' zircon surface $^{206}Pb/^{238}U$ or groundmass $^{40}Ar/^{39}Ar$ ages. Trace element concentrations, Ti-in-zircon temperatures, and model melt compositions are also discussed.

Ages of antecrysts and xenocrysts

The age of a sample's most recent zircon crystallization was calculated from the weighted mean of surface and/or polished rim ages that define a coherent population (e.g. where individual spot ages overlap within 2σ uncertainty; Chapter 1; Wall et al., 2018). Any spot analyses that yield ages older than this range are interpreted as inherited, i.e. antecrysts from earlier magma batches or xenocrysts from country rock (Table X, Figure 4.1). In Figure 4.1, spot ages are plotted against the sample's interpreted eruption age to highlight the range of populations sampled by each magma.

All samples contain inherited zircon, but some include particularly old crystals dating to much earlier stages of the Goat Rocks volcanic complex or pre-Goat Rocks basement. Zircons from sample GR16-36, the oldest lava flow known from the Lake Creek volcano, include two crystals with ages that overlap the end of the Tieton Peak eruptive stage (Figure 4.1). Another much older crystal yielded a spot age of 28.22 ± 0.51 Ma (1σ), which is within the time period of the Ohanapecosh Formation (this unit directly underlies the GR16-36 lava flow). One crystal analyzed from sample GR17-47A yielded a surface age of 3.69 ± 0.39 Ma (1σ), but it has elevated La (0.37 ppm) and no other analyzed zircons are close in age, so it is unclear whether this age (which predates the known Goat Rocks lifespan, and Miriam Creek volcano) is meaningful. Sample GR17-78, from the Clear Fork lava flow, contains inherited zircon crystals with a wide range of ages (Figure 4.1). One pair of ages lies between the age of the andesite of Countyline Ridge and the older Tieton andesite lava flow (Figure 4.1; Chapter 2, Figure 2.5). Four crystals have ages between 7.5-7.9 Ma, and two others are ~12 Ma, neither of which match any ages determined for volcanic or plutonic units in the area (though many undated units are mapped as "Oligocene to Miocene;" Chapter 2; Swanson, 1996a, 1996b). Another cluster of four crystals have ages ~55 Ma, overlapping the duration of the Summit Creek basalts (Figure 4.1; Chapter 2; Vance et al., 1987). Two of those spot analyses have elevated La and Fe (Appendix X), but the other two have clean compositions, so I take the cluster of ages to be robust. Finally, the oldest spot age is 177 ± 3 Ma (1σ), which predates the presumed age (Late Jurassic to Early Cretaceous) of the Rimrock Lake Inlier.

Zircon compositions and Ti-in-zircon thermometry

Compositions of zircons are included alongside ages in Appendix X and are shown in Figure 4.2, Figure 4.3, Figure 4.4. Only compositions of zircons younger than 1.2 Ma and presumed to be associated with the Lake Creek to Old Snowy Mountain magmatic system are discussed here. Ti concentration ranges from ~40 ppm to ~2ppm, extending to higher values for zircons from early Lake Creek time, with a much more restricted range (~2-10 ppm Ti) for zircons from late Lake Creek to Old Snowy Mountain stage (Figure 4.2a). The concentration of Y is generally lower in early Lake Creek time and extends to higher values for younger samples, except for some crystals from GR16-36 and an antecryst from GR16-30 that reach higher concentrations (Figure 4.2b). Hf concentrations follow a similar temporal trend: zircons in older samples tend to have a more restricted range, then extend to higher values in younger samples, except for those from the Clear Fork lava which also have a restricted range of ~7000-9000 ppm (Figure 4.2c). REE diagrams are generally similar but display slight differences through time (Figure 4.4). The late-Lake Creek aged zircons occupy a narrower range of compositions than the early-Lake Creek range (Figure 4.4b). Old Snowy Mountain aged zircons break into two populations. (Figure 4.4c). Zircons from Old Snowy Mountain and Goat Ridge lavas have the highest Ce values of the suite and a Eu anomaly (Eu/Eu*) comparable to older zircons. In contrast, zircons from the Clear Fork lava have lower Ce concentrations and a negligible Eu-anomaly (high Eu/Eu*).

Concentration of Hf in zircon can be considered a proxy for fractional crystallization of the magma (higher Hf = more evolved; Claiborne et al., 2006a). The ratio Ce/Nd can be used as an alternative to Ce/Ce* since La is in low concentration and difficult to measure in zircon. With increasing Hf, the range of Ce/Nd increases, indicating more oxidized conditions (more Ce^{4+} available to substitute for Zr^{4+}; Figure 4.3a). The highest Ce/Nd value is ~80, and most are <60, indicating that the magmas are typical of arc andesites and dacites and are not exceedingly oxidized (Nansen Olson, personal communication). Ce/Nd extends to the highest values at higher Hf concentration during late Lake Creek and early Old Snowy Mountain stage, indicating more evolved and more oxidized magmas (Figure 4.3a). Eu/Eu* occupies a narrow range for most of the analyzed zircons (~0.1-0.3), with a slight decrease in the direction of higher Hf concentration (Figure 4.3b). Sample GR17-78 (Clear Fork lava flow) is an exception, with Eu/Eu* between 0.4-0.7. This likely reflects more limited plagioclase crystallization (since Eu^{2+} is compatible in plagioclase) which is supported by the rare occurrence of plagioclase in hand sample and thin sections (e.g. Chapter 2, Figure 2.7g,h).

Ti-in-zircon temperatures span from ~650 to 950 °C, reaching their highest values in early Lake Creek time and their lowest from later Lake Creek through Old Snowy Mountain stage (Table X, Figure 4.5). The calculated temperatures typically span on the order of 50 to 100 °C within a given sample. Note that the uncertainty of the thermometer calibration is on the order of ±10 to 20 degrees (Ferry and Watson, 2007).

Model equilibrium melt compositions

Model melt compositions using the calculations of Claiborne et al. (2018) are given in Appendix X, and two examples (Hf and Y concentration) are shown in Figure 4.7. Claiborne et al. (2018) show that the zircon-melt partition coefficients (K_D) of HFSE such as Hf and Y decreases with increasing Ti in zircon; i.e. at higher temperatures these elements are less compatible and at cooler temperatures more readily accommodated by zircon. Recall that for zircons of early Lake Creek stage, Hf and Y concentrations do not extend as high as in younger zircons, but because Ti and temperature are at their highest (Figure 4.2a, Figure 4.5) the inverse K_D relationship indicates that melt concentrations were much higher during that time (Figure 4.7). These results align with the bulk rock data for early Lake Creek samples, which are higher in HFSE (like Hf, Y, Zr, Nb) than younger Lake Creek and Old Snowy Mountain stage samples (Chapter 2, Figure 2.9).

Zircon saturation temperatures of bulk rock compositions

As a gauge of the zircons' origin, zircon saturation temperatures were calculated for each sample (as well as other samples from Goat Rocks). The compositional parameter M [=(Na + K + 2Ca)/(Al*Si)](Watson and Harrison, 1983; see Hanchar and Watson, 2003, for worked example of molar calculations) was calculated from bulk compositions for use in the thermometer of Boehnke et al. (2013) alongside bulk rock Zr concentration. Note that the andesites and dacites from Goat Rocks typically contain ~10-30% phenocrysts/megacrysts, which means that a given bulk rock composition may not accurately represent the composition of the melt in which a zircon grew. In the future, one could estimate melt composition by subtracting the crystal cargo, but the simplicity of the bulk rock estimate at least enables broad scale comparisons and interpretations. The parameter M and zircon saturation temperature for all samples are given in Appendix X, and in Table X, zircon saturation temperatures are given alongside the Ti-in-zircon temperature range for each sample.

The zircon saturation temperatures range from 671 to 767 °C. Importantly, most of the Ti-in-zircon temperatures are higher than the zircon saturation temperature for their host sample ($T_{zircon}/T_{sat} > 1$, Figure 4.6). This means that a majority of zircons did not crystallize in their carrier magma, but in other magma(s) with a composition at which zircon became saturated at a higher temperature—even for coherent age populations within uncertainty of the interpreted eruption age. In general, younger samples record Ti-in-zircon temperatures that are closer to zircon saturation temperatures. Seven of the nine samples (GR17-78, GR16-38, GR17-71, GR17-75, GR17-72A, GR17-47A, and GR16-30) record Ti-in-zircon temperatures close to (within 25 °C) or below their host magma's zircon saturation temperature. Two of the oldest samples, GR16-34 and GR16-36, record no Ti-in-zircon temperatures below their respective saturation temperature.

Overall, the calculated zircon saturation temperatures decrease with time for this suite of samples as well as other age-constrained Goat Rocks samples (Figure 4.6). This trend reflects the decreasing Zr (and other HFSE) concentrations in the rocks over time (Chapter 2, Figure 2.9). Note that no compositions erupted at Goat Rocks have zircon saturation temperatures as high as the Ti-in-zircon temperatures recorded for early Lake Creek stage crystals (Figure 4.6).

Fe-Ti oxide thermometry

Touching pairs of magnetite and ilmenite were analyzed by electron microprobe in eight samples from Tieton Peak volcano, the Lost Lake andesite, Bear Creek Mountain (Tieton andesite, Qta_1), the Black Thumb dacite, late-stage Lake Creek volcano, and Old Snowy Mountain. Samples with touching pairs were selected from as narrow a range in silica as possible (59.9 to 64.5 wt% SiO_2), to allow comparison of thermometry results between samples, while still representing a broad range of time. The full composition dataset is given in Appendix X.

One of the Tieton Peak samples (GR20-16) did not yield many quality analyses: three of five touching pairs have magnetite with high silica (>0.5 wt%), and one of them has ilmenite with high silica and Al_2O_3. The remaining two oxide pairs have anomalous MnO and MgO concentrations in magnetite, as do the oxide pairs in the other Tieton Peak sample, GR20-15. These magnetites in Tieton Peak lava flows have anomalously high MnO (0.75-2.0 wt%) compared to the magnetites from other samples (<0.5 wt%), as well as extremely low MgO (<0.25 wt%). These compositions plot below the equilibrium line of Bacon and Hirschmann (1988; Figure 4.8), differing from the disequilibrium compositions that those authors show above/left of the equilibrium line for non-touching crystal pairs and exsolved plutonic oxides. These Tieton Peak samples have the highest MnO and MnO/FeO of the suite, which may be a sign of cryptic hydrothermal alteration (evidence of hydrothermal alteration can be readily observed in lava flows lower in the stratigraphy). The composition data are still included in Appendix X and Figure 4.8, but since they are not in Mg/Mn equilibrium, they are not suitable for thermometry.

Ilmenite compositions are similar among all samples, but magnetite compositions fall into two distinct temporal groups (Figure 4.8b,c). Magnetites in older samples (from Tieton Peak, Lost Lake andesite, and Bear Creek Mountain) are more TiO_2-enriched with lower FeO, while younger samples have magnetite with lower TiO_2 and higher FeO. This translates to a higher ulvospinel component (~0.4 to 0.6 mole fraction) compared to the younger magnetites (~0.2 to 0.4 mole fraction ulvospinel). In turn, the temperatures calculated for older samples are higher than those for the younger samples (Figure 4.9). Different thermometers yield the same overall result, with slight differences in exact temperatures. The Andersen and Lindsley (1985) thermometer yields higher temperatures at the cool end of the spectrum, and lower temperatures at the hotter end of the spectrum, compared to the Ghiorso and Evans (2008) thermometer (Figure 4.9a). The Ghiorso and Evans (2008) calibration is used when comparing Fe-Ti oxide temperatures to other thermometry results.

Amphibole thermobarometry

Amphibole occurs in some lava flows of late Lake Creek stage and is common in lava flows of Old Snowy Mountain stage. Amphibole was analyzed in thin sections from three Lake Creek stage samples (GR15-01C, GR15-02, and GR18-21) and three Old Snowy Mountain stage samples (GR16-17, GR16-25, GR16-38), in addition to a diorite of uncertain age in the Miriam Creek drainage (GR18-06, unit Tpd, late Pliocene? Chapter 2, Figure 2.1; Swanson and Clayton, 1983). Compositions are plotted in Figure 4.10, and the full dataset is given in Appendix X.

The amphiboles demonstrate a negative correlation between SiO_2 and Al_2O_3, emphasizing that Al dominantly substitutes into the tetrahedral cation site (Figure 4.10a). Indeed, most of the Al is assigned to the tetrahedral site by the Ridolfi et al. (2021) calculator, but for the more Al-rich samples, a small percentage is also incorporated into the octahedral site (Appendix X). Amphiboles in the two older samples from Lake Creek stage (GR15-01C and GR15-02) are notably higher in silica content and lower in aluminum than the rest of the sample suite (Figure 4.10a). The amphiboles in these two Lake Creek samples are also more enriched in K_2O, FeO, and MnO, and lower in Na_2O and MgO. They are classified as Mg-hornblende, while the other amphiboles are tschermakitic pargasite (Appendix X).

Temperature and pressure calculations are distinct for the two temporal-compositional groups. The older samples record lower temperatures and pressures than the younger samples (Figure 4.10e). The exact pressure and temperature values may be strongly affected by the thermometer or barometer calculation used. For example, the Ridolfi et al. (2021) barometer yields significantly higher pressures for amphiboles in GR16-38 compared to the earlier generation Ridolfi et al. (2010) barometer. Results from the Ridolfi et al. (2021) thermometer and Putirka (2016) thermometer are closely aligned, nearly 1:1, with a <25 °C offset to higher temperature for the Ridolfi (2021) formulation. Using the Ridolfi et al. (2021) calculator, the older suite ranges from ~775-850 °C and ~100-200 MPa, while the younger samples fall between ~875-1000 °C and ~200-700 MPa (Figure 4.10e).

Amphiboles in the diorite sample (GR18-06) are similar to the younger suite. They are slightly more enriched in MnO and depleted in TiO_2 and Na_2O. The compositions are classified as tschermakitic pargasite. Temperature and pressure are within range of the Old Snowy Mountain suite: ~900-950 °C and ~300-400 MPa.

Clinopyroxene and orthopyroxene compositions

Clinopyroxene and orthopyroxene pairs were analyzed in six samples with the goal to compare two-pyroxene barometry results against amphibole barometry results. However, the clinopyroxene compositions of these pairs are not sufficiently magnesian to be suitable to the Putirka (2008) thermobarometer, which is calibrated only for clinopyroxene with Mg# 75. The compositional data are included in Appendix X and are not further discussed in this chapter.

Whole-rock Sr, Nd, Hf, and Pb isotope compositions

Sr, Nd, Hf, and Pb isotope ratios were determined for sixteen samples from the four main Goat Rocks eruptive stages, plus one sample each from the Devils Horns rhyolite, Spiral Butte, and Round Mountain. Isotope ratios are given in Table 4.3 and are included with major and trace element data in Appendix X. Overall, the isotopic compositions of these intermediate to felsic lavas overlap significantly with the regional basalts and basaltic andesites discussed in Chapter 3 (Figure 3.5; Figure 4.11). Details of the samples from each temporal stage are described below, from oldest to youngest.

Devils Horns rhyolite

Sample TP19-08, from a glassy lava (presumed dome) in the Devils Horns rhyolite deposit, is isotopically similar to the Goat Rocks suite and the High Cascades basalt array (Figure 4.11a,b,c). It has higher 87Sr/86Sr and lower 143Nd/^{144}Nd than most of the Goat Rocks suite (apart from sample GR15-04 from the Lake Creek volcano, which is an outlier with high ^{87}Sr/^{86}Sr; a). Its Pb isotope ratios plot along the High Cascades array, in the direction toward N. Cascadia sediment. Its ^{176}Hf/^{177}Hf ratio is similar to the High Cascades array.

Tieton Peak stage

Two samples from the Tieton Peak volcano were analyzed, TP19-06 and TP19-15. These samples overlap the main Goat Rocks trend in 143Nd/144Nd (Figure 4.11a), and are on the higher side for Pb isotope ratios, similar to the slightly older Devils Horns rhyolite (Figure 4.11b). Their ^{176}Hf/^{177}Hf ratios are also on the lower side for this suite, like Devils Horns rhyolite, but not as low as the Tieton andesite (Qta_1) from Bear Creek Mountain (Figure 4.11c).

Bear Creek Mountain stage

A sample from each of the Tieton andesite lava flows from Bear Creek Mountain was analyzed: GR16-01 (Qta1) and GR16-05 (Qta2; Table 4.3). Their 143Nd/144Nd and 87Sr/86Sr isotopic ratios are very similar (Figure 4.11a). GR16-01 has slightly higher Pb isotope ratios (Figure 4.11b), and it also has the lowest ^{176}Hf/^{177}Hf ratio of the suite at 0.282986 (Figure 4.11c).

Lake Creek stage

Several samples were analyzed from the Lake Creek volcano (GR15-04, GR16-30, GR17-77A) as well as a sample of Black Thumb dacite (GR17-47A). Three of these are closely aligned with the rest of the Goat Rocks suite in their $^{143}Nd/^{144}Nd$ and $^{87}Sr/^{86}Sr$ range, but sample GR15-04 is anomalously high in 87Sr/86Sr compared to others with comparable 143Nd/144Nd (Figure 4.11a). The three Lake Creek samples are very similar in Pb isotope ratios, close to Tieton andesite sample GR16-01 and Tieton Peak sample GR20-15, whereas the Black Thumb dacite has lower values like the Tieton andesite sample GR16-05. These four samples have a small range in 176Hf/177Hf ratios that overlaps with the High Cascades array and compositions from the younger Old Snowy Mountain stage (Figure 4.11c). They have a diverse range in 1/Sr vs. 87Sr/86Sr, but higher 1/Sr can be attributed to plagioclase fractionation (Figure 4.11d).

Old Snowy Mountain stage

Isotopic ratios were also determined for samples from Old Snowy Mountain, Goat Ridge, the Clear Fork lava, Spiral Butte, and Round Mountain. These samples span a diverse range in 143Nd/144Nd and 87Sr/86Sr as well as Pb isotope values, and are displaced toward slightly higher 208Pb/204Pb values than the High Cascades array and most other Goat Rocks samples (Figure 4.11a,b). However, they represent a narrow range of 176Hf/177Hf compositions, like the Lake Creek stage andesites and dacites.

Petrologic models testing fractional crystallization

Petrologic modeling results are limited and preliminary. The following questions were posed to be investigated via modeling tools:

- Can andesitic compositions be produced by fractional crystallization of the regional basalt compositions erupted during each stage?
- Do andesitic to rhyolitic compositional arrays reflect primarily fractional crystallization, or is significant crustal melting required?
- Are the very different compositional suites of the Lake Creek and Old Snowy Mountain stages a product of distinct sources, different assimilants, or different storage conditions (or a combination of the above)?

Initial results of fractional crystallization models are presented below. There is much room for additional work to investigate the roles of crustal assimilation and magma storage conditions.

As discussed in Chapter 3 Results: Petrologic modelling, the primitive Devils Washbasin sample GRDH-2 was tested as a parent for fractional crystallization, mixing, and recharge models under various conditions to explain the compositional suite of Devils Washbasin. The best fitting conditions (1 to 1.5 wt% H_2O at 200 MPa and initial fO_2 at QFM) were also run to higher percentages of crystallization (cooler temperatures) to test whether the coeval Tieton Peak andesitic-dacitic suite could be achieved. Results of these two model runs are shown in Figure 4.12. These FC models are not a good match for Al_2O_3 (too low) and Na2O (too high), slightly too low in TiO_2, and do not match the slope of CaO. Further MCS testing has not been conducted, but I note that the Tieton Peak suite trends toward Devils Horns rhyolite on all plots, and so I propose that a combination of fractional crystallization of Devils Washbasin basalt plus assimilation of Devils Horns rhyolite is the most likely explanation for this array. This makes sense given the close proximity and age of these volcanoes (Chapter 2, Figure 2.1, Figure 2.2, Figure 2.5)

Initial testing supports that fractional crystallization could be the dominant process for differentiation from andesite to rhyolite in this suite. In Figure 4.13 I show two MCS FC models run at the same pressure as the best-fit Devils Washbasin models (200 MPa), one with 2 wt% water and the other at 3 wt% water. These two models are a close match for several major elements, but do not achieve the low CaO and high Na_2O values on the more felsic end. Trace element models could yield more valuable insight into the potential conditions or contaminants involved. Importantly, HFSE and REE are very high for the dacitic to rhyolitic end of this suite, which limits the possibility of Devils Horns rhyolite as a contaminant, since it is reduced in those elements (Chapter 2, Figure 2.9). Perhaps Devils Horns rhyolite was assimilated by the more mafic magmas but did not interact with more felsic magmas. Or, a unique composition not represented in the Goat Rocks suite (basement rock) was assimilated by these magmas. Or perhaps this compositional array instead indicates a partial melting trend. Additional petrologic modeling (and perhaps geochemical analysis of basement rocks) is required to test these ideas.

DISCUSSION

Mineral evidence of a thermally pulsing magmatic system

Zircon stability and declining crystallization temperatures

Zircon compositions can only preserve a small component of a magma's history and must be interpreted with caution, considering various factors such as analytical and thermometer uncertainty, textural observations, and magma composition. Despite these limitations, the zircons from Goat Rocks lavas provide insight into the changing conditions of the magma reservoir that align with other results such as bulk composition and Fe-Ti oxide temperatures. Overall, there is a trend toward cooler magma temperatures and more felsic compositions during the Lake Creek eruptive stage.

Zircon saturation temperatures are an important consideration for the meaning of temperatures recorded by zircon. At Goat Rocks, no erupted compositions have zircon saturation temperatures as high as the Ti-in-zircon temperatures recorded by early Lake Creek stage zircons (Figure 4.5, Figure 4.6). Zircon saturation temperatures are *higher* during that time, but the maximum saturation temperatures are ~765 °C, whereas temperatures recorded by zircon crystals are as high as ~950 °C. The magnitude of this difference suggests that it does not reflect the uncertainty of either thermometer, but that the zircons must have crystallized in a melt other than that by which they were carried to the surface. Zircon cannot crystallize in a melt that is above its zircon saturation temperature; the mineral is unstable. For the zircons to have crystallized at such high temperatures, they must have originated in a magma with different composition, either with a lower M parameter or higher Zr concentration (more likely the latter since the correlation is stronger between Zr and saturation temperature).

Zr concentration in the Lake Creek suite increases with SiO_2 until approximately 64 wt%, at which point the trend reverses—a clear sign of zircon saturation and fractional crystallization. Samples GR16-30, GR17-47A, GR17-72A, and GR17-75 (=GR15-02) are at the peak or on the downslope side, whereas GR16-36 and GR16-34 are less silicic and on the rising side of the peak, suggesting that those magmas had not yet reached zircon saturation. Recall that the latter two samples are those that contain only zircons with temperatures above their respective zircon saturation temperatures. For the zircon-undersaturated magma of GR16-36 to have entrained zircon crystals with a mean U-Pb age identical to its $^{40}Ar/^{39}Ar$ age suggests that a stratified magmatic system had already developed before the first eruption of that volcano. This further supports the idea presented in Chapter 2 that, based on overlapping $^{40}Ar/^{39}Ar$ ages of lava flows and similar bulk compositions, the Lake Creek volcano was fed by a long-lived, extensive magma reservoir that had also fed the Bear Creek Mountain volcano.

The Ti-in-zircon temperatures tell an incomplete but important story about magma temperatures through time, particularly during the Lake Creek stage. The crystals' recorded temperatures are in part dictated by the magmas' saturation temperatures, such that no zircon can form to record its temperature until the magma has sufficiently cooled or until the melt composition has evolved to make zircon a saturated phase. This means that much of a magma's cooling path is not recorded by these crystal temperatures. However, once zircon becomes saturated, it can continue to grow and record declining magma temperatures until the magma erupts. For zircons from the older three samples from Lake Creek stage (GR16-36, GR16-30, GR16-34), except for one analysis from GR16-30, the recorded temperatures do not extend as low as those recorded by younger zircons. This could mean that the older magmas did not reach temperatures as low as the younger magmas.

A caveat to the above interpretation is that most of the zircon analyses were on polished crystal interiors, which are biased toward earlier periods of crystallization when the magma may have been hotter. For the four samples (GR17-47A, GR17-75, GR17-71, GR17-78) for which zircon surfaces were analyzed in addition to polished interiors, the range of temperatures recorded by surfaces is offset to lower values than the range recorded by interiors. Therefore, in the case of the early Lake Creek magmatic system, there may once have been records of cooler temperatures in zircon rims that were subsequently lost to resorption when the crystals were entrained by magmas with zircon-undersaturated compositions. However, considering other evidence such as the trend toward more silicic compositions and a decrease in magnetite-ilmenite temperatures with time, I believe that these zircons preserve real evidence of a cooling upper crustal magmatic system.

Magnetite-ilmenite pairs connect zircon and amphibole information

Thermometry results from magnetite-ilmentite pairs and zircon for samples from middle to late Lake Creek stage are remarkably well aligned (Figure 4.14). The temporal resolution is only as good as the age of the sample, because Fe-Ti oxides diffuse so quickly, but the three samples GR17-47B, GR17-72A, and GR18-21 form a declining trend in time, with temperature ranges overlapping the zircon temperature estimates. This supports that the apparent cooling trend recorded by zircon is a meaningful indicator. The Fe-Ti oxide temperatures are not correlated with an increase in silica; conversely, sample GR18-21 is the least evolved of the trio.

The magnetite-ilmenite temperature data also correspond well with amphibole data. The amphibole temperatures recorded by late Lake Creek samples overlap the range of late Lake Creek oxide pairs. The amphibole temperatures are slightly elevated compared to zircons from that time period, but considering uncertainties of the thermometers, the multiple thermometers essentially yield indistinguishable results. This suggests that the magma reservoir system during this time was effectively homogenizing and stalling as opposed to a more disparate network of magma batches that mixed shortly before eruption. However, things appear to have changed by the start of Old Snowy Mountain stage. Interestingly, the sample GR18-21 (Lake Creek unit Qgrh) that records the lowest range of Fe-Ti oxide temperatures also contains amphibole that yield temperatures as high as those of Old Snowy Mountain (Figure 4.14). The oldest lava dated from Old Snowy Mountain, which follows the eruption of unit Qgrh by only ~15 kyr, contains magnetite-ilmenite pairs that record a higher range of temperatures, overlapping that of the amphibole. The compositions of GR18-21 and GR16-38 are very similar (Appendix X), and together they are intermediate between the main compositional clusters of Lake Creek and Old Snowy Mountain stage. This suggests that in the 10^4-10^5 year transition period between Lake Creek and Old Snowy Mountain volcanism, new input of hotter, more mafic magma was introduced to the system—at first disturbing a distinct, cooler reservoir ("mingled" assemblages of GR18-21), but soon more efficiently homogenizing (Fe-Ti oxide temperatures are more reset in GR16-38). Importantly, the zircons in GR16-38 still record temperatures as low as the preceding lake Creek samples, which suggests that the magmatic staging had not entirely shifted, but become more vertically stratified. As the geochronologic and bulk rock chemistry suggest for the Bear Creek Mountain and Lake Creek transition (Chapter 2), these mineral data support a model of a continuously active magmatic system between volcanic episodes.

Hf isotopic evidence for limited crustal assimilation

The Goat Rocks array (also including peripheral mafic volcanoes) extends over a relatively broad range of $^{176}Hf/^{177}Hf$, from High Cascades-like values to below the Simcoe-Adams IPB array, with no systematic relationship to $^{143}Nd/^{144}Nd$ or $^{87}Sr/^{86}Sr$ (Figure 4.11). Initially I was concerned that these results are erroneous and reflect contamination with a low-$^{176}Hf/^{177}Hf$ material (such as zircon) during sample preparation. However, several lines of evidence suggest that the low-$^{176}Hf/^{177}Hf$ trend records magma mixing with a crustal contaminant.

For samples from the same volcano, in most cases, the sample(s) with lower $^{176}Hf/^{177}Hf$ have higher Hf concentration (lower 1/Hf) as well as higher SiO_2. This is true for paired samples from the Devils Washbasin basalts, Tieton Peak volcano, Bear Creek Mountain, and several compositions from Lake Creek volcano (Figure X). This relationship suggests mixing with a Hf-enriched felsic composition with lower $^{176}Hf/^{177}Hf$. However, the vectors for each suite in 1/Hf vs $^{176}Hf/^{177}Hf$ do not converge on a clear endmember composition. This may reflect two possibilities. First, since Hf is a moderately incompatible element, Hf enrichment can be caused by fractional crystallization as well as mixing, such that the 1/Hf vs $^{176}Hf/^{177}Hf$ trend becomes steeper than by mixing alone. Second, there may be a variety of Hf-enriched mixing components with different Hf isotope ratios; for example, zircon-rich rocks of different ages.

A zircon-bearing rock is sensible as an assimilant given the mineral's composition as well as the evidence of inherited zircons in Goat Rocks samples. Since the element Hf behaves much like Zr, it is compatible in zircon—for example, the zircons analyzed in Goat Rocks samples generally have on the order of 10,000 ppm Hf (about 1%; Figure 4.3). Thus, a small amount of resorbed foreign zircon with distinct isotopic composition could significantly affect a magma's Hf isotope ratio without noticeably changing other isotopic ratios. As described in the results section, the zircon cargo provides proof of Goat Rocks magmas' interaction with old zircon-bearing basement rocks: several inherited zircons were dated in the ~55 Ma range, and one at ~177 Ma (Figure 4.1). The ~55 Ma zircons align in age with the Summit Creek basalts known to underlie the Goat Rocks area (~55-42 Ma; Vance et al., 1987), while the ~177 Ma zircon is a bit older than the Late Jurassic to Early Cretaceous age range of the Rimrock Lake Inlier (Miller, 1989)—within the realm of possibility that it was a detrital zircon in the Russell Ranch mélange. No Hf isotope data exist for zircons from Goat Rocks area basement rocks, but zircons from similar-aged terranes in the North Cascades provide some insight into the possible range of compositions. Zircons from that area with ages between 200 and 77 Ma have $^{176}Hf/^{177}Hf$ between ~0.2821 and ~0.2831 (Sauer et al., 2017), which is much lower than to overlapping with the Goat Rocks values. Therefore, the broad array of $^{176}Hf/^{177}Hf$ values represented by Goat Rocks magmas, in contrast to other High Cascades samples, is possibly explained by the unique regional basement. This hypothesis could be tested in the future with bulk-rock major and trace element and isotopic analyses of of the local basement units, and additional petrologic modelling with those compositions as mixing components.

Preliminary musings on andesite-dacite-rhyolite genesis

Only limited petrologic modeling was possible in the scope of this dissertation, but hypotheses about the petrogenesis of the Goat Rocks magmatic system can be constructed from multiple lines of geochemical evidence, to be properly tested in the future. First, isotopic evidence suggests that the ambient local basalts also fed the Goat Rocks composite volcanoes: their Sr, Nd, Hf, and Pb isotope ratios neatly overlap, except for minor outliers. The older eruptive deposits of Devils Horns rhyolite and Tieton Peak diverge slightly from the rest of the Goat Rocks suite (slightly higher Pb isotope ratios, and lower 176Hf/177Hf than most of the younger samples), which may indicate that the transcrustal magmatic system became more "mature" and overprinted by the mantle/basalt signature with time. If crustal melting/assimilation was contributing to magma genesis, it must have been limited (as suggested above, a whiff of zircon-bearing accreted terrane), and/or of a composition isotopically difficult to distinguish—perhaps slightly older igneous basement of a continuously evolving arc crust.

The thermodynamic modelling data are not yet sufficient to evaluate this, but the combined information from the local basalts and the mineral geothermobarometers lead me to hypothesize that the variability of Goat Rocks compositions over time are caused by changes in the flux of mantle melt delivery and/or the thermal state of the system. The compositional variability of the local basalts is limited, and the two slightly different CAB groups are represented across time and geography, essentially precluding a source difference as a cause of the major changes observed over time at the andesitic-dacitic Goat Rocks cluster. However, mineral thermometers provide clues about a thermally changing system. There are few data for the earlier stages of the system, but magnetite-ilmenite pairs from the Lost Lake andesite and Bear Creek Mountain record hotter temperatures than the samples from Lake Creek and Old Snowy Mountain stages. Zircon and magnetite-ilmenite pairs record a gradual decline in temperatures through the Lake Creek stage, and then a spectrum of crystallization temperatures are recorded by various minerals by the start of Old Snowy Mountain stage. The Bear Creek Mountain and Lake Creek volcanoes were voluminous edifices (Chapter 1), and there was significant basalt output during that time represented by the far-travelled Qob1 and Qob2 lava flows and the major shield volcano of Hogback Mountain. Lava flows from early Pleistocene to early Lake Creek time are commonly strikingly porphyritic, and have a restricted range in compositions that are relatively alkalic and trace element enriched, which may indicate a thermally sustained mushy reservoir with frequent recharge. During Old Snowy Mountain stage, compositions are varied in silica content and vents are distributed across a wide area (with small volcanoes along White Pass erupting similar compositions). For these reasons, I hypothesize that the mantle melt flux was at a climax during the Bear Creek Mountain to early Lake Creek stage, and the magmatic system was at its peak in size and its capability to capture, filter, and homogenize magmas. The thermal and mass input waned during Lake Creek stage, magmas were less enriched by recharge, and the system gradually cooled and waned. Deeper-staged, more mafic magmas began trickling through by the onset of Old Snowy Mountain stage, which may indicate a rejuvenating pulse of mafic input that has not yet thermally matured (the cycle beginning anew), or that the system had simply become too shriveled and diffusely organized to modify and filter compositions in the same way (death of the centralized system). There is abundant opportunity for future work to unveil these hidden processes.

CONCLUSIONS

The petrologic evolution of the Goat Rocks volcanic complex serves as a comparison to similar arc volcanic systems and represents a 3-million-year transcrustal transformation. A combination of zircon, Fe-Ti oxide, and amphibole thermobarometry data paint an image of a hot magmatic system between the early Pleistocene and Lake Creek time, gradual cooling during the Lake Creek stage, and a new influence of hotter, deeper magmas during Old Snowy Mountain stage. Sr, Nd, Hf, and Pb isotopes of the andesitic to rhyolitic compositions compared to local basalts indicate that crustal assimilation played a limited or cryptic role, and that the narrow variety of basalt compositions did not drive the major compositional changes that occurred. The present understanding is that the evolution of Goat Rocks records a cycle of waxing and waning magmatic flux, at its thermal and volumetric peak during the Bear Creek Mountain to early Lake Creek stage. A remarkably diverse array of arc magmatism can apparently be achieved by the self-organization of a limited range of mantle and crustal inputs.

TABLES

Table 4.1. Zircon age and composition data.

										Element concentration (ppm)														
Sample no.	$^{40}Ar/^{39}Ar$ age (Ma)	$^{40}Ar/^{39}Ar$ Age unc. (2σ, Ma)	Zircon wt. mean age (Ma)	Zircon age unc. (2σ, Ma)	Spot ID	Surface (S) or polished interior (I)	Used in wt. mean age	^{230}Th-corr. $^{206}Pb/^{238}U$ Age (Ma)	1σ error	48Ti	Fe	Y	La	Ce	Nd	Sm	Eu	Gd	Dy	Er	Yb	Hf	Ti-in-zircon temp. (°C) (a_{TiO2}=0.6)
GR16-38	0.440	± 0.003	0.453	± 0.008	GR16-38-7.1	I	Y	0.41	0.01	5.1	1.32	2034	0.012	53	1.33	3.8	0.42	37	164	311	613	10972	730
					GR16-38-1.1	I	Y	0.42	0.01	3.8	0.06	3383	0.009	131	2.19	7.2	1.00	67	293	511	952	10264	704
					GR16-38-5.1	I	Y	0.44	0.02	3.6	1.64	1814	**0.340**	55	7.37	7.1	1.56	48	200	318	581	5729	700
					GR16-38-8.1	I	Y	0.44	0.01	5.4	0.94	1574	0.034	44	1.02	3.3	0.38	26	132	232	456	8641	737
					GR16-38-2.1	I	Y	0.45	0.02	3.1	0.08	2242	0.009	44	1.35	4.7	0.77	49	203	331	569	10009	688
					GR16-38-6.1	I		0.46	0.01	4.2	0.10	2139	0.008	29	1.65	5.7	1.41	46	189	335	633	7593	712
					GR16-38-9.1	I		0.53	0.04	3.8	0.07	662	0.007	15	0.39	1.2	0.30	10	53	111	255	8771	704
					GR16-38-3.1	I		0.58	0.02	3.8	0.12	910	0.008	12	0.86	2.8	0.55	21	92	167	355	9780	705
					38-8.1	I	Y	0.47	0.01	5.6	3.88	2542	0.094	77.4	2.13	6.3	0.64	57.2	240	437	847	10968	739
					38-1.1	I	Y	0.48	0.01	4.1	0.09	2306	0.019	91.6	2.10	6.0	0.78	54.0	218	403	767	10745	712
					38-3.1	I	Y	0.48	0.01	8.6	**25.30**	4049	**0.573**	75.1	6.67	14.8	3.11	121.4	452	773	1387	9275	781
					38-2.1	I		0.57	0.03	3.7	0.22	550	0.015	12.4	0.40	1.0	0.26	9.2	45	100	220	10561	701
					38-7.1	I		0.56	0.02	4.6	0.47	1643	0.026	51.2	1.50	3.9	0.79	36.5	148	288	614	13078	721
					38-5.1	I		0.59	0.09	5.3	**20.94**	2567	0.094	59.0	1.76	5.2	0.46	50.0	228	460	954	13811	734
					38-4.1	I		0.65	0.03	4.6	0.04	604	0.020	14.5	0.53	1.3	0.30	10.2	49	110	244	10879	721
					38-6.1	I		0.73	0.03	7.4	0.04	1001	0.017	16.5	1.26	2.8	0.44	24.5	99	174	310	10761	766
GR16-30	0.969	± 0.004	0.987	± 0.057	GR16-30-5.1	I	Y	0.80	0.07	19.1	0.10	526	0.007	6	0.59	1.6	0.29	12	48	83	153	8281	868
					GR16-30-4.1	I	Y	0.87	0.13	25.1	0.08	1091	0.011	10	3.30	5.6	1.01	32	104	157	249	7163	901
					GR16-30-9.1	I	Y	0.97	0.08	21.7	0.52	701	0.010	10	1.19	2.7	0.40	19	68	108	183	7813	882
					GR16-30-8.1	I	Y	1.00	0.07	25.0	0.06	992	0.011	9	2.97	5.5	0.90	30	103	144	227	7374	900
					GR16-30-1.2	I	Y	0.99	0.23	16.6	0.09	381	0.007	6	0.31	1.0	0.15	7	34	60	112	8309	851
					GR16-30-3.1	I	Y	0.99	0.24	16.2	1.56	835	0.014	11	1.25	3.2	0.47	23	82	123	195	7501	848
					GR16-30-6.1	I	Y	1.04	0.07	5.1	0.03	449	0.006	14	0.17	0.6	0.07	7	37	73	142	12455	731
					GR16-30-1.1	I	Y	1.07	0.07	19.4	1.28	662	0.009	8	0.81	2.5	0.41	17	64	101	165	8650	869
					GR16-30-7.1	I	Y	1.08	0.07	16.6	2.49	613	0.006	7	1.03	2.4	0.33	15	60	99	170	8236	851
					GR16-30-11.1	I		1.13	0.03	19.5	0.78	4362	0.015	21	4.70	10.4	2.24	108	403	596	875	7904	870
GR17-78	0.115	± 0.004	0.107	± 0.005	78-5.1	I		0.03	0.02	16.5	4.5	1280	0.044	27.7	1.41	3.5	3.04	36	130	217	415	7235	851
					78-13.1	I		0.07	0.01	8.7	1.9	1374	0.019	8.8	0.93	2.4	1.59	30	135	209	380	7657	782
					78-4.1	I	Y	0.09	0.02	2.8	0.3	927	0.017	5.5	0.49	1.7	0.77	17	85	162	343	8790	679
					78-2.1	I	Y	0.10	0.00	8.9	1.2	1854	0.029	15.4	1.28	4.7	2.42	49	196	299	527	8069	784
					78-15.1	I	Y	0.11	0.01	9.1	2.4	2143	0.081	19.6	2.84	6.7	3.44	52	194	362	687	6881	787
					78-16.1	I	Y	0.11	0.01	7.1	3.3	1374	0.030	15.3	1.68	5.9	3.42	48	149	214	365	7187	762
					78-17.1	I	Y	0.13	0.01	6.7	3.0	1371	**0.292**	13.5	7.01	11.8	6.06	61	161	209	359	7329	756
					78-18.1	I		1.7	0.1	8.3	0.3	680	0.013	9.8	0.39	1.2	0.80	13	58	125	278	8657	777
					78-10.1	I		1.9	0.1	5.2	0.7	729	0.019	11.8	0.68	1.9	1.09	16	65	130	275	7764	733
					78-7.1	I		7.6	0.4	4.4	0.2	343	0.022	4.7	0.34	1.1	0.53	8	33	59	126	9023	718

Table 4.1 (continued)

			78-11.1	I		7.9	0.1	4.1	1.8	449	0.024	8.4	0.27	0.9	0.46	9	41	77	164	10845	712
			78-8.1	I		11.8	0.2	5.6	0.2	1018	0.019	14.5	0.67	2.1	1.24	21	91	180	377	8495	739
			78-9.1	I		12.6	0.3	6.6	2.1	2326	**0.214**	6.6	0.68	3.0	0.75	36	215	421	878	10881	755
			78-6.1	I		53.8	0.8	3.3	0.5	4166	0.068	18.1	3.36	9.5	1.63	100	451	771	1230	9331	692
			78-14.1	I		54.1	1.1	5.5	1.6	4572	**0.729**	23.6	3.94	11.6	1.57	116	511	846	1318	9674	737
			78-1.1	I		55.5	2.0	4.9	2.9	2819	**0.117**	12.8	2.15	6.9	1.12	69	307	515	833	8959	728
			78-12.1	I		56.6	1.2	7.7	0.2	2485	0.044	8.2	1.46	4.7	1.25	51	269	459	735	9106	770
			78-3.1	I		177	3	13.2	0.2	794	0.016	11.4	0.43	1.5	0.16	14	74	140	264	11792	826
			78-7.1	S	Y	0.04	0.04	7.3	1.44	1149	0.007	25.2	1.61	3.7	2.34	28.5	107	203	416	7379	764
			78-2.1	S	Y	0.12	0.01	5.5	3.15	5265	0.010	19.6	4.18	13.8	2.78	133.8	542	928	1589	7935	737
			78-5.1	S	Y	0.15	0.02	12.9	**8.58**	2281	0.093	59.2	13.93	20.4	12.20	106.5	259	387	604	6401	823
			78-4.1	S	Y	0.19	0.08	4.8	**9.86**	479	0.006	2.3	0.51	1.3	0.60	11.1	42	76	157	5723	725
			78-8.1	S		7.52	0.32	2.2	0.23	544	0.006	10.8	0.28	1.0	0.55	9.8	43	98	234	10275	660
			78-6.1	S		7.53	0.30	3.3	0.92	571	0.005	9.0	0.48	1.2	0.69	11.7	49	101	223	7940	693
GR17-72A	0.663 ± 0.003	0.742 ± 0.017	72A-7.1	I	Y	0.70	0.02	6.3	0.08	776	**0.925**	19.4	0.68	1.7	0.23	16	75	141	264	10686	751
			72A-11.1	I	Y	0.69	0.04	8.8	0.01	1861	0.086	18.9	2.82	6.3	1.69	53	202	324	538	7795	783
			72A-5.1	I	Y	0.72	0.04	4.9	0.01	539	0.017	12.4	0.24	0.8	0.16	10	49	98	191	10228	728
			72A-15.1	I	Y	0.72	0.03	6.6	0.02	615	0.015	12.1	0.40	1.3	0.21	12	58	107	203	8805	754
			72A-9.1	I	Y	0.73	0.04	5.9	0.01	709	0.019	16.7	0.39	1.4	0.25	13	66	128	249	10497	744
			72A-12.1	I	Y	0.75	0.03	6.4	0.01	810	0.009	15.7	0.43	1.5	0.27	15	74	150	295	10119	752
			72A-1.1	I	Y	0.75	0.04	7.4	0.01	1348	0.038	18.4	1.55	4.5	0.64	35	140	236	399	9988	766
			72A-10.1	I	Y	0.76	0.05	7.1	0.02	1314	**0.212**	15.0	1.26	3.9	0.67	32	133	235	392	9971	762
			72A-6.1	I	Y	0.76	0.04	6.1	0.35	1403	0.041	22.6	1.32	4.4	0.63	37	150	254	436	9808	748
			72A-13.1	I	Y	0.76	0.03	10.5	0.02	1566	0.083	15.0	2.49	5.6	1.10	43	166	276	462	9074	801
			72A-16.1	I	Y	0.77	0.02	6.8	0.47	1500	**0.800**	25.3	1.72	4.5	0.65	38	152	265	451	10500	758
			72A-3.1	I		0.84	0.02	8.5	4.84	1215	0.046	14.1	1.53	4.4	0.79	34	127	210	354	9335	779
			72A-2.1	I		1.05	0.09	13.5	0.01	456	0.016	8.1	0.37	1.2	0.18	10	45	80	146	9653	828
GR17-71	0.443 ± 0.01	0.443 ± 0.01	71-13.1	I	Y	0.39	0.17	3.4	0.08	359	0.076	2.5	0.22	0.7	0.24	6	32	63	134	7582	696
			71-9.1	I	Y	0.43	0.01	2.8	0.14	1434	0.032	20.2	0.79	2.5	0.38	26	129	261	550	10260	678
			71-5.1	I	Y	0.44	0.01	6.3	2.97	1817	**4.125**	46.1	1.66	4.0	0.59	37	171	328	662	9256	751
			71-2.1	I	Y	0.46	0.01	3.3	0.02	1592	0.026	45.7	0.96	3.2	0.41	33	153	279	570	11109	692
			71-10.1	I	Y	0.47	0.02	8.6	0.11	1115	0.025	25.6	0.49	1.5	0.64	14	84	208	457	8493	780
			71-3.1	S	Y	0.43	0.02	2.6	0.21	1487	0.005	23.4	1.09	2.9	0.66	29.0	130	265	537	7226	673
			71-1.1	S	Y	0.44	0.01	3.1	0.28	1755	0.008	31.1	1.22	3.2	0.72	32.0	152	316	654	8116	688
			71-2.1	S	Y	0.45	0.03	2.7	0.07	721	0.007	12.0	0.50	1.6	0.41	15.7	67	124	241	9548	677
			71-4.1	S	Y	0.57	0.06	2.2	0.66	513	0.017	10.8	0.34	0.9	0.20	9.0	43	92	203	10754	661
GR16-34	0.820 ± 0.003	0.874 ± 0.03	34-2.1	I	Y	0.84	0.05	14.5	0.01	791	0.016	9.2	0.85	2.7	0.41	22	83	135	222	9165	836
			34-3.1	I	Y	0.83	0.02	8.4	1.96	1963	**11.363**	57.5	6.34	8.2	0.66	59	212	337	564	9363	778
			34-6.1	I	Y	0.90	0.04	12.3	0.02	503	0.021	10.6	0.32	1.2	0.18	11	50	90	166	9722	818
			34-10.1	I	Y	0.90	0.05	18.6	0.01	743	0.021	8.2	0.98	2.7	0.49	22	80	125	209	8832	864
			34-9.1	I	Y	0.90	0.03	14.3	2.07	4166	**0.325**	49.9	7.74	20.3	2.50	152	490	707	1034	8860	834
			34-4.1	I	Y	0.93	0.04	1036.6	**311.78**	962	**0.394**	12.4	1.60	3.8	0.47	28	105	165	270	9542	1667

Table 4.1 (continued)

			34-8.1	I		0.95	0.07	15.7	0.65	866	0.041	9.0	1.21	3.3	0.56	26	95	148	244	9063	845
			34-1.1	I		0.97	0.05	18.4	0.16	757	0.029	8.2	1.39	3.3	0.55	25	85	131	208	8724	863
GR17-47A	0.812 ± 0.004	0.817 ± 0.024	47a-1.1	I	Y	0.69	0.10	17.3	0.00	904	0.026	8.9	1.48	3.9	0.59	29	101	152	247	8327	856
			47A-13.1	I	Y	0.79	0.03	8.4	0.01	540	0.015	10.0	0.38	1.1	0.15	11	52	95	183	9639	779
			47A-15.1	I	Y	0.81	0.03	8.8	0.20	1710	**0.318**	42.0	1.73	4.8	0.54	42	175	296	501	8284	783
			47a-11.1	I	Y	0.83	0.05	10.6	0.02	362	0.012	8.8	0.17	0.7	0.11	7	33	64	124	9483	802
			47A-5.1	I	Y	0.83	0.07	18.2	0.26	672	0.083	7.5	1.25	3.1	0.54	20	75	117	201	8162	862
			47A-6.1	I	Y	0.84	0.04	14.4	0.01	782	0.020	9.0	0.87	2.6	0.42	22	83	132	219	8968	835
			47A-14.1	I	Y	0.84	0.04	10.9	0.27	804	0.072	11.8	0.64	2.3	0.32	21	83	139	235	9041	805
			47A-7.1	I	Y	0.86	0.03	10.5	0.01	568	0.013	12.4	0.46	1.5	0.21	13	55	99	183	9374	801
			47A-2.1	I		0.93	0.02	11.0	0.12	1110	0.046	13.6	1.66	4.2	0.42	31	118	183	307	9493	806
			47A-11.2	I	Y	0.95	0.54	23.4	3.14	407	**1.266**	8.7	0.61	1.2	0.17	10	40	71	129	8691	892
			47AI-4.1	S	Y	0.74	0.05	10.0	0.06	843	0.006	10.2	0.95	2.7	0.40	22.9	86	146	243	9168	796
			47AI-7.1	S	Y	0.81	0.03	4.7	0.04	1139	0.005	25.1	0.81	2.3	0.19	23.3	106	198	353	12421	723
			47AI-2.1	S	Y	0.85	0.08	5.8	0.05	797	0.075	12.0	0.50	1.3	0.28	15.9	72	133	234	8255	742
			47AI-3.1	S	Y	0.88	0.07	6.7	0.03	979	0.004	15.3	0.77	2.5	0.34	23.4	95	167	287	9657	756
			47AI-1.1	S	Y	0.90	0.03	7.9	0.03	800	0.004	11.4	0.81	2.2	0.33	18.8	80	141	240	9088	772
			47AI-6.1	S		1.16	0.10	17.0	0.02	516	0.004	6.7	0.49	1.4	0.29	13.2	50	87	148	8279	854
			47AI-5.1	S		3.69	0.39	9.8	0.55	906	**0.371**	14.3	1.35	2.5	0.36	22.0	92	158	269	9451	794
GR17-75	0.559 ± 0.005	0.600 ± 0.029	75-3.1	I	Y	0.65	0.02	5.8	0.01	632	0.012	13.5	0.36	1.5	0.27	13	61	113	219	9894	743
			75-5.1	I	Y	0.64	0.04	5.2	0.27	2171	**0.119**	44.0	3.52	8.1	1.95	62	232	387	679	8063	733
			75-6.1	I	Y	0.68	0.10	6.7	-0.01	899	**0.284**	21.3	0.77	2.0	0.44	19	89	163	305	10226	756
			75-2.1	I	Y	0.69	0.03	5.4	0.01	614	0.022	15.4	0.32	1.3	0.22	12	57	112	221	10144	736
			75-10.1	I	Y	0.70	0.03	5.8	0.01	579	0.016	11.9	0.30	1.0	0.19	12	53	106	211	10309	743
			75-8.1	I	Y	0.68	0.02	10.7	0.12	3122	**1.059**	58.0	5.20	12.7	3.30	101	362	549	877	8266	803
			75-9.1	I	Y	0.71	0.03	5.4	0.01	878	0.012	15.1	0.39	1.8	0.28	18	87	159	278	10699	737
			75-4.1	I	Y	0.71	0.03	5.2	0.02	812	0.072	18.6	0.54	1.8	0.34	17	77	148	288	10289	733
			75-1.1	I	Y	0.84	0.10	11.9	1.08	1616	**0.302**	14.1	2.12	5.3	0.97	43	178	277	471	8963	814
			75I-1.1	S	Y	0.50	0.10	2.6	0.37	581	0.013	9.2	0.65	1.5	0.38	12.6	48	91	182	5947	672
			75I-9.1	S	Y	0.58	0.04	3.5	3.25	942	0.004	13.5	1.23	2.9	0.70	22.0	84	165	333	9290	696
			75I-8.1	S	Y	0.59	0.03	4.1	0.06	1133	0.005	16.6	1.41	3.1	0.70	27.5	107	205	384	10296	712
			75I-7.1	S	Y	0.59	0.02	3.0	0.10	1166	0.005	15.5	1.49	3.3	0.80	26.8	106	210	423	10250	686
			75I-4.1	S	Y	0.60	0.05	3.8	0.08	1071	0.010	15.3	1.24	2.9	0.68	26.5	102	189	354	9325	704
			75I-3.1	S	Y	0.62	0.09	3.6	0.31	922	0.010	13.7	0.93	2.4	0.61	20.9	83	160	319	9549	700
			75I-2.1	S	Y	0.63	0.04	3.5	0.10	1238	0.011	17.3	1.39	3.6	0.72	29.2	114	216	419	9664	697
			75I-6.1	S	Y	0.65	0.06	6.9	**12.17**	696	**18.873**	60.0	16.28	3.8	0.62	17.3	61	124	258	9545	758
			75I-5.1	S	Y	0.67	0.17	3.1	0.32	841	0.044	14.7	0.93	2.2	0.50	18.9	72	144	276	8014	688
			75I-10.1	S		0.77	0.05	4.4	1.39	1065	0.004	17.8	0.71	2.4	0.44	23.6	102	184	327	9932	717
GR16-36	1.11 ± 0.01	1.11 ± 0.03	36-12.1	I		0.78	0.09	20.0	0.11	385	0.011	6.0	0.47	1.2	0.21	9.8	39	67	115	8877	873
			36-6.1	I	Y	1.09	0.03	33.8	0.02	1800	0.076	12.7	5.04	8.2	1.08	59.2	195	289	424	7910	939
			36-10.1	I	Y	1.09	0.02	30.6	0.01	2110	0.070	11.2	4.61	8.4	1.49	66.5	227	353	523	7827	926
			36-1.1	I	Y	1.10	0.07	38.3	0.01	1395	0.084	9.2	4.40	6.0	1.20	41.7	143	222	334	7739	956

Table 4.1 (continued)

36-9.1	I	Y	1.10	0.05	28.9	0.03	1369	0.039	10.9	3.82	7.1	1.08	48.5	154	224	333	8236	918
36-7.1	I	Y	1.11	0.06	32.3	1.17	1285	**0.153**	10.0	3.63	5.5	1.07	43.2	141	209	326	7671	933
36-4.1	I	Y	1.12	0.02	24.4	2.25	2810	0.099	17.8	5.69	12.3	1.63	100.5	315	465	699	7507	897
36-3.1	I	Y	1.16	0.08	36.2	3.10	644	**0.166**	6.4	2.57	3.8	0.74	22.9	69	100	152	7344	948
36-11.1	I	Y	1.20	0.05	19.7	0.04	800	0.014	11.2	1.36	2.6	0.42	21.1	79	137	235	7901	871
36-5.1	I		2.56	0.08	13.8	0.09	675	0.022	10.5	1.13	2.5	0.45	18.1	66	116	200	9121	830
36-8.1	I		2.65	0.11	20.9	0.12	527	0.013	9.3	0.86	1.8	0.47	14.7	54	91	159	8442	878
36-2.1	I		28.22	0.51	5.2	0.77	905	0.012	38.0	0.58	1.6	0.90	15.1	72	166	406	9804	733

Table 4.2. Compositions and zircon saturation temperatures of samples analyzed for zircon.

Sample no.	Time period	Zircon sat. temp. (°C)	Bulk rock M	SiO_2 (wt%)	Zr (ppm)	Y (ppm)	Hf (ppm)
GR17-78	OSM	687	1.8	63.1	147	16.0	3.9
GR16-38	OSM	671	2.0	61.0	162	17.3	4.1
GR17-71	OSM	727	1.4	75.5	139	14.2	4.2
GR17-75	late LC	722	1.7	68.0	185	18.1	5.0
GR17-72A	late LC	710	1.8	64.3	196	21.8	5.1
GR17-47A	mid LC	725	1.8	64.5	225	23.1	5.8
GR16-34	early LC	729	1.9	62.6	273	24.1	6.7
GR16-30	early LC	767	1.9	64.1	357	29.2	8.8
GR16-36	early LC	731	2.1	61.2	320	28.3	7.7

Table 4.3. Sr, Nd, Hf, and Pb isotopic ratios of Goat Rocks area intermediate to felsic magmas.

Sample ID	Analysis ID	Rock class.	Latitude	Longitude	Unit	Age (ka) ±2σ	Age bin	$^{87}Sr/^{86}Sr$ ± 2 SE	$^{143}Nd/^{144}Nd$ ± 2 SE	$^{176}Hf/^{177}Hf$ ± 2 SE	$^{208}Pb/^{204}Pb$ ± 2 SE	$^{207}Pb/^{204}Pb$ ± 2 SE	$^{206}Pb/^{204}Pb$ ± 2 SE
Old Snowy Mountain stage													
GR18-14D	GR18-14D	Dac	46.6586	-121.3573	Qdwp	113 ± 4	0.0-0.2	0.703511 0.000008	0.512922 0.000006	0.283068 0.000005	38.5742 0.0022	15.5845 0.0009	18.9037 0.0010
GR17-78	GR17-78-rep	Dac	46.6791	-121.5480	Qacf	115 ± 4	0.0-0.2	0.703598 0.000007	0.512918 0.000006	0.283062 0.000003	38.6121 0.0020	15.5883 0.0008	18.9319 0.0009
GR18-07	GR18-07	And	46.6340	-121.3307	Qarn		0.0-0.2	0.703603 0.000008	0.512932 0.000007	0.283058 0.000005	38.6305 0.0019	15.5907 0.0007	18.9565 0.0007
GR17-66	GR17-66	And	46.4814	-121.5150	Qag		0.2-0.4	0.703639 0.000008	0.512915 0.000006	0.283063 0.000003	38.6832 0.0020	15.5939 0.0008	18.9817 0.0008
GR16-19	GR16-19	And	46.4999	-121.4550	Qao		0.2-0.4	0.703247 0.000007	0.512951 0.000005	0.283056 0.000004	38.4355 0.0025	15.5640 0.0010	18.8112 0.0011
GR16-19	GR16-19 Re	And	46.4999	-121.4550	Qao		0.2-0.4		0.512964 0.000006		38.4334 0.0021	15.5630 0.0008	18.8102 0.0009
GR16-25	GR16-25	Dac	46.5063	-121.4556	Qao	217 ± 5	0.2-0.4	0.703467 0.000008	0.512921 0.000008	0.283081 0.000005	38.5470 0.0026	15.5779 0.0009	18.8802 0.0010
GR16-25	GR16-25 re	Dac	46.5063	-121.4556	Qao	217 ± 5	0.2-0.4	0.703467 0.000008	0.512932 0.000006	0.283081 0.000005	38.5470 0.0026	15.5779 0.0009	18.8802 0.0010
GR16-38	GR16-38	And	46.5188	-121.4747	Qao	440 ± 3	0.4-0.6	0.703672 0.000008	0.512905 0.000006	0.283051 0.000004	38.6652 0.0020	15.5982 0.0008	18.9705 0.0010
GR17-71	GR17-71	Rhy	46.4866	-121.5400	Qrg	443 ± 10	0.4-0.6	0.703510 0.000008	0.512940 0.000008	0.283062 0.000005	38.6163 0.0028	15.5910 0.0010	18.9597 0.0012
Lake Creek stage													
GR15-04	GR15-04	Dac	46.5492	-121.5322	Qgr4	593 ± 4	0.4-0.6	0.704204 0.000010	0.512927 0.000010	0.283062 0.000007	38.6293 0.0029	15.5942 0.0011	18.9640 0.0012
GR17-77A	GR17-77A	Bas And	46.5523	-121.5416	Qgr3	735 ± 12	0.6-0.8	0.703650 0.000007	0.512914 0.000005	0.283074 0.000004	38.6265 0.0020	15.5911 0.0008	18.9497 0.0009
GR17-47A	GR17-47A	Dac	46.4916	-121.4241	Qdbt	812 ± 4	0.8-1.0	0.703436 0.000008	0.512945 0.000006	0.283061 0.000004	38.5729 0.0019	15.5838 0.0007	18.9343 0.0008
GR16-30	GR16-30	Dac	46.5184	-121.4944	Qgr2	969 ± 4	0.8-1.0	0.703451 0.000008	0.512945 0.000006	0.283045 0.000004	38.6111 0.0021	15.5891 0.0008	18.9661 0.0009
GR16-30	GR16-30 Re	Dac	46.5184	-121.4944	Qgr2	969 ± 4	0.8-1.0			0.283048 0.000004			
Bear Creek Mountain stage													
GR16-05	GR16-05	And	46.7297	-120.8129	Qta2	1390 ± 100	1.0-1.5	0.703373 0.000009	0.512951 0.000007	0.283055 0.000005	38.5763 0.0021	15.5844 0.0008	18.9319 0.0009
GR16-05	GR16-05 re	And	46.7297	-120.8129	Qta2	1390 ± 100	1.0-1.5	0.703373 0.000009	0.512955 0.000007	0.283058 0.000004	38.5752 0.0020	15.5841 0.0007	18.9310 0.0007
GR16-01	GR16-01	And	46.6675	-120.6467	Qta1	1640 ± 70	1.5-2.0	0.703404 0.000007	0.512946 0.000006	0.282996 0.000005	38.5755 0.0019	15.5844 0.0008	18.9272 0.0009
GR16-01	GR16-01 Dup	And	46.6675	-120.6467	Qta1	1640 ± 70	1.5-2.0	0.703401 0.000008	0.512944 0.000006	0.282986 0.000004	38.6450 0.0019	15.5866 0.0007	18.9566 0.0010
Tieton Peak stage													
GR20-15	GR20-15	And	46.5122	-121.3952	Tatp	2651 ± 38	2.5-3.0	0.703519 0.000009	0.512910 0.000007	0.283031 0.000004	38.6326 0.0020	15.5987 0.0008	18.9770 0.0010
GR20-15	GR20-15 dup	And	46.5122	-121.3952	Tatp	2651 ± 38	2.5-3.0	0.703517 0.000009	0.512909 0.000006	0.283030 0.000005	38.6356 0.0018	15.5998 0.0007	18.9786 0.0008
GR20-15	GR20-15 rep	And	46.5122	-121.3952	Tatp	2651 ± 38	2.5-3.0	0.703517 0.000009	0.512909 0.000006	0.283030 0.000005	38.6356 0.0018	15.5998 0.0007	18.9786 0.0008
TP19-06	TP19-06	And	46.4898	-121.3654	QTa	3081 ± 7	3.0-3.5	0.703670 0.000008	0.512917 0.000006	0.283014 0.000004	38.6810 0.0018	15.6075 0.0007	19.0234 0.0008
Pre-Goat Rocks: Devils Horns Rhyolite													
TP19-08	TP19-08	Rhy	46.4916	-121.3516	Tpr	3190 ± 20	3.0-3.5	0.703935 0.000008	0.512878 0.000007	0.283012 0.000004	38.6638 0.0019	15.6050 0.0007	19.0005 0.0009

FIGURES

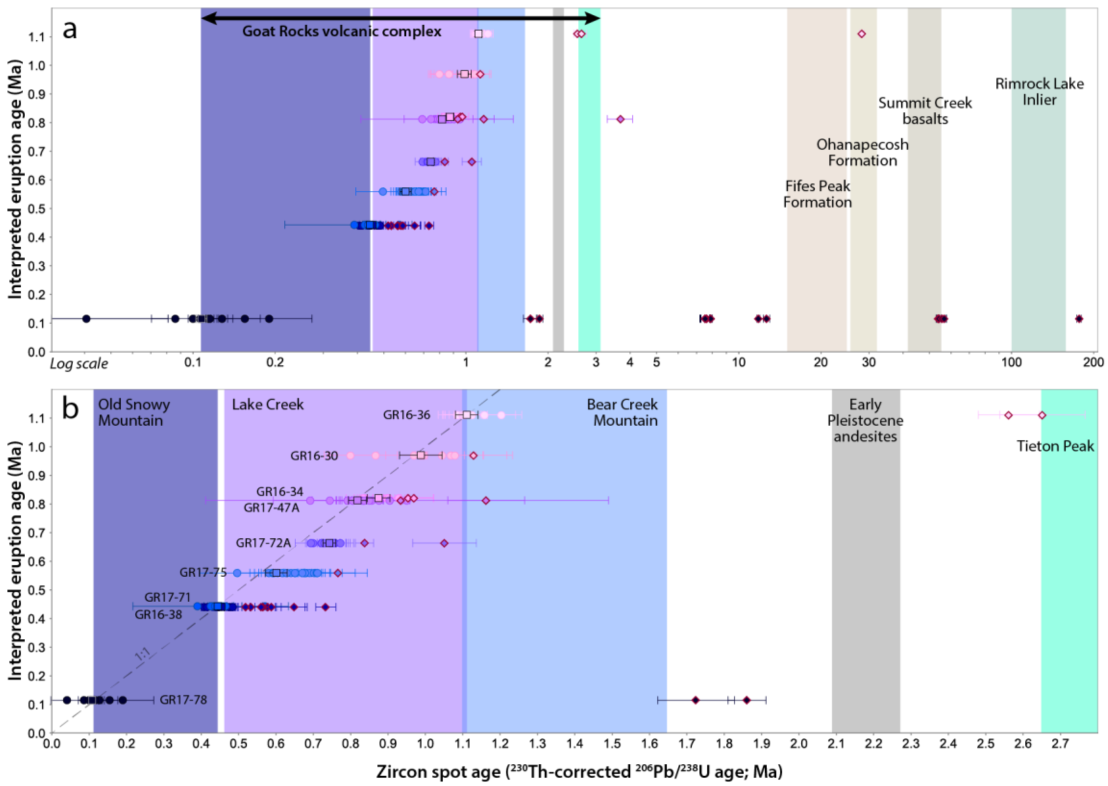

Figure 4.1. Individual spot ages of zircons plotted against interpreted eruption age of samples. **a)** All zircons, including those that define a coherent population of most recent crystallization (round symbols), in addition to antecrysts and xenocrysts (diamond symbols with red borders). Spot ages are plotted on a logarithmic scale. Error bars for spot ages show 1σ uncertainty. Square symbols with black border indicate weighted mean age of youngest zircon population (error bars for these show 2σ uncertainty). Colored bars indicate age range of Goat Rocks eruptive periods or basement rock units. **b)** The same data as in **a**, but zoomed in to show only zircons with ages within the lifespan of the Goat Rocks volcanic complex. A 1:1 line is plotted to highlight where zircon weighted mean ages are slightly older than $^{40}Ar/^{39}Ar$ ages, for example, samples GR17-72A and GR16-34.

Figure 4.2. Concentrations of select elements in Goat Rocks zircons over time. Individual spot analyses are plotted, including antecrysts in the Lake Creek to Old Snowy Mountain age range. a) Ti concentration decreases over time, particularly for zircons from early to middle Lake Creek stage. b) In general, the range of Y concentration in zircon extends to higher values with time. Crystals from sample GR16-36 are outliers in this trend, being relatively high in early Lake Creek time. c) Hf concentrations show a similar trend to Y concentrations: the range increases between zircons from early Lake Creek to early Old Snowy Mountain stage. Zircons from the Clear Fork lava have a more restricted range at lower Hf concentration.

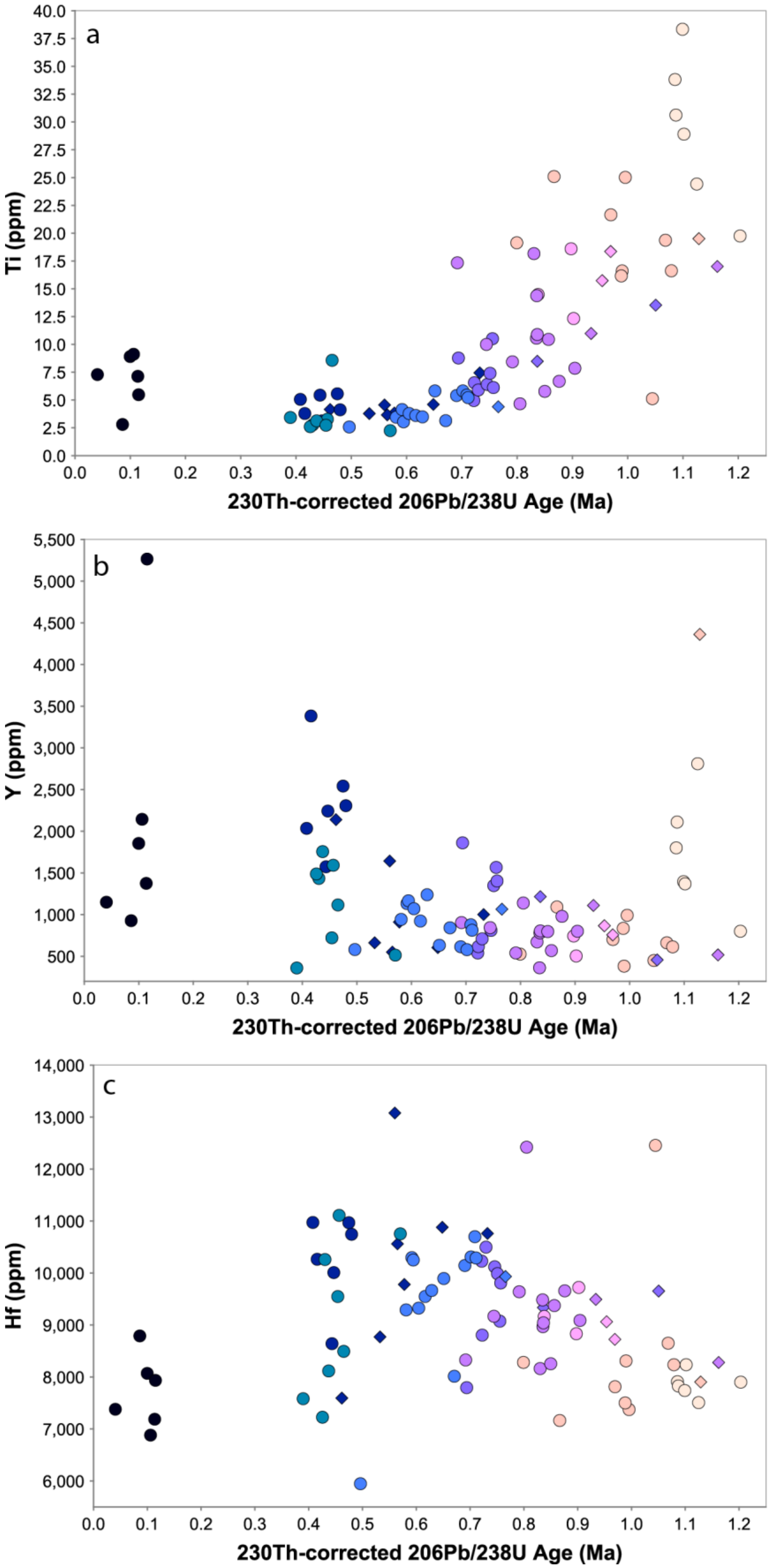
a
Ti (ppm)
230Th-corrected 206Pb/238U Age (Ma)
b
Y (ppm)
230Th-corrected 206Pb/238U Age (Ma)
c
Hf (ppm)
230Th-corrected 206Pb/238U Age (Ma)

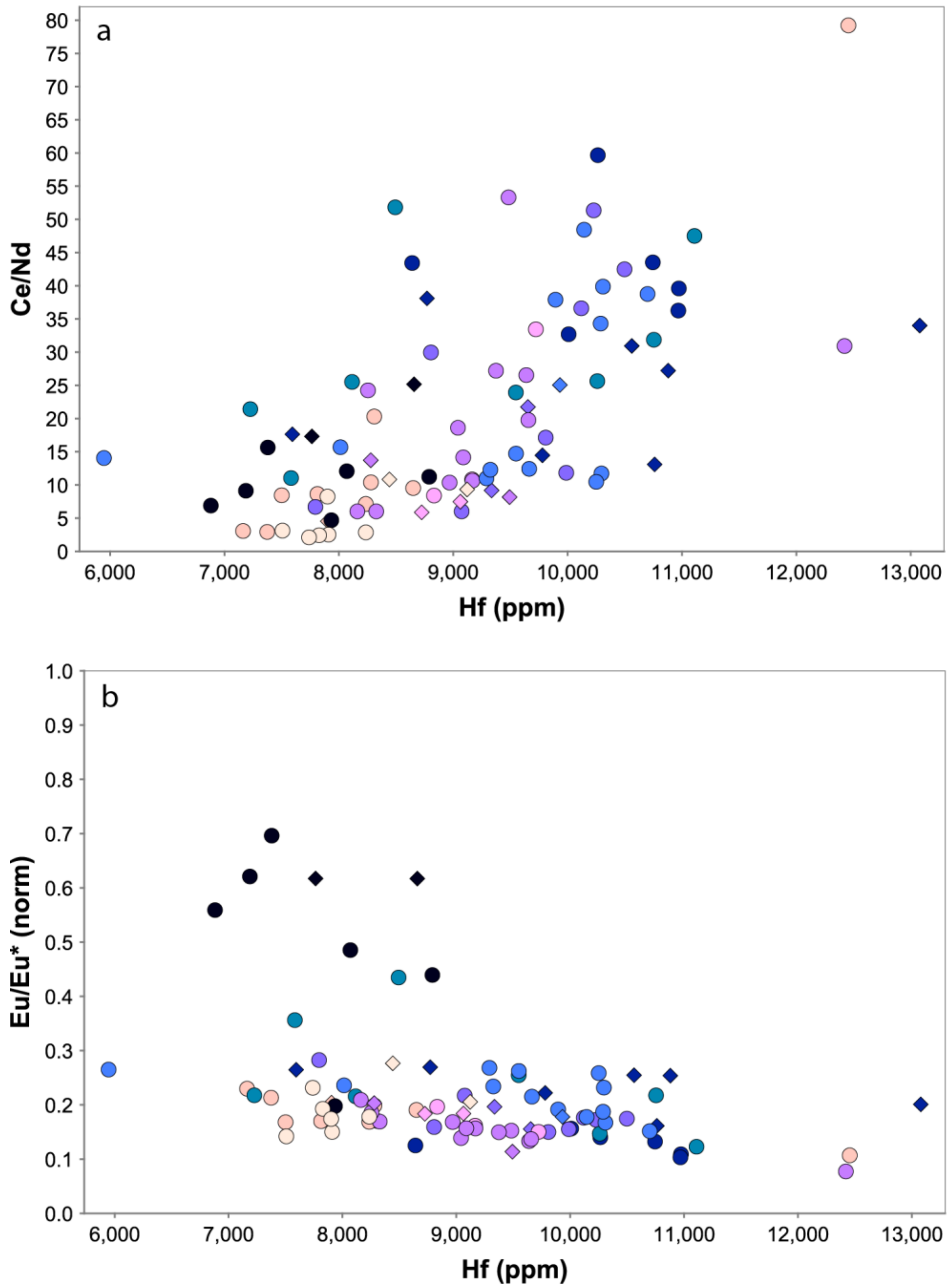

Figure 4.3. REE ratios plotted against Hf concentration.
Increasing Hf is a proxy for magma differentiation/fractional crystallization. a) Ce/Nd, a proxy for Ce/Ce*, since low La concentrations make the latter calculation difficult. Relatively low Ce/Nd for these zircons indicate typical oxidation state for arc andesites and dacites (as opposed to values <60 expected for oxidized, ore-forming magmas. b) Eu/Eu* normalized to chondrite values (Taylor and McLennan, 1985). Note much higher Eu/Eu* for zircons in the Clear Fork lava, suggesting limited plagioclase crystallization (supported by a lack of plagioclase in hand sample and thin section).

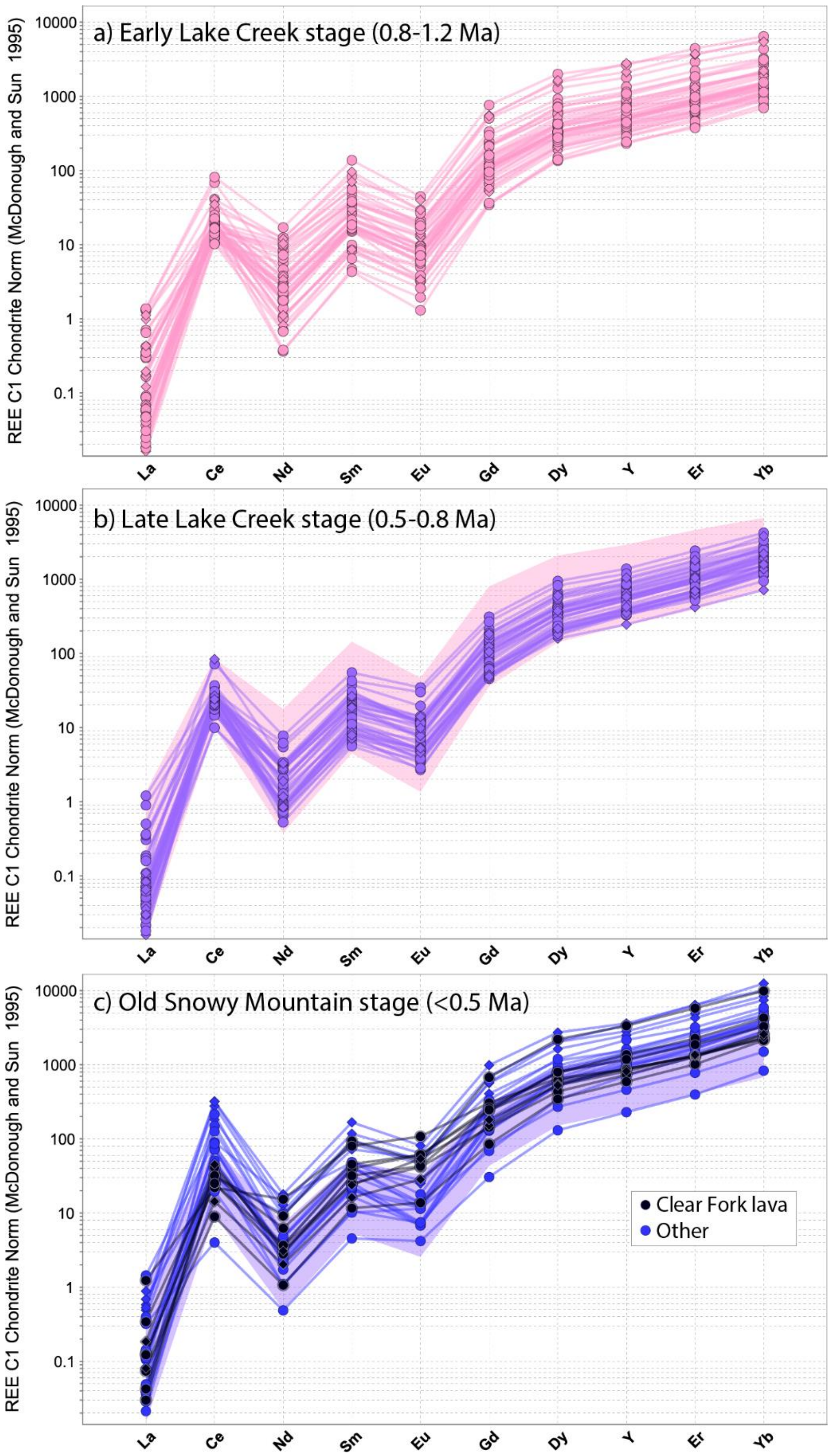

Figure 4.4. REE spider diagrams of zircon compositions.
Samples are distinguished by age. In b and c, the compositional range for the previous time period is shown with a transparent field. REE concentrations are normalized to C1 chondrite (McDonough and Sun, 1995).

Figure 4.5. Ti-in-zircon temperatures compared to zircon saturation temperatures. Only coherent age populations are shown, i.e. those interpreted to represent the most recent crystallization event (antecrysts and xenocrysts are not included). a) Ti-in-zircon temperature plotted against zircon saturation temperature for each sample. Points to the right of the 1:1 line have Ti-in-zircon temperatures higher than their samples' zircon saturation temperatures. b) Temperature vs. age. Individual spot analyses are plotted with their Ti-in-zircon temperature and ^{230}Th-corrected ^{206}Pb/^{238}U age. Overlain are the samples' zircon saturation temperatures vs. interpreted eruption age (hot pink borders and trendline; same scale on axes). The equation and R^2 of the trendline for sample age-zircon saturation temperature is shown in hot pink. c) T_{zircon}/T_{sat} [= (Ti-in-zircon temperature)/(zircon saturation temperature)] plotted against spot age. Zircon temperatures at or below zircon saturation temperature have $T_{zircon}/T_{sat} \leq 1$; higher values indicate crystallization temperatures above what is stable for the host magma's composition.

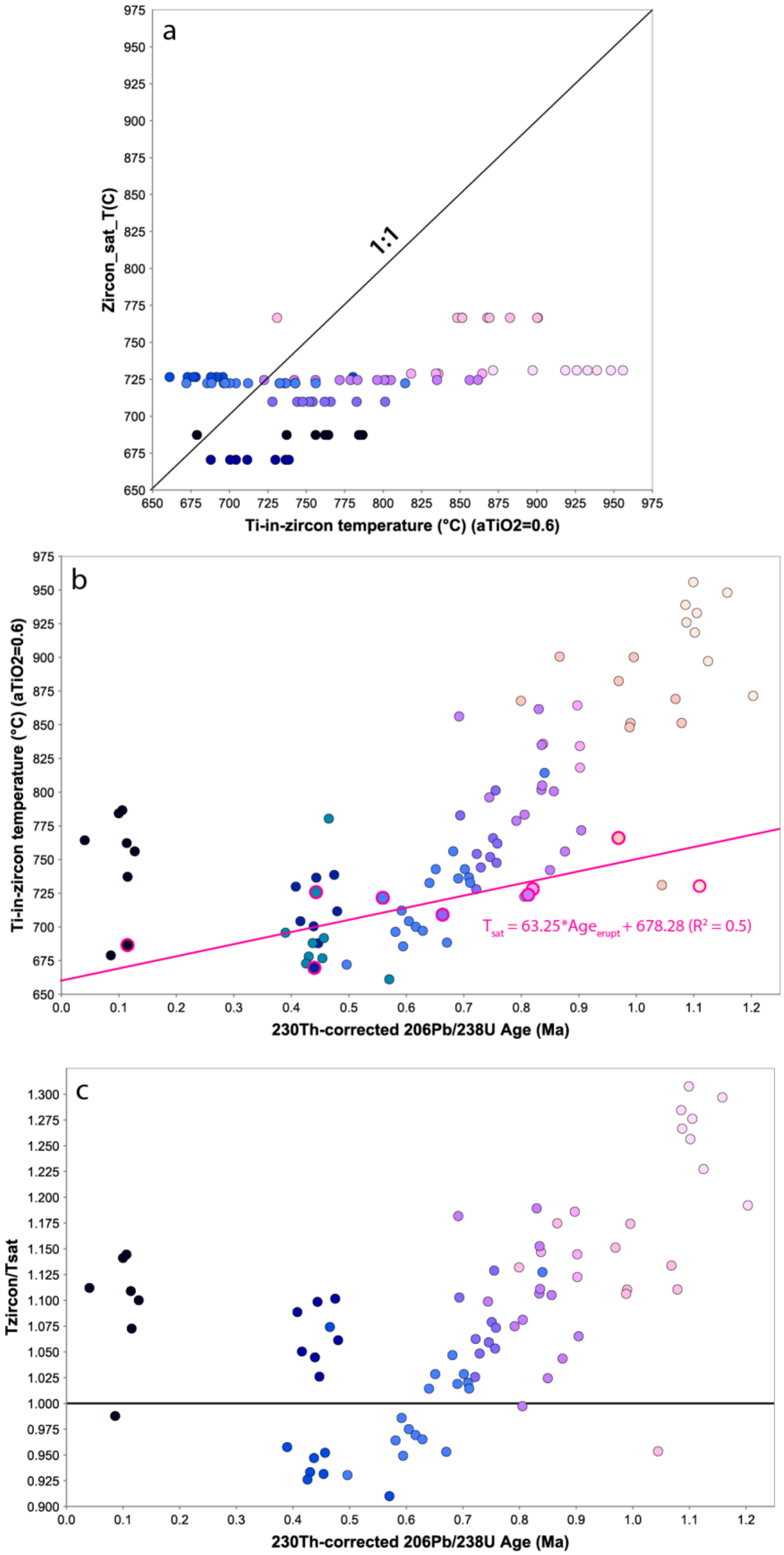
a
1:1
Zircon_sat_T(C)
Ti-in-zircon temperature (°C) (aTiO2=0.6)
b
Ti-in-zircon temperature (°C) (aTiO2=0.6)
T_{sat} = 63.25*Age_{erupt} + 678.28 (R^2 = 0.5)
230Th-corrected 206Pb/238U Age (Ma)
c
Tzircon/Tsat
230Th-corrected 206Pb/238U Age (Ma)

Figure 4.5.

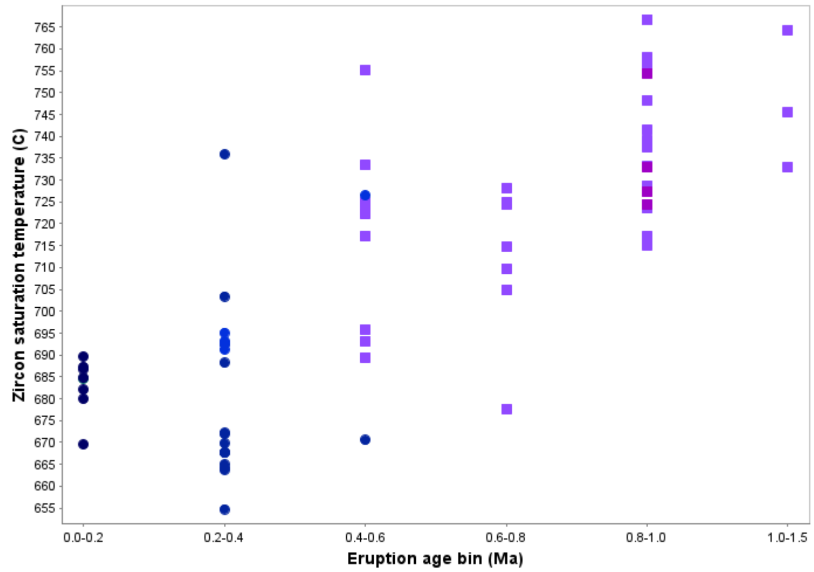

Figure 4.6. Zircon saturation temperatures of Goat Rocks magmas over time. Included only are those compositions with an M value ≤ 2.1, the upper limit of the Watson and Harrison (1983) compositional range for the calibration of their zircon saturation model.

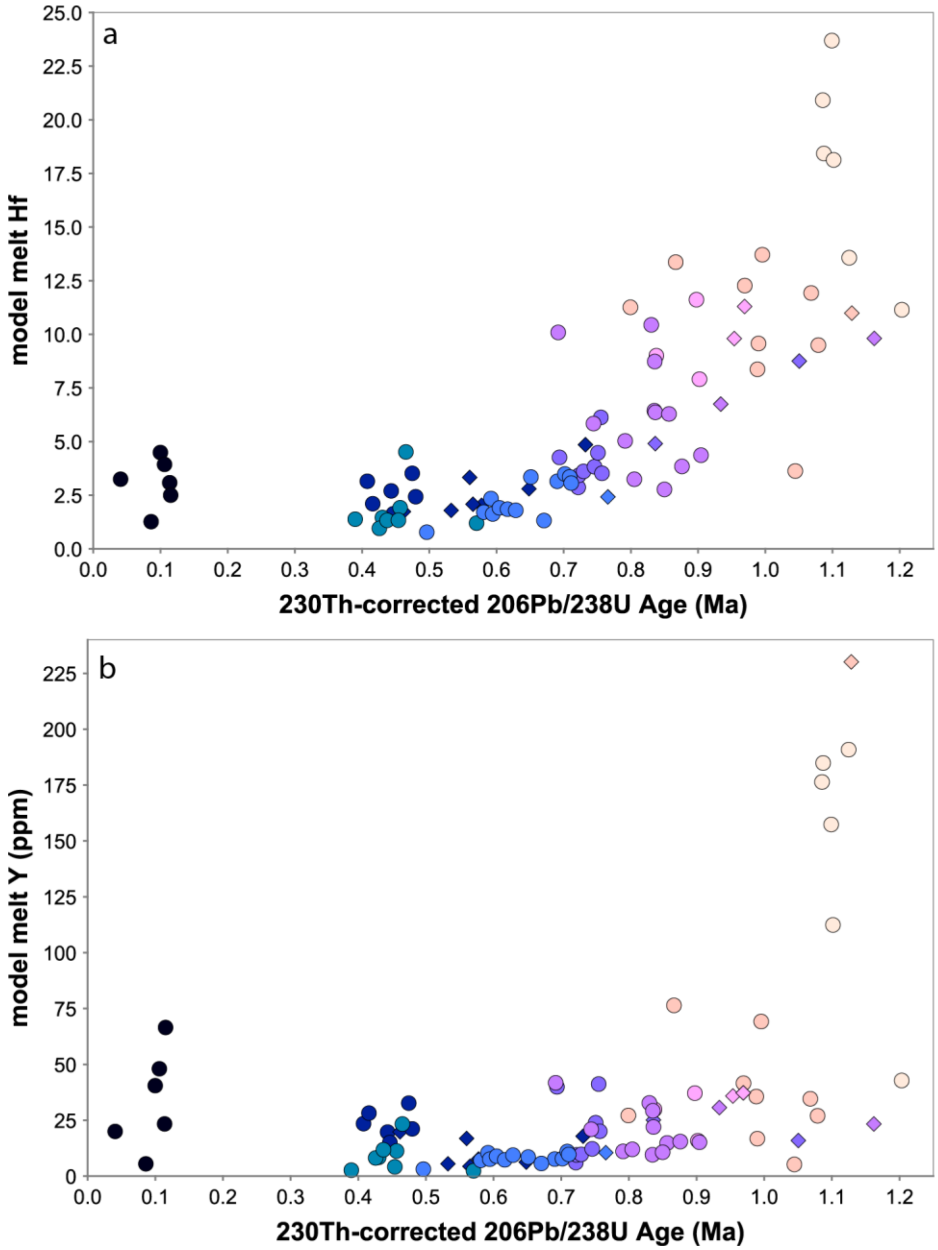

Figure 4.7. Model equilibrium melt compositions calculated from zircon compositions. The formulas by Claiborne et al. (2018) were used. Antecrysts are included in this figure.

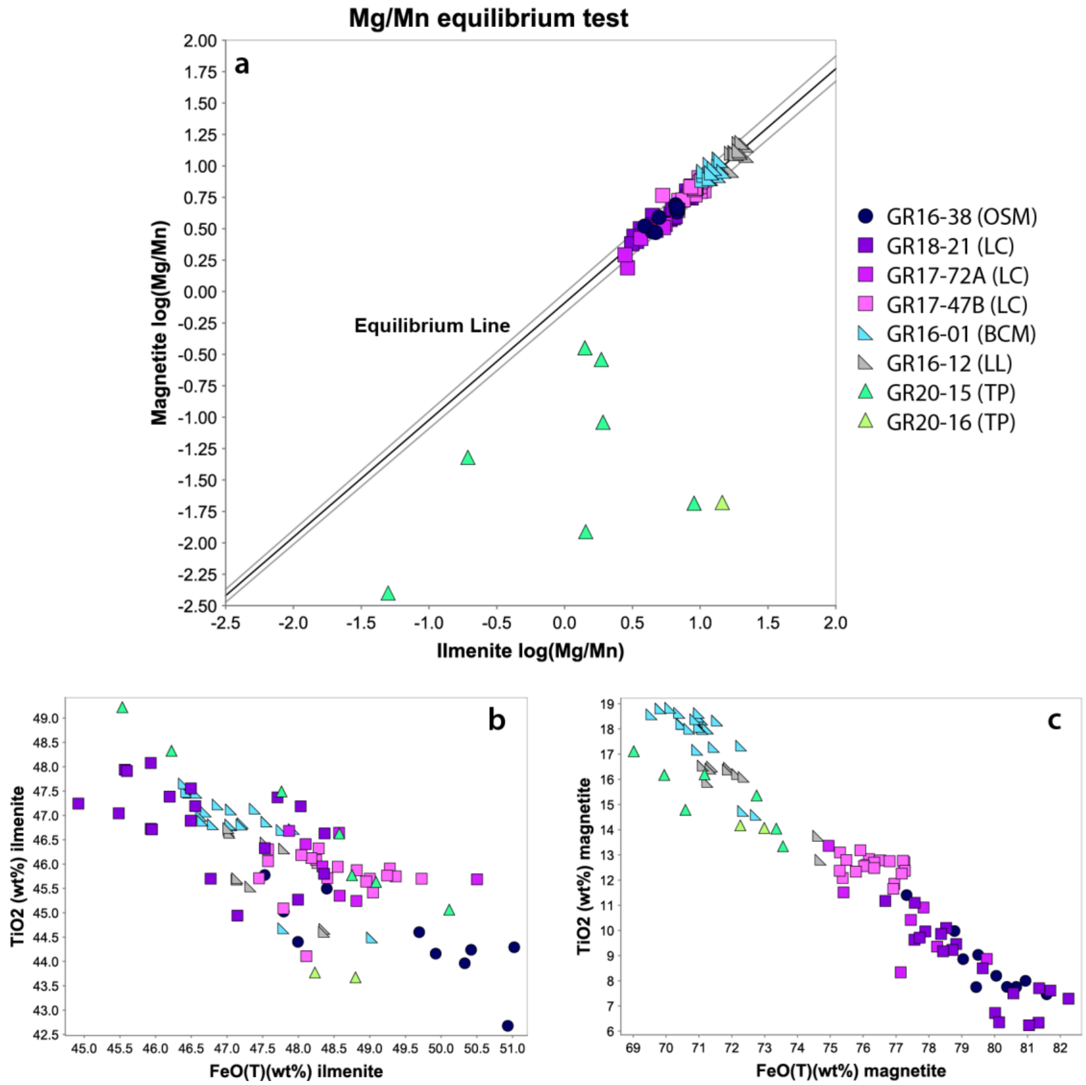

Figure 4.8. Compositions of paired magnetite and ilmenite in lava flows from the Goat Rocks volcanic complex.
Key to volcano/unit abbreviations in legend: OSM=Old Snowy Mountain, LC=Lake Creek, BCM=Bear Creek Mountain, LL=Lost Lake andesite, TP=Tieton Peak. a) Mg/Mn equilibrium diagram, after Bacon and Hirschmann (1988). Most compositions fall within the equilibrium envelope, but the magnetite-ilmenite pairs in samples from Tieton Peak are far outside of Mg/Mn equilibrium and therefore are not used for thermometry. b) TiO_2 vs. FeOT in ilmenite. The different samples overlap in composition. c) TiO2 vs. FeOT in magnetite. Samples from Tieton Peak, Lost Lake andesite, and Bear Creek Mountain form a population distinct from those samples from Lake Creek stage and Old Snowy Mountain.

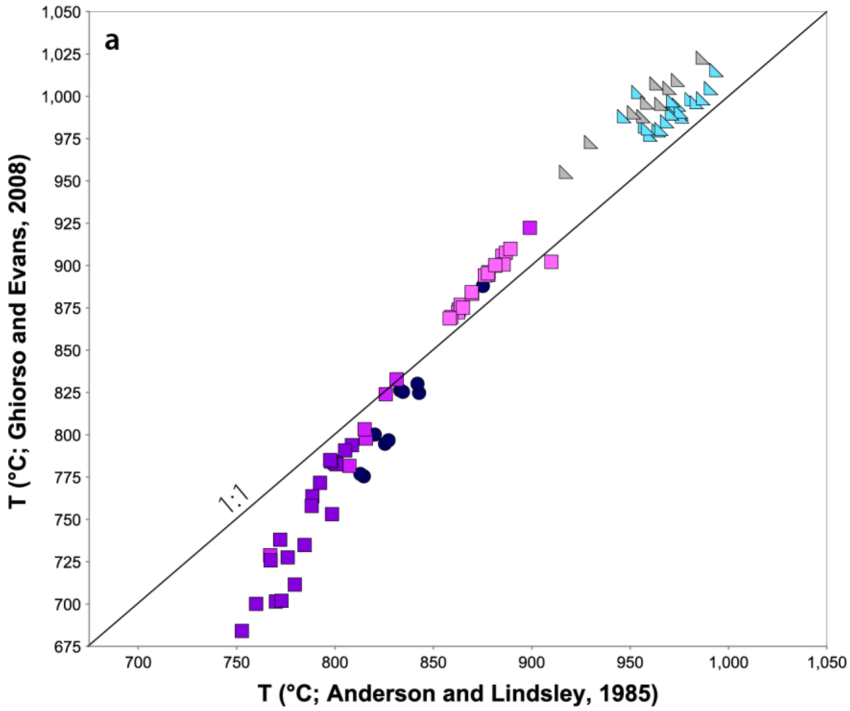

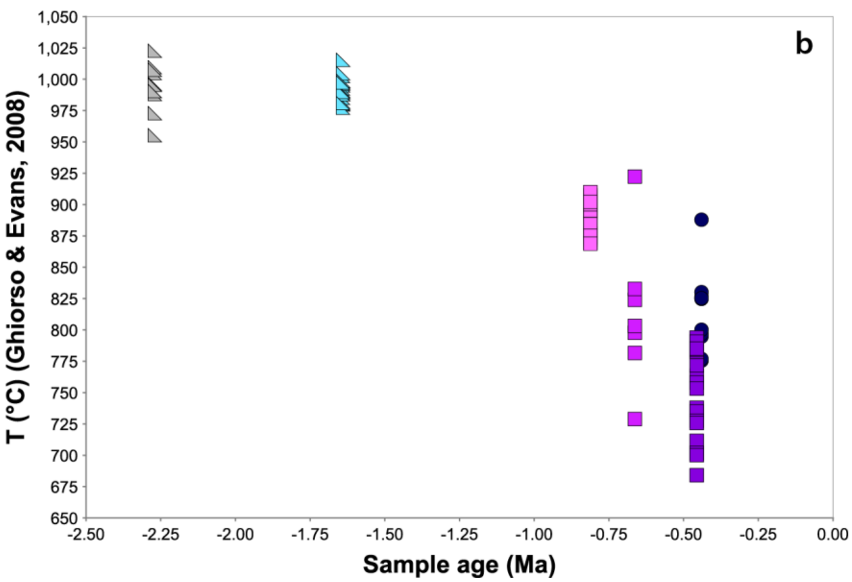

Figure 4.9. Thermometry results from magnetite-ilmenite pairs.
a) Different thermometer calibrations yield slightly different results. Here, compare results from the Ghiorso and Evans (2008) thermometer against those from the Andersen and Lindsley (1985) thermometer with stoichiometry formulation of Stormer (1983). b) Fe-Ti oxide temperatures (using Ghiorso and Evans, 2008) plotted against eruption age of samples. In addition to the decline in recorded temperatures between Bear Creek Mountain and Lake Creek samples, notice the overall decrease in recorded temperatures with time for the three samples from middle to late Lake Creek stage.

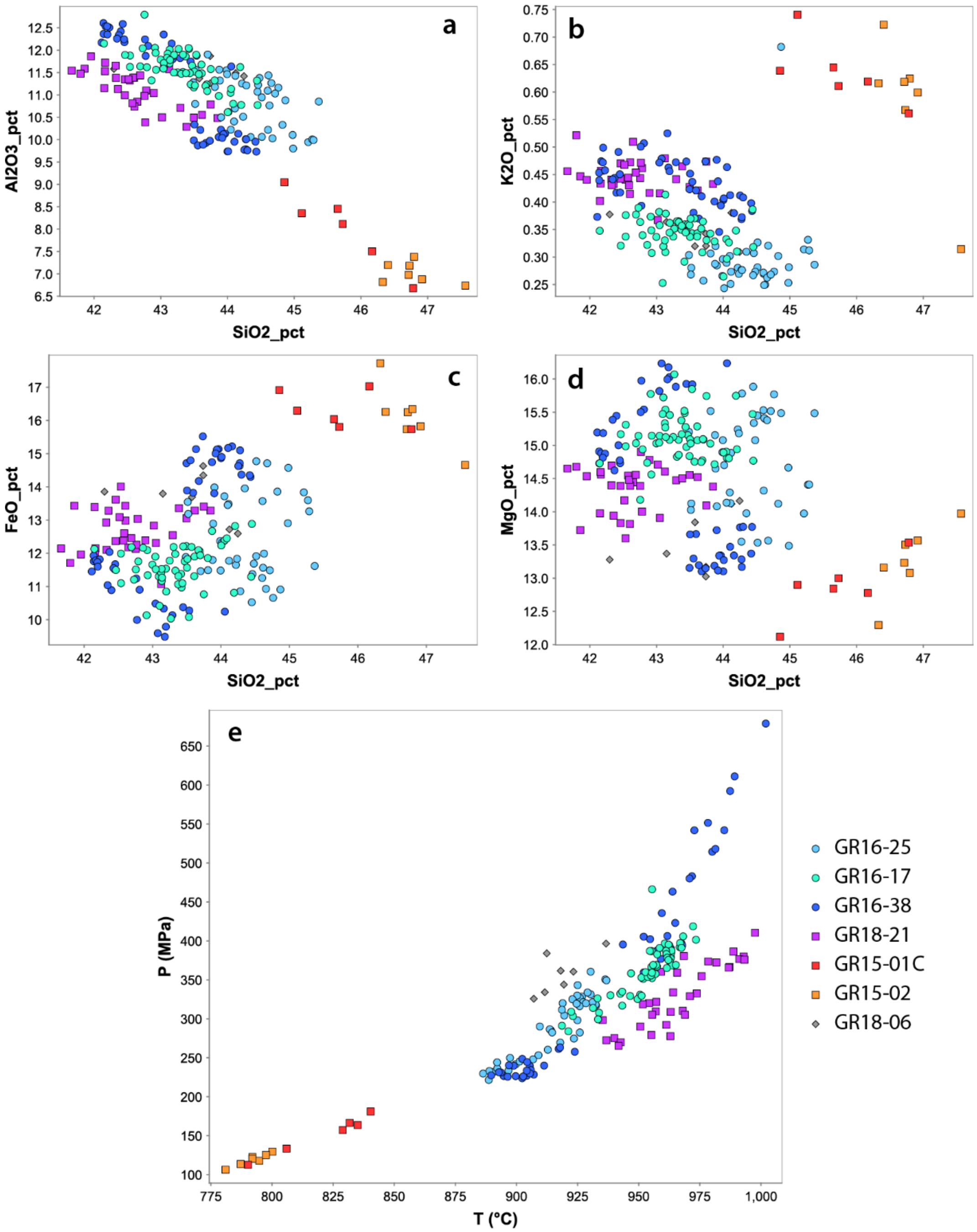

Figure 4.10. Compositions of amphibole in lava flows from the Goat Rocks area. Included are samples from the Lake Creek volcano, Old Snowy Mountain volcano, and late Pliocene diorite (unit Tpd; see geologic map in Chapter 2). a,b,c,d) concentrations of element oxides vs. SiO_2. Analyses which flagged an error in the Ridolfi et al. (2021) calculator (e.g. "low-B cations;" common for GR15-01C and GR15-02) are excluded. e) Pressure in megapascals (MPa) and temperature (°C) calculated using the Ridolfi et al. (2021) formulation. Note the distinction between older and younger samples from Goat Rocks. Sample GR18-06 (unit Tpd) records similar conditions as the younger Goat Rocks suite.

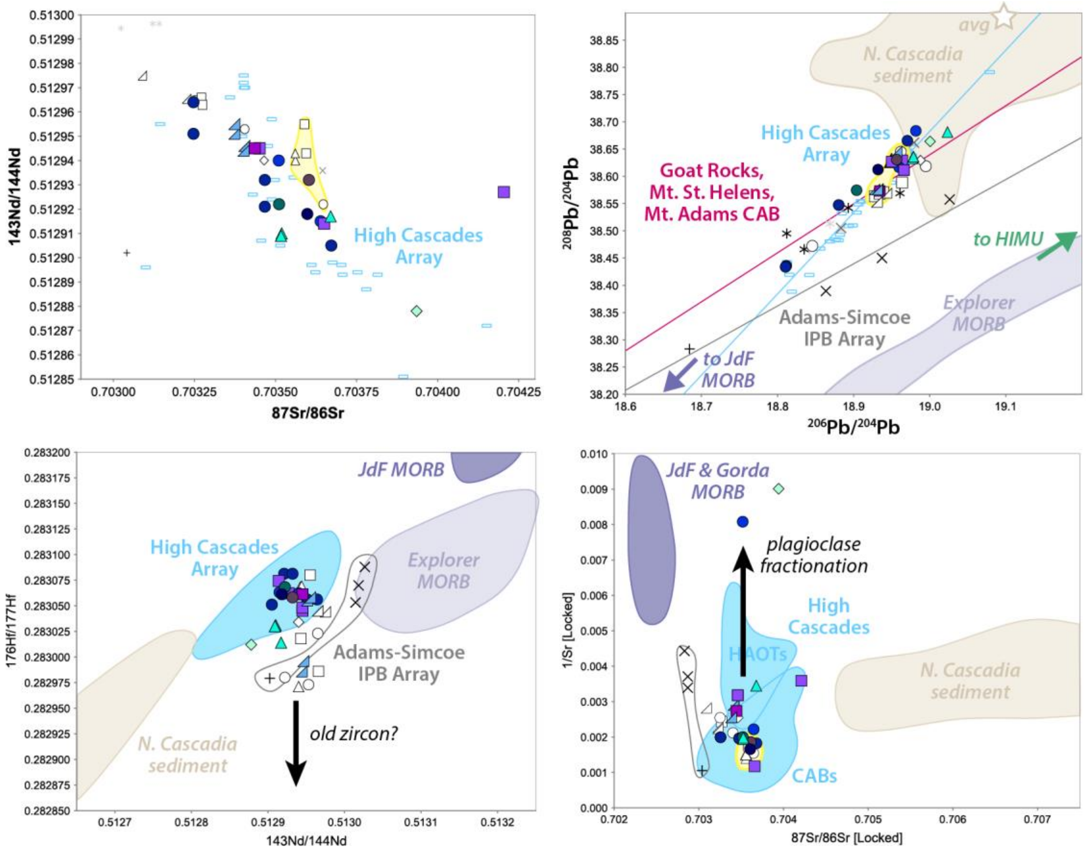

Figure 4.11. Bulk rock isotope ratios of intermediate to felsic lava flows from the Goat Rocks area.

Includes samples from the Goat Rocks volcanic complex as well as Devils Horns rhyolite, Spiral Butte, and Round Mountain. Basalt and basaltic andesite from peripheral mafic volcanoes are shown with white symbols (refer Chapter 3 for details). a) $^{143}Nd/^{144}Nd$ and $^{87}Sr/^{86}Sr$. Samples are mostly aligned with the High Cascades Array, overlapping the Goat Rocks basalt field and extending to lower $^{143}Nd/^{144}Nd$ and higher $^{87}Sr/^{86}Sr$. Sample GR15-04 is an outlier with much higher $^{87}Sr/^{86}Sr$ than other samples with comparable $^{143}Nd/^{144}Nd$. b) The intermediate to felsic samples are aligned with the basaltic High Cascades Array. Note that samples from Old Snowy Mountain extend over a broader range to lower Pb isotope values. c) $^{176}Hf/^{177}Hf$ values are mostly clustered with the High Cascades Array, but samples from Tieton Peak and Bear Creek Mountain extend to lower values, like the peripheral basalts. Zircon (or zircon-rich rock) from older basement is suggested as a contaminant that could pull down $^{176}Hf/^{177}Hf$ without significantly affecting other isotopes. d) There is not a clear correlation relating $^{87}Sr/^{86}Sr$ and concentration of Sr (or in this case, the inverse). Plagioclase fractionation complicates this diagram.

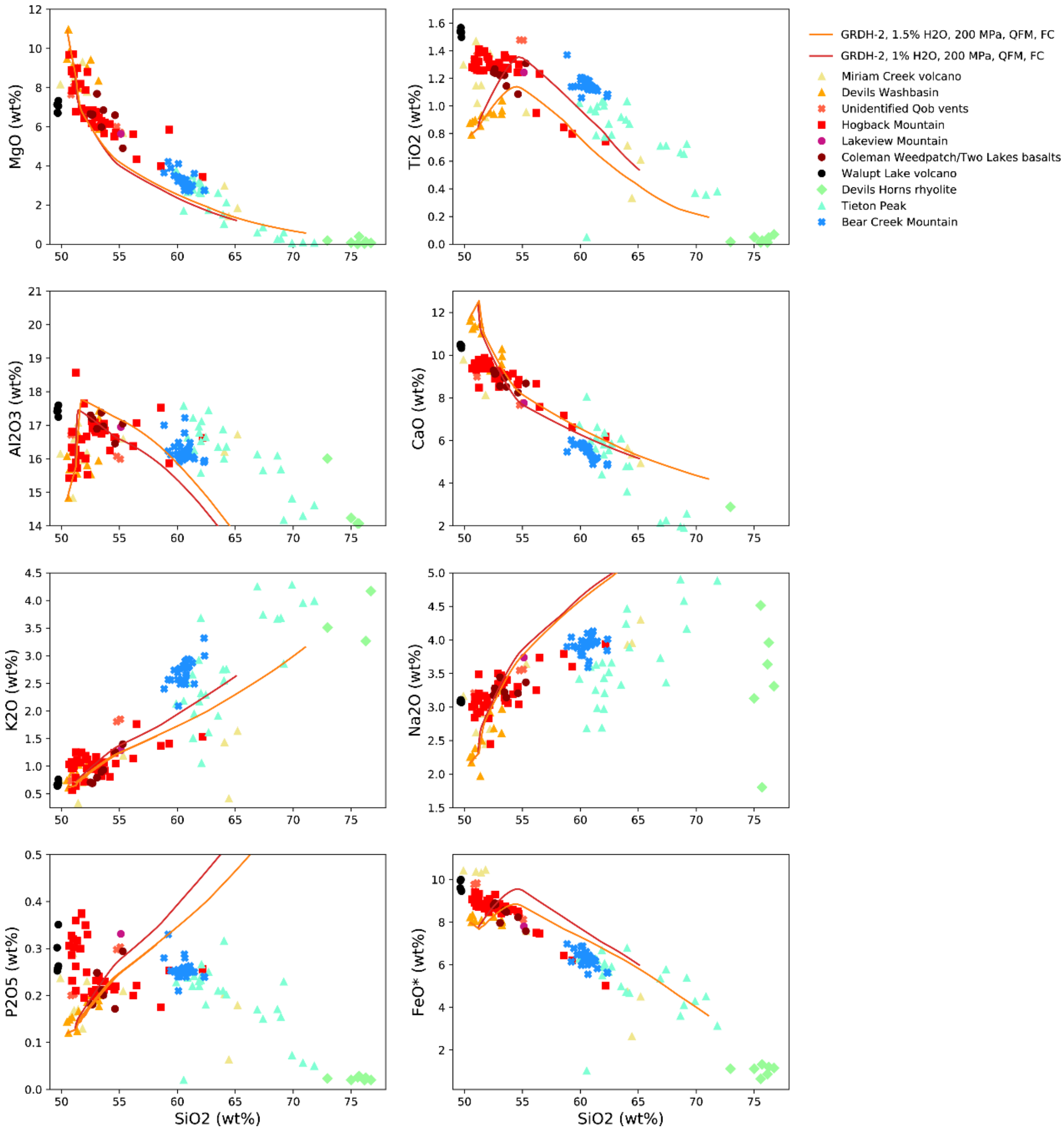

Figure 4.12. MCS fractional crystallization models of primitive Devils Washbasin basalt.

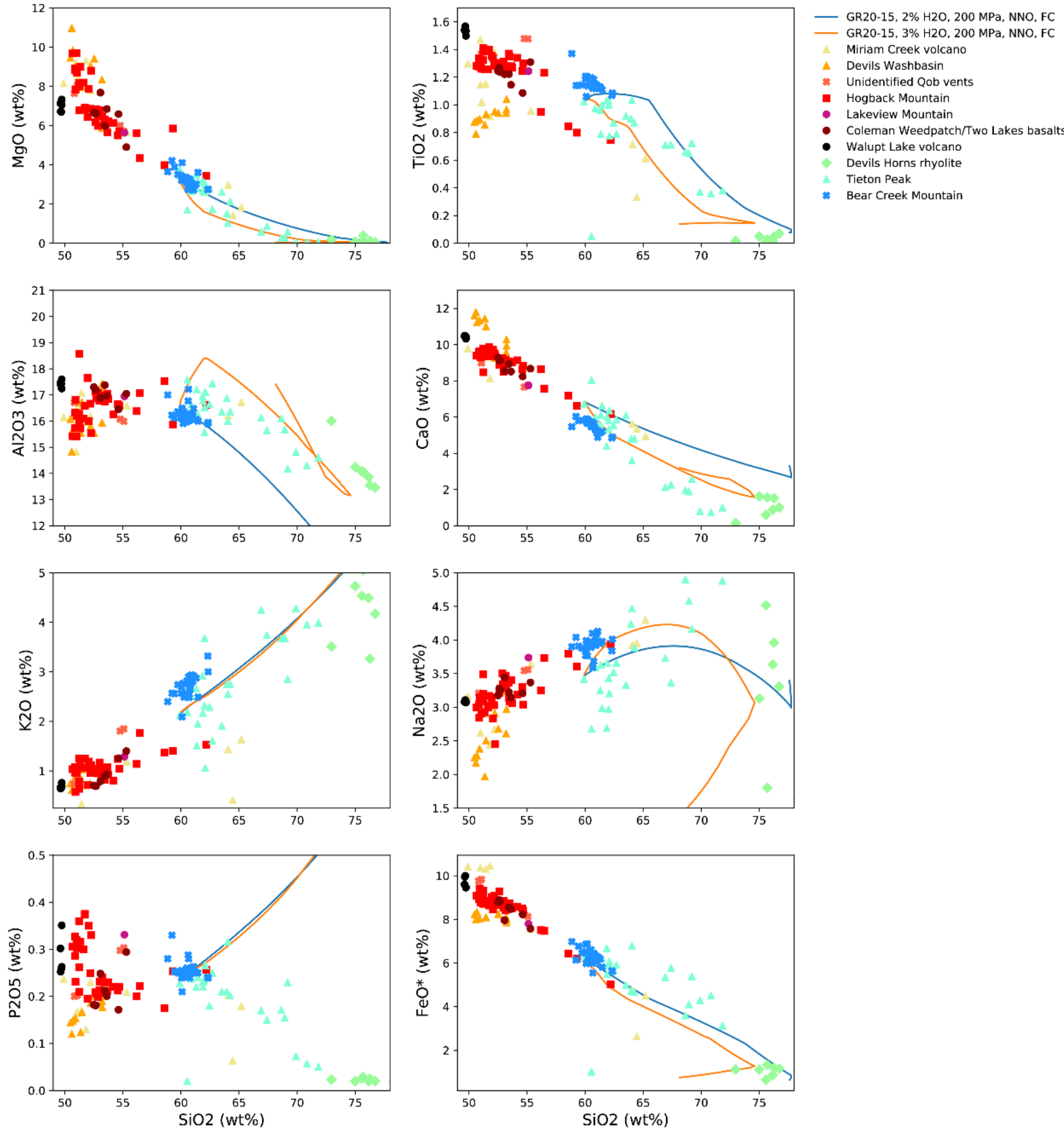

Figure 4.13. MCS models testing fractional crystallization of Tieton Peak andesite.

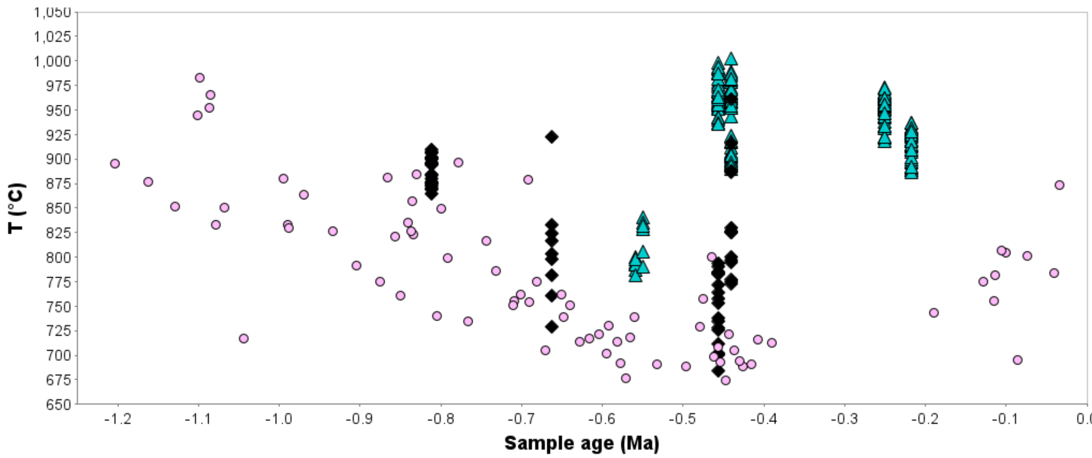

Figure 4.14. Comparison of thermometry results.
Data include zircon temperatures using the thermometer of Ferry and Watson (2007), paired magnetite-ilmenite temperatures using the thermometer of Ghiorso and Evans (2008), and amphibole temperatures using the thermometer of Ridolfi (2021). Zircon data are marked by pink circles and are plotted against their individual spot ages. For magnetite-ilmenite pairs (black diamonds) and amphibole (teal triangles), the age of the sample is used (constrained by geochronology in Chapter 2 or approximated based on stratigraphy).

REFERENCES

Anderson, A.T., 1968. Oxidation of the LaBlache Lake titaniferous magnetite deposit, Quebec. *The Journal of Geology*, *76*(5), pp.528-547. Andersen and Lindsley 1985 Fe Ti oxide thermometer

Bacon, C.R. and Hirschmann, M.M., 1988. Mg/Mn partitioning as a test for equilibrium between coexisting Fe-Ti oxides. *American Mineralogist*, *73*(1-2), pp.57-61.

Bohrson, W. A., Spera, F. J., Ghiorso, M. S., Brown, G. A., Creamer, J. B., and Mayfield, A., 2014, Thermodynamic model for energy-constrained open-system evolution of crustal magma bodies undergoing simultaneous recharge, assimilation and crystallization: The Magma Chamber Simulator: Journal of Petrology, v. 55, no. 9, p. 1685-1717.

Carmichael, I.S.E., 1967. The iron-titanium oxides of salic volcanic rocks and their associated ferromagnesian silicates. Contributions to Mineralogy and Petrology 14 (1), 36–64.

Claiborne, L.L., Miller, C.F., Walker, B.A., Wooden, J.L., Mazdab, F.K. and Bea, F., 2006. Tracking magmatic processes through Zr/Hf ratios in rocks and Hf and Ti zoning in zircons: an example from the Spirit Mountain batholith, Nevada. *Mineralogical Magazine*, *70*(5), pp.517-543.

Claiborne, L.L., Miller, C.F., Flanagan, D.M., Clynne, M.A. and Wooden, J.L., 2010. Zircon reveals protracted magma storage and recycling beneath Mount St. Helens. *Geology*, *38*(11), pp.1011-1014.

Claiborne, L.L., Miller, C.F., Gualda, G.A.R., Carley, T.L., Covey, A.K., Wooden, J.L. and Fleming, M.A., 2018, Zircon as Magma Monitor, *in* D.E. Moser, F. Corfu, J.R. Darling, S.M. Reddy and K. Tait, eds., Microstructural Geochronology, https://doi.org/10.1002/9781119227250.ch1

Clynne, M.A., Calvert, A.T., Wolfe, E.W., Evarts, R.C., Fleck, R.J. and Lanphere, M.A., 2008. *The Pleistocene eruptive history of Mount St. Helens, Washington, from 300,000 to 12,800 years before present* (No. 1750-28, pp. 593-627). US Geological Survey.

DeBari, S.M. and Greene, A.R., 2011. Vertical stratification of composition, density, and inferred magmatic processes in exposed arc crustal sections. In *Arc-continent collision* (pp. 121-144). Springer, Berlin, Heidelberg.

Ducea, M.N., Otamendi, J.E., Bergantz, G., Stair, K.M., Valencia, V.A. and Gehrels, G.E., 2010. Timing constraints on building an intermediate plutonic arc crustal section: U-Pb zircon geochronology of the Sierra Valle Fértil–La Huerta, Famatinian Arc, Argentina. *Tectonics*, *29*(4).

Ferry, J.M., and Watson, E.B., 2007, New thermodynamic models and revised calibrations for the Ti-in-zircon and Zr-in-rutile thermometers: Contributions to Mineralogy and Petrology, v. 154, p. 429-437, doi: 10.1007/s00410-007-0201-0.

Geschwind, C.H. and Rutherford, M.J., 1992. Cummingtonite and the evolution of the Mount St. Helens (Washington) magma system: an experimental study. *Geology*, *20*(11), pp.1011-1014.

Ghiorso, M.S., and Evans, B.W., 2008, Thermodynamics of rhombohedral oxide solid solutions and a revision of the Fe-Ti two-oxide geothermometer and oxygen-barometer: American Journal of Science, v. 308, p. 957-1039, DOI: 10.2475/09.2008.01

Ghiorso, M.S., and Prissel, K.B., 2020, ENKI Cloud App: Implementation of the Fe-Ti Oxide Geothermooxybarometer of Ghiorso and Evans, 2008, v. 1.0.0, Zenodo, https://doi.org/10.5281/zenodo.3866660

Grunder, A.L., Klemetti, E.W., Feeley, T.C., and McKee, C.M., 2008, Eleven million years of arc volcanism at the Aucanquilcha Volcanic Cluster, northern Chilean Andes: implications for the life span and emplacement of plutons: Transactions of the Royal Society of Edinburgh: Earth Sciences, v. 97, p. 415-436.

Gualda, G. A., Ghiorso, M. S., Lemons, R. V., and Carley, T. L., 2012, Rhyolite-MELTS: a modified calibration of MELTS optimized for silica-rich, fluid-bearing magmatic systems. Journal of Petrology, v. 53, no. 5, p. 875-890.

Gualda, G. A., and Ghiorso, M. S., 2015, MELTS _ Excel: A Microsoft Excel-based MELTS interface for research and teaching of magma properties and evolution: Geochemistry, Geophysics, Geosystems, v. 16, no. 1, p. 315-324.Hanchar, J.M. and Watson, E.B., 2003, Zircon saturation thermometry: Reviews in mineralogy and geochemistry, v. 53, no. 1, pp.89-112.

Jagoutz, O. and Behn, M.D., 2013. Foundering of lower island-arc crust as an explanation for the origin of the continental Moho. *Nature*, *504*(7478), pp.131-134.

Lepage, L.D., 2003, ILMAT: an Excel worksheet for ilmenite--magnetite geothermometry and geobarometry: Computers & Geosciences, v. 29, no. 5, pp.673-678.

Lindsley, D.H., Spencer, K.J., 1982. Fe–Ti oxide geothermometry: Reducing analyses of coexisting Ti-magnetite (Mt) and ilmenite (Ilm) abstract AGU 1982 Spring Meeting Eos Transactions. American Geophysical Union 63 (18), 471.

Miller, Robert B., Scott R. Paterson, Jennifer P. Matzel, and A. W. Snoke. "Plutonism at different crustal levels: Insights from the~ 5–40 km (paleodepth) North Cascades crustal section, Washington." *Crustal cross sections from the western North American*

Cordillera and elsewhere: Implications for tectonic and petrologic processes: Geological Society of America Special Paper 456 (2009): 125-149.

Otamendi, J.E., Ducea, M.N. and Bergantz, G.W., 2012. Geological, petrological and geochemical evidence for progressive construction of an arc crustal section, Sierra de Valle Fertil, Famatinian Arc, Argentina. *Journal of Petrology*, *53*(4), pp.761-800.

Powell, R., Powell, M., 1977. Geothermometry and oxygen barometry using coexisting iron-titanium oxides: a reappraisal. Mineralogical Magazine 41 (318), 257–263.

Putirka, K.D., 2008, Thermometers and barometers for volcanic systems: Reviews in Mineralogy and Geochemistry, v. 69, p. 61-120.

Putirka, K., 2016, Amphibole thermometers and barometers for igneous systems and some implications for eruption mechanisms of felsic magmas at arc volcanoes: American Mineralogist, v. 101, p. 841-858, DOI: http://dx.doi.org/10.2138/am-2016-5506.

Ridolfi, F., Renzulli, A., and Puerini, M., 2010, Stability and chemical equilibrium of amphibole in calc-alkaline magmas: an overview, new thermobarometric formulations and application to subduction-related volcanoes: Contributions to Mineralogy and Petrology, v. 160, p. 45-66, DOI 10.1007/s00410-009-0465-7.

Ridolfi, F., 2021, Amp-TB2: An updated model for calcic amphibole thermobarometry: Minerals 2021, v. 11, no. 324, https://doi.org/10.3390/min11030324.

Sauer, K.B., Gordon, S.M., Miller, R.B., Vervoort, J.D., and Fisher, C.M., 2017, Evolution of the Jura-Cretaceous North American Cordilleran margin: Insights from detrital-zircon U-Pb and Hf isotopes of sedimentary units of the North Cascades Range, Washington: Geosphere, v. 13, no. 6, p. 2094–2118, doi:10.1130/GES01501.1.

Spencer, K.J., Lindsley, D.H., 1981. A solution model for coexisting iron-titanium oxides. American Mineralogist 66 (11-12), 1189–1201.

Stormer Jr, J.C., 1983. The effects of recalculation on estimates of temperature and oxygen fugacity from analyses of multicomponent iron-titanium oxides. American Mineralogist 68 (5-6), 586–594.

Stormer Jr, J.C. and Nicholls, J., 1978, XLFRAC: a program for the interactive testing of magmatic differentiation models: Computers & Geosciences, v. 4, no. 2, pp.143-159.

Swanson, D.A., and Clayton, G.A., 1983, Generalized geologic map of the Goat Rocks Wilderness and Roadless Areas (6036, Parts A, C, and D), Lewis and Yakima Counties, Washington: U.S. Geological Survey Open-File Report 83-357.

Vance, J.A., Clayton, G.A., Mattinson, J.M., and Naeser, C.W., 1987, Early and Middle Cenozoic stratigraphy of the Mount Rainier-Tieton River area, southern Washington

Cascades: Washington Division of Geology and Earth Resources Bulletin, v. 77, p. 269-290.

Vervoort, J., 2014, Lu-Hf Dating: The Lu-Hf Isotope System in Encyclopedia of Scientific Dating Methods *in* Rink, W.J., and Thompson, J.W., eds., Encyclopedia of Scientific Dating Methods, Encyclopedia of Earth Sciences Series, Springer, Dordrecht, https://doi-org.ezproxy.proxy.library.oregonstate.edu/10.1007/978-94-007-6304-3_46

Wieser, P., Petrelli, M., Lubbers, J., Wieser, E., Kent, A., and Till, C., 2021, Thermobar: A critical evaluation of mineral-melt thermobarometry and hygrometry in arc magmas using a new open-source Python3 tool: Geological Society of America Abstracts with Programs, v. 53, no. 6, https://doi.org/10.1130/abs/2021AM-367080.